Two-length-scale multiblock copolymer self-assembly

Markov, Vladimir Aleksandrovich

Two-length-scale multiblock copolymer self-assembly:
theoretical investigations and computer simulations

Vladimir Aleksandrovich Markov

Two-length-scale multiblock copolymer self-assembly:

theoretical investigations and computer simulations

V.A. Markov

PhD thesis

University of Groningen

The Netherlands

January 2012

university of groningen

faculty of mathematics and natural sciences

zernike institute for advanced materials

RIJKSUNIVERSITEIT GRONIGEN

Two-length-scale multiblock copolymer self-assembly:
theoretical investigations and computer simulations

Proefschrift

ter verkrijging van het doctoraat in de

Wiskunde en Natuurwetenschappen

aan de Rijksuniversiteit Groningen

op gezag van de

Rector Magnificus, Dr. E. Sterken,

in het openbaar te verdedigen op

vrijdag 13 januari 2012

om 12:45 uur

door

Vladimir Aleksandrovich Markov

geboren op 14 maart 1983

Moskou, Rusland

The important thing in science is not so much to obtain new facts as to discover new ways of thinking about them.

William Bragg

CONTENTS

Chapter 1

Introduction

Chapter 2

Lamellar-*in*-Lamellar Self-Assembly in Linear Ternary Multiblock Copolymers: Alexander-de Gennes Approach and Dissipative Particle Dynamics Simulations

Chapter 3

Parallel versus perpendicular lamellar-*in*-lamellar self-assembly of linear ternary multiblock copolymer melts

Chapter 4

Self-Assembly of (A-comb-C)-b-(B-comb-C) diblock copolymer-based comb copolymers

Chapter 5

DNA-*b*-PFO block copolymer and SWNT complexes

Chapter 6

Chapter 7

Appendix

Chapter 1

Introduction

1.1 Block copolymers: magic of self-assembling

A **polymer** is a large molecule (macromolecule) composed of many repeating structural units typically connected by covalent chemical bonds [1-3]. The number of monomers N is called its degree of polymerization and the molecule is called a polymer if N >> 1. The chain length can vary within wide limits. The simplest polymer polyethylene ($-CH_2-)_N$, which is also the most widely used plastic, has a degree of polymerization N ≈ 10^2-10^5. This number is typical for synthetic polymers (polyethylene, polystyrene, polyisoprene, etc.). Natural polymers can be much longer even, for example, the longest natural polymer is DNA which consists of up to 10^9 monomer units. Because of the large number of monomer units it is often possible to ignore the specific chemical structure and to represent the polymer as beads freely linked together, Fig. 1.1. This allows the development of a polymer description in the framework of statistical mechanics where the microscopic details are not dominant in comparison with the large number of possible polymer conformations.
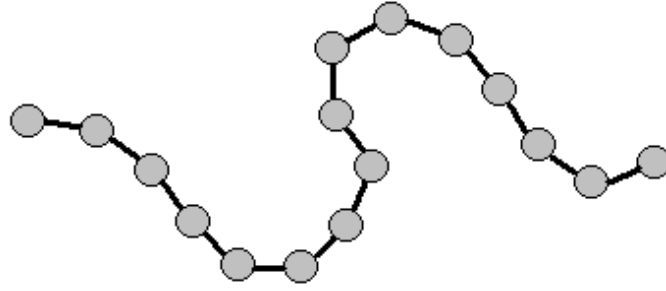
Figure 1.1. Schematic illustration of a homopolymer consisting of $N \gg 1$ monomer units.

If two chemically different homopolymer are connected by their ends a so-called called diblock copolymer is formed. The presence of two different units in the system introduces new interactions that are usually unfavorable. In a melt of two different homopolymers this tendency for the mutual interactions to be unfavorable often leads to macrophase separation in two phases. Due to the large chain length even small repulsive interactions are sufficient to drive the system to phase separation. If the chemically different homopolymers are connected macrophase separation is no longer possible and the system undergoes microphase separation. This phenomenon of microphase separation, or maybe more correctly nanophase separation, is one of the most interesting aspects of block copolymer systems, because it leads to a variety of different nanostructures that are of direct interest for many nanotechnology applications.

To describe the interactions between chemically different species the Flory-Huggins interaction parameter χ is introduced [4]. For monomer units A and B, it is defined by:

$$\chi_{AB} = \frac{z}{k_B T}\left(\varepsilon_{AB} - \frac{\varepsilon_{AA} + \varepsilon_{BB}}{2}\right) \tag{1.1}$$

where z is the number of nearest neighbor monomers, T denotes the temperature, k_B is the Boltzmann constant and ε_{AA}, ε_{BB} and ε_{AB} are the interaction energies of the A-A, B-B and A-B interactions respectively. For $\chi_{AB} > 0$ the A- and B-component interact unfavorably. In the opposite case, if $\chi_{AB} < 0$, the different species attract each other. As already mentioned above, there is a strong tendency for χ_{AB} to be positive, i.e., in most cases the chemically different species interact repulsively. Since the thermal translational energy per macromolecule is of the order $k_B T$, whereas the interaction energy per macromolecule is proportional to the length N, the product $\chi_{AB}N$ rather than χ_{AB} is the relevant quantity.
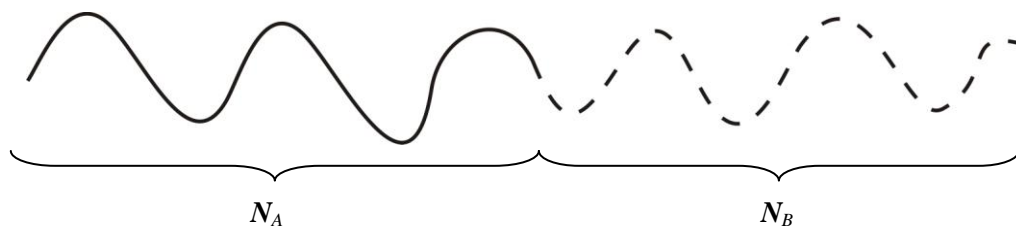
Figure 1.2. Schematic illustration of a diblock copolymer consisting of $N = N_A+N_B$ monomer units.

Fig. 1.2 presents a schematic illustration of a diblock copolymer with N_A and N_B A and B monomer units which for simplicity reasons often are assumed to have the same size. In terms of the volume fractions the composition is then given by $f_A = N_A/N$, respectively $f_B = 1\text{-}f_A = N_B/N$, where $N=N_A+N_B$. If $f_A = f_B$ the diblock copolymer is called symmetric, otherwise - asymmetric. By varying the interaction parameter χ and the composition f_A, the diblock copolymer will microphase separate in different well-ordered structures with a characteristic size of the order of a few times the radius of gyration, R_g, of the constituent blocks and thus in the range from 10 to 100nm [7].

Microphase separation of block copolymer systems has been the focus of attention for many years [7–12], because the nanostructures can be explored for nanotechnology applications, for example, for creating catalysts, membranes, arrays of nanowires, and photonic crystals [13]. The characteristic phase behavior of a *diblock copolymer melt*, as calculated by Matsen and Schick in 1994, [5] is presented in Figure 1.3. Only the lamellar, hexagonal(cylindrical), cubic(spherical) and gyroid morphologies were found to be stable. The corresponding nanostructures are schematically illustrated in Figure 1.4. In the meantime the phase diagram has been slightly refined, [6] but the main features remain as given. The diblock copolymer composition and the product χN determine the stability regions for the different morphologies.
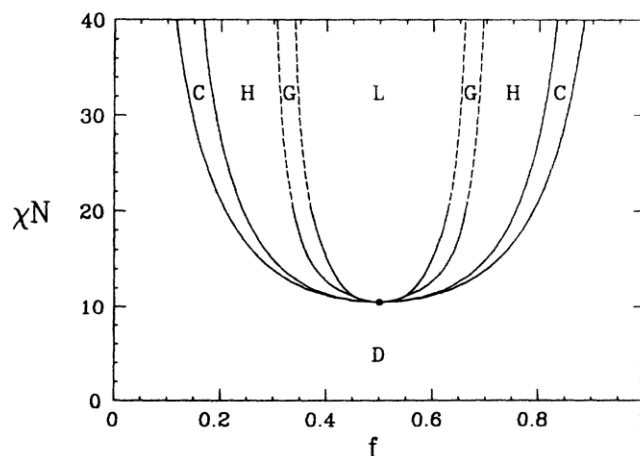
Figure 1.3. Phase diagram of diblock copolymer melt. L denotes the lamellar morphology, H - hexagonal, G - gyroid, C- spherical morphology, D – disordered state.
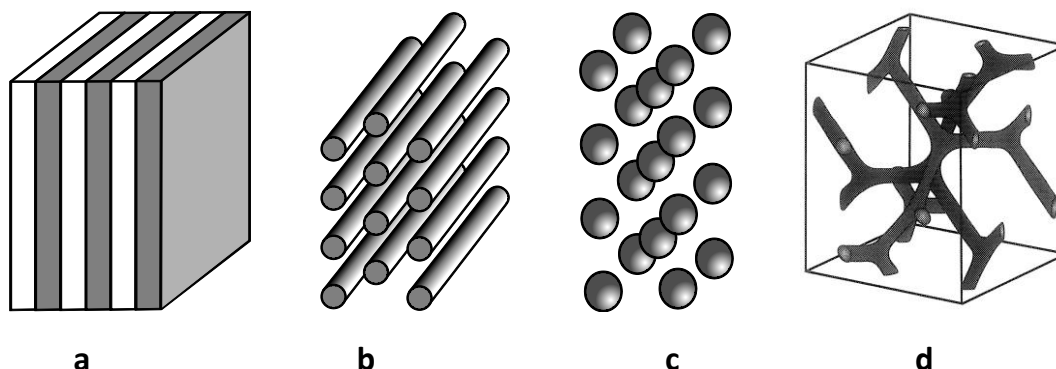
Figure 1.4. Schematic presentation of the different diblock copolymer microstructures: (a) lamellar, (b) cylindrical(hexagonal), (c) spherical, (d) gyroid.

Changing the diblock copolymer composition results in different nanophase separated structures because the system foremost tries to reduce the amount of contact surface where the unfavorable interactions take place. The periodicity length scale of a particular structure is determined by the competition between the interfacial energy F_{int} and the chain stretching free energy F_{str}. Apart from the above mentioned structures, many more morphologies may be found for block copolymers with a more complex molecular architecture, such as linear tri(multi)block copolymers, comb copolymers, star copolymers, etc. Multiblock copolymers will be briefly reviewed below because representatives of this class of block copolymers have been shown to exhibit hierarchical structure formation, i.e. structure formation at different length scales, which is the main topic of the work described in this thesis.

1.2 Multiblock copolymers: second characteristic length scale

As already discussed, simple AB diblock copolymers self-assemble in classical morphologies like lamellar, hexagonally ordered cylinders, body-centered cubic spheres and bicontinuous gyroid. All these morphologies have one thing in common: they can be described by one characteristic length. This fact is directly connected to the diblock structure. To obtain microphase separation involving two or more length scales (Fig. 1.5-1.7), more complex molecular architectures are needed. There are several ways to accomplish this. One possibility is to increase the number of chemically different monomers, as in ABC triblock copolymers, and another option is to change the diblock structure into, e.g., a linear *binary* multiblock copolymer structure.

1.2.1 Experimental overview

One of the first examples of self-assembled morphologies characterized by two different length scales is polystyrene-block-poly(4-vinylpyridine) (PS-*b*-P4VP) diblock copolymers with hydrogen-bonded pentadecylphenol (PDP) side chains attached to the P4VP block [13-15]. For common molar masses, the PS blocks separate from the comb-like P4VP(PDP) blocks, giving rise to the first characteristic length scale. At sufficiently low temperatures, below ca. 65°C, the alkyl tails of the PDP molecules start to microphase separate from the P4VP blocks introducing a second (small) characteristic length scale. By varying the volume fractions of the components and the temperature, a large number of different hierarchical microphase separated structures have been observed, see Fig. 1.5-1.6.
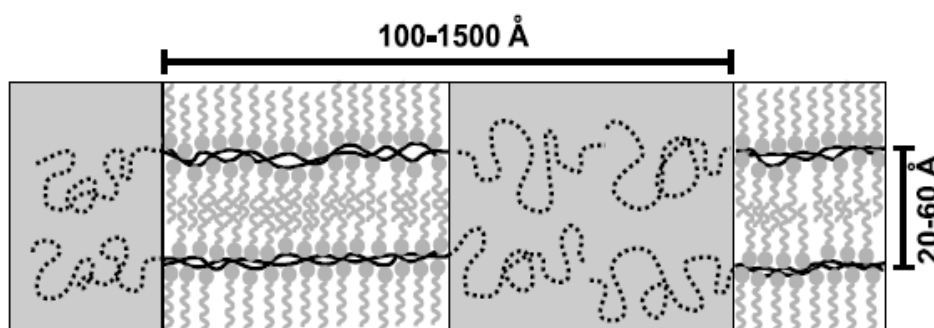
Figure 1.5. Schematic representation of PS-b-P4VP diblock copolymers with hydrogen-bonded PDP blocks self-assembled in a lamellar-*in*-lamellar morphology.
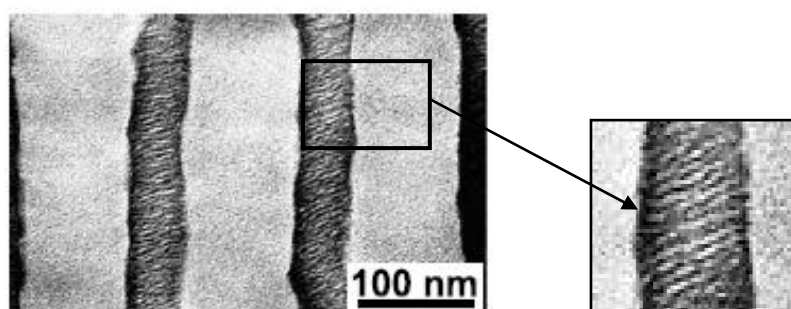
Figure 1.6. TEM pictures of lamellar-*in*-lamellar self-assembled PS-b-P4VP(PDP).

The above mentioned system is characterized by the presence of three chemically different species (PS, P4VP, PDP) and, in combination with the considerable difference in intrinsic length scales involved (PDP is much shorter than PS and P4VP), hierarchical structure formation seems quite natural Fig. 1.6. However, surprisingly enough, *binary* systems can also exhibit two-length-scale behaviour [16]. Experimentally, this was first demonstrated by Matsushita and co-workers. Based on polystyrene (S) and polyisoprene (I) blocks, they synthesized linear multiblock copolymers. A lamellar-*in*-lamellar structure was found for undecablock S-ISISISISI-

S copolymers with styrene end blocks that are much longer than the other blocks. The long polystyrene tails are responsible for the primary structure and the relatively short blocks of the multiblock part $(IS)_n$ are responsible for the secondary structure. For this particular system the multiblock part phase separated in three internal layers. The reason that phase separation in *binary* multiblock copolymers with a molecular architecture characterized by two length scales results in hierarchical structure formation has been discussed in some detail in ref. [43]
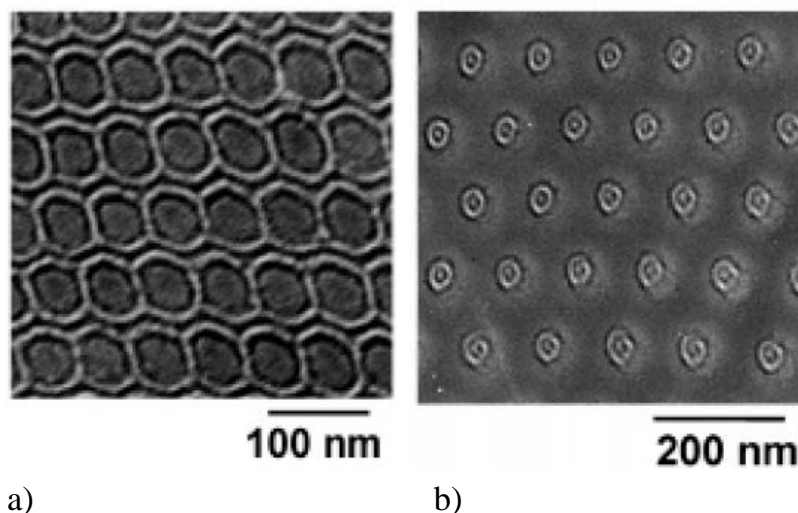
Figure 1.7. Structure inside structure a) P-*b*-(I-*b*-S)$_4$-I-*b*-P; b) P-*b*-(I-*b*-S)$_2$-*b*-I. (Reprinted with permission from J. Masuda, A. Takano, J. Suzuki, Y. Nagata, A. Noro, K. Hayashida and Y. Matsushita, Macromolecules, **2007**, *40* (11), 4023. Copyright 2007 American Chemical Society.)

In another study the polystyrene tails were replaced by poly(2-vinylpyridine)[17]. This turns the system from binary into ternary. Of course, due to its symmetric composition, the system still phase separates in a lamellar-*in*-lamellar morphology, however, now with five rather than three internal layers. By replacing the original S tails with a third type 2VP block, none of the blocks (S and I) of the multiblock middle part are able to penetrate in the layers formed by the long S blocks. This leads to the additional internal layers observed. In the systems described above, the molar mass (and, hence, also the volume fraction) of the tails and the multiblock was approximately the same and the blocks of the middle multiblock were also all of a similar, but much smaller, molar mass. Multiblock terpolymers with different volume fractions were also studied by Matsushita and co-workers [18]. An undecablock terpolymer of the P(IS)4IP type was found to exhibit a spheres-*in*-lamellar structure when P amounts to 8%w/w and terpolymers of the same type showed cylinders-*in*-lamellar (Fig. 1.7a) and lamellar-*in*-lamellar structures for weight percentage of the P component equal to 21% and 53%. In turn, hexablock terpolymers with P of 64%, 75%, and 87% exhibited a lamellar-*in*-lamellar structure, coaxial cylinders in a continuous matrix (Fig. 1.7b), and onionlike spheres in a continuous matrix, respectively. Figure 1.8 shows schematically the phase behavior for the multiblock terpolymers of A(BC)$_4$BA and A(BC)$_2$B type. The A(gray) domain transforms from spheres into cylinders into lamellae and finally into the matrix

with increasing fraction of the A component, while the domains of the B-C phase transform from matrix into lamellae, into cylinders and into spheres while keeping its alternating layered structure. This sequence of morphological transitions is very similar to the transitions in AB and ABA block copolymer systems.
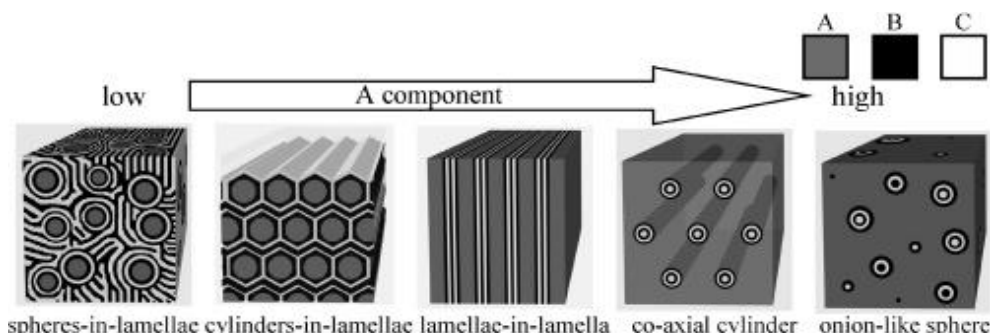
Figure 1.8. Schematic illustration of the composition-dependent morphological transitions of the multiblock terpolymers of $A(BC)_nBA$ type and $A(BC)_nB$ type. Gray, black, and white regions, correspond to A, B, and C domains, respectively.
(Reprinted with permission from J. Masuda, A. Takano, J. Suzuki, Y. Nagata, A. Noro, K. Hayashida and Y. Matsushita, Macromolecules, **2007**, *40* (11), 4023. Copyright 2007 American Chemical Society.)

Recently Fleury and Bates [19, 20] investigated the properties of a hexablock terpolymer C-E-C-E-C-P, consisting of cyclohexylethylene (C), ethylene (E) and propylene (P) blocks. This multiblock copolymer, which contained equal volume fractions of P and the compositionally symmetric CECEC, microphase separates due to the incompatibility between C, E, and P and exhibits a lamellar-*in*-lamellar morphology with two different length scales related to the local (C-E) and overall (C-E-P) sequences. They identified for the first time a *perpendicular* lamellar-*in*-lamellar mesostructure where the thin alternating CE layers are oriented perpendicularly to the P-layers. The issue of parallel versus perpendicular lamellar-*in*-lamellar structures will be discussed in more detail in Chapter 3.

In the case of a parallel lamellar-*in*-lamellar structure, the number of internal layers is directly connected to the probability of forming loops and bridges inside layers. Experimental efforts [22, 23] have been directed toward estimating the bridging fraction in A-B-A triblock systems. Monitoring the dynamics of the center block in poly(styrene-*block-cis*-isoprene-*block*-styrene) (S-I-S) with dielectric techniques, Karatasos et al.[22] estimated the bridging fraction to be in the range of 0.37–0.5, which agreed with the results of mean-field calculations [21].

Star copolymers are also able to phase separate in structures with a multi length scale character. ABC-like star-shaped terpolymers, where the three different components are connected at the same junction point, were investigated by Matsushita et al.[24, 25]. The systematic transitions of the two-dimensional tiling patterns have been studied extensively for two series of star-shaped terpolymers: $I_{1.0}S_{1.8}P_X$ and $I_{1.0}S_YP_{2.0}$. Investigation of the influence of the compositions X and Y on the periodic structures (Fig. 1.9) demonstrated that the transitions can be effectively described by the concept of the average coordination number, which is defined as the mean value of the side numbers of polygonal domains formed by each component.
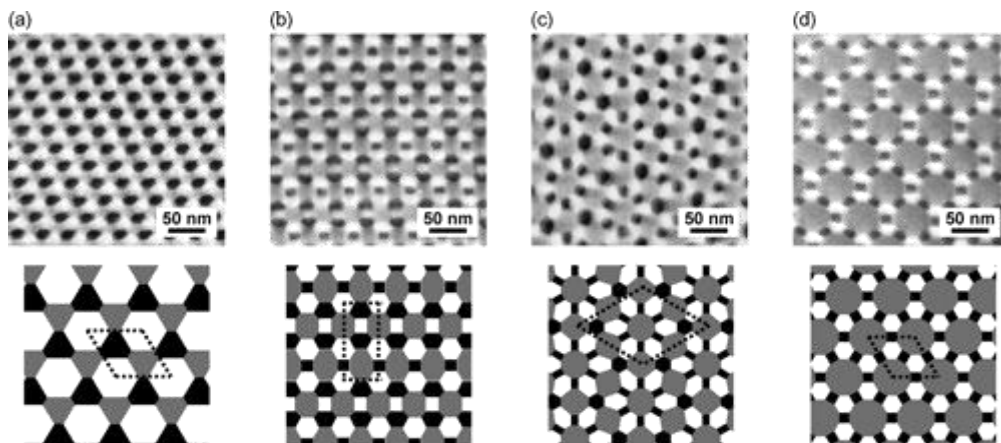
Figure 1.9. TEM images of four ISP star-shaped terpolymer samples (top) and the corresponding schematic tiling patterns (bottom): (a) I1.0S1.8P1.0, (b) I1.0S1.8P1.6, (c) I1.0S1.8P2.0, (d) I1.0S1.8P2.9.
(Reprinted with permission from K. Hayashida, A. Takano, S. Arai, Y. Shinohara, Y. Amemiya, and Y. Matsushita, *Macromolecules*, **2006**, 39, 9402. Copyright 2006 American Chemical Society.)

Another way to obtain multiscale structures is mixing copolymers with different topologies. Stadler proposed to construct self-assembled periodic noncentrosymmetric lamellar (NCL) structures oriented on the micrometer scale by mixing suitably chosen ABC triblock copolymers with AC diblock copolymers [26]. Such structures were indeed obtained in mixtures of polystyrene-block-polybutadiene-block-poly(tert-butyl methacrylate) (SBT) triblock copolymers with polystyrene-block-poly(tert-butyl methacrylate) (ST) diblock copolymers and in polybutadiene-block-polystyrene-block-poly(methyl methacrylate) (BSM) triblock copolymers mixed with polybutadiene-block-poly(methyl methacrylate) (BM) diblock copolymers.[26] Subsequently, the NCL structures were obtained in a blend of two SBT triblock copolymers, which differed only in the length of their middle blocks. Archimedean tiling structures were observed in bulk morphologies of block copolymer blends of AB/CD and ABA/CD types [27, 28]. It was found that the hierarchical structural formation is related to the bridged conformation of the B block chain in an ABA triblock copolymer. The symmetric PIP-91/SH-91 = 1/1 [poly(2-vinylpyridine-*block*-isoprene-*block*-2-vinylpyridine) / poly(styrene-*block*-4-hydroxystyrene)] blend showed a cylinder-*in*-lamellar three-phase structure with a cross section corresponding to the (33.42) two-dimensional Archimedean tiling pattern, while the asymmetric PIP-91/SH-91 = 2/1 blend exhibited another peculiar cylindrical three-phase structure with the (3.4.6.4) two-dimensional symmetry.

1.2.2 Theoretical overview

Already in 1994 Matsen and Shick [29] investigated microphase separation of binary multiblock copolymer melts. They calculated the relative stability of several ordered phases for a system consisting of a binary multiblock copolymer system consisting of a sequence of identical diblock copolymers in the limit of a large number of blocks. The results were similar as those obtained for diblocks [5]. They found that, in addition to the lamellar, hexagonal, and cubic phases, the gyroid phase is also stable. It was the first observation of a gyroid phase in multiblock copolymers systems. It exists between the lamellar and hexagonal phase but does not extend all the way to the weak- segregation limit. It was shown that phases which are nearly stable between the lamellar and hexagonal ones are also of interest. They predicted that ordered, bicontinuous, double-diamond phase can be stable. At intermediate segregations, they found that two mono-continuous catenoid-lamellar phases are close to being stable. Both these phases are characterized by a triangular array of tubes which penetrate the minority lamellae and connect the majority ones. In these phases, CL_{ab} and CL_{abc}, the tubes are staggered in **abab ...** and **abcabc ...** sequences, respectively.

Multiblock copolymers while forming lamellar structures make loops and bridges inside the layers. The bridging ability of the triblock system ABA has been examined by treating the middle B layer for the lamellar case as two polymer brushes, [30, 31] by self-consistent mean-field theories, [12] with generator-matrix methods, [32] and by Monte Carlo simulations [13]. At the other end of the multiblock copolymer spectrum—many-block systems—only a single calculation of the bridging fraction exists, [33] again with the self-consistent mean-field formalism. For many-block systems this study found the bridging fraction to be close to 0.45, decreasing slightly as the segregation strength increased. It has also been established that in the extremely strongly segregated regime this dependence scales as $\sim(\chi N)^{-1/9}$ [30]. Rasmussen et al. used the self-consistent field theory technique to establish that more than 25% of the blocks consisted of bridges in the already strongly segregated lamellar morphology [34].

Several studies involved the weak segregation limit [35 - 39]. Nap et al. showed the possibility of microphase separation at two different length scales in AB block copolymers consisting of a homopolymer A block and either a linear alternating AB copolymer block $(poly(A)_m\text{-block-poly}(B\text{-alt -}A)_n)$ or an AB comb copolymer block $poly(A)_m\text{-block-poly}(A\text{-graft-}B)_n$ [35, 36]. An analysis of the structure factor revealed that in the (n,m)-parameter space three different cases can be distinguished: I) The structure factor has only one minimum corresponding to the short length scale (i.e. the characteristic length of the repeating unit of the alternating or comb block). II) The structure factor has only one minimum corresponding to the long length scale (the characteristic length of the blocks). III) Two minima are present leading to a competition between microphase separation at the short and the long length scale. Depending on the choice of n and m, one of these three possibilities will occur. Later a more detailed analysis was performed for $A_m\text{-b-}(A\text{-graft-}B)_n$ block copolymers. On increasing the length of the A end block, the system goes through a

characteristic series of structural transitions. Starting from the pure comb copolymer, the first series of structures involve a short length scale followed by structures involving a large length scale. A maximum of two critical points exists. Furthermore, in the two parameter space characterizing the comb−coil diblock copolymer molecules considered, a nontrivial bifurcation point exists beyond which the structure factor can have two maxima. Within the weak segregation approach the possibility of microphase separation at two length scales in a melt of binary multiblock copolymers with two intrinsic length scales was studied by Kuchanov and co-workers. It was found that under certain conditions a pronounced change in the mesophase period may be observed, a phenomenon that appears to be characteristic for this type of multiblock copolymers [37, 38]. The same theoretical approach was used to investigate the phase behaviour of A-*b*-(B-*alt*-A)$_m$-*b*-B block copolymers [39]. It was shown that this system has far richer phase behaviour than simple multiblock block copolymer. The stability of the different phases strongly depended on the number of diblocks in the multiblock part of the considered polymer. If $m > 2$ the double gyroid structure became stable in a certain region. For $m > 3$ regions appeared where the nonconventional cubic phases FCC, SC, or the noncentrosymmetric cubic phase BCC$_2$ (single gyroid) replaced the LAM phase as the most stable low-temperature phase. For $n > 5$ a continuous change of m results in an abrupt jump not only in the symmetry but also in the periodicity of the ordered phases (for $n = 10$ up to ten times), which is the most transparent manifestation of the two-length-scale nature of the system.

In the group of An-Chang Shi many different self-consistent field theory (SCFT) investigations were performed during the last decade. In 2001 the phase behavior of blends of ABC triblock and ac diblock copolymers were examined [40]. Several different equilibrium lamellar structures were observed, depending on the volume fraction φ_2 of the diblocks, the monomer interactions, and the degrees of polymerization of the copolymers. For segregations just above the order−disorder transition the triblocks and diblocks mix together to form centrosymmetric lamellae. As the segregation is increased, the triblocks and diblocks spatially separate either by macrophase-separating or by forming a noncentrosymmetric (NCS) phase of alternating layers of triblock and diblock (...ABCcaABCca...). The NCS phase is stable over a narrow region near $\varphi_2 = 0.4$. This region is widest near the critical point on the phase coexistence curve and narrows to terminate at a triple point at higher segregation. Above the triple point there is two-phase coexistence between almost pure triblock and diblock phases. The theoretical phase diagram is consistent with experiments. Formation of noncentrosymmetric lammelae was predicted and found experimentally by Erukhimovich, Stadler and Leibler [26].

Later in 2005 by using a two-dimensional (2D) real-space self-consistent field theory, the phase diagrams of monodisperse ABC triblock copolymers (Fig. 1.10) were presented in a three-component triangle style with the interaction energies given between the distinct blocks; this system displays richer phase behavior when compared with the corresponding diblock copolymers [41]. Polydispersity of the end blocks or the middle block in the ABC linear block copolymer chains resulted in a completely different phase diagram. The presence of a polydisperse end block may cause strong segregation to occur among the three distinct components and larger domain sizes of

the dispersed phases; a polydisperse middle block may allow a connection to form between the two phases of the two end blocks.
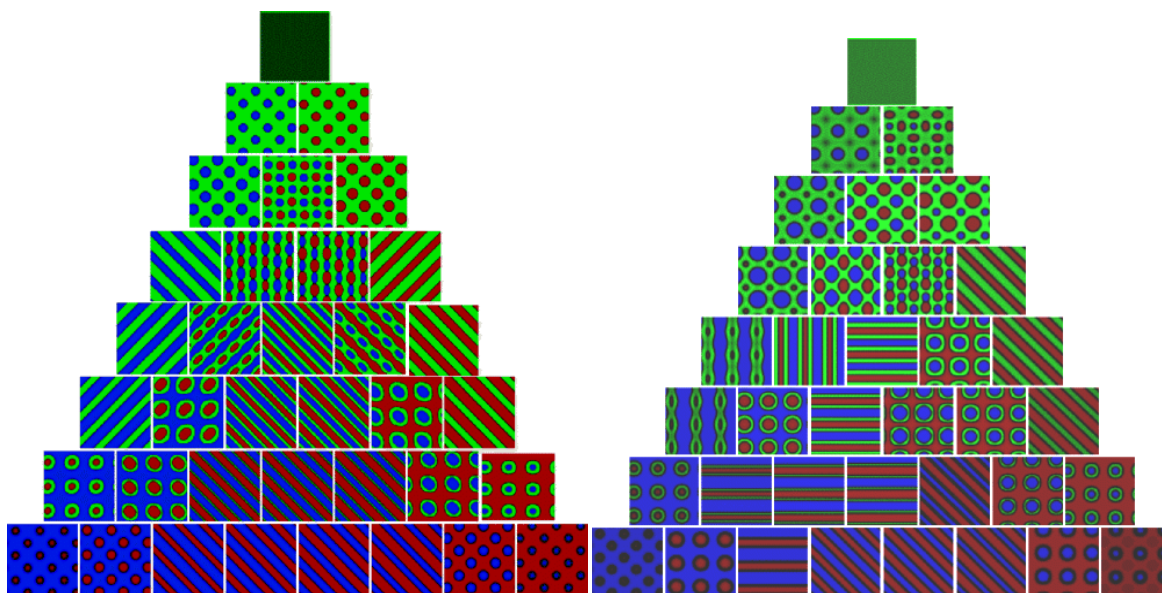
Figure 1.10. Phase diagram linear ABC triblock copolymers having binary interaction bparameters $\chi_{AB}N = \chi_{BC}N = \chi_{AC}N = 35$. The red, green, and blue regions represent the density distributions of the monomers belonging to the A, B, and C blocks, respectively a) monodisperse case b) ABC triblock copolymers exhibiting polydispersity in the C block at a polydispersity index of $I^C_{pdi} = 1.5$
(Reprinted with permission from Y. Jiang, X. Yan, H. Liang and A. Shi, *J. Phys. Chem. B*, **2005**, 109 (44), 21047. Copyright 2005 American Chemical Society.)

The phase behavior of A-*b*-(B-*b*-C)$_n$-*b*-B-*b*-A multiblock copolymer melts was also investigated using self-consistent field theory (SCFT) [42]. Solutions of the SCFT equations corresponding to hierarchical lamellar structures were obtained. The free energies of these structures were used to construct phase diagrams. It was predicted that hierarchical lamellar structures with different number of "internal" BC layers can be formed. More BC layers are preferred when the interactions between A and BC blocks are much stronger than that between B and C blocks.

In our group a strong segregation limit study was performed by Klymko. The number k of "internal" layers for the lamellar self-assembled state of a new class of multiblock copolymers A-*b*-(B-*b*-C)$_n$-*b*-B-*b*-A was determined as a function of n . Here the outer A-blocks are assumed to be considerably longer than the *m + 1* blocks of equal length of the (B-*b*-C)$_m$-*b*-B middle multiblock, and the self-assembled state is assumed to consist of k "thin" B- and C-layers sandwiched between "thick" A-layers. The predictions are in excellent agreement with the available experimental data. [43] Using the Alexander-de Gennes approximation and dissipative particle dynamics, the same results was obtained. [44]

Recently, a theoretical description of the lamellar-*in*-lamellar self-assembly of binary A-*b*-(B-*b*-A)$_m$-*b*-B-*b*-A multiblock copolymers in the strong segregation limit

was presented as well. The essential difference between this binary multiblock system and the previously considered C-*b*-(B-*b*-A)$_m$-*b*-B-*b*-C ternary multiblock copolymer system was discussed [45]. In the case of the binary system there exists a layer where the A blocks from the multiblock part penetrate into the layers of the long A tails. Because of this the stretching energy of the A tails close to junction points is strongly increased. The free energy of the lamellar-*in*-lamellar self-assembled state was analyzed as a function of the number k of "thin" internal layers for different numbers m of repeating (B-*b*-A) units and different values of the Flory-Huggins χ_{AB} interaction parameter.

In the group of An-Chang Shi the ordered phases of ABC star terpolymer melts were investigated using a generic reciprocal-space implementation of the self-consistent field theory (SCFT) of polymers [46]. It was shown that the distinct topology of ABC star terpolymers constraints the junction points on one-dimensional lines, resulting in novel microphase-separated morphologies such as tiling patterns Fig. 1.11. Two types of star triblock terpolymers, with symmetric and asymmetric interaction parameters, were studied in detail. A variety of tiling patterns in ABC star terpolymers were predicted from these SCFT calculations and characteristic phase diagrams were constructed. The phase transition sequences predicted were in qualitative agreement with experimental data and with Monte Carlo simulation results from Gemma et al. [47]

In this thesis both the strong segregation theory and SCFT calculations will be used to address the self-assembly in several two-length-scale copolymer systems. Furthermore, dissipative particle dynamics (DPD) simulations will be used to illustrate some of the hierarchical structure features predicted theoretically.
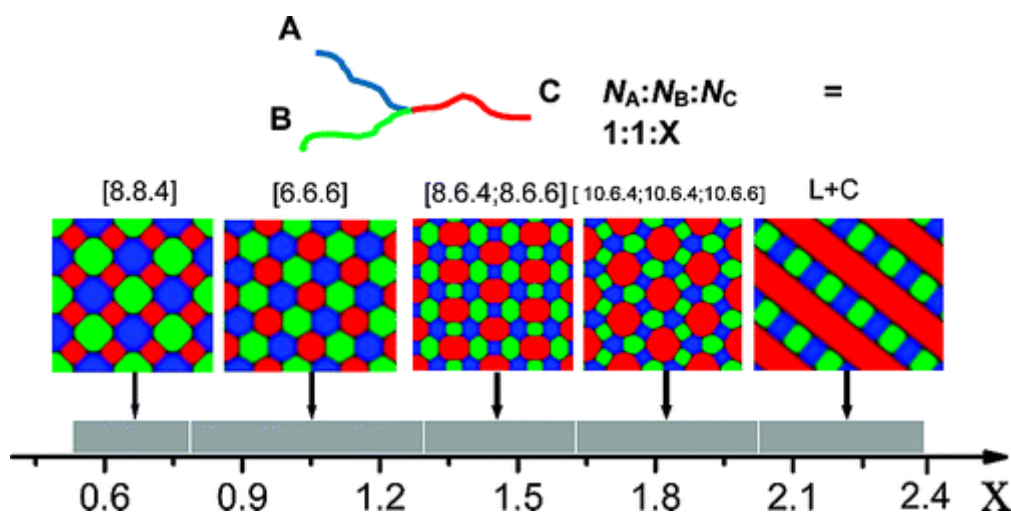
Figure 1.11. Phase behavior of an idealized $A_{1.0}B_{1.0}C_x$ star triblock terpolymer with symmetric interactions, $\chi_{AB}N = \chi_{BC}N = \chi_{AC}N = 30.0$, and with equal statistical segment lengths for each block. The structures shown are schematics that have been reconstructed from the nonzero Fourier weights of the density distribution functions of monomers A, B, and C, denoted by blue, green, and red colors.
(Reprinted with permission from G. Zhang, F. Qiu, H. Zhang, Y. Yang, A. Shi, *Macromolecules*, **2010**, 43 (6), 2981. Copyright 2010 American Chemical Society.)

In the literature it has been shown already that the DPD technique also can predict microphase separation with more than one characteristic length scale. A_2-*star*-(B-*alt*-C)$_n$ molecules were investigated by Huang and co-workers [48] using this technique. They observed various types of hierarchical structure-*in*-structures, such as A-spheres in a matrix formed by B and C alternating layers, hexagonally packed A-cylinders in the matrix of B and C segregated layers, B and C alternating layers-in-lamellae, coaxial B and C alternating domains within hexagonally packed BC-formed cylinders in the A-matrix, and co-centric BC-alternating domains within BC-spheres in the A-matrix, by increasing the A composition. The authors also investigated A-*block*-(B-*graft*-C) copolymers using the same simulation technique.

1.3 References

1. A.Y. Grosberg and A.R. Khokhlov. *Statistical Physics of Macromolecules*. American Institute of Physics, New York, **1994**.
2. M. Doi. *Introduction to polymer physics*. Clarendon Press, Oxford, **1996**.
3. G.R. Strobl. *The physics of polymers: concepts for understanding their structures and behavior*. Springer, Berlin, **1996**.
4. P.G. de Gennes. *Scaling concepts in polymer physics*. Cornell University Press, Ithaca, New York, **1979**.
5. M.W. Matsen, *J. Phys., Condens. Matter,* **2002**, *14*, 21.
6. C. Tyler, D.C. Morse, *Phys. Rev. Lett.,* **2005**, *94*, 208302.
7. F.S. Bates and G.H. Fredrickson, *Annu. Rev. Phys. Chem*., **1990,** *41*, 525.
8. F.S. Bates and G.H. Fredrickson*, Phys. Today,* **1999**, *52* (2), 32.
9. M.W. Matsen*, J. Phys.: Condens. Matter,* **2002,** *14* (2), 21.
10. M. Lodge, *Macromol. Chem. Phys*., **2003,** *204*, 265.
11. C. Park, J. Yoon, and E.L. Thomas, *Polymer* **2003,** *22*, 6725.
12. M.W. Matsen and M. Schick, *Phys. Rev. Lett*., **1994,** *72*, 2660.
13. J. Ruokolainen, R. Mäkinen, M. Torkkeli, T. Mäkelä, R. Serimaa, G. ten Brinke, O. Ikkala, *Science,* **1998**, *280*, 557.
14. J. Ruokolainen, G. ten Brinke, O. Ikkala, *Adv. Mater*., **1999**, *11*, 777.
15. O. Ikkala, G. ten Brinke, *Science,* **2002**, *295*, 2407.
16. J. Masuda, A. Takano, Y. Nagata, A. Noro, Y. Matsushita, *Phys. Rev. Lett.,* **2006***, 97*, 098301.
17. Y. Nagata, J. Masuda, A. Noro, D. Cho, A. Takano, Y. Matsushita, *Macromolecules,* **2005**, *38*, 10220.
18. J. Masuda, A. Takano, J. Suzuki, Y. Nagata, A. Noro, K. Hayashida and Y. Matsushita, *Macromolecules*, **2007**, *40* (11), 4023.
19. G. Fleury and F.S. Bates, *Macromolecules*, **2009**, *42*, 3598.
20. G. Fleury and F.S. Bates, *Macromolecules*, **2009**, *42*, 1691.
21. M.W. Matsen, M. Schick, *Macromolecules,* **1994**, *27*, 187.
22. K. Karatasos, S.H. Anastasiadis, T. Pakula, H. Watanabe, *Macromolecules,* **2000**, *33*, 523.
23. H. Watanabe, *Macromolecules,* **1995**, *28*, 5006.
24. K. Hayashida, N. Saito, S. Arai, A. Takano, N. Tanaka, and Y. Matsushita, *Macromolecules*, **2007**, *40*, 3695.

25.   K. Hayashida, A. Takano, S. Arai, Y. Shinohara, Y. Amemiya, and Y. Matsushita, *Macromolecules*, **2006**, *39*, 9402.

26.   T. Goldacker, V. Abetz, R. Stadler, I. Erukhimovich, L. Leibler, *Nature*, **1999**, *398*, 137.

27.   T. Asari, S. Matsuo, A. Takano, Y. Matsushita, *Macromolecules,* **2005,** *38,* 8811.

28.   T. Asari, S. Arai, A.Takano, Y. Matsushita, *Macromolecules,* **2006,** *29,* 2232.

29.   M.W. Matsen and M. Schick, *Macromolecules*, **1994**, *27*, 7157.

30.   E.B. Zhulina, A. Halperin, *Macromolecules,* **1992**, *25*, 5730.

31.   R.L. Jones, L. Kane, R.J. Spontak, *Chem. Eng. Sci.,* **1996**, *51*, 1365.

32.   L. Buqiang, E. Ruckenstein, *Macromol. Theory Simul.,* **1998**, *7*, 333.

33.   M.W. Matsen, *J. Chem. Phys.,* **1995**, *102*, 3884.

34.   K.O. Rasmussen, E.M. Kober, T. Lookman, A. Saxena, *J.Polym.Sci. Part B: Poly.Phys.,* **2003**, *41*, 101.

35.   R. Nap, C. Kok, G. Ten Brinke, and S. Kuchanov*, Eur. Phys. J., E*, **2001,** *4*, 515.

36.   R. Nap, N. Sushko, I.Ya. Erukhimovich, G. ten Brinke, *Macromolecules,* **2006**, *39*, 6765.

37.   S.I. Kuchanov, V.E. Pichugin, G. ten Brinke, *E-Polymers,* **2006**, 012.

38.   S.I. Kuchanov, V.E. Pichugin, G. ten Brinke, *Europhys. Lett.,* **2006**, *76*, 959.

39.   Y. Smirnova, G. ten Brinke, I.Ya. Erukhimovich, *J. Chem. Phys.,* **2006**, *124*, 054907.

40.   R.A. Wickham and A. Shi, *Macromolecules*, **2001**, *34* (18), 6487.

41.   Y. Jiang, X. Yan, H. Liang and A. Shi**,** *J. Phys. Chem. B*, **2005**, *109* (44), 21047.

42.   W. Li, A. Shi *Macromolecules*, **2009**, *42* (3), 811.

43.   A. Subbotin, T. Klymko, G. ten Brinke, *Macromolecules,* **2007**, *40*, 2915.

44.   T. Klymko, V. Markov, A. Subbotin, G. ten Brinke *Soft Matter,* **2009**, *5* (1) 98.

45.   T. Klymko, A. Subbotin, G. ten Brinke, *J. Chem. Phys*, **2009**, *129* (11) , 114902.

46.   G. Zhang, F. Qiu, H. Zhang, Y. Yang, A. Shi, *Macromolecules*, **2010**, *43* (6), 2981.

47.   T. Gemma, A. Hatano, T. Dotera, *Macromolecules*, **2002**, *35*,3225.

48.   C.I. Huang, C.-M.Chen, *Chem. Phys. Chem.*, **2007,** *8*, 2588.

Chapter 2

Lamellar-in-Lamellar Self-Assembly in Linear Ternary Multiblock Copolymers: Alexander-de Gennes Approach and Dissipative Particle Dynamics Simulations

2.1 Introduction

Hierarchically ordered block copolymer-based systems have become an active area of research recently [1-26]. In many cases diblock copolymers are involved where one of the blocks contains side chains that are either fully flexible or contain mesogenic units. Furthermore, the side chains can be covalently linked or attached via physical interactions such as, e.g., hydrogen bonding. Here the diblock copolymer introduces one of the length scales while a second one is associated with the side chains and thus with the graft-like nature of one of the blocks. Self-assembly in such systems with hierarchical structure formation was observed by ten Brinke and co-workes and is reported in Ref.[1,2].

Ternary P2VP-*b*-(PI-*b*-PS)$_4$-*b*-PI-*b*-P2VP linear undecablock copolymers, introduced and studied by Matsushita and co-workers [20], is an example of block copolymers with a linear architecture where double periodic behavior has been also observed experimentally. Here P2VP denotes poly-2-vinylpyridine end blocks, PI denotes polyisoprene and PS denotes polystyrene. In the multiblock copolymers used all chemically different species are mutually incompatible. It was observed that this undecablock copolymer self-assembled in a 5-layered lamellar-*in*-lamellar structure. The thick layers consist of the relatively long P2VP end blocks, and the thin layers are due to the PI-PS separation within the internal (PI-*b*-PS)$_4$-*b*-PI part of the multiblock.

In this Chapter we consider the simplest representative of this class of systems consisting of a C-*b*-(B-*b*-A)$_m$-*b*-B-*b*-C multiblock copolymers. We consider the situation when all three Flory-Huggins parameters χ_{AB}, χ_{AC}, χ_{BC} are relatively large and A- and B-layers are formed in between C-layers. Furthermore, strong segregation with respect to all chemically different species involved will be assumed. This situation corresponds to the experimental multiblock copolymer system investigated by Matsushita and co-workers [20].

The central problem addressed in this Chapter concerns the number *k* of internal A- and B-layers for lamellar-*in*-lamellar self-assembled C-*b*-(B-*b*-A)$_m$-*b*-B-*b*-C multiblock copolymers as a function of the pertinent parameters, notably *m*.

2.1   Theoretical investigation

A theoretical analysis of the lamellar-*in*-lamellar self-assembled state of ternary C-*b*-(B-*b*-A)$_m$-*b*-B-*b*-C multiblock copolymer melts in the strong segregation limit is presented using the Alexander-de Gennes approximation.

2.1.1 Model

Considering the ternary C-*b*-(B-*b*-A)$_m$-*b*-B-*b*-C multiblock copolymer melt in the Alexander-de Gennes approximation implies that we assume all $2m+1$ middle A- and B-blocks as well as the outer C-blocks to be stretched uniformly inside their respective layers. We assume that the $2m+1$ short middle blocks self-assemble into *k* internal layers confined between relatively "thick" C outer layers.

In general, a global multiblock conformation can be either a bridge or a loop as illustrated in Figure 2.1. Both global bridges and global loops consist in turn of local loops and bridges. Due to assumed strong incompatibility between the three chemically different species, the first and the last B-block of the middle multiblock will be present in the form of a local bridge conformation in the first and the last boundary B-layers (Figure 2.1).

Let x be the fraction of global bridges and *1-x* the fraction of global loops. The average free energy per multiblock copolymer chain is then given by

$$F = xF_{bridge} + (1-x)F_{loop} + x \ln x + (1-x)\ln(1-x) \tag{2.1}$$

where F_{bridge} and F_{loop} are the free energies of a global bridge and a global loop conformation. The last two terms in (2.1) represent the entropy of mixing between global loops and bridges. We will simply assume as a first approximation that $x \cong 1/2$, $F_{bridge} \cong F_{loop}$ and thus $F \cong F_{bridge} - \ln 2$. Hence, from now on we will restrict ourselves to a global bridge conformation and discuss its free energy in the Alexander-de Gennes approximation.
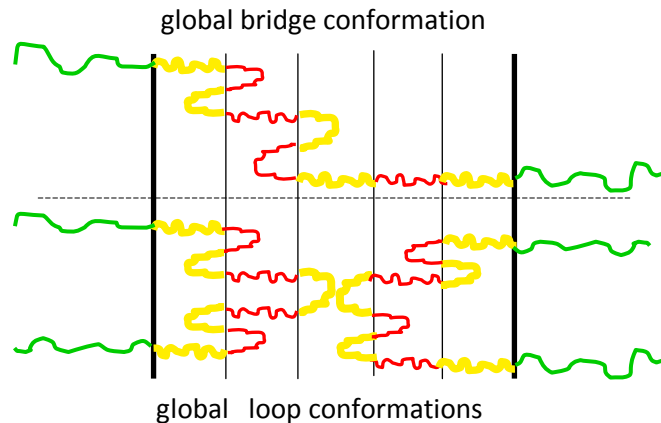
Figure 2.1. Schematic representation of a global bridge (top) and a global loop (bottom) conformation for a C-*b*-(B-*b*-A)₄-*b*-B-*b*-C multiblock copolymer. A, B and C blocks are denoted by red, yellow and green colors, respectively.

2.2.2 Theoretical analysis

Let n denote the degree of polymerization of the internal A- and B-blocks alike and N denote the degree of polymerization of the outer C-blocks, with $N \gg n$. The statistical segment length and monomer volume are denoted as a and υ, respectively, and are assumed to be equal for all chemically different components. The thickness of the internal layers and the outer layer are denoted as h and H (Figure 2.2). Furthermore Σ is used to denote the interfacial area per multiblock copolymer chain. The Flory-Huggins interaction parameters χ_{AB}, χ_{BC} and χ_{AC} are taken positive implying unfavourable interactions between all the chemically different species.
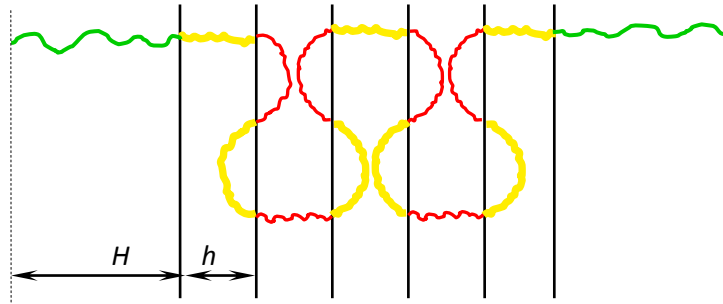
Figure 2.2. Schematic representation of a global bridge conformation of a C-*b*-(B-*b*-A)$_m$-*b*-B-*b*-C copolymer for $m = 2$. h and H denote the thickness of the internal layers and half of the outer layers, respectively.

Incompressibility implies

$$N\upsilon = H\Sigma \tag{2.2}$$

$$(2m+1)n\upsilon = kh\Sigma \tag{2.3}$$

The total free energy per multiblock copolymer bridge can be written as

$$F_{bridge} = 2F_{BC} + (k-1)F_{AB} + mF_{0A} + (m+1)F_{0B} + 2F_C + F_{conf} \tag{2.4}$$

Here F_{AB} and F_{BC} are the interfacial free energies related to the interfacial tensions and the average interfacial area Σ per multiblock copolymer by

$$F_{AB} = \gamma_{AB}\,\Sigma \qquad F_{BC} = \gamma_{BC}\,\Sigma \tag{2.5}$$

with interfacial tensions given by $\gamma_{AB} = \dfrac{a}{\upsilon}\sqrt{\dfrac{\chi_{AB}}{6}}$ and $\gamma_{BC} = \dfrac{a}{\upsilon}\sqrt{\dfrac{\chi_{BC}}{6}}$.

The elastic free energies of uniformly stretched short A- and B-blocks F_{0A} and F_{0B} are the same and are given by

$$F_0 = F_{0A} = F_{0B} = \frac{3h^2}{2na^2} \tag{2.6}$$

Likewise, the elastic free energy F_{0C} for the outer C-blocks is given by

$$F_C = \frac{3H^2}{2Na^2} \tag{2.7}$$

The conformational contribution F_{conf} takes into account the number of different possibilities to create multiblock conformations and, as in our previous work [21], will be considered in a simplified way by representing the middle multiblock by a chain of $k-2$ blobs propagating in one direction. The corresponding probability is $\left(\dfrac{1}{2}\right)^{k-2}$ resulting in an increase in free energy (in $k_B T$ energetic units) given by

$$F_{conf} = (k-2)\ln 2 \tag{2.8}$$

Taking into account Eqs. (2.2), (2.3) and Eqs. (2.5)-(2.8), the free energy expression (2.1) transforms into

$$F = \gamma^* \Sigma + \frac{Q}{\Sigma^2} + (k-3)\ln 2, \tag{2.9}$$

with $\gamma^* = 2\gamma_{BC} + (k-1)\gamma_{AB}$ and $Q = \dfrac{3(2m+1)^3 n\upsilon^2}{2k^2 a^2} + \dfrac{3N\upsilon^2}{a^2}$.

Minimization of the free energy (2.9) with respect to Σ yields the equilibrium interface area

$$\Sigma_0 = \left(\frac{2Q}{\gamma^*}\right)^{1/3} \tag{2.10}$$

which results in the final expression for the total free energy:

$$F = \frac{3}{2}\left(\gamma^*\right)^{2/3}(2Q)^{1/3} + (k-3)\ln 2 \tag{2.11}$$

2.2.3 Results and discussions

We consider first the only system investigated experimentally so far, i.e., P2VP-*b*-(PI-*b*-PS)$_4$-*b*-PI-*b*-P2VP. It corresponds to $\chi_{BC} = 0.4$, $\chi_{AB} = 0.1$, $\chi_{BC}N = 340$, $\chi_{AB}n = 17$, $m = 4$ and $n/N = 0.2$. The free energy (eq. 2.11) as a function of the number of internal layers k is presented in Figure 2.3a. The minimum occurs for $k = 5$, precisely as found experimentally [4]. Results for different values $m = 3$, 5 and 6 are presented in Figure 2.3b, c and d. The values of k found are 5, 5 and 7. Note, that for $m = 5$ the free energies for $k = 5$ and $k = 7$ are very close. These results are in good agreement with the ones obtained from a much more elaborated mean-field calculation using the same set of parameters, where the minima for $m = 3$, 4, 5 and 6 occurred for $k = 5$, 5, 7 and 7 [21].

a

b

c   d
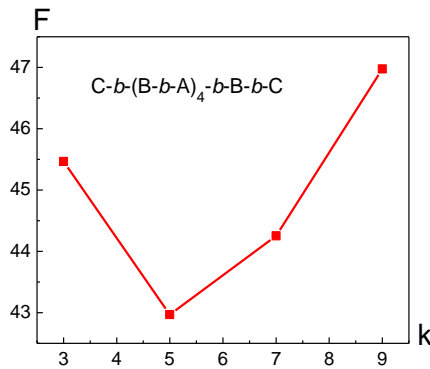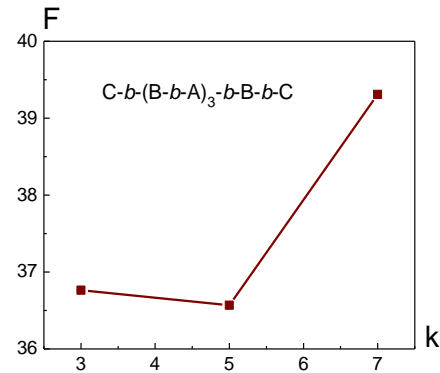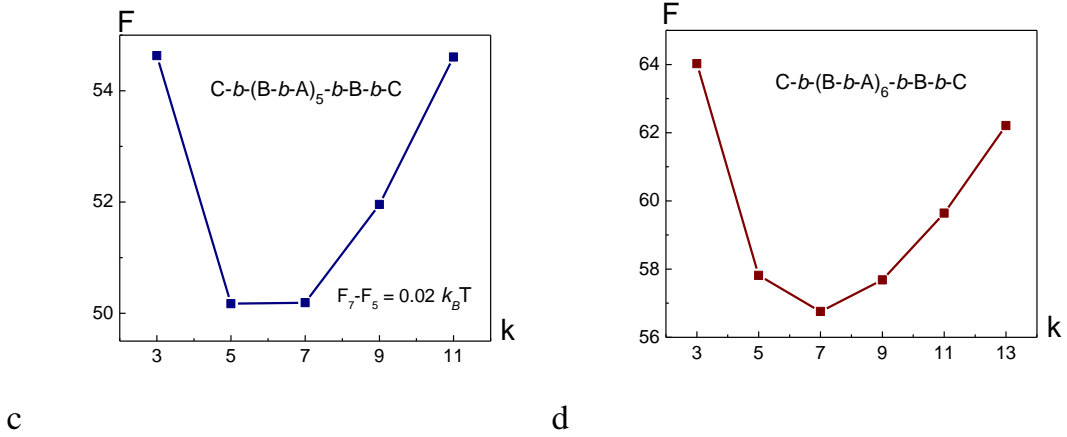
Figure 2.3. Free energy F of lamellar-*in*-lamellar self-assembled C-*b*-(B-*b*-A)$_m$-*b*-B-*b*-C multiblock copolymer melt as a function of the number k of internal layers for $\chi_{BC}N = 340$, $\chi_{AB}n = 17$, $n/N = 0.2$. (a) $m = 4$, (b) $m = 3$, (c) $m = 5$, (d) $m = 2$.

2.2.3.1 Influence of interaction strength

In order to investigate the effect of interfacial tension, numerical calculations were performed for different values of the Flory-Huggins χ_{BC}-parameter for $m = 3, 4, 5$ and 6, $\chi_{AB} = 0.1$ and fixed length of the internal blocks $n = 200$. Throughout the rest of this section the length N of the outer blocks is assumed to satisfy $(2m+1)n = 2N$, thus assuring an equilibrium lamellar structure. The results are summarized in Table 2.1. Figure 2.4a-d shows the free energy as function of k for $m = 4$ and Flory-Huggins parameter values $\chi_{BC} = 0.1, 0.4, 1.5$ and 5, where the minima are found at $k = 3, 5, 7$ and 9, respectively.

k_{opt}	χ_{BC}				
	$m = 3$ $N = 700$	$m = 4$ $N = 900$	$m = 5$ $N = 1100$	$m = 6$ $N = 1300$	$m = 7$ $N = 1500$
3	$0.1 - 0.25$	0.1	0.1	< 0.1	
5	$0.3 - 1.7$	$0.15 - 0.75$	$0.15 - 0.4$	$0.1 - 0.25$	$0.1 - 0.2$
7	≥ 1.75	$0.8 - 3.3$	$0.45 - 1.65$	$0.3 - 0.95$	$0.25 - 0.6$
9		≥ 3.35	$1.7 - 5.55$	$1.0 - 3.04$	$0.65 - 1.85$
11			≥ 5.6	$3.06 - 8.3$	$1.9 - 4.9$
13				> 8.35	$4.95 - 11.75$
15					≥ 11.8

Table 2.1. Equilibrium number of internal domains k_{opt} as a function of χ_{BC} for $\chi_{AB} = 0.1$ and $n = 200$.

Larger χ_{BC} values force a reduction in the BC interfacial area which in turn forces the internal short blocks to become more stretched. To relieve this stretching the system starts to create more AB interfaces, i.e. larger values of *k*. Of course, in reality the values of the Flory-Huggins interaction parameters hardly ever exceed unity. The calculations for larger values are nevertheless useful to track and understand the tendencies in the layer formation in ternary C-*b*-(B-*b*-A)$_m$-*b*-B-*b*-C multiblock copolymers.

a

b

c

d

Figure 2.4. Free energy *F* of lamellar-*in*-lamellar self-assembled C-*b*-(B-*b*-A)$_4$-*b*-B-*b*-C multiblock copolymer melt as a function of the number *k* of internal layers for $n = 200$, $N = 900$, $\chi_{AB} = 0.1$ and (a) $\chi_{BC} = 0.1$, (b) $\chi_{BC} = 0.4$, (c) $\chi_{BC} = 1.5$, (d) $\chi_{BC} = 5$.

2.2.3.2 Influence of chain length

To see how these results depend on the elastic stretching of the blocks, the length of the internal blocks was decreased to $n = 100$ with the outer block length N still satisfying $(2m+1)n = 2N$. We first consider fixed $\chi_{AB} = 0.1$. The equilibrium number of internal domains k_{opt} as a function of m and χ_{BC} are given in Table 2.2. A comparison with Table 2.1 shows that the decreased length of the blocks, implying "stiffer" springs, indeed requires larger values of χ_{BC} to obtain the same number of internal layers.

k_{opt}	χ_{BC}				
	$m = 3$ $N = 350$	$m = 4$ $N = 450$	$m = 5$ $N = 550$	$m = 6$ $N = 650$	$m = 7$ $N = 750$
3	$0.05 - 0.25$	$0.05 - 0.15$	$0.05 - 0.1$	$0.05 - 0.08$	$0.05 - 0.07$
5	$0.3 - 2.05$	$0.2 - 0.9$	$0.15 - 0.5$	$0.09 - 0.3$	$0.08 - 0.2$
7	≥ 2.1	$0.95 - 4.1$	$0.55 - 2.0$	$0.35 - 1.15$	$0.25 - 0.75$
9		≥ 4.15	$2.05 - 2.85$	$1.2 - 3.7$	$0.8 - 2.25$
11			≥ 2.9	$3.75 - 10.35$	$2.3 - 2.05$
13				≥ 10.4	$2.1 - 14.6$
15					≥ 14.65

Table 2.2. Equilibrium number of domains k_{opt} as a function of χ_{BC} for $n = 100$ and $\chi_{AB} = 0.1$.

Numerical calculations were also performed for a constant $\chi_{BC} = 0.1$ as a function of χ_{AB} with internal block lengths of $n = 200$ and $n = 100$. The results are collected in Table 2.3 and 2.4. Figure 2.5 presents free energy graphs as a function of k for $m = 4$, $n = 200$, $N = 900$, $\chi_{BC} = 0.1$ and $\chi_{AB} = 0.05$ (a), $\chi_{AB} = 0.15$ (b).

χ_{AB}	$2n \cdot \chi_{AB}$	k_{opt}				
		$m = 3$ $N = 700$	$m = 4$ $N = 900$	$m = 5$ $N = 1100$	$m = 6$ $N = 1300$	$m = 7$ $N = 1500$
0.05	20	3	5	5	5	5
0.1	40	3	3	3	5	5
0.15	60	3	3	3	3	5
0.2	80	3	3	3	3	3
0.25	100	3	3	3	3	3

Table 2.3. Equilibrium number of domains k_{opt} as a function of χ_{AB} for $n = 200$ and $\chi_{BC} = 0.1$.

χ_{AB}	$2n \cdot \chi_{AB}$	k_{opt}				
		$m = 3$ $N = 350$	$m = 4$ $N = 450$	$m = 5$ $N = 550$	$m = 6$ $N = 650$	$m = 7$ $N = 750$
0.1	20	3	3	3	5	5
0.15	30	3	3	3	3	3
0.2	40	3	3	3	3	3
0.25	50	3	3	3	3	3

Table 2.4. Equilibrium number of domains k_{opt} as a function of χ_{AB} for $n = 100$ and $\chi_{BC} = 0.1$.
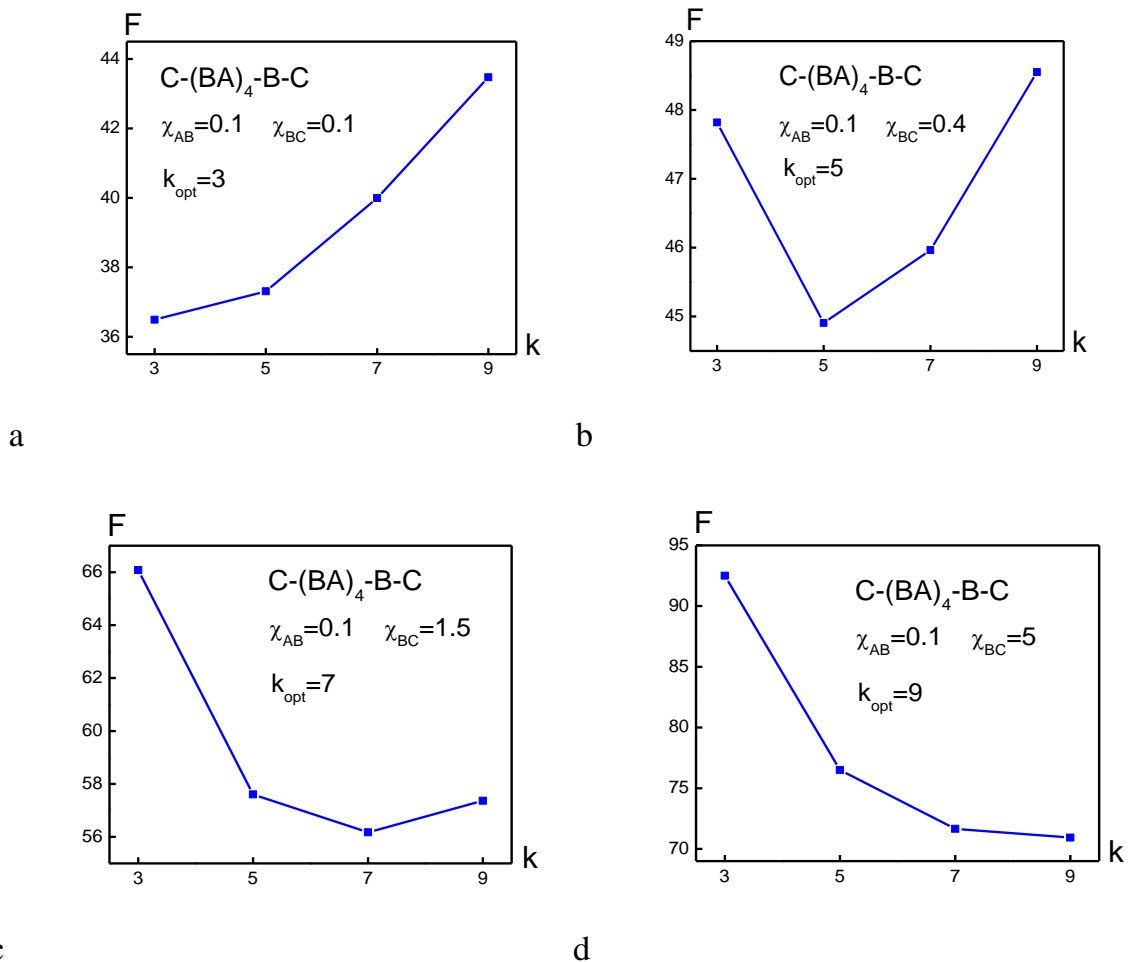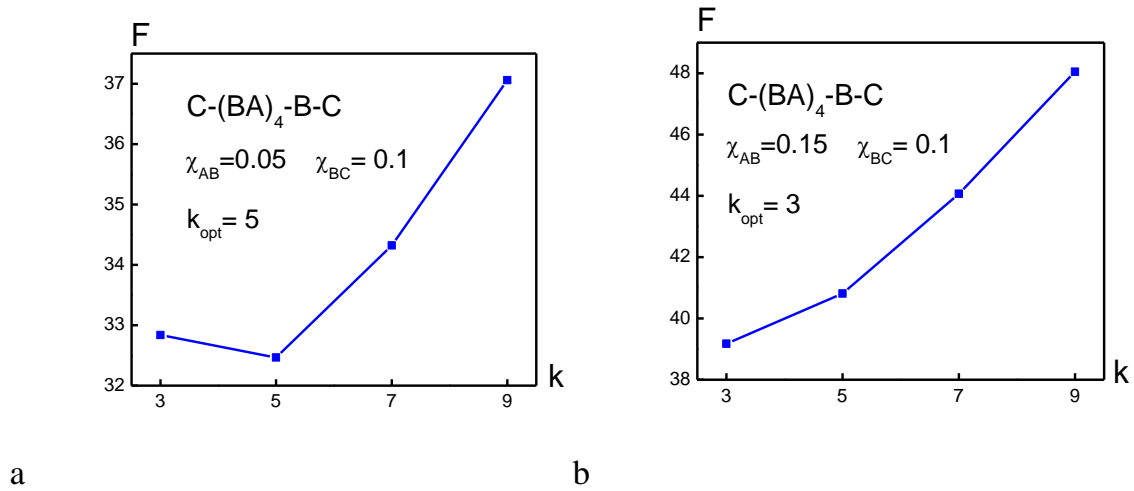

Figure 2.5. Free energy F of lamellar-*in*-lamellar self-assembled C-*b*-(B-*b*-A)$_4$-*b*-B-*b*-C multiblock copolymer melt as a function of the number k of internal layers for $n = 200$, $N = 900$, $\chi_{BC} = 0.1$ at (a) $\chi_{AB} = 0.05$, (b) $\chi_{AB} = 0.15$.

For the given value of $\chi_{BC} = 0.1$, nearly always the minimal number of $k = 3$ internal layers are found. Only when χ_{AB} is sufficiently small a transition to a 5-layered structure (more A/B interface) is observed. Of course, $2n\chi_{AB}$ has to be considerably larger than 10 to really have a strongly segregated lamellar-*in*-lamellar self-assembled state. The interfacial contribution to the free energy is given by $F_{interface} = 2F_{BC} + (k-1)F_{AB}$, which can be simply rewritten as $F_{interface} = \dfrac{(2m+1)n\upsilon}{h}\left[\gamma_{AB} + \dfrac{2\gamma_{BC} - \gamma_{AB}}{k}\right]$ where Eqs.2.3 and 2.5 have been used. From this expression it follows straightforward that when $\chi_{AB} > 4\chi_{BC}$ ($\gamma_{AB} > 2\gamma_{BC}$) a 3-layered has a lower interfacial free energy than a 5-layered one. The results presented in the various tables, however, show that in reality a 3-layered structure is already formed at considerably smaller values of χ_{AB}, thus demonstrating in particular the importance of the conformational $(k-3)\ln 2$ contribution (see eq. 2.9) favoring small values of k. The tendencies observed are corroborated by the results of computer simulations obtained by using dissipative particle dynamics simulation technique. The

results are described in the next section, whereas the computational details are presented in the Appendix.

2.3 Dissipative particle dynamic simulations of C-*b*-(B-*b*-A)$_m$-*b*-B-*b*-C multiblock copolymers

In the dissipative particle dynamics simulation technique, described in more detail in Ch. 7 Appendix, a large series of monomers are collected into a few bead-and-spring particles which interact with each other by soft sphere like potential. Only repulsive interactions are possible. This technique allows the simulation of the molecular behavior on a longer time- and length-scale [23-31].

2.3.1 Model

In our study one block from the multiblock part of the terpolymer was represented by one or two DPD beads. In Fig. 2.6. the DPD model C$_4$-(B$_1$A$_1$)$_4$B$_1$-C$_4$, where one bead is used to describe the small blocks, is shown. Due to spring type bonds one bead is enough to simulate bridge and loop formation.
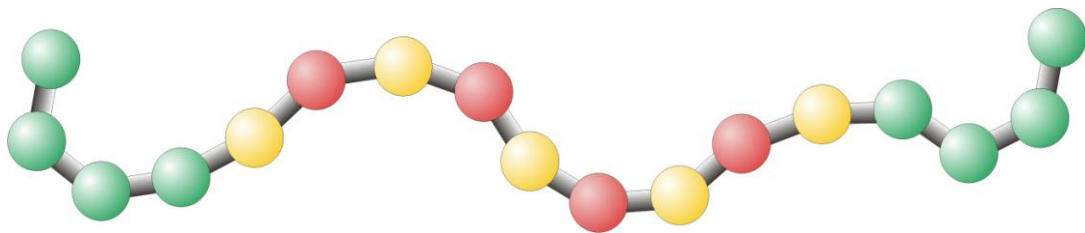
Figure 2.6. DPD model of C-*b*-(B-*b*-A)$_4$-*b*-B-*b*-C terpolymer. Green beads represent C blocks, yellow – B blocks and red – A blocks.

2.3.2 Computational details

The following values of the constants were used: $\lambda = 0.65$, $\Delta t = 0.06$, $\rho = 3$ and $\sigma = 3$. The DPD simulations are performed in a cubic box of L^3 grids with periodic boundary conditions. Since the particle density ρ is set equal to 3, the total number of simulated DPD beads equal $3L^3$. As reported in Refs. 28-30, the morphology obtained by DPD simulations may depend on the finite size of the simulation box. In our simulations we have periodic structures with large periods and to exclude finite size effects we have to take the simulation box sufficiently large. The number of DPD beads per chain is in the range 9-17. The size of the simulation box volume used was taken in the range $V = 10^3$ - 30^3, in such a way that for each case considered L exceeded the length of the chains. All simulations were started from random positions.

Following the work of Groot and Warren [25], the repulsive parameters between the same types of particles is taken as $a_{ii} = 25$. For different types of particles a_{ij} can be

chosen from the relation between the energy parameter a_{ij} and the Flory–Huggins interaction parameter χ_{ij}

$$a_{ij} = a_{ii} + 3.497 \, \chi_{ij} \qquad (2.12)$$

2.2.3 Results

In the dissipative particle dynamics simulation technique a large series of monomers are collected into a few bead-and-spring particles in order to simulate the molecular behavior on a longer time- and length-scale [23-31]. The first situation simulated resembled the experimentally studied ternary P2VP-*b*-(PI-*b*-PS)$_4$-*b*-PI-*b*-P2VP linear undecablock copolymer system, i.e. *m* = 4 [5]. Figure 2.6 shows the corresponding self-assembled state observed for C$_4$-(B$_1$A$_1$)$_4$B$_1$-C$_4$ with the energy parameters representing the soft repulsion (see eq. A2) equal to a_{BA} = 85, a_{BC} = 320. Using equation 2.12 for the relation between these energy parameters and the familiar Flory-Huggins parameters this corresponds to $N\chi_{BC} \cong 338$ and $n\chi_{AB} \cong 17.2$. Figure 2.7 demonstrates that a self-assembled lamellar state is formed with 5 "thin" internal layers as observed experimentally [4] and calculated theoretically (Figure 2.3a and ref. 21). The same result is obtained for internal blocks that are twice as long C$_4$-(B$_2$A$_2$)$_4$ B$_2$-C$_4$ (the subscripts of A, B and C denote the number of beads taken for the calculations).

Subsequently, we address the issue of the dependence of the number of internal layers on the interfacial tension. Tables 2.1-2.3 suggest that for this purpose it may be best to take *m* = 5 because then reasonable variations in the values of the Flory-Huggins parameters are theoretically predicted to induce transitions between different number of internal layers. That this is also the case in the simulations is shown in Figure 2.8, where 3 snapshots of the same system C$_4$-(B$_1$A$_1$)$_5$ B$_1$-C$_4$ are presented for different energy parameters a_{AB}, a_{BC}.

Figure 2.7 demonstrates that when the A-B interaction becomes less unavorable and the B-C interaction becomes more unfavorable, indeed transitions are observed from 3 to 5 to 7 internal layers. There is the obvious tendency to decrease the BC interface with a corresponding increase in the AB interface. For the system with *m* = 4, C$_4$-(B$_1$A$_1$)$_4$ B$_1$-C$_4$, 3 and 5 internal layers were observed varying the energy parameters.

To illustrate the dependence of the number of internal layers on the length of the internal blocks two systems C$_3$-(B$_1$A$_1$)$_3$ B$_1$-C$_3$ and C$_3$-(B$_2$A$_2$)$_3$ B$_2$-C$_3$ were simulated using the same energy parameter values. Figure 2.9 shows that in the former case 3 internal layers are formed and 5 in the latter.

Similar simulations have been performed for *m* equal to 4, 5 and 6 for the same a_{AB} = 75, a_{BC} = 120 taking *n* =1 and *n* =2. The number of internal layers found were 5, 5 and 7 for *m* = 4, 5 and 6, respectively, independently of *n*.
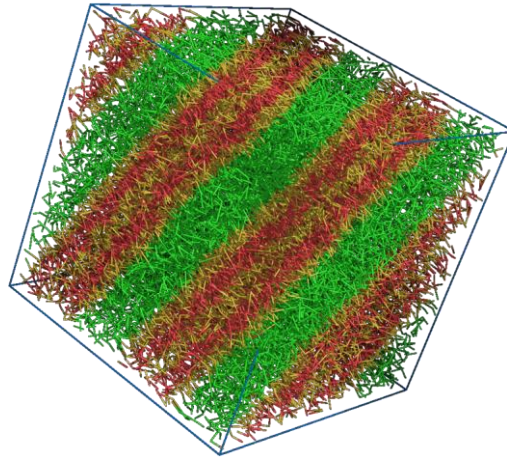
Figure 2.7. Snapshot of C_4-$(B_1A_1)_4B_1$-C_4 for $a_{BA} = 85$, $a_{BC} = 320$.

a. **b.** **c.**
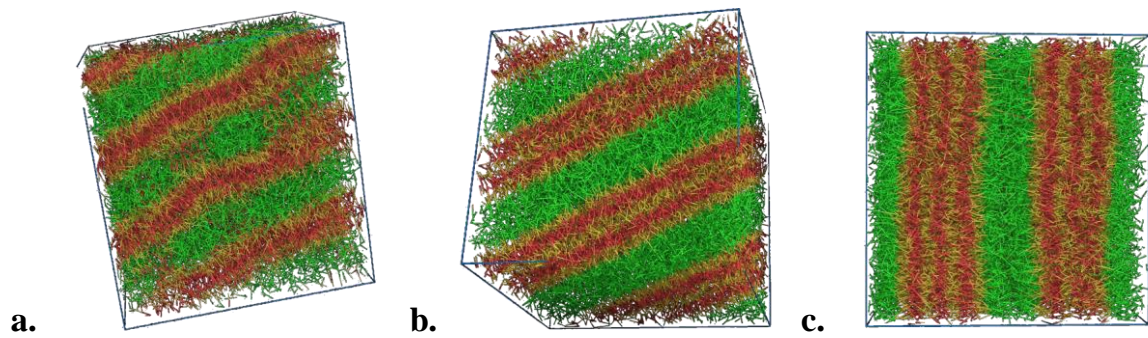
Figure 2.8. Snapshots of self-assembled C_4-$(B_1A_1)_5$ B_1-C_4 multiblock copolymer melt for: (a) $a_{AB} = 250$, $a_{BC} = 50$; (b) $a_{AB} = 75$, $a_{BC} = 120$; (c) $a_{AB} = 65$, $a_{BC} = 300$

a. **b.**
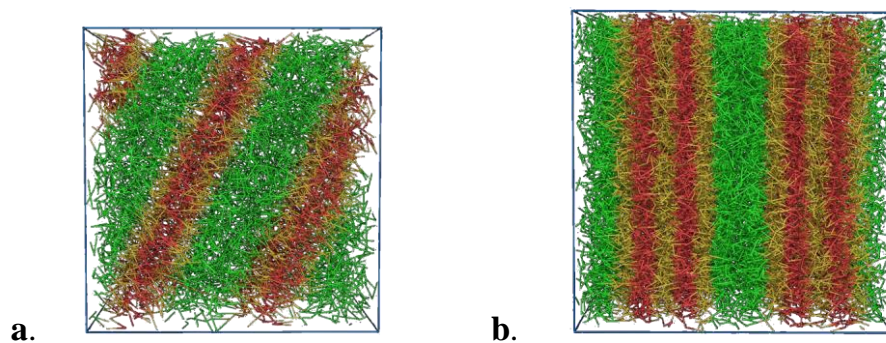
Figure 2.9. Snapshots of (a) C_3-$(B_1A_1)_3$ B_1-C_3 and (b) C_3-$(B_2A_2)_3$ B_2-C_3 for $a_{AB} = 75$ and $a_{BC} = 120$.

2.4 Concluding remarks

In this Chapter, we presented a simple theoretical analysis of the strongly segregated lamellar-*in*-lamellar self-assembled state of ternary C-*b*-(B-*b*-A)$_m$-*b*-B-*b*-C multiblock copolymers using the Alexander-de Gennes approach. This simplified description allowed us to discuss in detail the influence of the pertinent parameters on the number of internal layers k formed. The main observation concerns the sensitivity of k on the interfacial tension between the outer C-layers and the adjacent internal B-layers. The theoretically observed general tendencies were corroborated by the results of computer modeling using dissipative particle dynamics technique.

2.5 References

1. J. Ruokolainen, R. Mäkinen, M. Torkkeli, T. Mäkelä, R. Serimaa, G. ten Brinke, O. Ikkala, *Science,* **1998**, *280*, 557.
2. O. Ikkala, G. ten Brinke, *Science,* **2002,** *295*, 2407.
3. J. Ruokolainen, G. ten Brinke, O. Ikkala, *Adv. Mater.,* **1999**, *11*, 777.
4. J. Masuda, A. Takano, Y. Nagata, A. Noro, Y. Matsushita, *Phys. Rev. Lett.*, **2006,** *97*, 098301.
5. Y. Nagata, J. Masuda, A. Noro, D. Cho, A. Takano, Y. Matsushita, *Macromolecules,* **2005**, *38*, 10220.
6. C.C. Evans, F.S. Bates, M.D. Ward, *Chem. Mater.*, **2000,** *12*, 232.
7. A.F. Thünemann, S. General, *Macromolecules,* **2001,** *34*, 6978.
8. C. Osuji, C.Y. Chao, I. Bita, C.K. Ober, E.L. Thomas, *Adv. Funct. Mater.,* **2002,** *12*, 753.
9. I.A. Ansari, V. Castelletto, T. Mykhaylyk, I.W. Hamley, Z.B. Lu, T. Itoh, C.T. Imrie, *Macromolecules,* **2003**, *36*, 8898.
10. G.O.R. Alberda van Ekenstein, E. Polushkin, H. Nijland, O. Ikkala, G. ten Brinke, *Macromolecules,* **2003,** *36*, 3684.
11. C.Y. Chao, X. Li, C.K. Ober, C. Osuji, E.L. Thomas, *Adv. Mater.*, **2004,** *14*, 364.
12. O. Ikkala, G. ten Brinke, *Chem. Com.*, **2004**, 2131.
13. C.S. Tsao, H.L. Chen, *Macromolecules,* **2004**, *37*, 8984.
14. I.W. Hamley, V. Castelletto, P. Parras, Z.B. Lu, C.T. Imrie, T. Itoh, *Soft Matter,* **2005,** *1*, 355.
15. B. Nandan, C.H. Lee, H.L. Chen, W.C. Chen, *Macromolecules,* **2005**, *38*, 10117.
16. R. Nap, C. Kok, G. ten Brinke, S.I. Kuchanov, *European Phys. J. E,* **2001,** *4*, 515.
17. R. Nap, N. Sushko, I.Ya. Erukhimovich, G. ten Brinke, *Macromolecules,* **2006,** *39*, 6765.
18. Y. Smirnova, G. ten Brinke, I.Ya. Erukhimovich, *J. Chem. Phys.*, **2006**, *124*, 054907.
19. S.I. Kuchanov, V.E. Pichugin, G. ten Brinke, *E-Polymers,* **2006**, 012.
20. S.I. Kuchanov, V.E. Pichugin, G. ten Brinke, *Europhys. Lett.*, **2006,** *76*, 959.
21. A. Subbotin, T. Klymko, G. ten Brinke, *Macromolecules,* **2007,** *40*, 2915.
22. T. Klymko, A. Subbotin, G. ten Brinke, *J. Chem. Phys.,* **2008**, *129*, 114902.
23. P.J.Hoogerbrugge, J.M.V.A. Koelman, *Europhys. Lett.,* **1992**, *19*, 155.
24. R.D. Groot, T.J. Madden, *J. Chem. Phys.*, **1998**, *108*, 8713.
25. R.D. Groot, P.B. Warren, *J. Chem. Phys.*, **1997**, *107*, 4423.
26. P. Español, P.B.Warren, *Europhys. Lett*., **1995**, *30*, 191.
27. M.P.Allen, D.J. Tildesley, *Computer Simulation of Liquids*, **1987**, Clarendon, Oxford.
28. U. Micka, K. Binder, *Macromol. Theory Simul*., **1995**, *4*, 419.
29. Y. Bahbot-Raviv, Z.G. Wang, *Phys. Rev. Lett*., **2000**, *85*, 3428.
30. Q. Wang, P.F.Nealey, J.J. de Pablo, *Macromolecules,* **2001**, *34*, 3458.
31. C.-I. Huang, C.-M. Chen, *Chem. Phys. Chem.*, **2007**, *8*, 2588.

Chapter 3

Parallel versus perpendicular lamellar-in-lamellar self-assembly of linear ternary multiblock copolymer melts

3.1 Introduction

In recent years, multiblock copolymers that self-assemble in the form of periodical hierarchical structures involving different length scales have become an attractive area both for experimental [1-12] and theoretical [13-21] investigations. The simplest hierarchical structures characterized by two length scales can best be described as a structure-*in*-structure morphology. One of the first observations of a system having two periods concerned comb-shaped supramolecules consisting of polystyrene-block-poly(4-vinylpyridine) (PS-*b*-P4VP) diblock copolymers and hydrogen-bonded pentadecylphenol (PDP) side chains attached to the P4VP blocks. [1-3] Depending on the relative volume fraction of the polystyrene block the hierarchical structures lamellar-*in*-lamellar, lamellar-*in*-spheres, spheres-*in*-lamellar, etc. were identified.

Undecablock copolymers PS-*b*-(PI-*b*-PS)4-*b*-PI-*b*-PS and P2VP-*b*-(PI-*b*-PS)4-*b*-PI-*b*-P2VP appeared to be the first examples of block copolymers with a linear architecture forming a double periodic parallel lamellar-*in*-lamellar structure. [4,5] Here P2VP, PI and PS denote poly(2-vinylpyridine), polyisoprene and polystyrene, respectively, components that are mutually strongly immiscible. Recently Fleury and Bates demonstrated [11,12] that a terpolymer A-B-A-B-A-C, consisting of cyclohexylethylene (A), ethylene (B) and propylene (C) blocks, self-assembled in the form of a perpendicular lamellar-*in*-lamellar structure when the copolymer chain length exceeded some critical value. The authors attributed this particular mutual arrangement of the layers to a relatively small value of the Flory-Huggins interaction parameter between the B and C blocks as compared to that between the A and C blocks.

Multiblock copolymers have been extensively studied theoretically in the framework of a self-consistent field theory, [13-16] the weak segregation Landau approach [17, 18] as well as the strong segregation theory. [19-21] In this paper we focus on a theoretical description of the lamellar structure formation in A-*b*-(B-*b*-A)$_n$-*b*-C ternary multiblock copolymers in the strong segregation regime.

3.2 Theoretical investigation of A-b-(B-b-A)n –b–C ternary multiblock copolymer melts in strong segregation limit

Different types of the lamellar-*in*-lamellar structure formation in A-b-(B-b-A)$_n$-b-C terpolymer melts, with volume fraction of components A, B and C in the ratio 1:1:2, are analyzed in the strong segregation limit using a simple theoretical approach. We consider the lamellar, parallel lamellar-*in*-lamellar and perpendicular lamellar-*in*-lamellar self-assembled states. The influence of the copolymer chain length N, the value of the Flory-Huggins interaction parameters $\chi_{AB}, \chi_{AC}, \chi_{BC}$ and the number of blocks n in the AB multiblock chain on the phase behavior will be discussed.

3.2.1 Model and simple lamellar structure

We assume that all blocks are Gaussian chains, the total A-*b*-(B-*b*-A)$_n$-*b*-C copolymer chain length is N and the length of the C block $N_C = N/2$ equals the length of the total AB multiblock. The fraction of A and B segments are assumed to be equal, hence the length of the A and B blocks are $N_A = \dfrac{N}{4(n+1)}$ and $N_B = \dfrac{N}{4n}$, respectively. The volume and the length of the statistical segments of all components are assumed to be equal and denoted as v and a. The interaction energy between the different species are described by the Flory-Huggins interaction parameters χ_{AB}, χ_{AC} and χ_{BC}. They are assumed to be positive in accordance with unfavorable interactions.

We first consider the transition from the disordered (D) phase to the ordered lamellar phase consisting of alternating layers of C-blocks and AB multiblocks. The dominating contribution to the free energy of the disordered phase is due to interactions between different segments. Per copolymer chain this energy is given by

$$F_I = \frac{\chi_{AB}N}{16} + \frac{\chi_{AC}N}{8} + \frac{\chi_{BC}N}{8} \tag{3.1}$$

For a fixed chain architecture and positive interaction parameters an increase in the chain length N will result in incompatibility between the different blocks and the

lamellar (L) structures formation. The simplest one is the lamellar structure with one periodicity length scale corresponding to phase separation between the C blocks and the AB multiblocks (fig. 3.1).
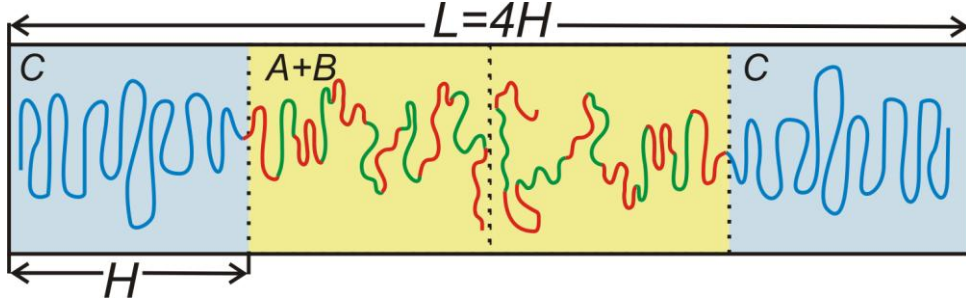
Figure 3.1. Schematic representation of the simple lamellar structure consisting of C and AB layers.

It is easy to see that this structure can appear only if $\frac{\chi_{AB}}{2} < \chi_{AC} + \chi_{BC}$. Indeed, complete separation between the AB and C components without taking the polymer connectivity into account gives an interaction energy per chain equal to $\frac{1}{2} \times \frac{\chi_{AB} N}{4} + \frac{1}{2} \times 0$, where the first term represents the interaction energy of A and B segments, which occupy half of the volume, and the second term represents the energy of C segments occupying the other half of the volume. Comparison of this energy with eq.(3.1) gives the desired condition. The polymer connectivity of the segments leads to an additional contribution to the free energy due to conformational loss associated with the non-homogeneous structure formation. In the strong segregation limit, where the thickness of the interfacial layer Δ between the C and AB domains is much smaller than the Gaussian size of the copolymer chain $R_0 = aN^{1/2}$, the stretching energy of the blocks and the interfacial energy should be taken into account (we will omit the translational energy of the chains). The interfacial energy can be derived from minimization of the free energy with respect to the profiles of the components. Let us denote the thickness of the C layer as H (it is equal to the thickness of the AB layer) and the concentration profile of C segments as $\phi_C(z)$. Assuming that the size of a AB diblock, which equals $a(N_A + N_B)^{1/2}$, is smaller than the thickness of the interfacial layer Δ (the concentration profiles of A and B segments are nearly equal, $\phi_A(z) = \phi_B(z) = \frac{1 - \phi_C(z)}{2}$), the free energy per copolymer chain in the scope of the Alexander de Gennes approximation is given by

$$F_L = 2\left[\frac{3H^2}{a^2N} + \frac{a^2\Sigma}{24v}\int_{-H}^{H} dz \frac{\phi_C'^2}{\phi_C(1-\phi_C)} + \frac{\Sigma}{v}\int_{-H}^{H} dz\left(\chi_{AB}\frac{(1-\phi_C)^2}{4} + \frac{\chi_{AC}+\chi_{BC}}{2}\phi_C(1-\phi_C)\right)\right] \quad (3.2)$$

Here $2H\Sigma = Nv$, with Σ the interface surface per chain, and the period of the lamellar structure is $L = 4H$. The total energy (2) includes the elastic energies of C and AB blocks, the gradient term due to the non-homogeneous composition profiles of the components and the interaction energy between A, B and C segments. After minimization of this free energy with respect to $\phi_C(z)$ using the additional condition

$\frac{\Sigma}{v}\int_{-H}^{H} dz \phi_C(z) = N/2$ (in eq. (3.2) we can put $(1-\phi_C)^2 = 1 - \phi_C - \phi_C(1-\phi_C)$ and then use the

method of ref.22) to arrive at $\phi_C(z) = \frac{1}{2}\left(1 + \tanh\left(\frac{z}{\Delta}\right)\right)$, where

$\Delta = R_0\sqrt{\dfrac{1}{3(\chi_{AC}N + \chi_{BC}N - 0.5\chi_{AB}N)}}$ is the interfacial thickness. With this the free energy becomes

$$F_L \cong 2\frac{3H^2}{a^2N} + \frac{Na}{2H}\sqrt{\frac{\chi_{AC}+\chi_{BC}-0.5\chi_{AB}}{12}} + \frac{\chi_{AB}N}{8} \quad (3.3)$$

Further minimization with respect to H gives

$$F_L \cong \frac{3}{2^{5/3}}(\chi_{AC}N + \chi_{BC}N - 0.5\chi_{AB}N)^{1/3} + \frac{\chi_{AB}N}{8} \quad (3.4)$$

For large values of N the free energy (3.4) increases linearly with N. The period of the lamellar structure equals to

$$L = 4H \cong 0.916R_0(\chi_{AC}N + \chi_{BC}N - 0.5\chi_{AB}N)^{1/6} \quad (3.5)$$

The transition between the isotropic and lamellar phases occurs when the free energies (3.1) and (3.4) are equal. Hence, the lamellar phase becomes stable for

$$\chi_{AC}N + \chi_{BC}N - 0.5\chi_{AB}N > 20.8 \qquad (3.6)$$

As an example we consider the copolymer A-B-A-B-A-C consisting of cyclohexylethylene (A), ethylene (B) and propylene (C) blocks as investigated in the group of Bates. [11, 12] The Flory-Huggins interaction parameters (at 140° C) satisfy $\chi_{AB} \cong 0.054, \chi_{AC} \cong 0.034$ and $\chi_{BC} \cong 0.0054$. The last ones were calculated using the fitting formulas proposed in ref.23. According to eq. (3.6) the transition to the simple lamellar phase should occur at $N = N_C \cong 1680$. This value is indeed in the range of the molecular masses where the lamellar phase was observed experimentally.

3.2.2 Perpendicular lamellar-*in*-lamellar structure

With increasing N additional separation between the A and B blocks inside the AB layer will occur resulting in the formation of more complicated lamellar structures such as parallel lamellar-*in*-lamellar ($LL_{//}$, fig. 3.2a) or perpendicular lamellar-*in*-lamellar ($LL_{\perp}$, fig. 3.2b). First we consider the perpendicular lamellar-*in*-lamellar structure. In this case thin A and B layers are arranged perpendicularly with respect to the thick C layers. We denote the thickness of the C-layer as $2H$ (along z-axis) and the thickness of the A and B layers as $2d$ (along x-axis). In the perpendicular lamellar-*within*-lamellar structure both A and B layers have the same thickness since we assume that their volume fractions are equal. The period of the lamellar structure in x-direction is $L_x = 4d$ and in z-direction it is $L_z = 4H$. For further calculation we consider the volume containing half of the periods along the z- and x-direction and take the origin of the (x, z) plane on the line where the A, B and C layers intersect (see fig. 3.3). The y-axis is perpendicular to the (x, z) plane. The junction points between the A and C blocks are located on a strip of width $2d$ and are characterized by the distribution function $\rho(x)$.
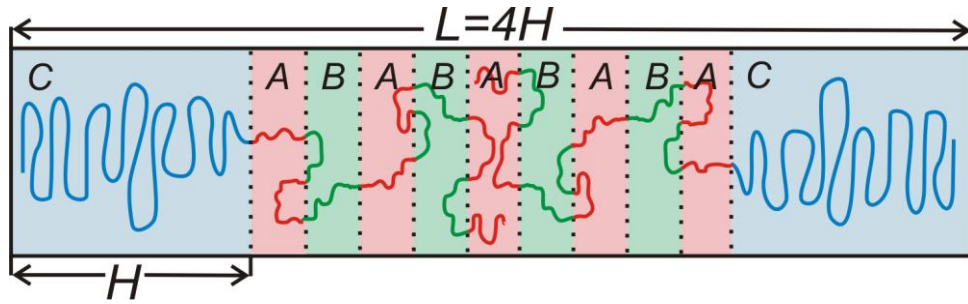
(a)
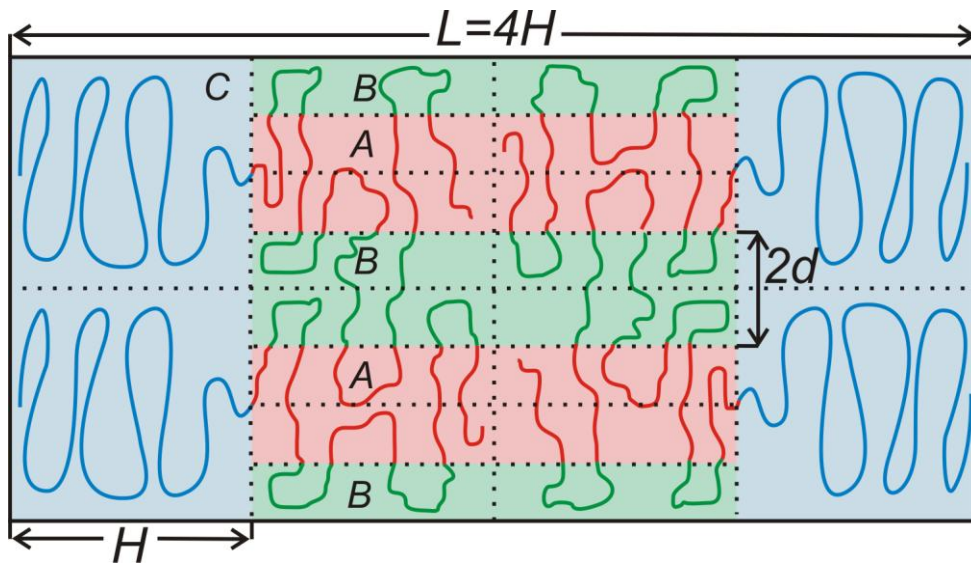
(b)

Figure 3.2. Schematic representation of parallel lamellar-*in*-lamellar (a) and perpendicular lamellar-*in*-lamellar (b) structure.

We start with the elastic stretching energy of the C-blocks which are extended inside the C layers so that their conformations can be described by trajectories. For simplicity we assume that these trajectories are straight lines characterized by a bending angle $\theta(x)$ with the *x*-axis, fig. 3.3.
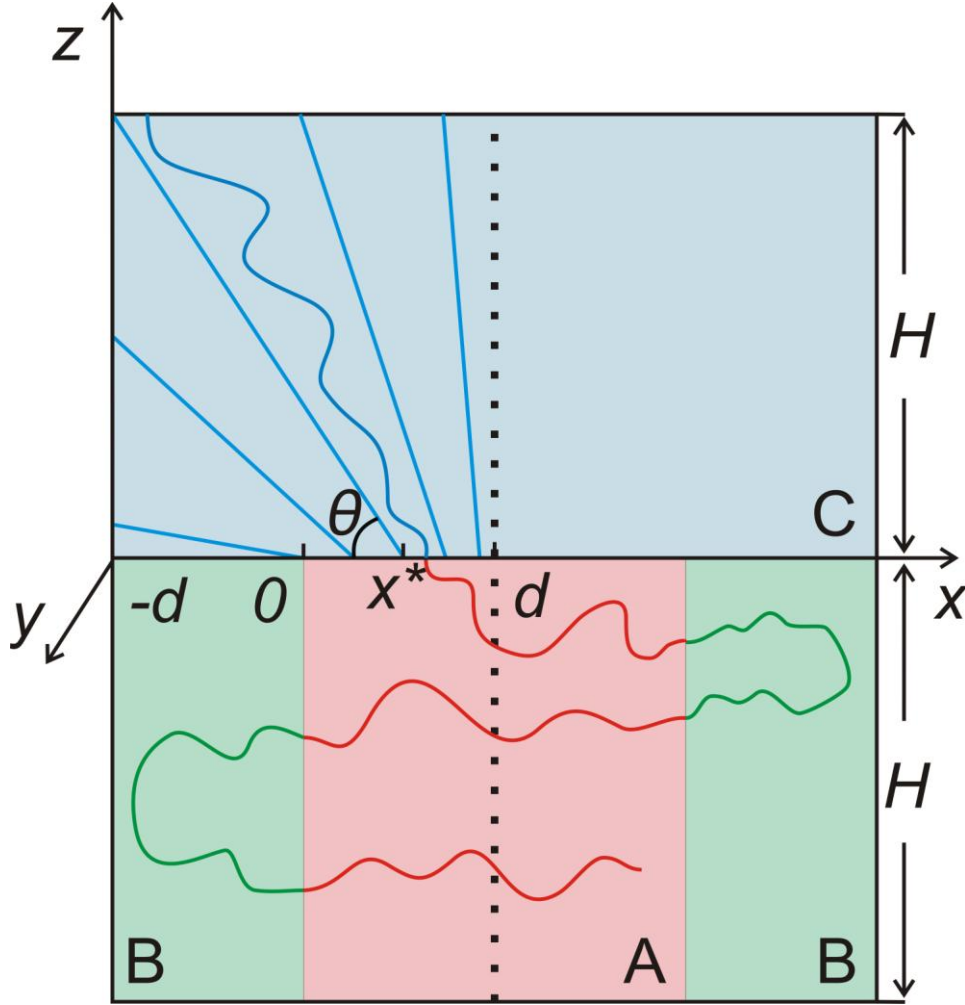
Figure 3.3. Conformation of C-*b*-(A-*b*-B)$_m$-*b*-A copolymer chain in the perpendicular lamellar-*in*-lamellar structure.

On average a C-block occupies a box of size $2dHl$, where $l = \dfrac{N_C v}{2dH}$ is its dimension along the *y*-axis. The length of the trajectory which start at the point *x* is equal to $\dfrac{d+x}{\cos\theta(x)}$ if $0 \leq \theta \leq \theta^*$ and $0 \leq x \leq x^*$, and $\dfrac{H}{\sin\theta(x)}$ if $\theta^* \leq \theta \leq \dfrac{\pi}{2}$ and $x^* \leq x \leq d$, where $\tan\theta^* = \dfrac{H}{d+x^*}$. Coordinate x^* can be found from the incompressibility condition. The number of C-blocks that start on the surface area $dxdy$ in the vicinity of point *x* is $dQ = \rho(x)dxdy$ and the volume occupied is given by $dV = vN_C dQ$. This volume can also be obtained using the incompressibility condition and simple geometrical arguments,

$$dV = \frac{d+x}{\cos\theta}\left(\sin\theta + \frac{d+x}{2\cos\theta}\frac{d\theta}{dx}\right)dxdy, \quad 0 < \theta < \theta*$$

$$dV = \frac{H}{\sin\theta}\left(\sin\theta + \frac{H}{2\sin\theta}\frac{d\theta}{dx}\right)dxdy, \quad \theta* < \theta < \frac{\pi}{2}$$

(3.7)

Thus we arrive to the following equations

$$\frac{d\theta}{dx} = \frac{\sin 2\theta}{d+x}\left(\frac{vN_C\rho(x)}{(d+x)\tan\theta} - 1\right), \quad 0 \le \theta \le \theta*$$

$$\frac{d\theta}{dx} = \frac{2\sin^2\theta}{H}\left(\frac{vN_C\rho(x)}{H} - 1\right), \quad \theta* \le \theta \le \frac{\pi}{2}$$

(3.8)

The solutions to these equations can be written in the form

$$\tan\theta(x) = \frac{2vN_C}{(d+x)^2}\int_0^x \rho(x')dx', \qquad 0 \le x \le x*$$

$$\cot\theta(x) = \frac{2}{H}\left(d+x - \frac{vN_C}{H}\int_0^x \rho(x')dx'\right), \quad x* \le x \le d$$

(3.9)

The normalization condition implies that $\int_0^d \rho(x')dx' = \frac{2dH}{vN_C}$. For $0 \le \theta(x) \le \theta*$, the z–coordinate of the free end of the trajectory is $z_N(x) = (d+x)\tan\theta(x)$ and its x-coordinate is $x_N(x) = -d$. Similarly, for $\theta* \le \theta(x) \le \pi/2$ the free end has coordinates $x_N(x) = x - H\cot\theta(x)$ and $z_N(x) = H$.

The local stretching of the C-block can be obtained from similar arguments. The number of segments that are inside the interval dr at a distance r along the trajectories starting at the point with coordinate x is $dN = \frac{1}{v}\left(\sin\theta + r\frac{d\theta}{dx}\right)dxdydr$. Therefore, the number of segments belonging to one block equals $dn = \frac{dN}{dQ} = \frac{1}{v\rho(x)}\left(\sin\theta + r\frac{d\theta}{dx}\right)dr$. The equation for the local chain stretching is given by

$$E(x,r) = \frac{3}{2a^2}\frac{dr}{dn} = \frac{3v\rho(x)}{2a^2}\left(\sin\theta + r\frac{d\theta}{dx}\right)^{-1} \tag{3.10}$$

The elastic energy of stretching for the C-block can be written as

$$F_C = 2\frac{vN_C}{4dH}\left[\int_0^{x^*} dx\rho(x)\int_0^{\frac{d+x}{\cos\theta}} drE(x,r) + \int_{x^*}^{d} dx\rho(x)\int_0^{\frac{H}{\sin\theta}} drE(x,r)\right] \tag{3.11}$$

Using eq. (3.10) we get

$$F_C = \frac{3v^2N_C}{4a^2 dH}\left[\int_0^{x^*} dx\frac{\rho^2(x)}{\theta_x'}\ln\left(1+\frac{(d+x)\theta_x'}{\sin\theta\cos\theta}\right) + \int_{x^*}^{d} dx\frac{\rho^2(x)}{\theta_x'}\ln\left(1+\frac{H\theta_x'}{\sin^2\theta}\right)\right] \tag{3.12}$$

θ_x' can be eliminated from the last equation using relationship (8) and results in

$$F_C = \frac{3v^2N_C}{4a^2 dH}\left[\int_0^{x^*} dx\frac{(d+x)\rho^2(x)}{\sin 2\theta\left(\frac{vN_C\rho(x)}{(d+x)\tan\theta}-1\right)}\ln\left(\frac{2vN_C\rho(x)}{(d+x)\tan\theta}-1\right) + \right.$$

$$\left. \int_{x^*}^{d} dx\frac{H\rho^2(x)}{2\sin^2\theta\left(\frac{vN_C}{H}\rho(x)-1\right)}\ln\left(\frac{2vN_C}{H}\rho(x)-1\right)\right] \tag{3.13}$$

To simplify further calculations we assume that the junction points between the A and C blocks are distributed homogeneously on the AC interface. This implies that $\rho(x) = \rho_{0x} = \frac{2H}{vN_C} = \frac{4H}{vN}$. From the incompressibility condition we get $x^* = d/3$, and after some calculations the final equation for the elastic energy of the C block becomes

$$F_C = 2.65 \frac{H^2}{a^2 N} + 5.29 \frac{d^2}{a^2 N} \qquad (3.14)$$

The situation is more complicated for the short period AB lamellar structure, where the blocks are stretched both in the *x*- and *z*-direction and their ends located at the AB interface. Here we use a simple approach assuming that the blocks are stretched homogeneously. A AB multiblock occupies the volume $2dHl = vN/2$. Therefore its average end-to-end distance along the *z*-axis is H and the average stretching force of the multiblock along the *z*-direction is $E_z = \frac{3}{a^2} \frac{H}{N}$. The internal A and B blocks form either bridge or loop conformations. Assuming that the energy of a bridge and a loop is the same, which implies that the middle of a loop is located on a distance d from the interface, the average tension of the A and B blocks are $E_{x,A} = \frac{12(n+1)d}{a^2 N}$ and $E_{x,B} = \frac{12nd}{a^2 N}$, respectively. The total elastic energy of the AB multiblock is given by

$$F_{AB} = E_z H + 2(n+1)E_{x,A}d + 2nE_{x,B}d = \frac{3}{a^2 N}\left[H^2 + 8\left((n+1)^2 + n^2\right)d^2\right] \qquad (3.15)$$

The interfacial energy is determined by the Flory-Huggins interaction parameters χ_{AB}, χ_{AC} and χ_{BC}, and is given by

$$F_{\text{inf}} = \frac{a}{v\sqrt{6}}\left(\Sigma_{AB}\sqrt{\chi_{AB}} + \Sigma_{AC}\sqrt{\chi_{AC}} + \Sigma_{BC}\sqrt{\chi_{BC}}\right) = \frac{aN}{4H\sqrt{6}}\left[\frac{H}{d}\sqrt{\chi_{AB}} + \sqrt{\chi_{AC}} + \sqrt{\chi_{BC}}\right] \qquad (3.16)$$

Here $\Sigma_{AB} = \frac{vN_C}{2d}, \Sigma_{AC} = \Sigma_{BC} = \frac{vN_C}{2H}$ are the areas of contact between the different components per copolymer chain. The total free energy is equal to the sum of the elastic energies of the C, A and B blocks and the interfacial energy.

$$F_{LL_\perp} = 5.65 \frac{H^2}{a^2 N} + 48(n(n+1) + 0.61)\frac{d^2}{a^2 N} + \frac{aN}{4d}\sqrt{\frac{\chi_{AB}}{6}} + \frac{aN}{4H\sqrt{6}}\left[\sqrt{\chi_{AB}} + \sqrt{\chi_{BC}}\right] \qquad (3.17)$$

Further minimization of this energy with respect to H and d is trivial. The periods of the structure are

$$L_z = 4H \cong 0.84R_0\left(\sqrt{N\chi_{AC}} + \sqrt{N\chi_{BC}}\right)^{1/3}, \quad L_x = 4d \cong 0.41\frac{R_0\left(N\chi_{AB}\right)^{1/6}}{\left(n(n+1)+0.61\right)^{1/3}} \tag{3.18}$$

The final equation for the free energy is given by

$$F_{LL_\perp} = \frac{3}{2}\left(n(n+1)+0.61\right)^{1/3}\left(N\chi_{AB}\right)^{1/3} + 0.73\left(\sqrt{N\chi_{AC}} + \sqrt{N\chi_{BC}}\right)^{2/3} \tag{3.19}$$

This energy scales as $F_{LL_\perp} \propto N^{1/3}$. Comparison of the energies F_L (eq. 3.4) and $F_{LL_\perp}$ (eq. 3.19) shows that the perpendicular lamellar-*in*-lamellar becomes stable when N exceeds some critical value N_{c1}. For the terpolymer A-B-A-B-A-C consisting of cyclohexylethylene (A), ethylene (B) and propylene (C) blocks this value is $N_{c1} \cong 2200$.

3.2.3 Parallel lamellar-*in*-lamellar structure

Next we address the parallel lamellar-*in*-lamellar structure where the thin A and B layers are parallel to the thick C layers. We assume that two neighboring C layers are separated by $m+1$ A layers and m B layers (the total number of thin layers inside the AB multiblock domain is $k = 2m+1$, fig.3.4) . A similar structure has been considered before for copolymer chains with the chemical structure C-b-(A-b-B)ₙ-b-A-b-C. [19-21]
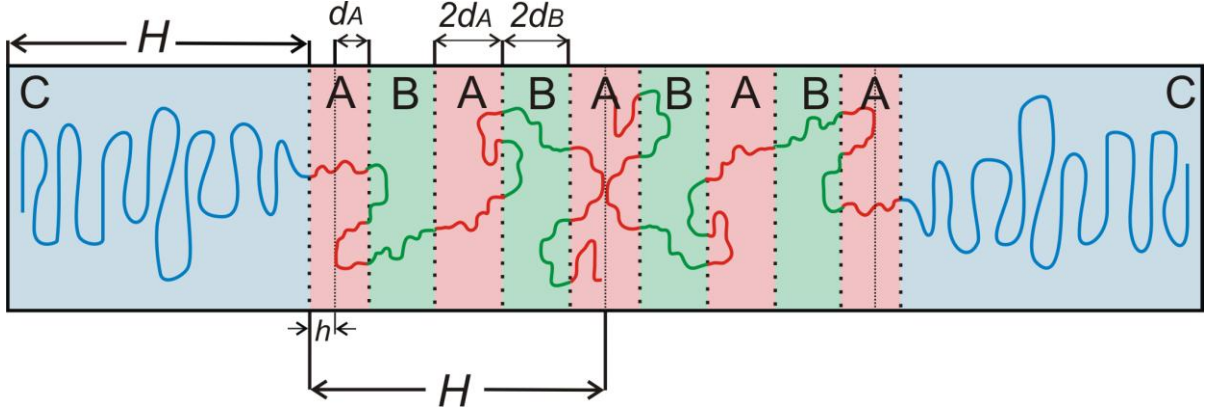
Figure 3.4. Conformation of C-*b*-(A-*b*-B)$_m$-*b*-A copolymer chain in the parallel lamellar-*in*-lamellar structure.

We denote the thickness of the B layers as $2d_B$ and the thickness of the C layers as $2H$. Among the A layers we will distinguish between the boundary layers which are in a contact with C layers and have thickness $h+d_A$ and the internal A layers having thickness $2d_A$. Homogeneous stretching of the blocks in the proposed structure imply that the stretching force of the C blocks is $E_C = \dfrac{3H}{a^2 N}$, the stretching force of the B blocks is $E_B = \dfrac{12nd_B}{a^2 N}$ and the stretching force of the A blocks is $E_{A1} = \dfrac{12(n+1)d_A}{a^2 N}$. The exception is the first half of those A blocks that are directly connected to C blocks and occupy a domain of thickness h in the boundary A layer. The stretching force of this section is $E_{A2} = \dfrac{12(n+1)h}{a^2 N}$. If the interfacial area per copolymer chain equals Σ, incompressibility implies

$$\frac{vN}{2} = H\Sigma, \quad 2md_B\Sigma = \frac{vN}{4}, \quad h\Sigma = \frac{vN}{8(n+1)}, \quad 2md_A\Sigma = \frac{vN(2n+1)}{8(n+1)} \qquad (3.20)$$

The total free energy per multiblock copolymer chain includes the local stretching energy of A, B and C blocks, AB and AC interfacial energy and a combinatorial term which takes into account the different ways that the AB multiblock chain can pass through the m AB interfacial layers.

$$F_{LL_{//}} = \frac{12(n+1)h^2}{a^2 N} + \frac{12(n+1)(2n+1)d_A^2}{a^2 N} + \frac{24n^2 d_B^2}{a^2 N} + \frac{3H^2}{a^2 N} + \frac{a\Sigma}{v\sqrt{6}}\left[m\sqrt{\chi_{AB}} + \sqrt{\chi_{AC}}\right] + F_{comb}$$

(3.21)

The combinatorial term F_{comb} can be estimated from imagining the extended multiblock conformation as a one-dimensional random walk consisting of $2n$ steps [21] (this is the total number of AB links) drifting on a distance m: i.e., the number of steps in the positive direction is $(2n+m)/2$ and in the opposite direction is $(2n-m)/2$

$$F_{comb} \cong \left(\frac{2n+m}{2}\right)\ln\left(\frac{2n+m}{2}\right) + \left(\frac{2n-m}{2}\right)\ln\left(\frac{2n-m}{2}\right) - 2n\ln(n)$$

(3.22)

After minimization of $F_{LL_{//}}$ with respect to Σ using eq.(3.20) we get

$$F_{LL_{//}} = \frac{3}{2}\left(m\sqrt{N\chi_{AB}} + \sqrt{N\chi_{AC}}\right)^{2/3}\left(\frac{m^2 + (2n+1)^3}{16m^2(n+1)} + \frac{n^2}{2m^2} + \frac{1}{4}\right)^{1/3} + F_{comb}$$

(3.23)

The period of the structure is given by

$$L_z = 4H \cong 0.82R_0\left(m\sqrt{N\chi_{AB}} + \sqrt{N\chi_{AC}}\right)^{1/3}\left(\frac{m^2 + (2n+1)^3}{16m^2(n+1)} + \frac{n^2}{2m^2} + \frac{1}{4}\right)^{1/3}$$

(3.24)

For large N the free energy scales as $F_{LL_{//}} \propto N^{1/3}$. The transition between the simple lamellar phase (L) and the parallel lamellar-*in*-lamellar structure occurs when the energies (3.4) and (3.23) are equal. Turning back to the terpolymer A-B-A-B-A-C consisting of cyclohexylethylene (A), ethylene (B) and propylene (C) blocks we find that $N_{c2} \cong 2040$. The transition occurs to a structure with $k = 5$ thin layers.

3.2.4 Discussion and concluding remarks

The analysis of the terpolymer A-B-A-B-A-C consisting of cyclohexylethylene (A), ethylene (B) and propylene (C) blocks shows that for large chain lengths N the parallel lamellar-*in*-lamellar structure is more preferable than the perpendicular lamellar-*in*-lamellar structure (the transition to the lamellar-*in*-lamellar structure occurs first for $N_{c2}\chi_{AB} \cong 110 < N_{c1}\chi_{AB} \cong 119$. This result is in contradiction with the experimental observations. [11,12] However, we note that these two transition points are very close to each other and using more rigorous calculations in part concerning the energy of the terminal A blocks may well change this sequence. The self-consistent field method seems the most appropriate way for the analysis of terpolymers with a small numbers of blocks in the AB multiblock chain.

When the number of blocks in the multiblock is large ($n >> 1$) the contribution of the terminal A blocks to the free energy is small and the transition between the different lamellar structures can be done using the approach presented. In this limiting case the dominating contribution to the free energy of the complex lamellar structures appears to be due to the AB multiblock. This energy is the same both for the parallel and perpendicular lamellar-*in*-lamellar structures. An expansion of the free energies eqs. (3.19, 3.23) with respect to the small parameter $1/n << 1$, with the additional assumption that $1 << m << n$ (this inequality should be verified after the calculations), results in

$$F_{LL_\perp} \cong \frac{3}{2}n^{2/3}\left(N\chi_{AB}\right)^{1/3} + 0.73\left(\sqrt{N\chi_{AC}} + \sqrt{N\chi_{BC}}\right)^{2/3} \qquad (3.25a)$$

$$F_{LL_{//}} \cong \frac{3}{2}n^{2/3}\left(N\chi_{AB}\right)^{1/3}\left(1 + \frac{2}{3m}\left(\frac{\chi_{AC}}{\chi_{AB}}\right)^{1/2} + \frac{m^2}{12n^2}\right) + \frac{m^2}{4n} \qquad (3.25b)$$

In the last equation we used the approximation $F_{comb} \cong \dfrac{m^2}{4n}$. Minimization of the free energy (3.25.b) with respect to m gives

$$m \cong \left(2n\right)^{2/3}\left(\frac{\chi_{AC}}{\chi_{AB}}\right)^{1/6} \qquad (3.26)$$

After substitution of this value in eq.(3.25.b) we get the final formula for the free energy of the parallel lamellar-*in*-lamellar structure

$$F_{LL_{//}} \cong \frac{3}{2} n^{2/3} (N\chi_{AB})^{1/3} + \frac{3}{2^{5/3}} (N\chi_{AC})^{1/3} + \frac{1}{2^{2/3}} n^{1/3} \left(\frac{\chi_{AC}}{\chi_{AB}} \right)^{1/3} \qquad (3.27)$$

The last term is connected with the combinatorial energy and is small since $\chi_{AB}(N/2n) \gg 1$. Here, the parameter $\chi_{AB}(N/2n)$ determines the energy of the (A-B) diblock. In our case this parameter is responsible for the transition between the simple lamellar and the complex lamellar structures. Comparing the free energies eq.(3.4) and eqs. (3.25a, 3.25b) gives the range of stability of the complex lamellar structures

$$\chi_{AB} \left(\frac{N}{2n} \right) > \chi^* M = 6 \cdot \sqrt{12} \cong 20.8 \qquad (3.28)$$

Here $M = N/2n$ is the length of AB diblock. This value exceeds the critical value $\chi^* M = 15.1$ of the lamellar phase formation in AB multiblock copolymers obtained using the random phase approximation approach. [24, 25] The essential discrepancy between these two values appears because in the present approach loops and bridges have the same energy. The separation line between the parallel and perpendicular lamellar-*within*-lamellar structures can be found by equating the energies (3.25a) and (3.27). The perpendicular lamellar-*in*-lamellar structure becomes stable when

$$\frac{\chi_{BC}}{\chi_{AC}} < 0.22 \qquad (3.29)$$

According to this criterion the transition to the perpendicular lamellar-*in*-lamellar phase for the terpolymer A-b-(B-b-A)$_n$-b-C consisting of cyclohexylethylene (A), ethylene (B) and propylene (C) blocks with $n \gg 1$ should occur before the transition to the parallel lamellar-*in*-lamellar phase as far as $\chi_{BC}/\chi_{AC} \cong 0.16 < 0.22$. Contrary to the direct calculations the formal application of this criterion to the case when $n = 2$ is in agreement with the experimental observations. [11, 12]

(a)

(b)
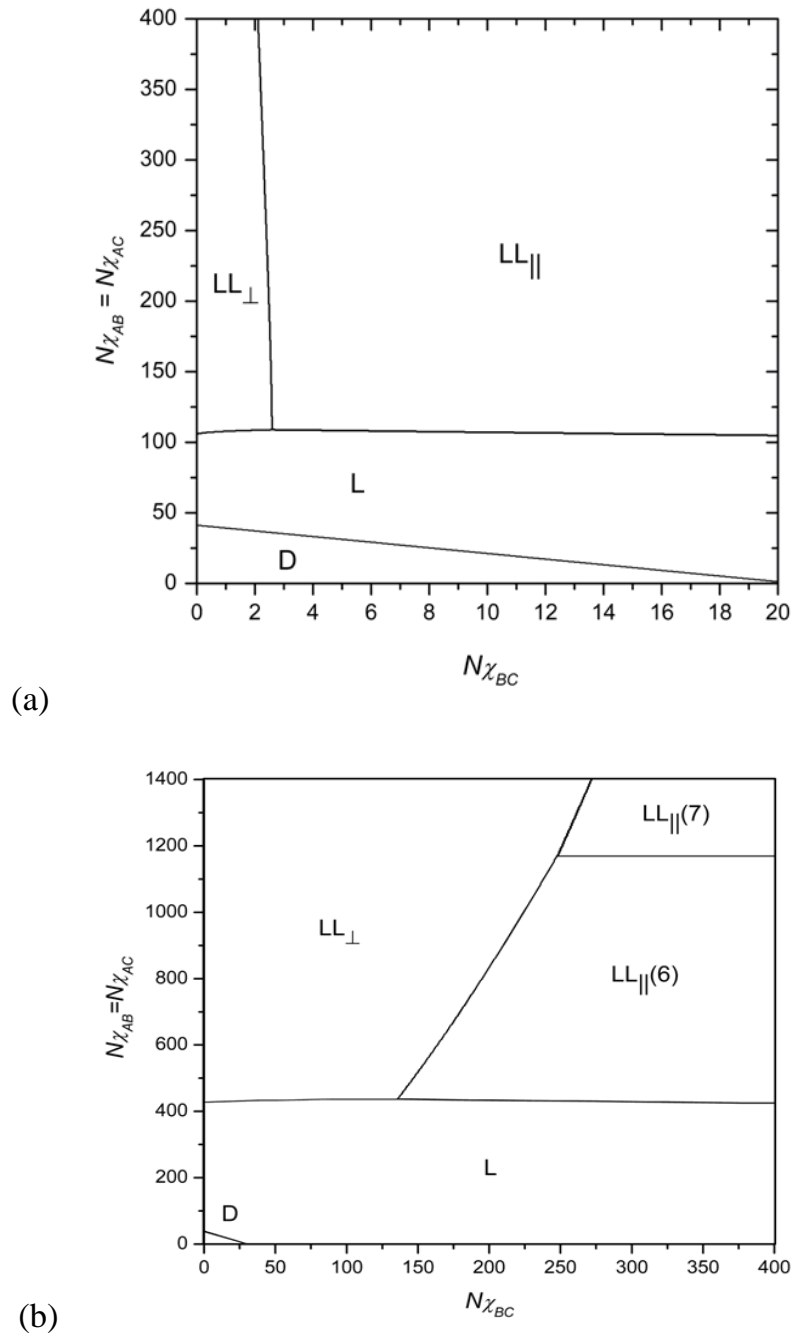
Figure 3.5. Phase diagram for $n = 2$ (a) and $n = 10$ (b) when $\chi_{AB} = \chi_{AC}$.

Two different phase diagrams for $n = 2$ and $n = 10$ and $N\chi_{AB} = N\chi_{AC}$ are shown in fig. 3.5. One can see that the area of stability of the parallel lamellar-*in*-lamellar structure exceeds the area of stability of the perpendicular lamellar-*in*-lamellar structure, which occurs for small values of χ_{BC}. When χ_{BC} is very small, i.e. $\chi_{BC}(N/n) \leq 1$, the B blocks start to penetrate inside the C-layers and the BC interface is destroyed. In this case we expect stabilization of the parallel lamellar-*in*-lamellar structure.

3.3 Dissipative particle dynamics simulations of A-*b*-(B-*b*-A)₂–*b*–C and (B-*b*-A)₂–*b*–C ternary multiblock copolymer melts

The SSL method has as a disadvantage that only the most obvious structures are investigated, which makes it difficult to find new ones. As will be shown in part 3.4 of this Chapter, the SCFT also suffers from limitations for systems with three types of monomers. Hence, it is interesting to look at the type of systems under investigation using another approach. For this the dissipative particle dynamics DPD simulation method was chosen.

3.3.1 Model

In order to simulate linear ternary multiblock copolymers the chains are replaced by a coarse grained version. As it is typical for the DPD technique a number of monomers, usually this number corresponds the Kuhn segment, is considered as one bead. For the A-b-(B-b-A)₂ -b–C copolymer, the blocks of type A were replaced by two, B – by three and C – by twelve DPD beads. For the (B-b-A)₂ -b–C copolymer the DPD chain is the same except that the A blocks are now represented by three DPD beads in order to maintain the volume fraction of the multiblock part and the C tail at 50/50. Furthermore, the volume fraction of the A and B blocks are in both cases equal to 0.25. The total length of the polymer chain was in both cases equal to $N = 24$.

3.3.2 Technique

The chains were placed in a box size of $L = 30$ in each direction, with density equal to three. One advantage of the DPD method is that it allows to use large time steps in order to solve the equations of motion, which was chosen to be *Δt = 0.06*. Each numerical experiment was done by a fixed protocol. For the first $5*10^4$ time steps all interaction parameters in system were equal to 25 ($a_{ij} = 25$ for any i and j). After that the annealing technique was applied to obtain the desired values for the interaction parameters. This annealing took place during 10^6 time steps where at each step the interaction parameter value was increased with $a_{max}/10^6$ (a_{max} corresponding to the final increment). Subsequently the relaxation time was equal to $4*10^6$ time steps. The interaction parameter values were changed in the ranges listed in Table 3.1 (see also Ch. 7 Appendix).

a_{ij}	A	B	C
A	25	70-160	47.5-67.5
B	70-160	25	25-50
C	47.5-67.5	25-50	25

a)

χ_{ij}	A	B	C
A	0	70-160	6.4-19.3
B	12.8-38.6	0	0-7.14
C	6.4-19.3	0-7.4	0

b)

Table 3.1. Range of interaction parameter in term of a) a_{ij}; b) χ_{ij}

3.3.3 Results

Using the DPD technique it is possible to investigate the transition from the ternary to binary system by changing χ_{BC} from 7.14 (ternary case) to 0 (binary).

3.3.3.1 Highly fluctuating disordered structure

As shown in Table 3.1, the values of χ_{AB} and χ_{AC} are always quite big to achieve phase separation between A and C and between A and B blocks. Let us consider the structures formed by the A-b-(B-b-A)$_n$ -b–C copolymer system. When a_{BC} = 25 (χ_{BC} = 0) and a_{AB} = 2a_{AC} = 70 (χ_{AB} = 2χ_{AC} = 12.8), a highly fluctuating disordered structure is formed. As shown in Fig. 3.6, the A blocks form blobs covered by B blocks and these blobs are disordered in the matrix of C blocks. Because χ_{BC} = 0, for the B blocks it is preferable to be mixed with C blocks. Due to the geometrical structure of the copolymers this leads to two possibilities. One possibility is to increase the stretching of the C blocks close to AC interface to allow for the B blocks and the

other is to increase the area of the AC interface by bending making it possible to allocate parts of C blocks and B blocks close to interface without extra stretching. From the picture one can conclude that the free energy of the system is lower in the second case. It appears that χ_{AB} is not too high to increase the interface surface and lower the free energy as compared to the case where parts of the C blocks and the B blocks are severely stretched.
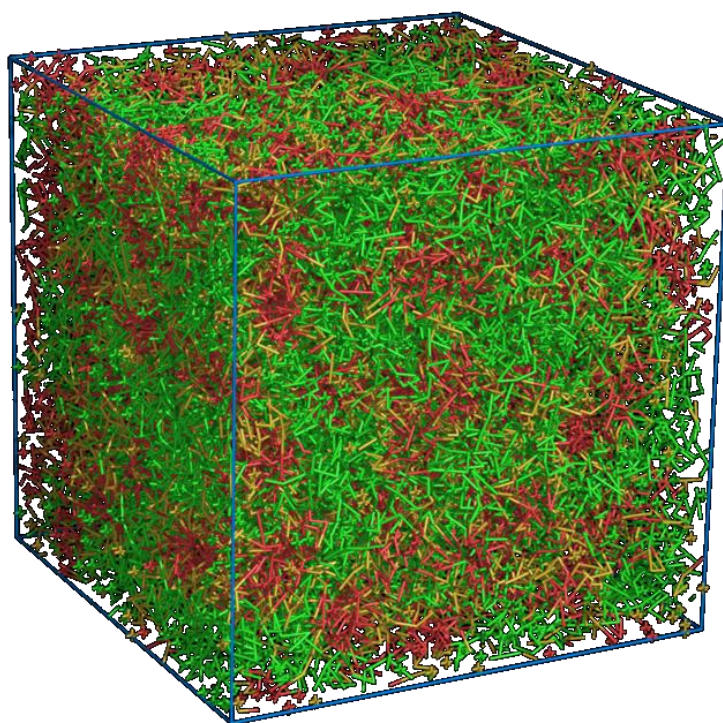
Figure 3.6. Snapshot of highly fluctuating disordered structure formed by A-*b*-(B-*b*-A)$_n$-*b*–C chains for $a_{BC} = 25$ ($\chi_{BC} = 0$) and $a_{AB} = 2a_{AC} = 70$ ($\chi_{AB} = 2\chi_{AC} = 12.8$).

a)   b)
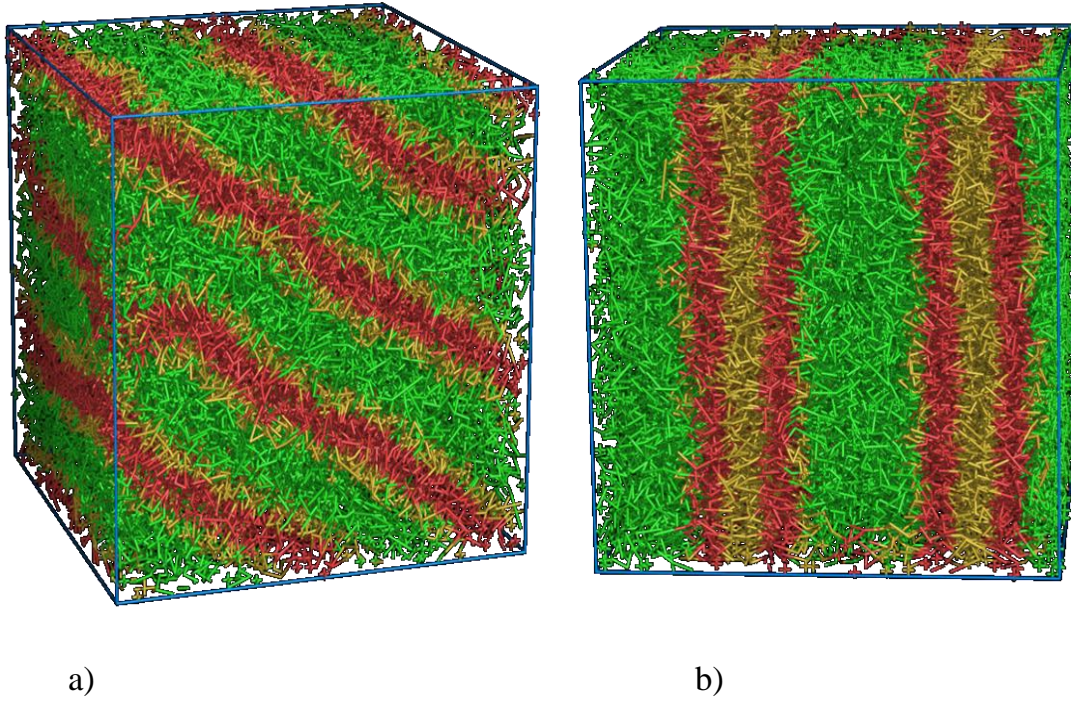
Figure 3.7. Snapshot of inverted lamellar structure formed by A-*b*-(B-*b*-A)$_n$-*b*–C chains
a) Three internal layers $a_{BC} = 25$ ($\chi_{BC} = 0$) and $a_{AB} = 2a_{AC} = 130$ ($\chi_{AB} = 2\chi_{AC} = 30$).
b) Five internal layers $a_{BC} = 30$ ($\chi_{BC} = 1.4$) and $a_{AB} = 2a_{AC} = 130$ ($\chi_{AB} = 2\chi_{AC} = 30$)

3.3.3.2 Inverted lamellar structures

By increasing $\chi_{AB} = 2\chi_{AC}$, the system transforms to a lamellar state. Increasing of the AC interface is no longer the best way to minimize the free energy and the system tries to decrease this interface by adding extra stretching to the C and B blocks. Because $\chi_{BC} = 0$, the B blocks mix with the C blocks but separate from the A blocks. Increasing χ_{BC} leads to separation between B and C blocks. First the C blocks segregate and make C channels in B layers. This is how the BC interface appears. Then, if χ_{BC} becomes larger it is preferable for the system to add one more B layer to decrease the BC interface with extra stretching of C blocks. We call this structure *inverted lamellar* because the order of the layers C-B-A in lamellar phase is not the same as in the molecular structure of the polymer (see Fig. 3.7).

3.3.3.3 Perpendicular lamellar-*in*-lamellar structure

Further increasing the incompatibility between the B and C blocks forces the system to minimize the BC interface as well. Due to sufficiently high incompatibility between B and A blocks, it is still not preferable to form the parallel lamellar-*in*-lamellar ($L_\parallel$) structure. Instead a perpendicular lamellar-*in*-lamellar ($L_\perp$) structure is formed, Fig. 3.8. From our theoretical investigations it is known that the free energies of the parallel and perpendicular states are quite close to each other. A delicate balance between stretching and interfacial energies makes one of the structures preferable over the other. In the case of $L_\perp$ the stretching energy of the C blocks is more complex and higher than for the $L_\parallel$, but the interfacial energy is lower. DPD is not accurate enough to find difference between shifted and not shifted $L_\perp$ structures. According to the DPD experiments these two structures are identical. Structures where A and B lamellae from one layer are perpendicular to AB lamellas from another one are also possible. During experiments such kind of structures occurred very infrequently compared to shifted and not shifted $L_\perp$ structures, one out of ten. Therefore we believe this structure to be metastable
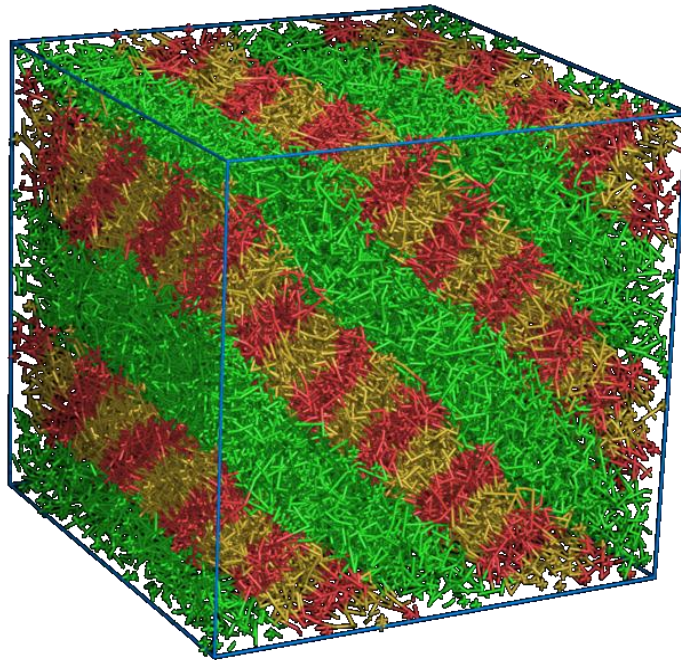
Figure 3.8. Snapshot of perpendicular lamellar-*in*-lamellar structure formed by A-*b*-(B-*b*-A)$_n$-*b*–C chains at $a_{BC} = 35$ ($\chi_{BC} = 2.85$) and $a_{AB} = 2a_{AC} = 130$ ($\chi_{AB} = 2\chi_{AC} = 30$).

3.3.3.4 Parallel lamellar-*in*-lamellar

When the incompatibility between the B and C blocks increases even further, it is no longer preferable to have a BC interface and the system can easily avoid it because there are no direct bonds between the B and C blocks. Now parallel lamellar-*in*-lamellar structures are formed with a different number of internal layers, Fig.3.9. These kinds of structures were already investigated using the DPD simulations and the SSL approach presented in Chapter 2 of this thesis. The only difference is in the primary structure of the polymers considered.

a)   b)
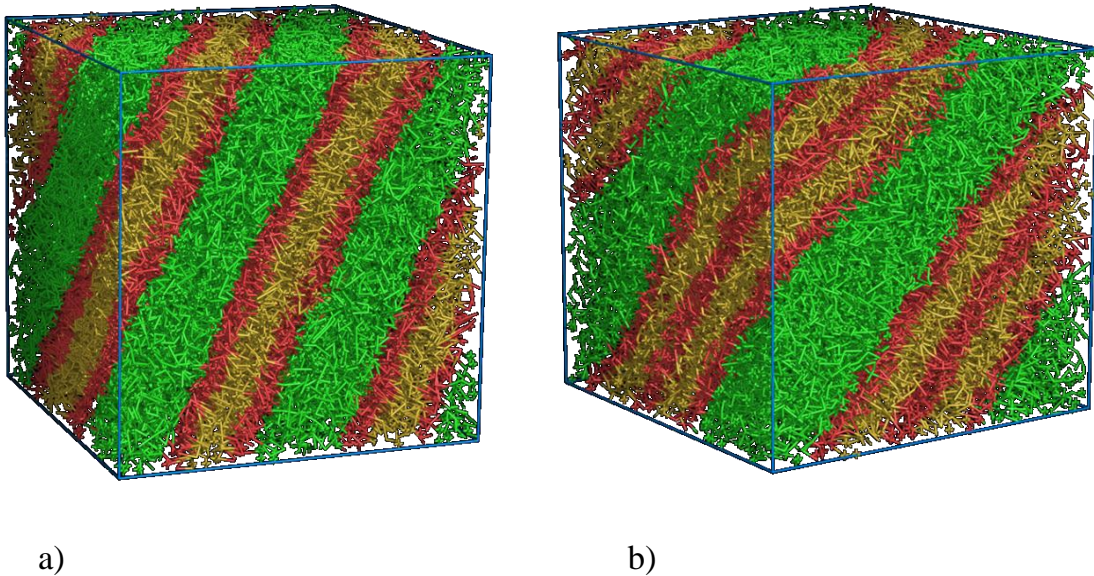
Figure 3.9. Snapshot of parallel lamellar-*in*-lamellar structure formed by A-*b*-(B-*b*-A)$_2$-*b*–C chains

a) Three internal layers $a_{BC} = 25$ ($\chi_{BC} = 0$) and $a_{AB} = 2a_{AC} = 130$ ($\chi_{AB} = 2\chi_{AC} = 30$ n).

b) Five internal layers $a_{BC} = 30$ ($\chi_{BC} = 1.4$) and $a_{AB} = 2a_{AC} = 130$ ($\chi_{AB} = 2\chi_{AC} = 30$)

3.3.3.5 Morphology diagrams

To summarize the results conformational diagrams for the two types of polymers were plotted. Fig. 3.10 presents the conformational diagram for A-*b*-(B-*b*-A)$_2$-*b*–C. The diagram shows that there are several pathways by which ternary systems by decreasing χ_{BC} to zero transform into binary systems. One possibility is the sequence:

highly fluctuating disordered state – perpendicular lamellar-*in*-lamellar - parallel lamellar-*in*- lamellar. Another, and longest with respect to the number of different structures, is: inverted lamellae with three internal layers - inverted lamellae with five internal layers - perpendicular lamellar-*in*-lamellar - parallel lamellar-*in*-lamellar. It is interesting to notice that inverted lamellae with 3 and 5 internal layers appear simultaneously while increasing $\chi_{AB} = 2\chi_{AC}$. The stability area of $L_\perp$ increases with increasing of incompatibility between A and B and between A and C blocks.

The morphology diagram of (B-b-A)$_2$ -b–C is presented in Fig. 3.11. Due to the smaller number of blocks in the multiblock part but at the same fixed volume fractions blocks of A type are now longer. The order-disorder transition line lies lower with respect to $\chi_{AB} = 2\chi_{AC}$ because $n\chi_{AB}$ is now larger than for the previous structure. Another influence of the smaller number of blocks is that lamellae with five internal layers no longer exist. The stability region of the perpendicular lamellar-*in*-lamellar structure is more restricted
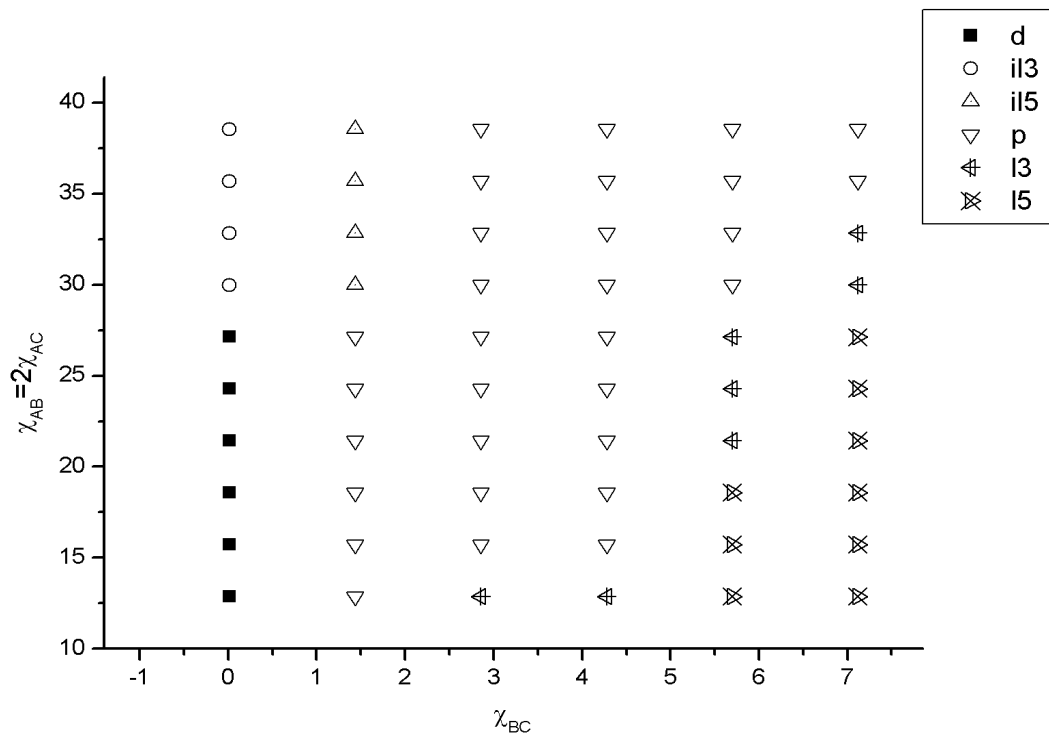
Figure. 3.10. Conformational diagram for polymer melt consist of A-*b*-(B-*b*-A)$_2$-*b*–C chains. Here: d – disordered; il3 - inverted lamellae with three internal layers; il5 - inverted lamellae with five internal layers; p - perpendicular lamellar-*in*-lamellar; l3 – parallel lamellae with three internal layers; l5 - parallel lamellae with five internal layers.
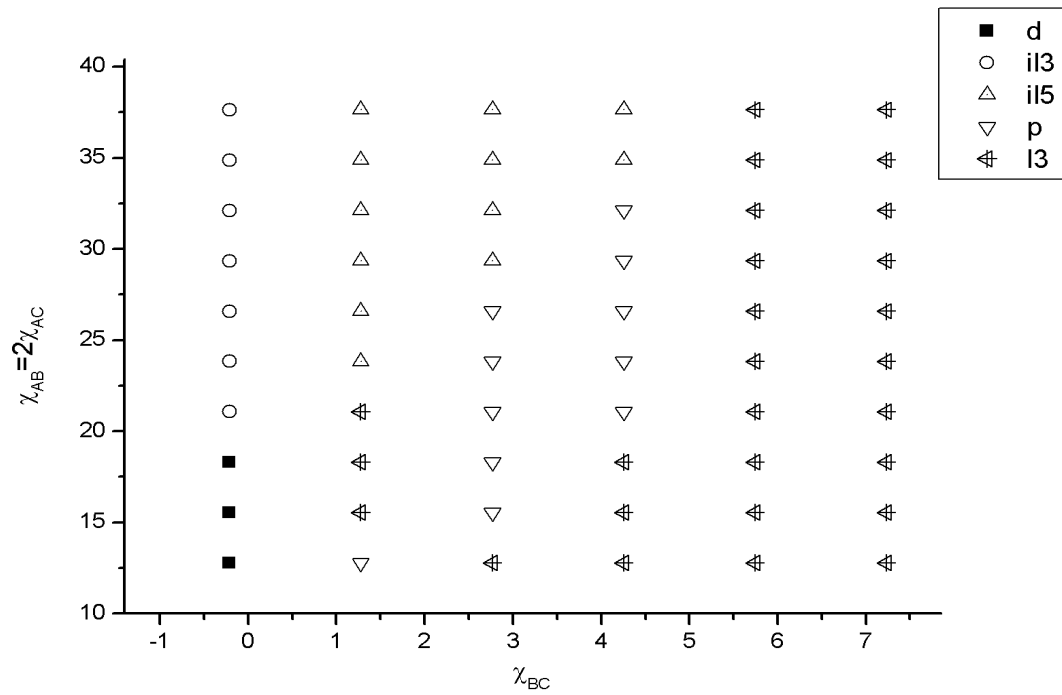
Figure. 3.11. Conformational diagram for polymer melt consist of (B-*b*-A)$_2$-*b*–C chains. For notation see Fig. 3.10.

3.3.3.6 Conclusions

The phase behavior of A-*b*-(B-*b*-A)$_2$-*b*–C and (B-*b*-A)$_2$-*b*–C copolymer melts were investigated using the DPD technique. It was shown that the perpendicular lamellar-*in*-lamellar structure is more likely to occur for the A-*b*-(B-*b*-A)$_2$-*b*–C copolymers. The results are compared with those obtained by SSL (Chapter 2, Part 3.3) and SCFT (Chapter 2, Part 3.5).

3.4 Self-consistent field theory investigation of A-*b*-(B-*b*-A)$_2$–*b*–C and (B-*b*-A)$_2$–*b*–C ternary multiblock copolymer melts

First, the restrictions of the self-consistent field theory approach as applied to ternary block copolymer systems are discussed and a new self-consistent field theory technique is introduced. Then the lamellar-*in*-lamellar structure formation in A-*b*-(B-*b*-A)$_2$-*b*-C and (B-*b*-A)$_2$-*b*-C terpolymer melts, with volume fraction of components A, B and C in the ratio 1:1:2, is analyzed with the self-consistent field theory. Depending on the values of the Flory-Huggins interaction parameters $\chi_{AB}, \chi_{AC}, \chi_{BC}$, the different layers will be parallel or perpendicular. Two types of perpendicular lamellar-*in*-lamellar structures, shifted and not-shifted, are investigated.

3.4.1 Model and the SCFT technique

A SCFT analysis of the phase behavior of A-*b*-(B-*b*-A)$_2$-*b*–C (fig. 3.12a) and (B-*b*-A)$_2$-*b*–C (fig. 3.12b) copolymers with volume fraction of components A, B and C in the ratio 1:1:2 is presented.
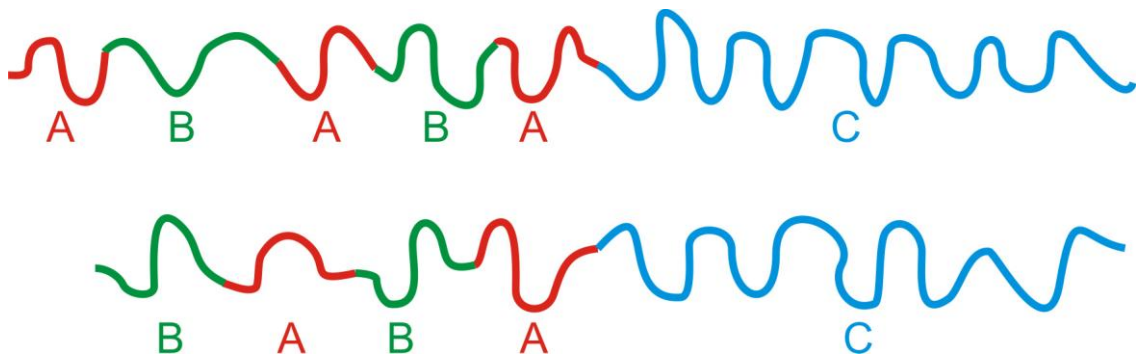
Figure 3.12. Ternary undecablock copolymers. a) A-*b*-(B-*b*-A)$_2$-*b*–C; b) (B-*b*-A)$_2$–*b*-C.

The two strategies that have been applied to solve the SCFT equations are the spectral method [26] and the real-space method. [27-31] The first strategy is based on the representation of the spatially varying density fields in a Fourier-type basis, using a large number of harmonic terms.[32] The second computational formalism employs an

appropriate relaxation iterative procedure in order to reach a local minimum of the free energy functional, adjusting simultaneously the chemical potential fields and the conjugate monomer densities at every iteration step. Both schemes have advantages and disadvantages. A disadvantage of the fully spectral schemes is that the computational effort per single iteration scales very poorly as nF^3, where nF is the number of basis functions. Also, it requires that the symmetry of a formed microstructure be specified in advance so that a proper set of harmonic terms can be utilized. The real-space methods do not require the system symmetry in advance but are rather time consuming in three dimensions even on supercomputers. Recent progress in this field has been achieved by using the so-called pseudo-spectral technique. [33-36] In the context of polymer physics, this technique was first applied by Rasmussen and Kalosakas [34] in order to solve the modified diffusion equation that describes the propagation of monomer densities. Subsequently, Ceniceros and Fredrickson [35] further extended this approach. In particular, they introduced a robust class of semi-implicit numerical methods that employ supplementary information about the nonlocal density operators. As a result, the total computational cost has been reduced by an order of magnitude. Another way to speed up convergence of the SCFT equations for polymeric systems, we employ here, is to use the iterative scheme by Ng, [37] linearizing the solution around stationary points. A similar procedure was used by Thompson *et al.* [38]. We believe that incompressible multicomponent block copolymers need a new SCFT technique due to the degeneracy problem taking place when the χ-parameters belong to some specified set. This degeneracy problem has not been considered yet. The new technical details can be easily understood in the case of incompressible three-component block copolymers.

To discuss this we consider an incompressible melt of linear ternary ABC triblock copolymers consisting of end blocks A and C and middle block C. The free energy functional for the system under consideration reads [27]:

$$
\begin{aligned}
F/nk_BT = V^{-1}\int d^3\mathbf{r}[&\chi_{AB}\lambda_A(\mathbf{r})\lambda_B(\mathbf{r}) + \chi_{BC}\lambda_B(\mathbf{r})\lambda_C(\mathbf{r}) + \chi_{AC}\lambda_A(\mathbf{r})\lambda_C(\mathbf{r}) \\
&- w_A(\mathbf{r})\lambda_A(\mathbf{r}) - w_B(\mathbf{r})\lambda_B(\mathbf{r}) - w_C(\mathbf{r})\lambda_C(\mathbf{r}) + \xi(\mathbf{r})(\lambda_A(\mathbf{r}) + \lambda_B(\mathbf{r}) + \lambda_C(\mathbf{r}))] \\
&- V\ln Q\big(\{w_\alpha(\mathbf{r})\}\big)
\end{aligned}
$$

$$(3.30)$$

where the Flory-Huggins parameters $\chi_{\alpha\beta}$ describe the interaction between the monomers of the sorts α and β, $V-$ is the volume of the system, n is the total number of chains in the volume V, k_B is Boltzmann's constant and T is the absolute (Kelvin) temperature. From here on we set $k_B = 1$ (in other words, we measure the temperature

in energetic units). The deviation of the local volume fraction $\varphi_\alpha(\mathbf{r})$ of component α from its average (over the volume V) value f_α is designated in (3.30) as follows:

$$\lambda_\alpha(\mathbf{r}) = \varphi_\alpha(\mathbf{r}) - f_\alpha \tag{3.31}$$

The quantity $Q(\{w_\alpha(\mathbf{r})\})$ is the partition function of a single ideal chain subject to the external fields $w_\alpha(\mathbf{r})$, acting on the component α

$$Q(\{w_\alpha(\mathbf{r})\}) = V^{-1} \int d^3\mathbf{r}\, q(\mathbf{r},1) \tag{3.32}$$

where the density distribution $q(\mathbf{r},s)$ satisfies the modified diffusion equation

$$\partial q(\mathbf{r},s)/\partial s = \nabla^2 q(\mathbf{r},s) - \psi(\mathbf{r},s)q(\mathbf{r},s), \qquad q(\mathbf{r},0) = 1 \tag{3.33}$$

in which the variable $s \in [0,1]$ labels the monomer's relative distance from an end of the chain, therewith the field $\psi(\mathbf{r},s) = w_\alpha(\mathbf{r})$ in case the monomer located on the distance s belongs to the sort α. Finally, $\xi(\mathbf{r})$ is the Lagrange multiplier corresponding to the incompressibility condition:

$$\lambda_A(\mathbf{r}) + \lambda_B(\mathbf{r}) + \lambda_C(\mathbf{r}) = 0 \tag{3.34}$$

When we consider the melt in bulk then we stipulate periodic boundary conditions on the computation cell boundaries; when the melt is confined then some special boundary conditions have to be used that will have to be defined more precisely.

Varying the free energy functional (3.30) both over the fields $w_\alpha(\mathbf{r})$ and volume fractions $\varphi_\alpha(\mathbf{r})$, one gets the full set of the self-consistent field equations:

$$w_A(\mathbf{r}) = \chi_{AB}\lambda_B(\mathbf{r}) + \chi_{AC}\lambda_C(\mathbf{r}) + \xi(\mathbf{r}) \tag{3.35}$$

$$w_B(\mathbf{r}) = \chi_{AB}\lambda_A(\mathbf{r}) + \chi_{BC}\lambda_C(\mathbf{r}) + \xi(\mathbf{r}) \tag{3.36}$$

$$w_C(\mathbf{r}) = \chi_{AC}\lambda_A(\mathbf{r}) + \chi_{BC}\lambda_B(\mathbf{r}) + \xi(\mathbf{r}) \tag{3.37}$$

appended by the incompressibility condition (5).

Therewith, the local volume fractions $\varphi_A(\mathbf{r})$, $\varphi_B(\mathbf{r})$ and $\varphi_C(\mathbf{r})$ are defined by equations

$$\varphi_A(\mathbf{r}) = \frac{1}{Q[w_A, w_B, w_C]} \int_0^1 ds\, \sigma_A(s) q(\mathbf{r},s) \tilde{q}(\mathbf{r},1-s) \tag{3.38}$$

$$\varphi_B(\mathbf{r}) = \frac{1}{Q[w_A, w_B, w_C]} \int_0^1 ds\, \sigma_B(s) q(\mathbf{r},s) \tilde{q}(\mathbf{r},1-s) \tag{3.39}$$

$$\varphi_C(\mathbf{r}) = \frac{1}{Q[w_A, w_B, w_C]} \int_0^1 ds\, \sigma_C(s) q(\mathbf{r},s) \tilde{q}(\mathbf{r},1-s) \tag{3.40}$$

where the multiplier $\sigma_\alpha(s) = 1$ in case the monomer located on the distance s belongs to the sort α, and $\sigma_\alpha(s) = 0$ otherwise.

The distribution function $\tilde{q}(\mathbf{r},s)$ satisfies the modified diffusion equation

$$\partial \tilde{q}(\mathbf{r},s)/\partial s = \nabla^2 \tilde{q}(\mathbf{r},s) - \psi(\mathbf{r},1-s)\tilde{q}(\mathbf{r},s), \qquad \tilde{q}(\mathbf{r},0) = 1 \tag{3.41}$$

with the same boundary conditions as in the case of eq. (3.33).

Eqs. (3.34)-(3.37) can be considered as simultaneous linear equations with respect to the variables $\lambda_\alpha(\mathbf{r}) = \varphi_\alpha(\mathbf{r}) - f_\alpha$ and $\xi(\mathbf{r})$:

$$\begin{pmatrix} w_A \\ w_B \\ w_C \\ 0 \end{pmatrix} = \begin{pmatrix} 0 & \chi_{AB} & \chi_{AC} & 1 \\ \chi_{AB} & 0 & \chi_{BC} & 1 \\ \chi_{AC} & \chi_{BC} & 0 & 1 \\ 1 & 1 & 1 & 0 \end{pmatrix} \begin{pmatrix} \lambda_A \\ \lambda_B \\ \lambda_C \\ \xi \end{pmatrix} \tag{3.42}$$

If the matrix

$$M = \begin{pmatrix} 0 & \chi_{AB} & \chi_{AC} & 1 \\ \chi_{AB} & 0 & \chi_{BC} & 1 \\ \chi_{AC} & \chi_{BC} & 0 & 1 \\ 1 & 1 & 1 & 0 \end{pmatrix}$$

(3.43)

is not degenerate then the auxiliary field $\xi(\mathbf{r})$, which assures that the incompressibility condition (3.34) is fulfilled, can be expressed in terms of the fields $\{w_\alpha(\mathbf{r})\}$ and, thus, eliminated:

$$\xi = \frac{C_2 C_3 (w_A + w_B) + C_1 C_3 (w_B + w_C) + C_1 C_2 (w_A + w_C)}{2(C_1 C_2 + C_2 C_3 + C_1 C_3)}$$

(3.44)

Where

$$C_1 = \chi_{AC} + \chi_{BC} - \chi_{AB}, \quad C_2 = \chi_{AC} + \chi_{AB} - \chi_{BC}, \quad C_3 = \chi_{AB} + \chi_{BC} - \chi_{AC} \quad (3.43)$$

The set of equations (3.34)-(3.41) can be represented as a non-linear operator

$$x = A[x]$$

(3.46)

with respect to an unknown vector-function

$$x = (w_A(\mathbf{r}), w_B(\mathbf{r}), w_C(\mathbf{r}))$$

(3.47)

Here the operator A is defined as follows:

$$A[x] = \begin{pmatrix} \chi_{AB}(\varphi_B(\mathbf{r}) - f_B) + \chi_{AC}(\varphi_C(\mathbf{r}) - f_C) + \xi(\mathbf{r}) \\ \chi_{AB}(\varphi_A(\mathbf{r}) - f_A) + \chi_{BC}(\varphi_C(\mathbf{r}) - f_C) + \xi(\mathbf{r}) \\ \chi_{AC}(\varphi_A(\mathbf{r}) - f_A) + \chi_{BC}(\varphi_B(\mathbf{r}) - f_B) + \xi(\mathbf{r}) \end{pmatrix} \qquad (3.48)$$

where the functions $\varphi_\alpha(\mathbf{r})$ are expressed in terms of the fields $w_A(\mathbf{r})$, $w_B(\mathbf{r})$ and $w_C(\mathbf{r})$ via the integral operators (3.38) - (3.40) and the auxiliary field $\xi(\mathbf{r})$ is given via equalities (3.42) – (3.44). The operator equation (3.46) can be solved using the Picard iteration procedure

$$x_{n+1} = x_n + \tau(A[x_n] - x_n), \qquad n = 0,1,2,... \qquad (3.49)$$

with a positive parameter τ.

To speed up the iteration procedure convergence, after certain number of the Picard iterations (3.47) one should switch to the iteration method by Ng, which is characterized by a faster convergence. The details of the Ng method are described in [37,40].

If the matrix (3.43) is degenerate then it can be shown that the Flory-Huggins parameters $\chi_{\alpha\beta}$ satisfy the Hildebrand condition[39]

$$\chi_{\alpha\beta} \sim (\delta_\alpha - \delta_\beta)^2 \qquad (3.50)$$

where δ_α are so-called Hildebrand solubility parameters.

Indeed, the determinant of the matrix (14) $\Delta = 2(C_1C_2 + C_2C_3 + C_1C_3)$ is a quadratic form of three variables χ_{AB}, χ_{BC} and χ_{AC}. This quadratic form is reducible to the diagonal form via the following change of variables:

$$\chi_{AB} = \frac{x_3}{\sqrt{3}} - \frac{x_2 - x_1}{2\sqrt{2}}, \quad \chi_{BC} = \frac{x_3}{\sqrt{3}} - \frac{x_1 + x_2}{2\sqrt{2}}, \quad \chi_{AC} = \frac{x_2}{\sqrt{6}} + \frac{x_3}{\sqrt{3}} \tag{3.51a}$$

$$x_1 = \sqrt{2}\left(\chi_{AB} - \chi_{BC}\right), \quad x_2 = \sqrt{6}\,\frac{2\chi_{AC} - \chi_{AB} - \chi_{BC}}{3}, \quad x_3 = \frac{\chi_{AB} + \chi_{BC} + \chi_{AC}}{\sqrt{3}} \tag{3.51b}$$

In terms of the new variables, the determinant of the matrix (3.43) reads $\Delta = -x_1^2 - x_2^2 + 2x_3^2$, which implies that the degeneration condition for the matrix $\Delta = 0$ holds on the cone surface in the space (x_1, x_2, x_3), the upper inner part of the cone $x_3 \geq \sqrt{\left(x_1^2 + x_2^2\right)/2}$ describes the region where the self-consistent approximation is physically applicable (outside of the region the SCFT solution corresponds to a saddle point or maximum rather than to a minimum of the free energy). Introducing new variables

$$\chi_0 = \sqrt{2\,\frac{\left(x_1^2 + x_2^2\right)}{3}}, \quad \cos\phi = \frac{x_1}{\sqrt{x_1^2 + x_2^2}}, \quad \sin\phi = \frac{x_2}{\sqrt{x_1^2 + x_2^2}}, \quad \varepsilon = \frac{1}{2}\frac{\sqrt{2}x_3 - \sqrt{x_1^2 + x_2^2}}{\sqrt{x_1^2 + x_2^2}} \tag{3.52}$$

We get a trigonometric representation of the three Flory-Huggins parameters:

$$\chi_{AC} = \chi_0 \left(\frac{1 + \sin\phi}{2} + \varepsilon \right)$$

$$\chi_{AB} = \chi_0 \left(\frac{1 + \sin\left(\phi + 2\pi/3\right)}{2} + \varepsilon \right) \tag{3.53}$$

$$\chi_{AB} = \chi_0 \left(\frac{1 + \sin\left(\phi - 2\pi/3\right)}{2} + \varepsilon \right)$$
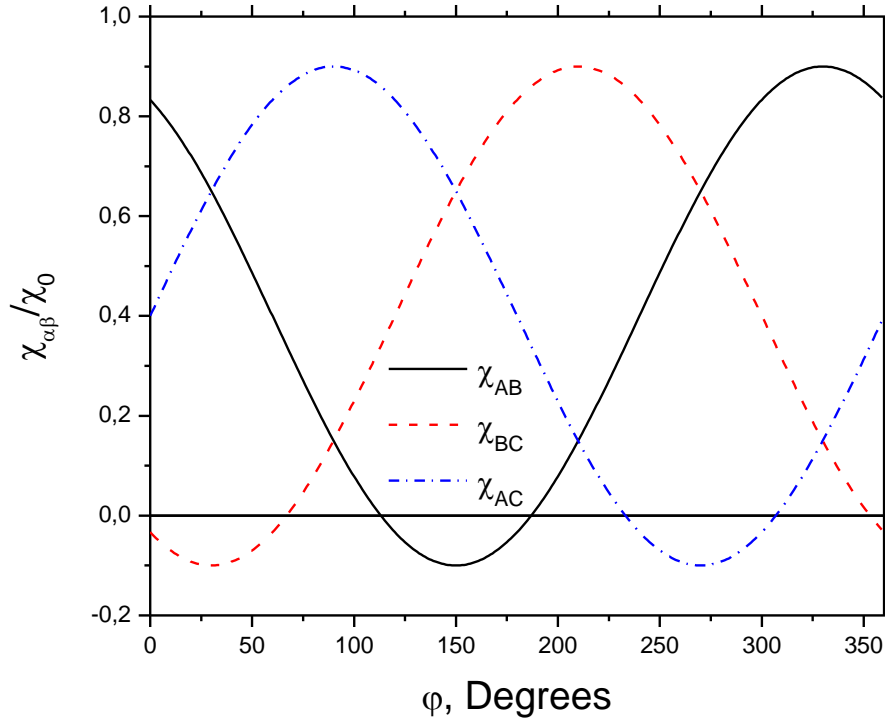
Figure 3.13. The φ-parameter set (24) with $\varepsilon\chi_0 = -0.1$

In the trigonometric variables the determinant Δ takes the form $\Delta = 6\varepsilon\chi_0^2(\varepsilon+1)$. The region $\varepsilon \geq 0$ coincides with the upper inner part of the cone $x_3 \geq \sqrt{\left(x_1^2 + x_2^2\right)/2}$. If the value of ε is fixed, the point $(\chi_{AB}, \chi_{BC}, \chi_{AC})$ defined by Eqs.(3.53) belongs to the φ-parameter set represented by three curves in Fig. 3.13. If $\varepsilon \geq 0$, these curves lie in the upper halfplane $(\varphi, \chi_{\alpha\beta})$. Otherwise $(\varepsilon < 0)$, this set contains points $(\chi_{AB}, \chi_{BC}, \chi_{AC})$ with $\chi_{\alpha\beta} < 0$. Notice that if $\varepsilon < 0$, the iterations (3.49) do not converge for any point $(\chi_{AB}, \chi_{BC}, \chi_{AC})$ belonging to the set (3.53), including the case $\chi_{AB} > 0$, $\chi_{BC} > 0$, $\chi_{AC} > 0$.

Now, let the matrix (3.43) be degenerate (ε=0), and, for definiteness, let $\chi_{AB} = \max(\chi_{AB}, \chi_{AC}, \chi_{BC})$. Then it follows from (3.53) that

$$\sqrt{\frac{\chi_{AC}}{\chi_{AB}}} + \sqrt{\frac{\chi_{BC}}{\chi_{AB}}} = 1 \tag{3.54}$$

It is easy to show that Eq.(3.54) is equivalent to the Hildebrand conditions (3.50). Let designate the second addendum in the left hand side of eq. (3.54) as g:

$$g = \sqrt{\chi_{BC}/\chi_{AB}} \qquad (3.55)$$

We can show now that if the Hildebrand approximation is valid then the simultaneous equations (3.30)- (3.41) for the three-component ABC triblock copolymer are equivalent to those for the two-component AB multiblock copolymer shown in Fig. 3.14.

In this case *i*) the field $w_C(\mathbf{r})$ can be expressed as a linear combination of the fields $w_A(\mathbf{r})$ and $w_B(\mathbf{r})$:

$$w_C(\mathbf{r}) = g w_A(\mathbf{r}) + (1-g) w_B(\mathbf{r}) \qquad (3.56)$$

and *ii*) formally, the original three-component system of triblock copolymers becomes equivalent to the two-component system of triblock copolymers in which the middle block C can be represented as a mixture of the A and B monomers with fractions g and *1-g* of the sorts A and B, respectively:

.

Figure 3.14. Cartoon explaining the idea of the SCFT implementation for the degenerated system of the χ-parameters appearing in the case of the Hildebrand Approximation.

$$\varphi_C(\mathbf{r}) = g\varphi_A(\mathbf{r}) + (1-g)\varphi_B(\mathbf{r}) \tag{3.57}$$

Let g_A, g_B and $\mu_A(\mathbf{r})$, $\mu_B(\mathbf{r})$ be the average and local volume fractions of the components A and B, respectively, for the two-component multiblock copolymer shown in Fig.3.14. One can check readily that

$$\mu_A(\mathbf{r}) = \phi_A(\mathbf{r}) + g\phi_C(\mathbf{r}), \quad \mu_B(\mathbf{r}) = \phi_B(\mathbf{r}) + (1-g)\phi_C(\mathbf{r}) \tag{3.58a}$$

$$g_A = f_A + gf_C, \quad g_B = f_B + (1-g)f_C \tag{3.58b}$$

Substitution of the relations (3.58) into eqs. (3.34)-(3.37) shows that the latter are equivalent to equations

$$w_A(\mathbf{r}) = \chi_{AB}(\mu_B(\mathbf{r}) - g_B) + \eta(\mathbf{r}) \tag{3.59a}$$

$$w_B(\mathbf{r}) = \chi_{AB}(\mu_A(\mathbf{r}) - g_A) + \eta(\mathbf{r}) \tag{3.59b}$$

$$\mu_A(\mathbf{r}) + \mu_B(\mathbf{r}) = 1 \tag{3.59c}$$

where

$$\eta(\mathbf{r}) = \left(w_A(\mathbf{r}) + w_B(\mathbf{r})\right)/2, \quad \xi(\mathbf{r}) = \eta(\mathbf{r}) + \chi_{AB}g(1-g)(g\phi_A(\mathbf{r}) + (1-g)\phi_B(\mathbf{r}) - f_C)$$

Recall that solution of the self-consistent field equations for two-component copolymer melts can be achieved via iteration procedures as described in ref [15].

It is also worth to consider explicitly small values of the parameter ε corresponding to the ill-conditioned matrix (3.43) since the iterative algorithm (3.49) becomes unstable when $\varepsilon \to 0$. The physical solutions correspond to positive values of the parameter ε ($\Delta > 0$). The longest block C can be represented as a mixture of A, B, and D monomers:
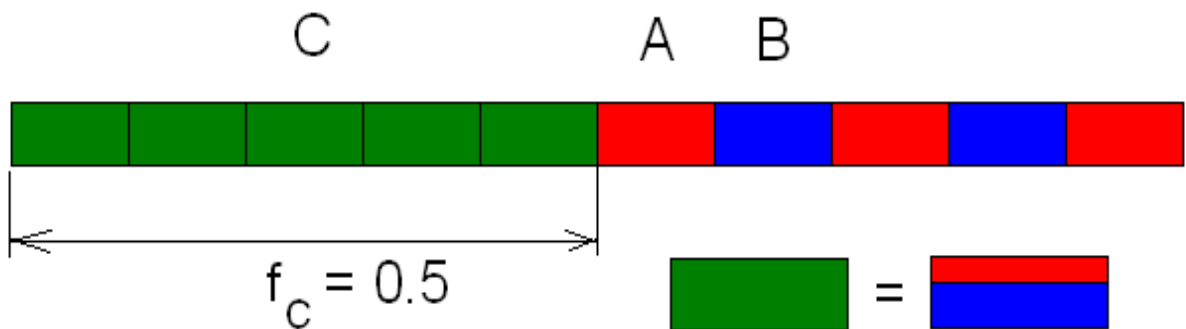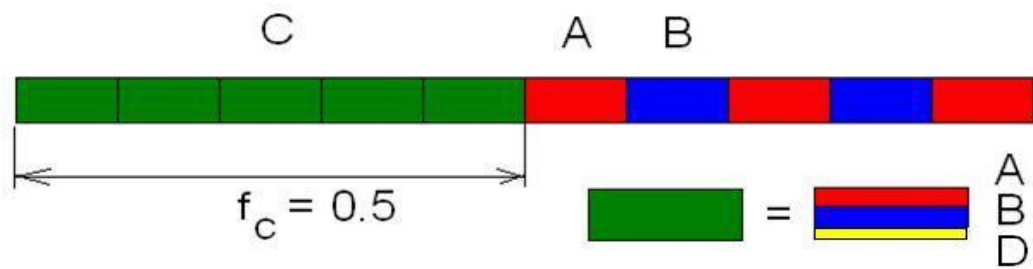
Figure 3.15. Cartoon explaining the idea of the SCFT implementation for the ill-conditioned system of χ-parameters appearing close to the Hildebrand Approximation ($\varepsilon \to 0$).

Species D is found in such a way that the three parameters χ_{AB}, χ_{BD}, and χ_{AD} are far enough from Hildebrand condition (3.54). Then the matrix (3.43), where the parameters χ_{AB}, χ_{BC}, and χ_{AC} are replaced by χ_{AB}, χ_{BD}, and χ_{AD}, is well-conditioned. E.g., the parameters χ_{AB}, χ_{BD}, and χ_{AD} may be the sides of a triangle (see Fig.3.16). The best choice is the equilateral triangle.
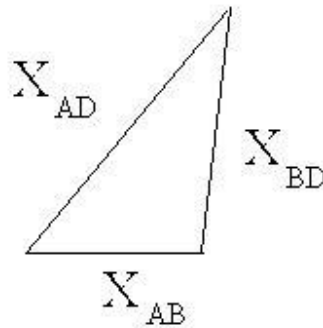
Figure 3.16. The triangle with side lengths χ_{AB}, χ_{BD}, and χ_{AD}.

To find the composition of C block consisting of A, B, and D species providing the prescribed values of χ_{AB}, χ_{BC}, χ_{AC} we consider the block C as composed of the species D and E (see Fig. 3.17).
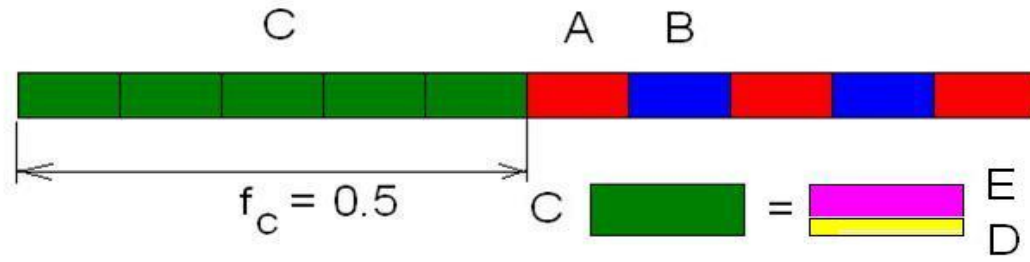
Figure 3.17. Cartoon explaining the idea of representing block C as a mixture of the species D and E.

It can be shown readily that

$$\chi_{AC} = (1 - g_E)\chi_{AD} + g_E\chi_{AE} - g_E(1 - g_E)\chi_{DE} \tag{3.60a}$$

$$\chi_{BC} = (1 - g_E)\chi_{BD} + g_E\chi_{BE} - g_E(1 - g_E)\chi_{DE} \tag{3.60b}$$

where g_E is the volume fraction of E in block C. Notice that E is a mixture consisting of A and B with a volume fraction g_A of A monomer units. Therefore,

$$\chi_{AE} = (1 - g_A)^2 \chi_{AB} \tag{3.61a}$$

$$\chi_{BE} = g_A^2 \chi_{AB} \tag{3.61b}$$

$$\chi_{DE} = (1 - g_A)\chi_{BD} + g_A\chi_{AD} - g_A(1 - g_A)\chi_{AB} \tag{3.61c}$$

Eqs. (3.60)-(3.61) can be considered as the conditions that determine the parameters g_A and g_E. The parameters χ_{BC}, χ_{AC}, χ_{AB}, χ_{AD}, and χ_{BD} are assumed to be known. The parameter g_A can be eliminated. The parameter g_E is the root of the quadratic equation

$$p(1 - g_E)^2 - q = 0 \tag{3.62}$$

with

$$p = a - b^2/2 - 1/2, \qquad q = c - d^2/2 - 1/2, \qquad \text{(3.63a)}$$

$$a = \chi_{AB}^{-1}(\chi_{AD} + \chi_{BD}), \qquad b = \chi_{AB}^{-1}(\chi_{AD} - \chi_{BD}), \qquad \text{(3.63b)}$$

$$c = \chi_{AB}^{-1}(\chi_{BC} + \chi_{AC}), \qquad d = \chi_{AB}^{-1}(\chi_{BC} - \chi_{AC}), \qquad \text{(3.63c)}$$

If $p/q > 0$, equation (3.62) has two real roots. Only the roots g_E and g_A, which belong to the interval (0,1), have physical meaning. Finally, the desired solution of eqs. (3.60)-(3.61) reads

$$g_E = 1 - \sqrt{p/q}, \; g_A = [1 - b + (d + b)/g_E]/2 \qquad \text{(3.64)}$$

As a result, we obtain a mathematically equivalent polymer system with the C block (see Fig. 3.15) consisting of monomer units A, B, and D. This system is described by eqs. (3.34)-(3.41), where C is replaced by D. The recalculated average volume fractions of A, B, and D are

$$f_A' = f_A + f_C g_E g_A, \; f_B' = f_B + f_C g_E (1 - g_A), \; f_D' = f_C(1 - g_E) \qquad \text{(3.65)}$$

For the results presented further on, the calculations in the region near the Hildebrand line were carried out using the equilateral triangle with the side lengths $\chi_{AD} = \chi_{BD} = \chi_{AB}$. The contour step size was taken to be equal to $\Delta s = 0.01$. Smaller values were tested as well, but had no effect on the free energy value. The simulations were done in two dimensions with periodic boundary conditions because all observed structures are 2D. The free energy was optimized with respect to the size of simulation box. The spatial resolutions were equal to $\Delta x = 0.03 R_g$, $\Delta y = 0.015 R_g$. The numerical simulations proceeded until the relative free energy changes at each iteration were smaller than 10^{-5} and the incompressibility condition was achieved.

3.4.2 Results and discussions

Using the SCFT outlined in the previous section we calculated phase diagrams for (B-*b*-A)$_2$-*b*–C (Fig. 3.18) and A-*b*-(B-*b*-A)$_2$-*b*–C (Fig. 3.19) as a function of $N\chi_{BC}$ and $N\chi_{AB} = 2N\chi_{AC}$, up to and including the Hildebrand line where the solubility parameter approximation holds. As shown in the Section 2, the Hildebrand line satisfies Eq. (3.54). In the case of $N\chi_{AB} = 2N\chi_{AC}$ considered, this implies $N\chi_{AB} = 11.66 N\chi_{BC}$. The composition of both multiblock copolymers is assumed to satisfy $\varphi_C = 0.5$, $\varphi_A = \varphi_B = 0.25$. N denotes the total length of the multiblock copolymer.

Figure 3.18 Phase diagram of (B-*b*-A)$_2$-*b*–C as a function of $N\chi_{BC}$ and $N\chi_{AB} = 2N\chi_{AC}$. $LAM_{\parallel}$, $LAM_{\perp}$ and $SLAM_{\perp}$ denote the parallel, the perpendicular and the shifted perpendicular layered morphologies. The number in between brackets, i.e. $LAM_{\parallel}(5)$, denotes the total number of "internal"A plus B layers. Circles represent the points where the transitions occur according to the calculations.

Under the conditions selected, the multiblock copolymers self-assemble in three different morphologies $LAM_\parallel$, $LAM_\perp$ and $SLAM_\perp$. These denote the parallel lamellar-*in*-lamellar, the perpendicular lamellar-*in*-lamellar and the shifted perpendicular lamellar-*in*-lamellar structure. In the $LAM_\parallel$ a parallel layered structure is formed, where the layer in between successive C-layers contains a number of A- and B-layers. The precise number of "internal" layers depends on the multiblock copolymer and the values of the interaction parameters and is indicated by the number in between brackets, i.e. $LAM_\parallel(3)$ denotes 3 internal layers (A-B-A). In the $LAM_\perp$ morphology the "internal" A- and B-block layers are oriented perpendicularly to the C-layers. The same is true for the $SLAM_\perp$ structure except that now the successive "internal" layers are shifted with respect to each other over half the long period of the A/B structure (see also Figures 3.23 and 3.24 further on).

Figure 3.18 shows the phase diagram of the (B-*b*-A)$_2$ -*b*–C multiblock copolymer and demonstrates the stability of both perpendicular lamellar-*in*-lamellar structures. In the interaction parameter region covered the parallel lamellar-*in*-lamellar structure contains 5 internal layers. Note that 9 would be the maximum number. Figure 3.19 presents the phase diagram of the A-*b*-(B-*b*-A)$_2$-*b*–C multiblock copolymer. Significant differences with the previous diagram are the absence of a stability region for the $LAM_\perp$ structure, the appearance of $LAM_\parallel(5)$ and a small region of the simple lamellar structure *L* where C-rich layers microphase separate from mixed A- and B-rich layers. Figure 3.20 illustrates the composition profile for the latter case. Furthermore, the position of the ODT line in both figures differ due to the increased number of A blocks in A-*b*-(B-*b*-A)$_2$ -*b*–C and the concurrent smaller length of the A blocks. But even more striking is the increase of the $SLAM_\perp$ region of the A-*b*-(B-*b*-A)$_2$-*b*–C multiblock copolymer for increasing $N\chi_{AB} = 2N\chi_{AC}$, whereas exactly the opposite happens for the (B-*b*-A)$_2$ -*b*–C multiblock copolymers. In the latter case the $SLAM_\perp$ region diminishes as a function of $N\chi_{AB} = 2N\chi_{AC}$ to the expense of the $LAM_\parallel(5)$ region.
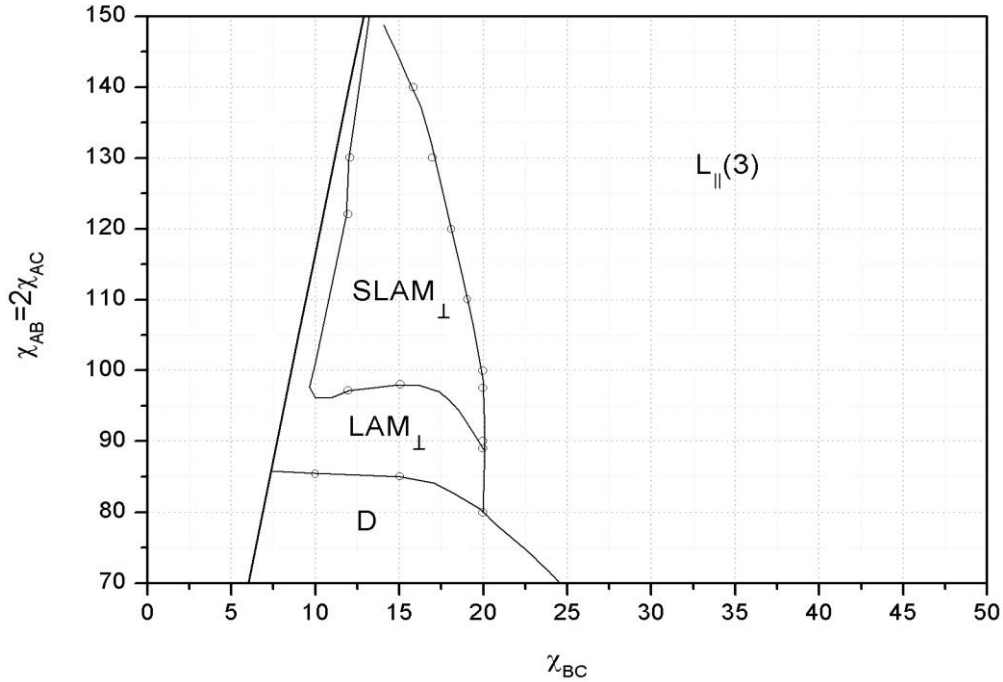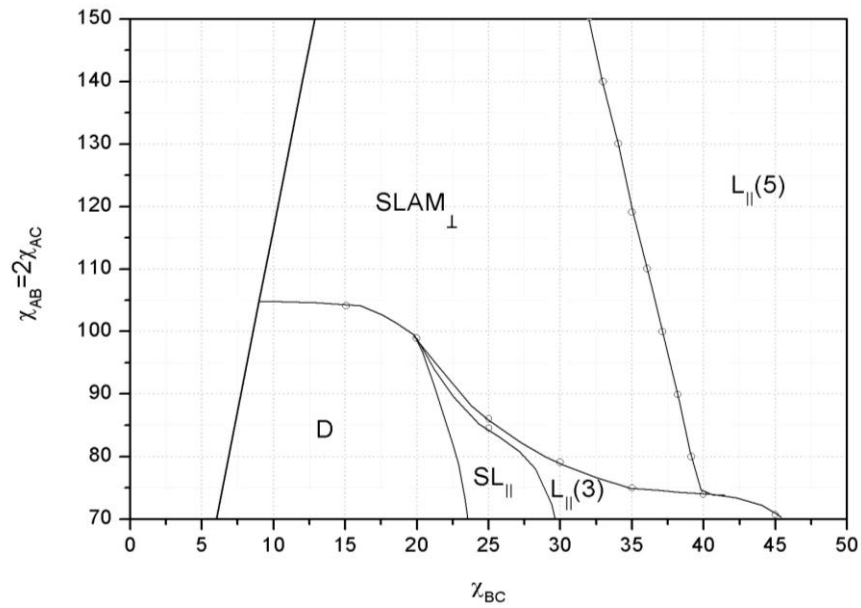
Figure 3.19. Phase diagram of A-*b*-(B-*b*-A)$_2$-*b*–C as a function of $N\chi_{BC}$ and $N\chi_{AB} = 2N\chi_{AC}$. $LAM_{\parallel}$, $LAM_{\perp}$ and $SLAM_{\perp}$ denote the parallel, the perpendicular and the shifted perpendicular lamellar-*in*-lamellar morphologies. The number in between brackets, i.e. $LAM_{\parallel}(5)$, denotes the total number of "internal" A plus B layers. Circles represent the points where the transitions occur according to the calculations.
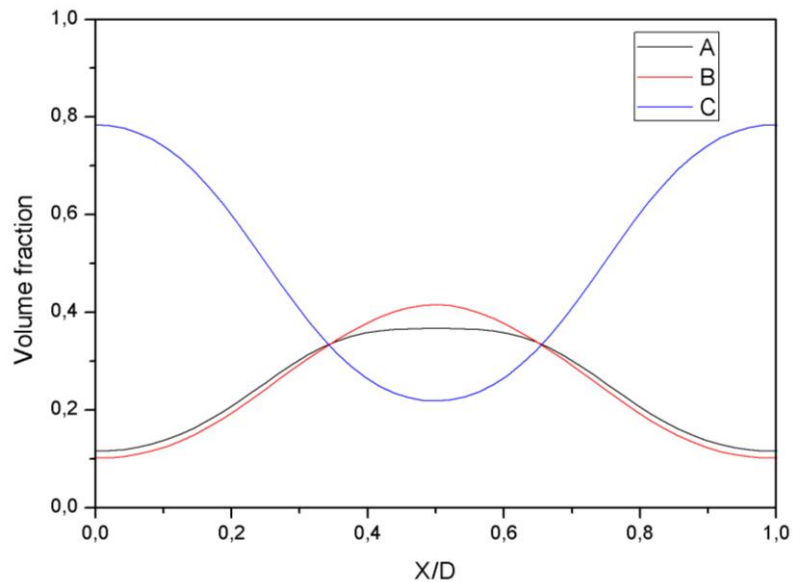
Figure 3.20. Composition profile of A-*b*-(B-*b*-A)$_2$-*b*-C for simple lamellar structure for $N\chi_{AB} = 2N\chi_{AC} = 80$ and $N\chi_{BC} = 24$

To discuss the self-assembly characteristics in more detail we will consider specific points of the phase diagram.

Figure 3.21 shows the volume densities maps for the parallel lamellar-*in*-lamellar structure $LAM_\parallel$ of A-(B-*b*-A)$_2$-*b*–C for $N\chi_{AB} = 2N\chi_{AC} = 100$ and $N\chi_{BC} = 40$. In this particular case 2 A-layers and 1 B-layer are formed in between two successive C-layers. For a slightly larger value of $N\chi_{AB} = 2N\chi_{AC} = 120$ (Figure 3.22) the number of internal A- resp. B-layers increases to 3 resp. 2.

a)   b)   c)
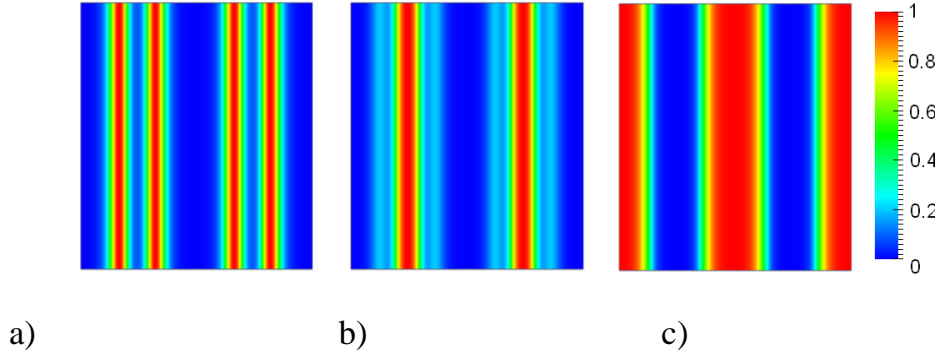
Figure 3.21. Volume density maps for the parallel lamellar-*in*-lamellar $LAM_\parallel$ structure of A-*b*-(B-*b*-A)$_2$-*b*–C with two A-type internal layers at $N\chi_{AB} = 2N\chi_{AC} = 100$ and $N\chi_{BC} = 40$. a) A blocks; b) B blocks; c) C blocks

a)   b)   c)
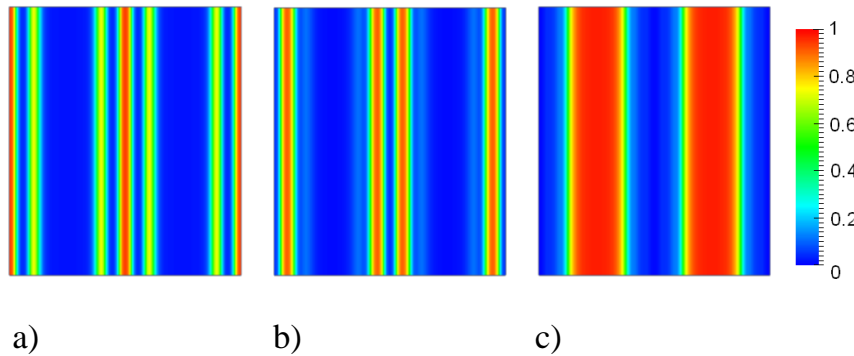
Figure 3.22. Volume density map for the parallel lamellar-*in*-lamellar structure $LAM_\parallel$ of A-*b*-(B-*b*-A)$_2$-*b*–C with three A-type internal layers at $N\chi_{AB} = 2N\chi_{AC} = 120$ and $N\chi_{BC} = 40$. a) A blocks; b) B blocks; c) C blocks.

Figure 3.23 shows the composition profiles in more detail. Besides the strong peaks corresponding to the various layers there are two additional smaller peaks due to the presence of B-blocks, which are not directly linked to the C-blocks, at the A/C interface. This is, obviously, due to the least unfavorable BC interactions, i.e. $N\chi_{BC} = 40$.
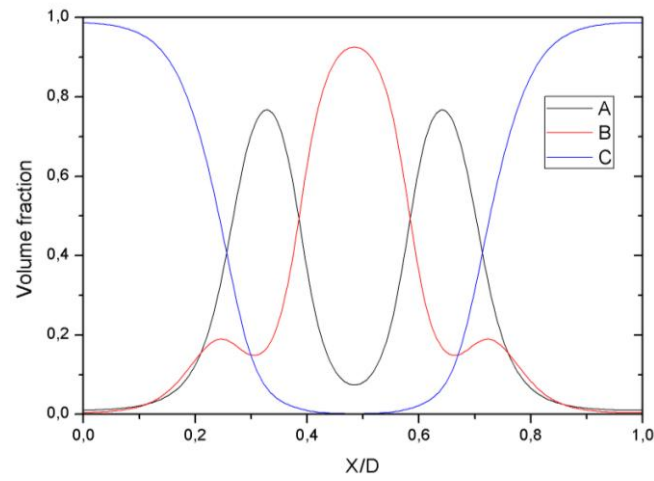
a)
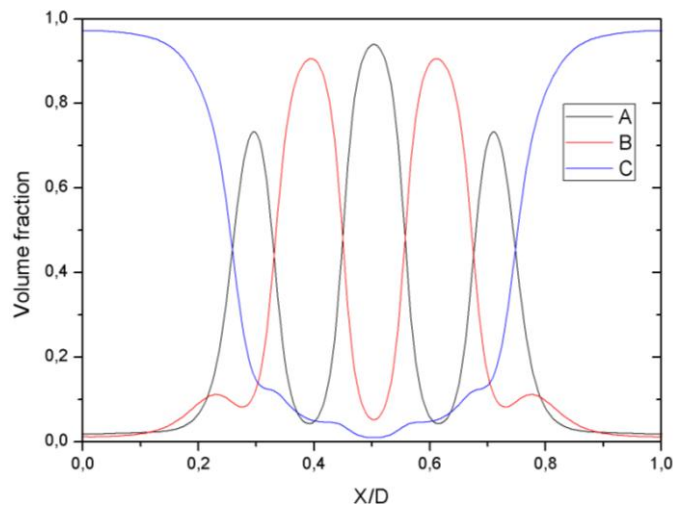
b)

Figure 3.23. Composition profiles of A-*b*-(B-*b*-A)₂-*b*–C
for parallel lamellar-*in*-lamellar $LAM_\parallel$ with

a) $N\chi_{AB} = 2N\chi_{AC} = 100$ and $N\chi_{BC} = 40$;

b) $N\chi_{AB} = 2N\chi_{AC} = 120$ and $N\chi_{BC} = 40$.

Next we turn our attention to smaller values of $N\chi_{BC} = 20$, where the perpendicular lamellar-*in*-lamellar structure becomes favorable. Figures 3.24-3.26 show the $LAM_\perp$ resp. $SLAM_\perp$ morphology for the A-*b*-(B-*b*-A)$_2$-*b*–C multiblock copolymer. For this particular set of interaction parameter values the $SLAM_\perp$ structure is the stable state and the non-shifted $LAM_\perp$ is a metastable (see phase diagram Fig. 3.19). In fact for the A-*b*-(B-*b*-A)$_2$-*b*–C multiblock copolymer

a)   b)   c)
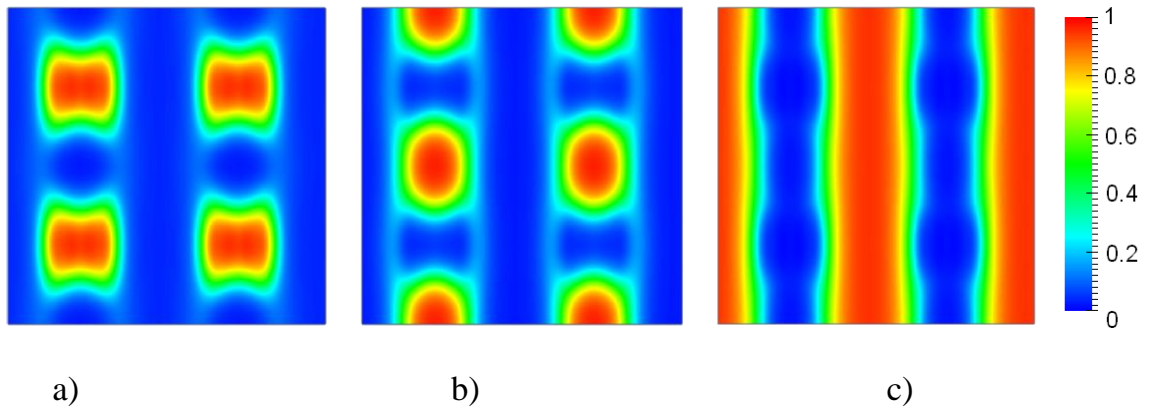
Figure 3.24. Volume density maps for *non-shifted* perpendicular lamellar-*in*-lamellar structure $LAM_\perp$ of A-*b*-(B-*b*-A)$_2$-*b*–C at $N\chi_{AB} = 2N\chi_{AC} = 120$ and $N\chi_{BC} = 20$ a) A blocks; b) B blocks; c) C blocks.

a)   b)   c)
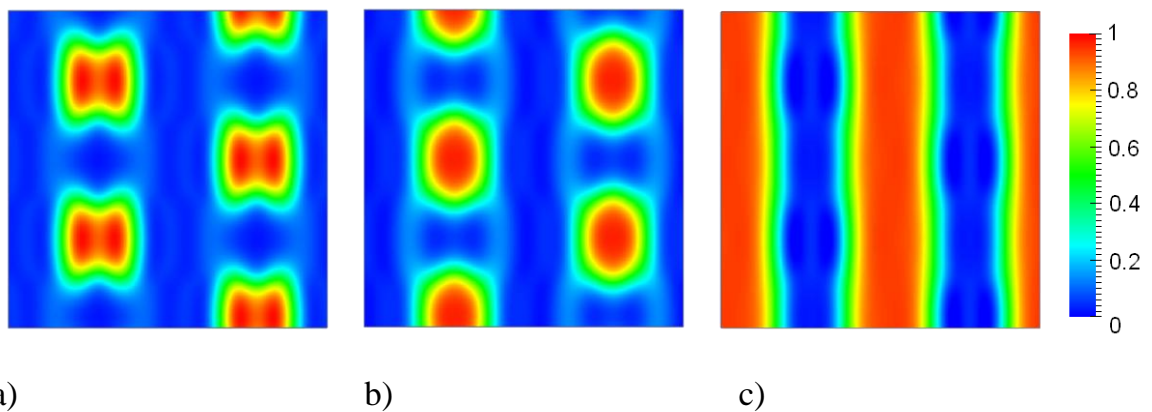
Figure 3.25. The volume density maps of the *shifted* perpendicular lamellar-*in*-lamellar structure $SLAM_\perp$ of A-*b*-(B-*b*-A)$_2$-*b*–C at $N\chi_{AB} = 2N\chi_{AC} = 120$ and $N\chi_{BC} = 20$ a) A blocks; b) B blocks; c) C blocks.

Figures 3.26 and 3.27 present similar composition profile maps for the (B-*b*-A)$_2$ -*b*–C multiblock copolymer for $N\chi_{AB} = 2N\chi_{AC} = 90$, $N\chi_{BC} = 15$ resp. $N\chi_{AB} = 2N\chi_{AC} = 120$ and $N\chi_{BC} = 15$. As shown in the phase diagram Fig. 3.18, in the former case the non-shifted $LAM_\perp$ is the equilibrium state, whereas in the latter case the shifted $SLAM_\perp$ is the equilibrium structure.

a)   b)   c)
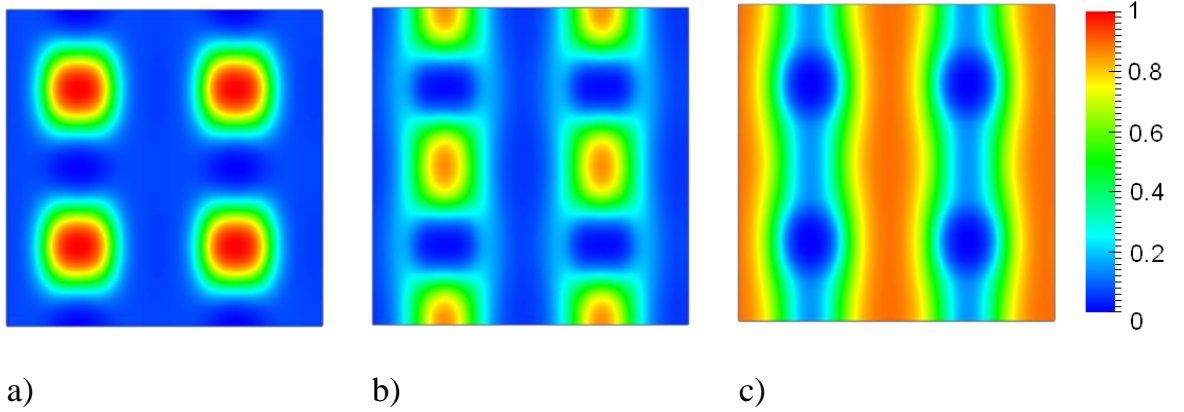
Figure 3.26. Volume density maps for the non-shifted perpendicular lamellar-*in*-lamellar structure $LAM_\perp$ of (B-*b*-A)$_2$ -*b*–C at $N\chi_{AB} = 2N\chi_{AC} = 90$ and $N\chi_{BC} = 15$ a) A blocks; b) B blocks; c) C blocks.

a)   b)   c)
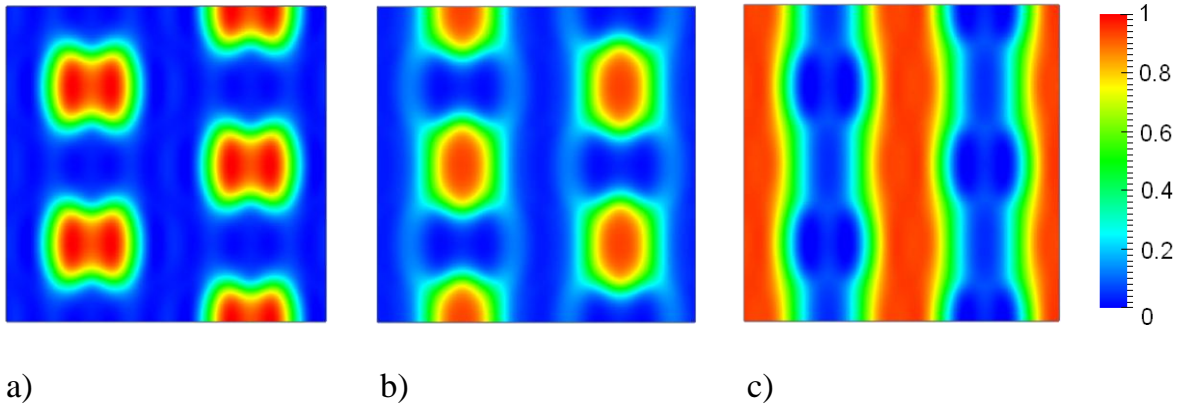
Figure 3.27. Volume density maps of the shifted perpendicular lamellar-*in*-lamellar structure $SLAM_\perp$ of (B-*b*-A)$_2$-*b*–C for $N\chi_{AB} = 2N\chi_{AC} = 120$ and $N\chi_{BC} = 15$ a) A blocks; b) B blocks; c) C blocks.

In order to understand how the copolymer chains fold in the perpendicular lamellar-*in*-lamellar structure ($LAM_\perp$, $SLAM_\perp$) it is useful to present volume density maps for the most relevant parts of the chains. Fig. 3.28a shows the volume density map of the A blocks of (B-*b*-A)$_2$-*b*–C that are directly connected to the long C blocks under conditions where $LAM_\perp$ is the equilibrium state. Because of this connection these A blocks are near the AC interface. The A blocks that are not directly linked to the C blocks form the core of the structure (Fig. 3.28b). The first B blocks that are connected at both ends to A blocks are preferentially present near the AB interface but also near the AC interface where they shield the AC interactions (Fig. 3.28c). The B end blocks form the core of the B domains but are also present at the AC interface (Fig. 3.28d).

a)   b)

c)   d)
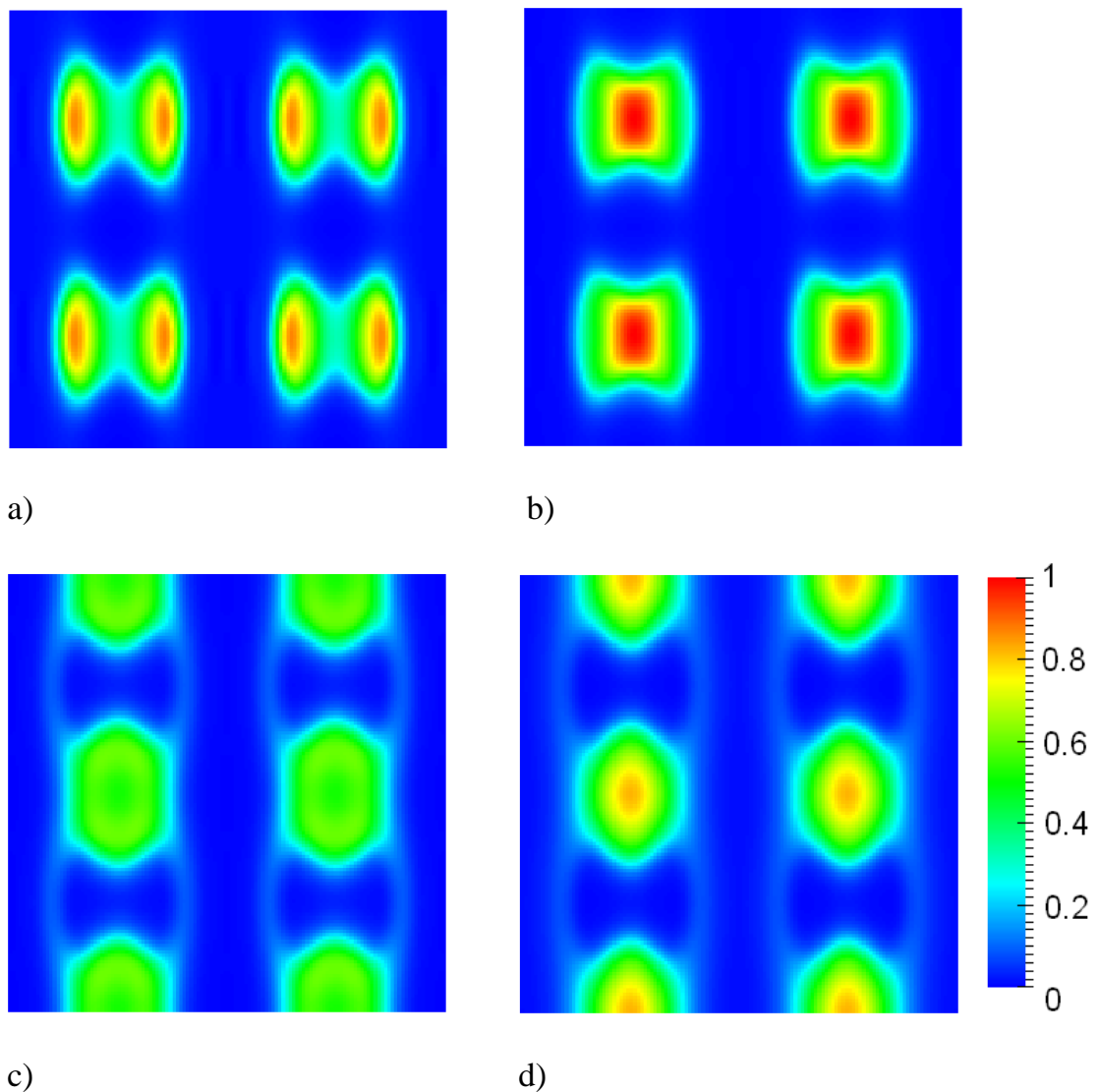
Figure 3.28. Volume density maps of the different A and B blocks of the multiblock part of the (B-*b*-A)₂-*b*–C multiblock copolymers at $N\chi_{AB} = 2N\chi_{AC} = 120$ and $N\chi_{BC} = 12$ where $LAM_\perp$ is the equilibrium state. a) A blocks connected to the C blocks; b) A blocks that are not directly connected to the C blocks; c) the B blocks that are connected at both ends to an A block; d) the B end blocks.

Another interesting issue is the observation that the AC interface is not a straight line for the perpendicular lamellar-*in*-lamellar structures, as would be required to minimize the unfavorable contact between the A and C monomers (Fig. 3.24-3.27). This is due to the fact that the interface is formed by the junction points between the A and C blocks. As discussed in our previous theoretical work, the C blocks have to fill the space that equals that of the A and B blocks together. As a consequence, the C blocks are stretched in the direction perpendicular and parallel to this interface. In order to fill this space uniformly, and in particularly the region opposite the B phase, the polymers should be stretched a lot at the AC interface and much less far away from

the interface. To minimize the stretching close to the interface the shape of the interface becomes curved inwards into the region of the C blocks. The distance between successive AC junction point increases and the stretching energy of the C blocks decreases. Additionally the B blocks that are also present at the AC interface reduce the interfacial energy.

As it is shown in Figs. 3.24c and 3.25c the shape of the interface between the C blocks and the AB blocks looks sinusoidal. In Fig. 3.24c, corresponding to the $LAM_\perp$ structure, the AC interfaces in successive layers are in phase, whereas in Fig. 3.25c, corresponding to $SLAM_\perp$ phase, they are out of phase. Obviously this phenomenon should affect the stretching of the long C blocks. To illustrate this, the volume density maps of the ends of the C blocks are presented in Figure 3.29. For the non-shifted $LAM_\perp$ (Fig. 3.29a) the concentration of the open ends exhibits maxima. Not surprisingly, these are located in the middle of the C layers opposite the middle of the domains formed by the B blocks. In the shifted $SLAM_\perp$ case the C ends are distributed more uniformly along the midplane of the C layers with less pronounced maxima in front of the AB interfaces. This is the reason why the shifted structure is usually the preferred state (see phase diagrams Figs. 3.18 and 3.19). From an entropy point of view the system will have lower free energy when the C ends are uniformly distributed along the midplane.

a)   b)
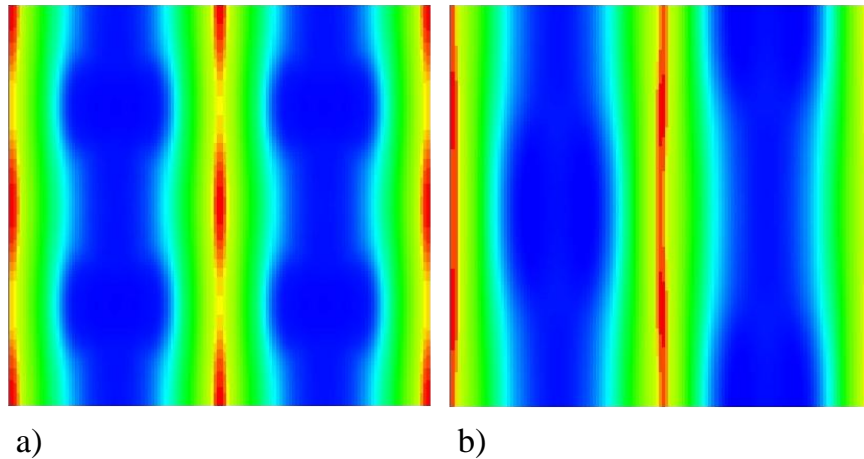
Figure 3.29. Volume density maps of the free ends of C blocks of (B-*b*-A)₂-*b*–C for $N\chi_{AB} = 2N\chi_{AC} = 120$ and $N\chi_{BC} = 15$. a) Not shifted structure $LAM_\perp$; b) Shifted structure $SLAM_\perp$ (equilibrium state).

It is interesting to show how the key harmonics depend on the interaction parameters in order to investigate the transition from $LAM_\perp$ to $SLAM_\perp$. In Fig. 3.30 the amplitudes of the key harmonics are presented for both structures of (B-*b*-A)₂ -*b*–C

polymers as a function of $N\chi_{AB} = 2N\chi_{AC}$ at fixed $N\chi_{BC} = 15$ (see phase diagram Fig. 3.18). We see that the amplitude of the (2,0) harmonic approaches zero at the transition point between $LAM_{\perp}$ and $SLAM_{\perp}$, i.e. $N\chi_{AB} = 2N\chi_{AC} = 97$. The phase of this harmonic also changes significantly. The (2,1) harmonic also decreases to zero but at $N\chi_{AB} = 2N\chi_{AC} = 105$.
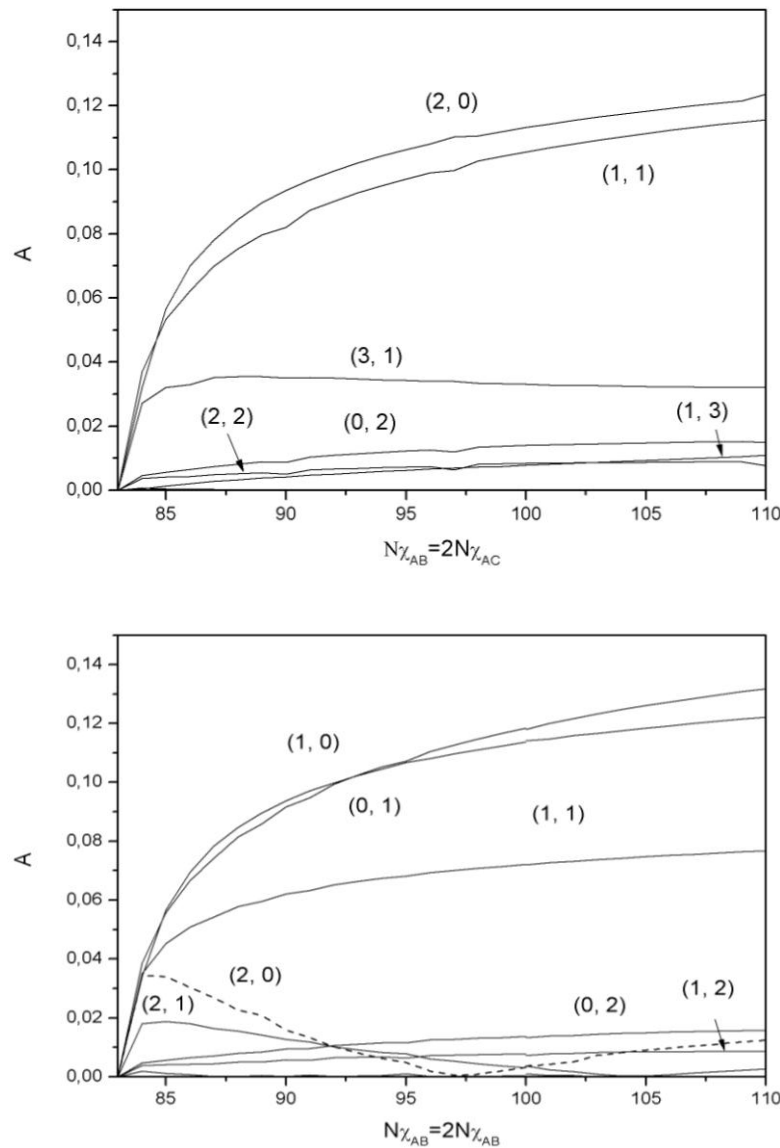
Figure 3.30. Amplitudes of key harmonics for (B-*b*-A)$_2$-*b*–C polymers as a function of $N\chi_{AB} = 2N\chi_{AC}$ for fixed $N\chi_{BC} = 15$. Top: $SLAM_{\perp}$; bottom: $LAM_{\perp}$.

Another difference between SPLAM and PLAM structures is periods along the AB interface L_x and along AC interface L_y. Interesting that L_x for the SPLAM

structure is a little bit more than for PLAM and L_x less at $N\chi_{AB} = 2N\chi_{AC} = 100$ and $N\chi_{BC} = 15$. In the transition point L_x and L_y for both states are equal. At $N\chi_{AB} = 2N\chi_{AC} < 97$ the PLAM structure becomes more extended in *y* direction.

3.4.3 Conclusion

A new SCFT technique for incompressible three-component block copolymers is developed. This technique is more general because it takes into account all possible cases when the matrix (3.43) is degenerate or non degenerate. The limits of the SCFT applicability are outlined for such copolymer systems.

Two types of multiblocks copolymers were investigated using SCFT method. It was shown that the standart technique to solve system of SCFT equation for ternary systems has restrictions. The standart iteration scherm do not converge in, on and close to so called Hildenbrand surface. Therefore different ways were introduced to solve the system of SCFT equations on and close to this surface. The parameter space inside the Hildenbrand surface can, however, still not be calculated using the standard ways of solving the system of SCFT equations.

It was shown that (B-*b*-A)$_2$-*b*–C and A-*b*-(B-*b*-A)$_2$-*b*–C ternary copolymers self-assembly in such structures as: parallel lamellar-*in*-lamellar, shifted perpendicular lamellar-*in*-lamellar and perpendicular lamellar-*in*-lamellar. Phase diagrams were presented. A significant difference was found between the phase behavior of (B-*b*-A)$_2$-*b*–C and A-*b*-(B-*b*-A)$_2$-*b*–C copolymers. PLAM is stable only for first one. Furthermore, the region of stability of the SPLAM structure extended to higher values of $N\chi_{AB} = 2N\chi_{AC}$ for the second copolymer. By comparing the volume fraction profiles it was shown that the free ends of the C blocks distributed more uniformly along the midplane in the case of SPLAM compared to PLAM.

Different parallel lamellar-*in*-lamellar structures were observed. For relatively small values of $N\chi_{BC}$ an extra layer of the A, B and C blocks mixture appears. The blocks of type B, due to the reduced incompatibility with the C blocks, penetrate into the interface formed by the directly connected A and C blocks. Increasing the value of $N\chi_{AB} = 2N\chi_{AC}$, results into reconfiguration of internal layers composition. Due to fact that investigation was done in 2d, it is still an open question how the B blocks are distributed in the AC interface in three dimensions.

3.5 Summary

A-*b*-(B-*b*-A)$_n$–*b*–C and (B-*b*-A)$_n$–*b*–C ternary multiblock copolymer melts were investigated using different theoretical approaches. The first part of this chapter is devoted to the SSL approach. The free energies for the four different structures found experimentally by Bates and co-workers, disordered, simple lamellae, parallel and perpendicular lamellar-*in*-lamellar, were calculated. By comparing these free energies it was found that the perpendicular lamellar-*in*-lamellar state becomes stable when the interaction parameters satisfy the relation $0 < \chi_{BC} < 0.22\,\chi_{AC}$. In order to find new structures DPD was performed and the results are presented in part two of this chapter. A few new structures were found: inverted lamellae with different number of internal layers and two perpendicular lamellar-*in*-lamellar structures, i.e. "shifted" and "not shifted." A metastable perpendicular lamellar-*in*-lamellar state that occurred sometimes involved AB lamellae from one layer which were perpendicular to the AB lamellae from the next one. By changing χ_{BC} from zero to $N\chi_{BC} >> 10$ the transition from binary to ternary multiblock copolymer melts were investigated. DPD allowed us to find different pathways for this transition. One sequence is: highly fluctuating disordered state – perpendicular lamellar-*in*-lamellar - parallel lamellar-*in*- lamellar. Another one is: inverted lamellae with three internal layers - inverted lamellae with five internal layers - perpendicular lamellar-*in*-lamellar - parallel lamellar-*in*-lamellar. To verify the DPD and SSL data a SCFT study was next performed. We restricted ourselves to 2d in order to save calculation time. The traditional SCFT approach has some limitations for ternary systems which implies that not every point in the parameter space ($\chi_{AB}, \chi_{AC}, \chi_{BC}$) is accessible. A new technique of solving SCFT system of equations was implemented in order to extend the accessible parameter value space. With SCFT stability regions of shifted and not shifted perpendicular lamellar-*in*-lamellar states were found. Complex phase behavior and alignment of blocks in different structures were discussed. It was shown that the distribution of the C end blocks is involved in the reduction of the free energy of the shifted structure with respect to the not shifted. Phase diagrams were calculated and they were shown to be in good agreement with SSL and DPD results.

3.6 References

1.   J. Ruokolainen, R. Mäkinen, M. Torkkeli, T. Mäkelä, R. Serimaa, G. ten Brinke, O. Ikkala, *Science*, **1998**, *280*, 557.
2.   J. Ruokolainen, G. ten Brinke, O. Ikkala, *Adv. Mater.*, **1999**, *11*, 777.
3.   O. Ikkala, G. ten Brinke, *Science,* **2002**, *295*, 2407.
4.   J. Masuda, A. Takano, Y. Nagata, A. Noro, Y. Matsushita, *Phys. Rev. Lett.*, **2006**, *97*, 098301.
5.   Y. Nagata, J. Masuda, A. Noro, D. Cho, A. Takano, Y. Matsushita, *Macromolecules,* **2005**, *38*, 10220.
6.   A.F. Thünemann, S. General, *Macromolecules,* **2001**, *34*, 6978.
7.   C. Osuji, C.Y. Chao, I. Bita, C.K. Ober, E.L. Thomas, *Adv. Funct. Mater.*, **2002**, *12*, 753.
8.   I.A. Ansari, V. Castelletto, T. Mykhaylyk, I.W. Hamley, Z.B. Lu, T. Itoh, C.T. Imrie, *Macromolecules,* **2003**, *36*, 8898.
9.   B. Nandan, C.H. Lee, L.H. Chen, W.C. Chen, *Macromolecules,* **2005**, *38*, 10117.
10. I.W Hamley, V. Castelletto, P. Parras, Z.B. Lu, C.T. Imrie, T. Itoh, *Soft Matter,* **2005**, *1*, 355.
11. G. Fleury, F.S. Bates, *Macromolecules*, **2009**, *42*, 1691.
12. G. Fleury, F.S. Bates, *Macromolecules*, **2009**, *42*, 3598.
13. R. Nap, C. Kok, G. ten Brinke, S.I. Kuchanov, *European Phys. J. E,* **2001**, *4*, 515.
14. R. Nap, N. Sushko, I.Y. Erukhimovich, G. ten Brinke, *Macromolecules,* **2006**, 39, 6765.
15. Y.A. Kriksin, I.Y. Erukhimovich, P.G. Khalatur, Y. Smirnova, G. ten Brinke, *J. Chem. Phys.*, **2008**, *128,* 244903.
16. Y.A. Kriksin, I.Y. Erukhimovich, Y. Smirnova, P.G. Khalatur, G. ten Brinke, *J. Chem. Phys.*, **2009**, *130*, 204901.
17. Y. Smirnova, G. ten Brinke, I.Y. Erukhimovich, *J. Chem. Phys.,* **2006**, *124*, 054907.
18. S.I. Kuchanov, V.E. Pichugin, G. ten Brinke, *Europhys. Lett.,* **2006**, *76*, 959.
19. A. Subbotin, T. Klymko, G. ten Brinke, *Macromolecules,* **2007**, *40,* 2915.
20. T. Klymko, A. Subbotin, G. ten Brinke, *J. Chem. Phys.*, **2008**, *129*, 114902.
21. T. Klymko, V. Markov, A. Subbotin, G. ten Brinke, *J. Soft Matter*, **2009**, *5*, 98.
22. A.N. Semenov, *Sov. Phys. JETP*, **1985**, *61*, 733.
23. E.W Cochran, F.S. Bates, *Macromolecules*, **2002**, *35*, 7368.
24. H. Benoit, G. Hadziioannou, *Macromolecules*, **1988**, *21*, 1449.
25. T.A. Kavassalis, M.D. Whitmore, *Macromolecules*, **1991**, *24*, 5340.
26. M.W. Matsen, M. Schick, *Phys. Rev. Lett.*, **1994**, *72*, 2660.
27. F. Drolet, G.H. Fredrickson, *Phys. Rev. Lett.*, **1999**, *83*, 4317.
28. J. G. E. M. Fraaije, *J. Chem. Phys.*, **1993**, *99*, 9202.
29. N.M. Maurits, J. G. E. M. Fraaije, *J. Chem. Phys.*, **1997**, *107*, 5879.
30. E. Helfand, Z.R. Wasserman, Developments in Block Copolymers, edited by I. Goodman Applied Science, London, **1982**, 99.
31. E. Helfand, Z.R. Wasserman, *Macromolecules*, **1976**, *9*, 879.
32. M.W. Matsen, *Phys. Rev. Lett.*, **1995**, *74*, 4225.
33. M.D. Feit, J.A. Fleck, A.J. Steiger, *Comput. Phys.*, **1982**, *47*, 412.
34. K.O. Rasmussen, G.J. Kalosakas, *Polym. Sci., Part B: Polym. Phys.*, **2002**, *40*, 1777.
35. H.D. Ceniceros, G.H. Fredrickson, *Multiscale Model. Simul.*, **2004**, *2*, 452.
36. G. H. Fredrickson, *The Equilibrium Theory of Inhomogeneous Polymers* (Oxford University Press, New York, **2006**).

37. K.-C. Ng, *J. Chem. Phys.*, **1974**, *61*, 2680.
38. R.B. Thompson, K.Ø. Rasmussen, T. Lookman, *J. Chem. Phys.*, **2004**, *120*, 31.
39. J. H. Hildebrand, *The Solubility of Non-Electrolytes* (Reinhold, New York, **1936**).
40. Y.A Kriksin, I.Y. Erukhimovich, P.G. Khalatur, Y. Smirnova, G. ten Brinke, *J. Chem. Phys.*, **2008**, *128*, 244903

Chapter 4

Self-Assembly of
(A-*comb*-C)-*b*-(B-*comb*-C) diblock
copolymer-based comb copolymers

4.1 Introduction

The ability of block copolymer-based systems to form highly ordered complex nanostructures has been the focus of attention for many years [1-10]. This continued interest is driven by the prospects to develop nanotechnology applications, such as nanostructured membranes, complex catalysts, nanowires, photonic crystals, to mention only a view [11-14]. The self-assembly of diblock copolymers is well understood by now [5,6], although new developments still occur [7,8], and much of the research shifted to the study of self-assembly in copolymers with a more complex molecular architecture, such as tri- star- and multiblock copolymers, where already many new structures have been found experimentally and theoretically [15-24].

In the present paper we focus on comb copolymers, where the same types of side chains are attached to both blocks of a diblock copolymer. The structure formation in conventional comb copolymers, i.e. with a homopolymer backbone, has already been presented in some detail in the literature [25-30]. Phase diagrams of various comb copolymer systems have been published and, although different in details, the general trends are the same as for diblock copolymers. Most importantly, rather than the overall chain length, it is the length of the "repeat unit" that determines the order-disorder transition temperature as well as the characteristic length scale of the ordered structures. Gido and co-workers [31-34] used this observation to initiate a strong segregation description of comb copolymers based on the so-called "constituting block copolymer hypothesis." According to this hypothesis, the repeat unit of a comb copolymer system is the determining factor for the microphase separated morphology. The weak segregation description of these systems lends further support to this proposition. The behavior of molecules with large, complex architectures is dictated by the behavior of the smaller architectural units from which they are comprised. Existing theory (e.g. ref. 35) is then used to predict the behavior of the repeat unit (i.e. the constituting block copolymer), which is then applied to the overall multigraft architecture.

Since the length scale of the structures corresponds to the length scale of the repeat unit, the characteristic domain size will usually be smaller than in the case of linear diblock copolymers. Combining a comb copolymer and a homopolymer into a comb-coil diblock copolymer molecule, the microphase separation between the homopolymer block and the comb block gives rise to a large length scale structure. Subsequent microphase separation inside the comb block containing domains will introduce the second shorter length scale [36, 37]. The experimental realizations of these kinds of structures are all based on comb-coil diblock copolymer-based supramolecules, where the side chains of the comb block are bonded by physical interactions [38-42]. So far mainly diblock copolymers of polystyrene and poly(4-vinylpyridine), PS-*b*-P4VP, have been used in combination with, e.g., pentadecylphenol (PDP) or dodecylbenzenesulfonic acid (DBSA), that form hydrogen bonds with the pyridine moiety of P4VP. Our current experimental activities seek to replace the PS block by another polymer block that also allows hydrogen bonding to PDP, thus obtaining supramolecular diblock copolymer-

based comb copolymers [43]. In the present paper we present a theoretical strong segregation analysis of the self-assembly in such systems, assuming the side chains to be covalently linked to both blocks of the diblock copolymer backbone.

4.2 Theoretical investigation

The phase behavior of (A-*comb*-C*)-b-*(B-*comb*-C) diblock copolymer melts is investigated using the strong segregation theory approach introduced by Semenov.

4.2.1 Model and theoretical approach

A schematic representation of the (A-*comb*-C)-*block*-(B-*comb*-C) comb diblock-copolymer chains investigated is shown in Fig. 4.1. Before we start with the analysis we will introduce our notation.
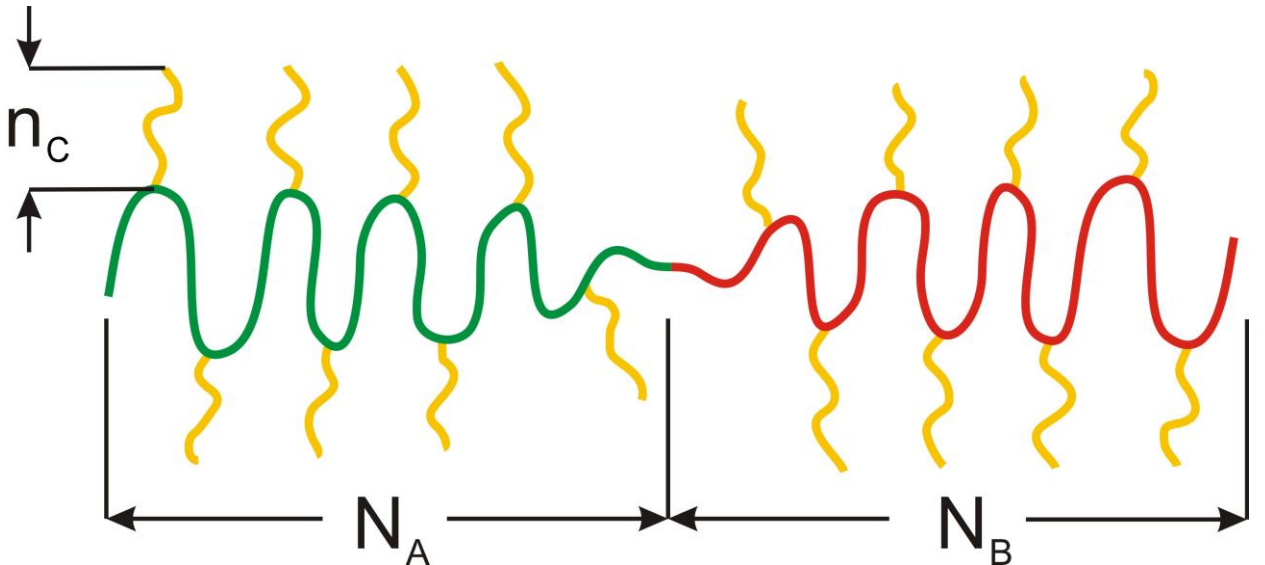
Figure 4.1. Schematic representation of comb-like diblock-copolymer chain.

The A- and B-blocks consist of N_A and N_B statistical segments, respectively. The C side chains contain n_C segments and the number of all C-segments per copolymer chain is denoted by N_C. Hence, the number m_C of C side chains per molecule is given by $m_C = \dfrac{N_C}{n_C}$. The total number of segments per copolymer chain is denoted by $2N$ and equals $N_A + N_B + N_C = 2N$. It is assumed that all chain segments have the same length a and volume υ. The volume fraction of C segments is denoted by ϕ_C. The volume fractions of A- and B-blocks are $\phi_A = \left(1-\phi_C\right)\varphi_A$ and $\phi_B = \left(1-\phi_C\right)\varphi_B$, respectively, where φ_A, resp. φ_B, denotes the volume fractions of the diblock backbone in absence of side chains, i.e.

$\varphi_B + \varphi_A = 1$. The length of the chain section between two neighbouring C blocks is $n_b = \dfrac{N_A + N_B}{m_C}$, so that the A-blocks contain $m_A = \dfrac{N_A}{n_b}$ short blocks of length n and the B-blocks $m_B = \dfrac{N_B}{n_b}$ of such short blocks. Each of these short A- and B-blocks contain one C side chain grafted to the middle of it. The total number of AC + BC repeat units in the copolymer chain is denoted as m ($m \equiv m_C$). Hence, the total number of segments in the AC (BC) repeat unit equals $n = \dfrac{2N}{m}$. Obviously, $m_A = \varphi_A m$, $m_B = \varphi_B m$, $n_b = n(1 - \phi_C)$, $n_C = n\phi_C$. We will assume that n is sufficiently larger than n_C so that the comb-copolymer chains do not form a bottle-brush. The interactions between the segments of different types are described by the Flory-Huggins interaction parameters χ_{AB}, χ_{AC} and χ_{BC}, all of which are assumed to be positive.

We first consider the disordered state, which is realized when the values of the interaction parameters are sufficiently small. The dominating contribution to its free energy comes from the interactions between the different components, which per copolymer chain is given by

$$F_{DIS} = 2N \left(\chi_{AB} (1 - \phi_C)^2 \varphi_A \varphi_B + \chi_{AC} \phi_C (1 - \phi_C) \varphi_A + \chi_{BC} \phi_C (1 - \phi_C) \varphi_B \right) \qquad (4.1)$$

Increasing the unfavorable interactions between the segments various kinds of microphase separation between the different blocks become possible. We focus on three different situations, (1) – microphase separation occurs between the AC and BC comb-blocks only, (2) – microphase separation occurs between the C blocks and the AB diblocks and (3) – microphase separation occurs between all block species A, B and C. We will analyse these three situations employing the strong segregation limit (SSL). We will furthermore restrict our discussion to the simplest (classical) structures.

To denote the different self-assembled structures, superscripts will be used to indicate the different phases and subscripts to denote the minority phase. As an example, $HEX_{AC}^{AC/BC}$ denotes hexagonal microphase separation between the AC and BC comb blocks with the AC blocks forming the core of the cylinders.

4.2.2 AC comb blocks microphase separated from BC comb blocks

In the case of microphase separation between the AC and BC comb-blocks only, the concentration profile of the C component may assumed to be constant throughout the system, $\phi_C = const$. In the strong segregation limit the thickness of the interface layer Δ between the AC and BC domains is much smaller than the Gaussian size of the

copolymer chain which is of the order of $R_0 = aN^{1/2}$. In this case the free energy can be presented in the form

$$F = F_{el} + F_{grad} + F_{int} \tag{4.2}$$

Here F_{el} is the stretching energy of the A and B blocks (it is assumed that the C-blocks are not stretched), F_{grad} is the conformational free energy loss due to the non-homogeneous profiles of the A and B species (the corresponding free energy density is given by $f_{grad} = \dfrac{a^2}{24\upsilon}\left[\dfrac{\phi_A'^2(z)}{\phi_A(z)} + \dfrac{\phi_B'^2(z)}{\phi_B(z)}\right]$) and F_{int} is the interaction energy. The free energy (4.2) per one copolymer chain, which occupies on average an interface area Σ, is given by

$$F = F_{el} + \frac{\Sigma}{\upsilon}\int_{-\infty}^{\infty} dz\left(\frac{a^2}{24}\frac{(1-\phi_C)\varphi_A'^2(z)}{\varphi_A(z)(1-\varphi_A(z))} + \chi_{AB}(1-\phi_C)^2\,\varphi_A(z)(1-\varphi_A(z))\right) +$$
$$\chi_{AC}\phi_C N_A + \chi_{BC}\phi_C N_B \tag{4.3}$$

Here we use $\phi_j(z) = (1-\phi_C)\varphi_j(z)$, $j = A, B$. After minimization this expression with respect to $\varphi_A(z)$ we obtain $\varphi_A(z) = \dfrac{1}{2}\left(1+\tanh\left(\dfrac{z}{\Delta}\right)\right)$, where $\Delta = a\sqrt{\dfrac{1}{6\chi_{AB}(1-\varphi_C)}}$ is the interfacial thickness. With this the free energy becomes

$$F_{tot} = F_{el} + \Sigma\gamma_{AC/BC} + F_{AC/BC} \tag{4.4}$$

where $\gamma_{AC/BC} = \dfrac{a}{\upsilon}(1-\varphi_C)^{3/2}\sqrt{\dfrac{\chi_{AB}}{6}}$ is the effective surface tension and $F_{AC/BC}$ is the interaction energy of the AC/BC mixture

$$F_{AC/BC} = 2N(1-\phi_C)\phi_C\left(\chi_{AC}\varphi_A + \chi_{BC}\varphi_B\right) \tag{4.5}$$

4.2.2.1 Lamellar structure

When the volume fraction of the A and B components are sufficiently close to each other a lamellar structure will be formed. The layers consist of alternating AC and BC mixtures (Fig. 4.2). The A and B blocks are stretched in the direction perpendicular to the interface on a distance d_A and d_B respectively. The C blocks are assumed not to be stretched.
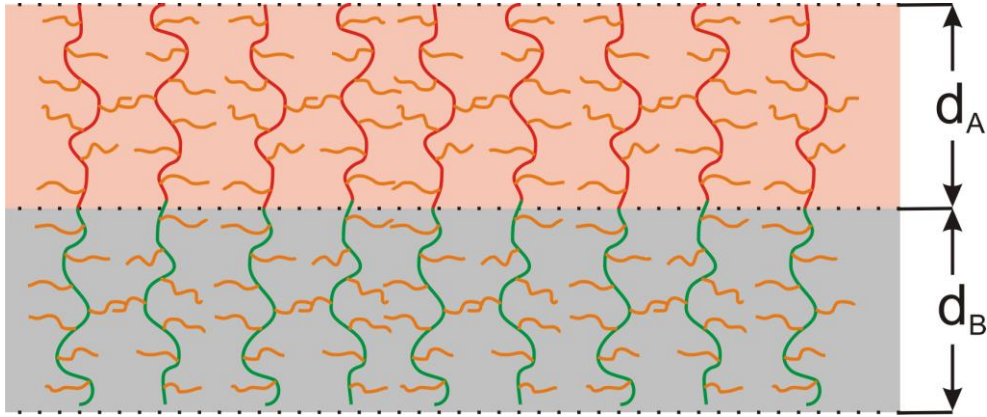
Figure 4.2. Schematic representation of the lamellar phase $LAM^{AC/BC}$ when AC blocks microphase separate from BC blocks.

We will use the Alexander – de Gennes approximation for the stretching energy of the A- and B-blocks, which implies that the free energy per copolymer chain is given by

$$F_{LAM^{AC/BC}} = \frac{3}{2}\frac{d_A^2}{N_A a^2} + \frac{3}{2}\frac{d_B^2}{N_B a^2} + \Sigma\gamma_{AC/BC} + F_{AC/BC} \tag{4.6}$$

Here the first two terms represent the stretching energy of the A- and B-blocks, the third term is the interfacial free energy and the last term the interaction energy of the AC and BC mixtures. Minimization of this free energy with respect to the interfacial area Σ taking into account the incompressibility conditions

$$d_A\Sigma = 2N\varphi_A\upsilon, \quad d_B\Sigma = 2N\varphi_B\upsilon \tag{4.7}$$

results in the following period of the lamellae structure

$$2(d_A + d_B) = \frac{4}{\sqrt{6}}R_0\left[\chi_{AB}N(1-\phi_C)^5\right]^{1/6} \tag{4.8}$$

and a free energy

$$F_{LAM^{AC/BC}} = 1.5(N\chi_{AB})^{1/3}(1-\phi_C)^{2/3} + 2N(1-\phi_C)\phi_C\left(\chi_{AC}\varphi_A + \chi_{BC}\varphi_B\right) \tag{4.9}$$

4.2.2.2 Hexagonal structure

When the volume fraction of B-blocks (A-blocks) decreases the formation of the hexagonal structure $HEX_{BC}^{AC/BC}$ ($HEX_{AC}^{AC/BC}$) is expected.
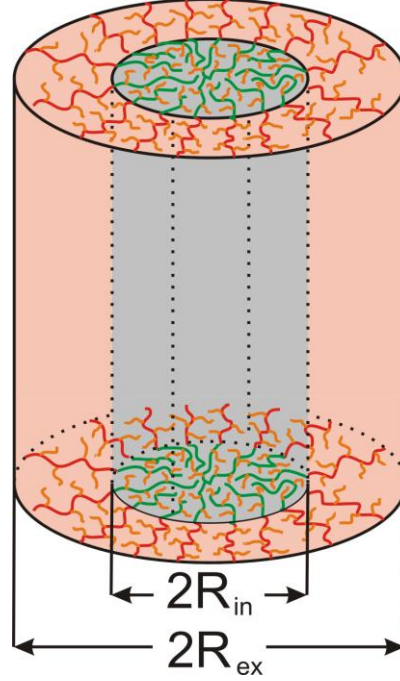
Figure 4.3. Schematic representation of the hexagonal phase $HEX_{BC}^{AC/BC}$ when the AC blocks microphase separate from the BC blocks that form the core.

Assuming that the chains are stretched non-uniformly in the core [2] and uniformly in the shell, the free energy per copolymer chain in the hexagonal structure with the BC comb-blocks forming the core can be written as:

$$F_{HEX_{BC}^{AC/BC}} = \frac{R_{in}^2}{N_B a^2}\left(\frac{\pi^2}{16} + \frac{3}{8}\ln\left(\frac{1}{\varphi_B}\right)\right) + 2\pi R_{in} L \gamma_{AC/BC} + F_{AC/BC} \qquad (4.10)$$

where $\dfrac{R_{in}^2}{N_B a^2}\dfrac{\pi^2}{16}$ is the stretching energy of the polymer chains forming the core and

$\dfrac{R_{in}^2}{N_B a^2}\dfrac{3}{8}\ln\left(\dfrac{1}{\varphi_B}\right)$ is the stretching energy of the chains in the shell. The second term is the interfacial energy, with L the length of the cylinder per copolymer chain. After minimization of this energy with respect to R_{in} using the incompressibility conditions

$$\pi R_{ex}^2 L = 2N\upsilon, \quad \pi R_{in}^2 L = 2N\varphi_B \upsilon \qquad (4.11)$$

we get

$$R_{in} = 4R_0 \left[\frac{\varphi_B^4 (1-\phi_C)^5 \chi_{AB} N}{6\left(\pi^2 - 6\ln\varphi_B\right)^2} \right]^{1/6}, \quad R_{ex} = R_{in}\,\varphi_B^{-1/2}$$

(4.12)

The corresponding free energy per copolymer chain is

$$F_{HEX_{BC}^{AC/BC}} = 0.83(1-\phi_C)^{2/3}\,\varphi_B^{1/3}\left(\pi^2 - 6\ln\varphi_B\right)^{1/3}\left[N\chi_{AB}\right]^{1/3} +$$
$$2N(1-\phi_C)\phi_C\left(\chi_{AC}\varphi_A + \chi_{BC}\varphi_B\right)$$

(4.13)

Of course, when the AC comb-blocks form the core a similar expression is obtained.

4.2.2.3 BCC structure

At a sufficiently small volume fraction of B blocks the $BCC_{BC}^{AC/BC}$ structure, with BC comb blocks forming the spheres, becomes preferable (Fig. 4.4). Using the same assumptions as for the hexagonal structure, the free energy per copolymer chain is given by

$$F_{BCC_{BC}^{AC/BC}} = \frac{R_{in}^2}{N_B a^2}\left(\frac{3\pi^2}{80} + \frac{1}{2}\left(1-\varphi_B^{1/3}\right)\right) + \frac{1}{Q}4\pi R_{in}^2\gamma_{AC/BC} + F_{AC/BC}$$

(4.14)

where Q is the number of copolymer chains in the spherical domain. The stretching energy for the core is $\dfrac{R_{in}^2}{N_B a^2}\dfrac{3\pi^2}{80}$, and for the shell $\dfrac{R_{in}^2}{N_B a^2}\dfrac{1}{2}\left(1-\varphi_B^{1/3}\right)$. The second term is the interfacial energy.
Incompressibility implies:

$$\frac{4}{3}\pi R_{ex}^3 = 2N\upsilon Q, \quad \frac{4}{3}\pi R_{in}^3 = 2N\varphi_B\upsilon Q$$

(4.15)

After minimization with respect to R_{in} the free energy is found to be

$$F_{BCC_{BC}^{AC/BC}} = 0.63(1-\phi_C)^{2/3}\,\varphi_B^{1/3}\left(3\pi^2 + 40\left(1-\varphi_B^{1/3}\right)\right)^{1/3}\left[N\chi_{AB}\right]^{1/3} +$$
$$2N(1-\phi_C)\phi_C\left(\chi_{AC}\varphi_A + \chi_{BC}\varphi_B\right)$$

(4.16)

The internal and external radii of the micelle are given by

$$R_{in} = 4R_0 \left[\frac{75\varphi_B^4(1-\phi_C)^5 \chi_{AB} N}{8\left(3\pi^2 + 40\left(1-\varphi_B^{1/3}\right)\right)^2} \right]^{1/6} , \quad R_{ex} = R_{in}\,\varphi_B^{-1/3}$$

(4.17)

Again, the opposite case of AC comb-blocks forming the core follows by a simple AB permutation.
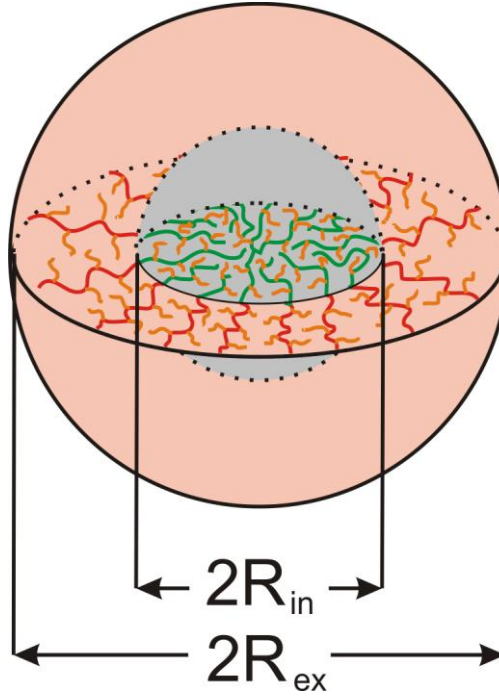
Figure 4.4. Schematic representation of $BCC_{BC}^{AC/BC}$ phase where the AC blocks microphase separate from the BC blocks that form the core.

4.2.2.4 Phase diagram

Equations 4.1, 4.9, 4.13 and 4.16 allows us to construct phase diagrams for different volume fractions of the C-component, where the transition from the disordered to the ordered state is estimated by comparing the free energy of the disordered state (eq. 4.1) with any of the SSL expressions 4.9, 4.13 and 4.16. Figure 4.5 shows the phase diagram in terms of $N\chi_{AB}$ versus the volume fraction of φ_B of the B-block in the A-*b*-B diblock for $\phi_C = 0.5$, $N\chi_{AC} = N\chi_{BC} = 10$ and total number of side chains $m = 20$. The critical Flory-Huggins parameter $\chi_{AB,c}$ corresponding to the order - disorder transition at fixed $\varphi_B = 0.5$ is $2N\chi_{AB,c} \cong \dfrac{10.4}{(1-\phi_C)^2}$. When the volume fraction of C blocks equals zero we

arrive back at the simple diblock copolymer case of $2N\chi_{AB,c} \cong 10.4$. In the phase diagram, Fig. 4.5, the order – disorder transition occurs at $2N\chi_{AB,c} \cong 42$ for $\varphi_B = 0.5$.
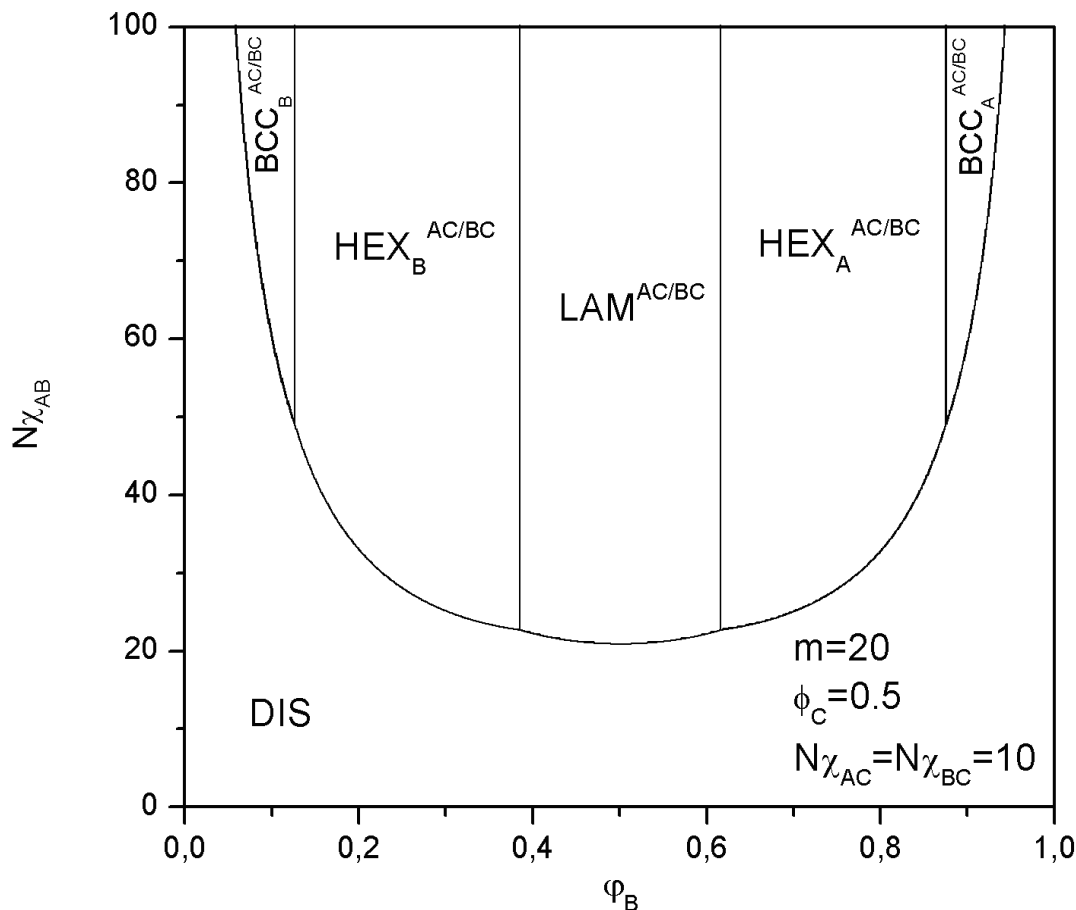
Figure 4.5. Phase diagram for (A-*comb*-C)-*block*-(B-*comb*-C) when the C blocks are molecularly mixed with the microphase separated A and B blocks for fixed $m = 20, \phi_C = 0.5, N\chi_{AC} = N\chi_{BC} = 10$. Note, e.g. $HEX_{AC}^{AC/BC}$ denotes microphase separation between A-*comb*-C and B-*comb*-C with the former forming the core of the cylinders.

4.2.3 AB backbone microphase separated from C side chains

Increasing the repulsion between the backbone and the side chains while at the same time reducing the repulsion between the A- and B-blocks results in the second type of microphase separation that we consider, i.e. microphase separation between the side chains C on the one hand and the AB backbone on the other. In the SSL approach the free energy of the resulting microstructures is given by

$$F^{AB/C} = F_{el} + \frac{\Sigma}{\upsilon} \int\limits_{-\infty}^{\infty} dz \left(\frac{a^2}{24} \frac{\phi_C'^2(z)}{\phi_C(z)(1-\phi_C(z))} + \left[\chi_{AC}\varphi_A + \chi_{BC}\varphi_B - \chi_{AB}\varphi_A\varphi_B \right] \phi_C(z)(1-\phi_C(z)) \right)$$
$$+ \chi_{AB}\varphi_A\varphi_B (N_A + N_B) \tag{4.18}$$

where F_{el} is the elastic free energy of the A, B and C blocks. Minimization of this free energy with respect to the concentration profile $\phi_C(z)$ gives $\phi_C(z) = \frac{1}{2}\left(1 + \tanh\left(\frac{z}{\Delta}\right)\right)$

where $\Delta = R_0 \sqrt{\dfrac{1}{6(\chi_{AC}\varphi_A + \chi_{BC}\varphi_B - \chi_{AB}\varphi_A\varphi_B)}}$ is the interfacial thickness. With this the free energy becomes

$$F_{tot} = F_{el} + \Sigma\gamma_{AB/C} + \chi_{AB}\varphi_A\varphi_B (N_A + N_B) \tag{4.19}$$

Here $\gamma_{AB/C} = \dfrac{a}{\upsilon} \sqrt{\dfrac{\chi_{AC}\varphi_A + \chi_{BC}\varphi_B - \chi_{AB}\varphi_A\varphi_B}{6}}$ is the surface tension of the AB/C interface.

4.2.3.1 Lamellar structure

Varying the volume fraction of the side chains and the value of the interaction parameters different microphase separated morphologies can be formed. The simplest case corresponds to the lamellar structure where the alternating layers consist of C blocks and mixed A and B blocks. As shown in Fig. 4.6, the A and B chain sections between two successive C blocks can form either bridges or loops. To deal with this we will use the approximation that the stretching energies of loops and bridges are equal. A schematic picture of the lamellar structure with period $2(H_1+H_2)$ is shown in Fig. 4.6.
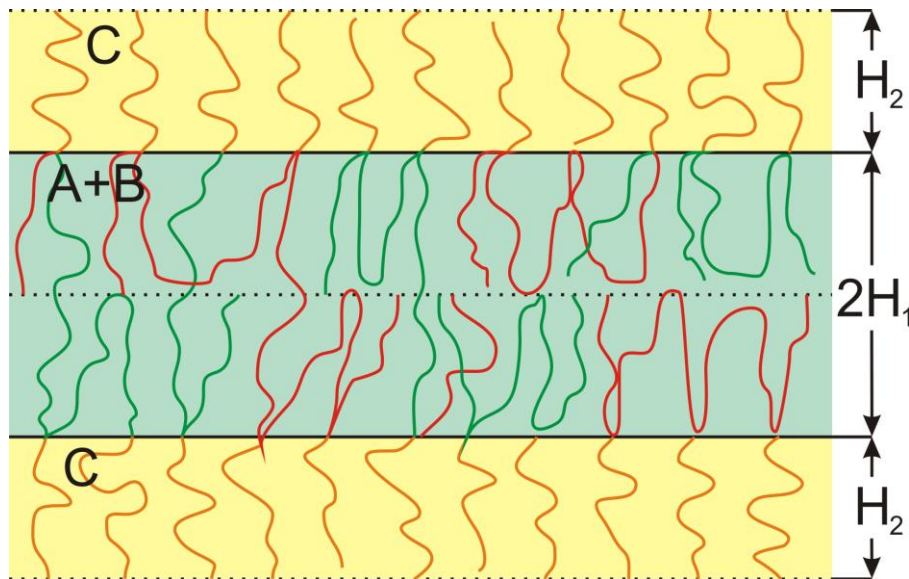

Figure 4.6. Lamellar structure $LAM^{AB/C}$ with C and AB lamellae.

The free energy of the lamellar structure per copolymer chain is given by

$$F_{LAM^{AB/C}} = m\frac{3H_2^2}{2n_Ca^2} + m\frac{3(2H_1)^2}{2n_ba^2} + \Sigma\gamma_{AB/C} + \chi_{AB}\varphi_A\varphi_B(N_A + N_B) \tag{4.20}$$

Here the first term corresponds to stretching free energy of the C blocks, the second term represents the stretching free energy of the A and B blocks, the third term is the surface free energy of the (AB)/C interface and the last term is the interaction energy of the AB mixture.

Incompressibility implies

$$H_1\Sigma = 2N(1-\phi_C)\upsilon; \quad H_2\Sigma = 2N\phi_C\upsilon \tag{4.21}$$

After minimization of the free energy with respect to Σ using Eq. (4.20) we obtain for the period of the structure

$$2(H_1 + H_2) = \frac{4}{\sqrt{6}}R_0\left[\frac{N\chi_{AC}\varphi_A + N\chi_{BC}\varphi_B - N\chi_{AB}\varphi_A\varphi_B}{m^4(4-3\phi_C)^2}\right]^{1/6} \tag{4.22}$$

Its free energy is

$$F_{LAM^{AB/C}} = 1.5m^{2/3}(4-3\phi_C)^{1/3}\left[N\chi_{AC}\varphi_A + N\chi_{BC}\varphi_B - N\chi_{AB}\varphi_A\varphi_B\right]^{1/3} + 2N\chi_{AB}\varphi_A\varphi_B(1-\phi_C) \tag{4.23}$$

For large values of N the free energy increases linearly with N.

4.2.3.2 Hexagonal structures

Besides the lamellar structure, two different hexagonally ordered cylindrical structures, denoted as $HEX_{AB}^{AB/C}$ and $HEX_C^{AB/C}$, are possible (Fig. 4.7). In the former the core of the cylinders is formed by the AB diblocks and in the latter by the C side chains. The internal and external radii of the cylinders are denoted as R_{in} and R_{ex}, and L denotes the cylinder length per copolymer chain. When the core is formed by AB diblocks, the "short" A and B sections between consecutive side chains form only loops. The free energy of the $HEX_{AB}^{AB/C}$ phase can be written as:

$$F_{HEX_{AB}^{AB/C}} = \frac{mR_{in}^2}{a^2n_b}\left(\frac{\pi^2}{4} + \frac{3}{8}\ln\left(\frac{1}{1-\phi_C}\right)\right) + 2\pi R_{in}L\gamma_{AB/C} + \chi_{AB}\varphi_A\varphi_B(N_A + N_B) \tag{4.24}$$

Taking into account the incompressibility conditions $\pi R_{ex}^2 L = 2N\upsilon$ and $\pi R_{in}^2 L = 2N(1-\phi_C)\upsilon$, we obtain after minimization of the free energy with respect to R_{in}

$$R_{in} = R_0 \left[\frac{4(1-\phi_C)^2}{\sqrt{6}\lambda_1 m^2} \right]^{\frac{1}{3}} \left(N\chi_{AC}\varphi_A + N\chi_{BC}\varphi_B - N\chi_{AB}\varphi_A\varphi_B \right)^{1/6}, \quad R_{ex} = R_{in}(1-\varphi_C)^{-1/2} \quad (4.25)$$

where $\lambda_1 = \dfrac{\pi^2}{4} + \dfrac{3}{8}\ln\left(\dfrac{1}{1-\phi_C}\right)$. Using the expressions for R_{in} and $\gamma_{AB/C}$ the free energy can be written as

$$F_{HEX_{AB}^{AB/C}} = 2.08\left(\lambda_1 m^2 (1-\phi_C)\right)^{1/3}\left[N\chi_{AC}\varphi_A + N\chi_{BC}\varphi_B - N\chi_{AB}\varphi_A\varphi_B \right]^{1/3}$$
$$+2N\chi_{AB}\varphi_A\varphi_B(1-\phi_C) \quad (4.26)$$

The other possibility arises when the volume fraction of the backbone is much higher than that of the side chains. In that case the AB diblocks form the matrix and, therefore, the copolymer chain can belong to more than one cylinder. Assuming again that the stretching free energy of the loops and the bridges connecting different elementary cells is equal, the free energy per copolymer chain is given by

$$F_{HEX_C^{AB/C}} = \frac{mR_{in}^2}{n_C a^2}\left(\frac{\pi^2}{16} + \frac{3}{2}\ln\left(\frac{1}{\phi_C}\right)\right) + 2\pi R_{in}L\gamma_{AB,C} + \chi_{AB}\varphi_A\varphi_B(N_A + N_B) \quad (4.27)$$

After minimization with respect to the radius of the core taking into account the incompressibility conditions $\pi R_{ex}^2 L = 2N\upsilon$ and $\pi R_{in}^2 L = 2N\phi_C\upsilon$ we get

$$R_{in} = R_0 \left[\frac{4\phi_C^2}{\sqrt{6}\lambda_2 m^2} \right]^{\frac{1}{3}} \left(N\chi_{AC}\varphi_A + N\chi_{BC}\varphi_B - N\chi_{AB}\varphi_A\varphi_B \right)^{1/6}, \quad R_{ex} = R_{in}\phi_C^{-1/2} \quad (4.28)$$

where $\lambda_2 = \dfrac{\pi^2}{16} + \dfrac{3}{2}\ln\left(\dfrac{1}{\phi_C}\right)$. Using this expression for R_{in} and the expression for $\gamma_{AB/C}$ the free energy becomes

$$F_{HEX_C^{AB/C}} = 2.08\left(\lambda_2 m^2 \phi_C\right)^{1/3}\left[N\chi_{AC}\varphi_A + N\chi_{BC}\varphi_B - N\chi_{AB}\varphi_A\varphi_B \right]^{1/3} + 2N\chi_{AB}\varphi_A\varphi_B(1-\phi_C) \quad (4.29)$$

a)   b)
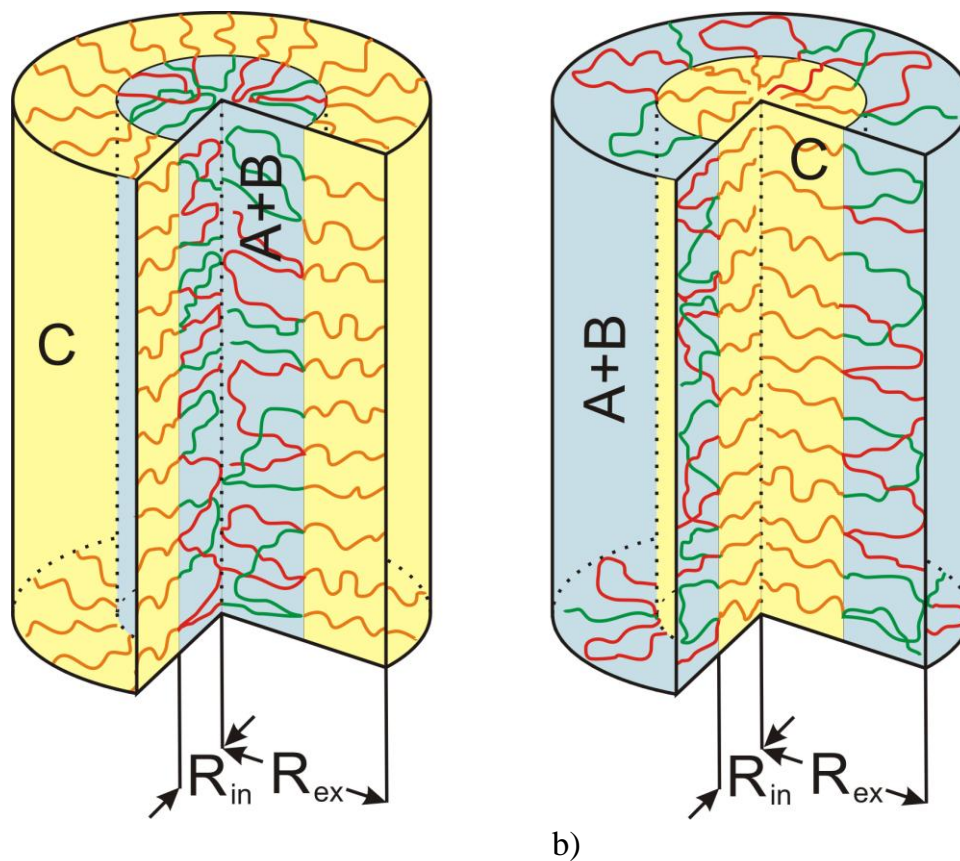
Figure 4.7. Schematic illustration of hexagonal structure: a) $HEX_{AB}^{AB/C}$ with core of the cylinder formed by the AB diblocks, b) $HEX_C^{AB/C}$ with core of the cylinder formed by the C side chains.
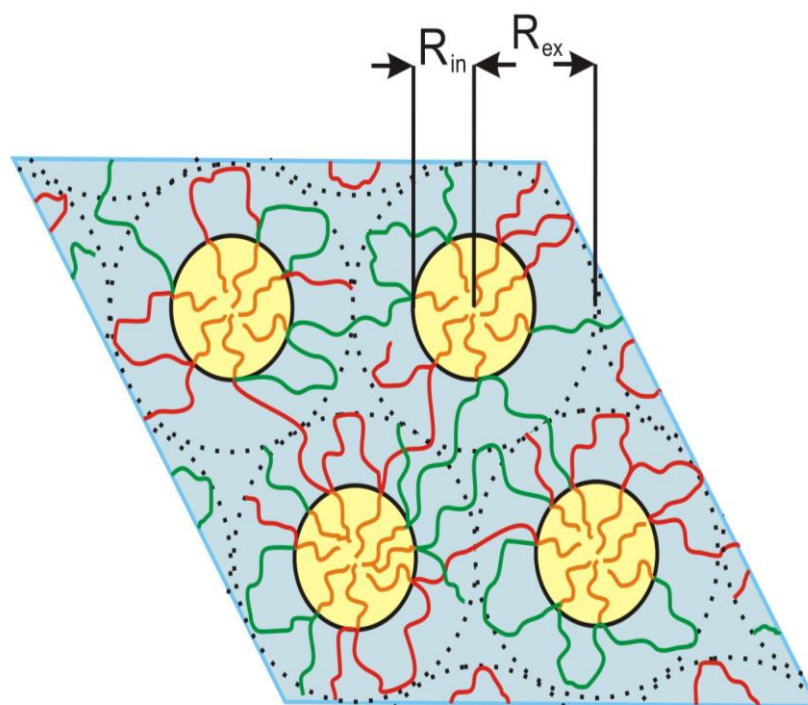
Figure 4.8. Schematic illustration of hexagonal structure $HEX_C^{AB/C}$ where the core of the cylinders is formed by the C side chains.

4.2.3.3 BCC structures

When the volume fraction of either C or AB is sufficiently small BCC structures may appear (see Fig. 4.9). Using the standard approach [2], the free energy of the $BCC_{AB}^{AB/C}$ structure when the core of the cylinders is formed by the AB diblocks is given by

$$F_{BCC_{AB}^{AB/C}} = \frac{mR_{in}^2}{n_b a^2}\left(\frac{3\pi^2}{20} + \frac{1}{2}\left(1 - (1-\phi_C)^{\frac{1}{3}}\right)\right) + \frac{4\pi}{Q}R_{in}^2\gamma_{AB/C} + \chi_{AB}\varphi_A\varphi_B\left(N_A + N_B\right) \qquad (4.30)$$
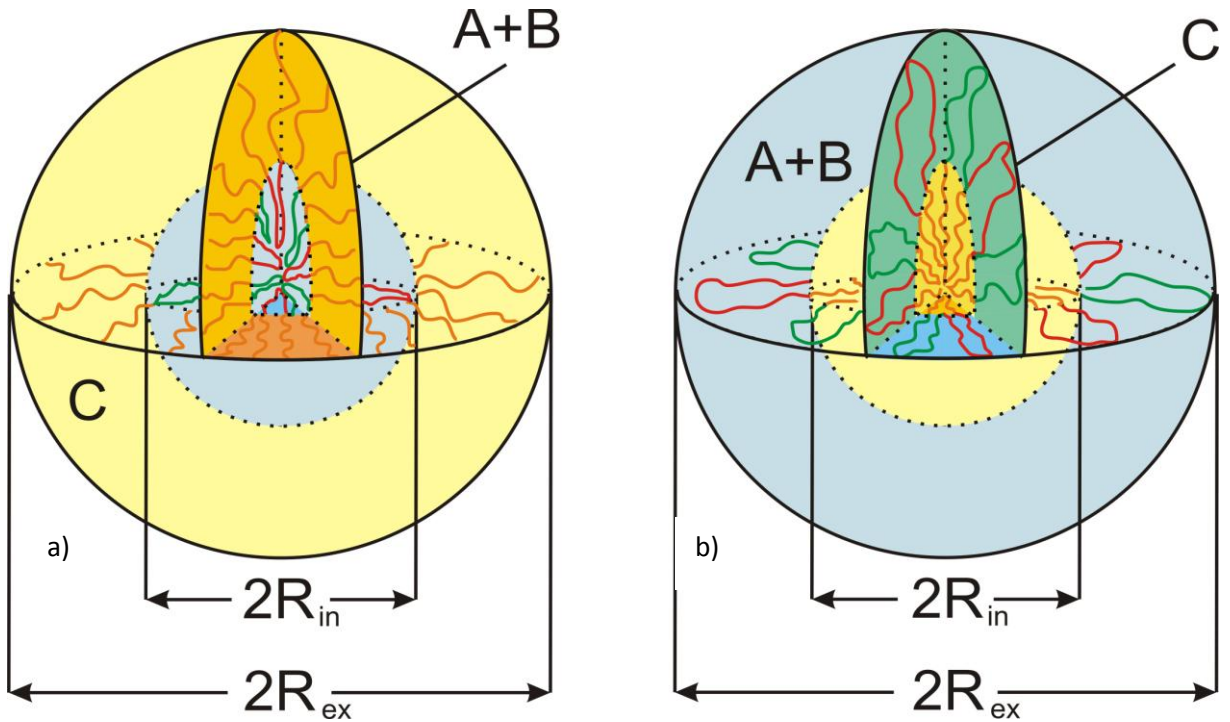
Figure 4.9. Schematic illustrations of the two BCC structures: a) $BCC_{AB}^{AB/C}$, where core of the sphere is formed by AB diblocks and b) $BCC_C^{AB/C}$, where core of the sphere is formed by the C side chains.

The incompressibility conditions are $\frac{4}{3}\pi R_{ex}^2 = 2N\upsilon Q$ and $\frac{4}{3}\pi R_{in}^2 = 2N(1-\phi_C)\upsilon Q$. When the matrix consists of the AB diblocks the free energy is given by

$$F_{BCC_C^{AB/C}} = \frac{mR_{in}^2}{n_C a^2}\left(\frac{3\pi^2}{80} + 2\left(1 - (\phi_C)^{\frac{1}{3}}\right)\right) + \frac{4\pi R_{in}^2}{Q}\gamma_{AB/C} + \chi_{AB}\varphi_A\varphi_B\left(N_A + N_B\right) \qquad (4.31)$$

The incompressibility conditions in this case read $\frac{4}{3}\pi R_{ex}^2 = 2N\upsilon Q$ and $\frac{4}{3}\pi R_{in}^2 = 2N\phi_C\upsilon Q$.

After minimization of the corresponding free energies we arrive at the following results:

$$R_{in,1} = R_0 \left[\frac{\sqrt{6}(1-\phi_C)^2}{\mu_1 m^2} \right]^{\frac{1}{3}} \left(N\chi_{AC}\varphi_A + N\chi_{BC}\varphi_B - N\chi_{AB}\varphi_A\varphi_B \right)^{1/6}, \quad R_{ex,1} = R_{in,1}\left(1-\phi_C\right)^{-1/3},$$

$$R_{in,2} = R_{in} = R_0 \left[\frac{\sqrt{6}\phi_C^2}{\mu_2 m^2} \right]^{\frac{1}{3}} \left(N\chi_{AC}\varphi_A + N\chi_{BC}\varphi_B - N\chi_{AB}\varphi_A\varphi_B \right)^{1/6}, \quad R_{ex} = R_{in}\phi_C^{-1/3} \qquad (4.32)$$

Where $\mu_1 = \dfrac{3\pi^2}{20} + \dfrac{1}{2}\left(1-(1-\phi_C)^{\frac{1}{3}}\right)$, $\mu_2 = \dfrac{3\pi^2}{80} + 2\left(1-\phi_C^{\frac{1}{3}}\right)$.

Using eqs. (4.30-4.32) the free energy of the $BCC_{AB}^{AB/C}$ phase (matrix of C-blocks) can be written as

$$F_{BCC_{AB}^{AB/C}} = 2.72\left(\mu_1 m^2(1-\phi_C)\right)^{1/3}\left[N\chi_{AC}\varphi_A + N\chi_{BC}\varphi_B - N\chi_{AB}\varphi_A\varphi_B\right]^{1/3}$$
$$+2N\chi_{AB}\varphi_A\varphi_B\left(1-\phi_C\right) \qquad (4.33)$$

For the second *BCC* phase (matrix of AB diblocks) we find

$$F_{BCC_C^{AB/C}} = 2.72\left(\mu_2 m^2\phi_C\right)^{1/3}\left[N\chi_{AC}\varphi_A + N\chi_{BC}\varphi_B - N\chi_{AB}\varphi_A\varphi_B\right]^{1/3}$$
$$+2N\chi_{AB}\varphi_A\varphi_B\left(1-\phi_C\right) \qquad (4.34)$$

4.2.3.4 Phase diagram

Free energies as a function of the volume fraction of C blocks for the different morphologies are shown in Fig. 4.10. It is easy to see that the free energy behavior of all the structures is asymmetric. This effect can be explained by the way the matrix is formed by either AB diblock chains or by C side chains. In Fig. 4.11 the stretching energy for the lamellar case of the AB diblocks and the C blocks versus the volume fraction of C blocks is presented at fixed values of the Flory-Huggins interaction parameters. It is easy to see that the stretching energy of the AB loops becomes equal to the stretching energy of C side chains when the volume fraction of the latter approximately equals $\phi_C = 0.8$. This big difference in stretching energies automatically leads to the asymmetric behavior observed.
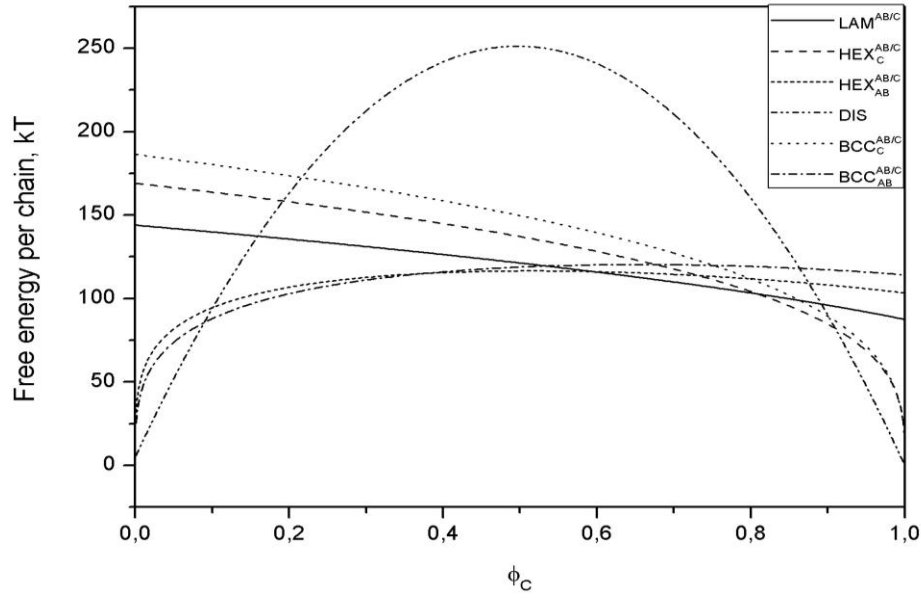
Figure 4.10. Free energies as a function of the volume fraction ϕ_C of the C blocks for Flory-Huggins interaction parameters $\chi_{AB} = 0.01$, $\chi_{BC} = 0.5$, $\chi_{AC} = 0.5$ and $m = 20, N = 1000$. Here the notation of, e.g., Hex C denotes hexagonal structure with C blocks forming the matrix.
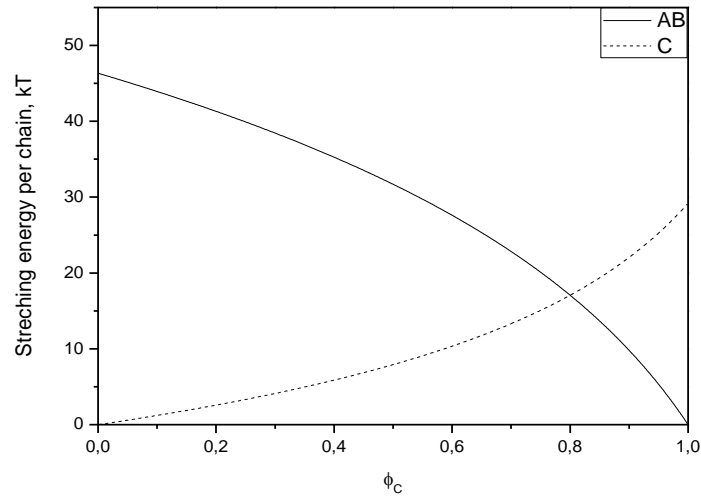
Figure 4.11. Streching energy for lamellar case for the AB diblocks and the C blocks versus the volume fraction ϕ_C of the C blocks for Flory-Huggins interaction parameters $\chi_{AB} = 0.01$, $\chi_{BC} = 0.5$, $\chi_{AC} = 0.5$ and $m = 20, N = 1000$. Solid line corresponds to stretching energy of AB blocks and dotted line to that of the C blocks.

Figure 4.12 presents one possible phase diagram in terms of the volume fraction of the C blocks and the interaction between C and AB diblocks, for fixed values $N\chi_{AB} = 10, m = 20, \varphi_A = \varphi_B = 0.5$.
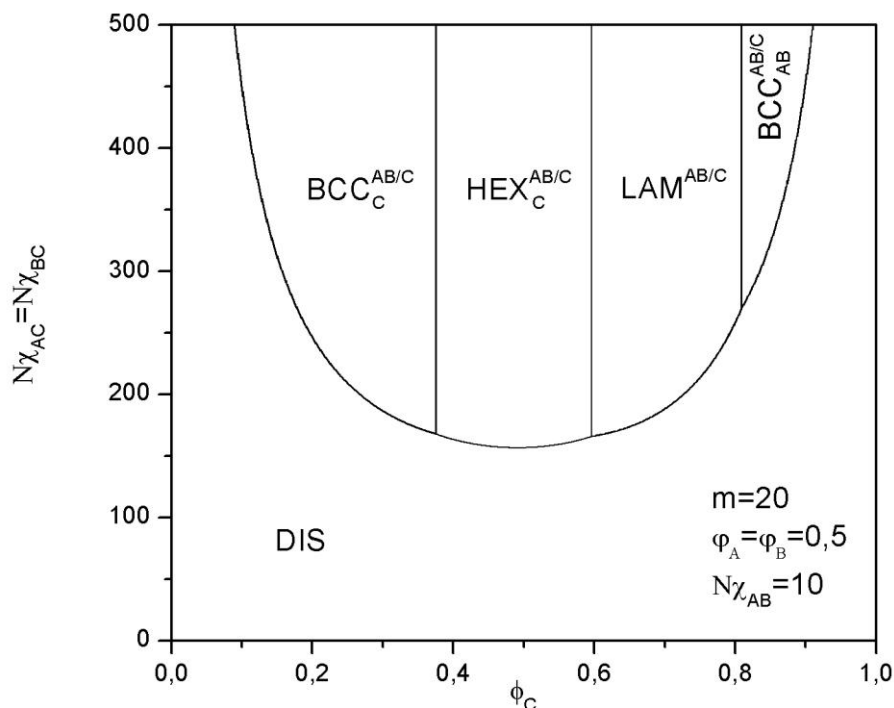
Figure 4.12. Phase diagram of (A-*comb*-C*)-b-*(B-*comb*-C) when A and B are mixed as a function of the volume fraction ϕ_C of C blocks and interaction strength $N\chi_{AC} = N\chi_{BC}$ for fixed $N\chi_{AB} = 10, \varphi_A = \varphi_B = 0.5, m = 20$.

The effect of the asymmetry is obvious. Compared to simple diblocks, the lamellar region shifts, in agreement with the analysis presented in ref. 35, to higher values of the C volume fraction. At small values of the volume fraction of C blocks $\phi_C < 0.38$ the $BCC_C^{AB/C}$ structure with the cores formed by the C blocks becomes stable. At higher values of ϕ_C the hexagonal structure becomes preferable. For $0.6 < \phi_C < 0.8$ the lamellar structure is formed. A further increase of ϕ_C transfers the system directly into the $BCC_{AB}^{AB/C}$ phase where the core is formed by the AB blocks, thus bypassing the hexagonal structure. The hexagonal structure becomes unfavorable because of an insufficient amount of AB blocks to form the core.

4.2.4 Hierarchical Structure Formation

Finally we consider the most interesting case where all three different types of blocks microphase separate from each other. For simplicity we restrict ourselves to the case where the C and A+B monomers form a lamellar structure, with additional microphase separation between the A- and B-blocks inside the corresponding layer.

Three different morphologies, namely a perpendicular lamellar-*in*-lamellar, a parallel lamellar-*in*-lamellar and a hexagonally packed disks-*in*-lamellar structure will be considered.

4.2.4.1 Perpendicular lamellar-*in*-lamellar structure

The perpendicular lamellar-*in*-lamellar structure can appear when the volume fraction of the B blocks is close to the volume fraction of the A blocks, Fig. 4.13. As above, we assume that the loops formed by the "short" A and B sections are stretched in the y direction (the direction perpendicular to the C layers) up to the mid plane (= distance H_1). In the x direction, which is perpendicular to the secondary lamellar structure, the full A resp. B blocks are stretched up to a distance d_A (d_B), respectively (see Fig. 4.13). The C blocks are stretched only in the y direction up to a distance H_2.

The free energy (per copolymer chain) of this structure can be approximated as the sum of the stretching and interfacial free energies :

$$F_{ll} = F_A + F_B + F_C + F_{AB} + F_{AC} + F_{BC} \tag{4.35}$$

Here F_A, F_B, F_C are the stretching free energies of the A, B and C blocks, respectively, given by

$$F_A = F_{A,x} + F_{A,y} = \frac{3d_A^2}{2N_A a^2} + m_A \frac{3(2H_1)^2}{2n_b a^2}; \quad F_B = F_{B,x} + F_{B,y} = \frac{3d_B^2}{2N_B a^2} + m_B \frac{3(2H_1)^2}{2n_b a^2}$$

$$F_C = F_{C,y} = m_C \frac{3H_2^2}{2n_C a^2} \tag{4.36}$$

and F_{AB}, F_{AC}, F_{BC} are the interfacial energies:

$$F_{AB} = \Sigma_{AB}\, \gamma_{AB}; \quad F_{AC} = \Sigma_{AC}\, \gamma_{AC}; \quad F_{BC} = \Sigma_{BC}\, \gamma_{BC} \tag{4.37}$$

where Σ_{AB}, Σ_{AC}, Σ_{BC} are the interfacial areas per copolymer chain. Incompressibility implies

$$\Sigma_{AC} H_1 = \Sigma_{AB} d_A = N_A \upsilon; \quad \Sigma_{BC} H_1 = \Sigma_{AB} d_B = N_B \upsilon; \quad (\Sigma_{AC} + \Sigma_{BC})H_2 = N_C \upsilon \tag{4.38}$$
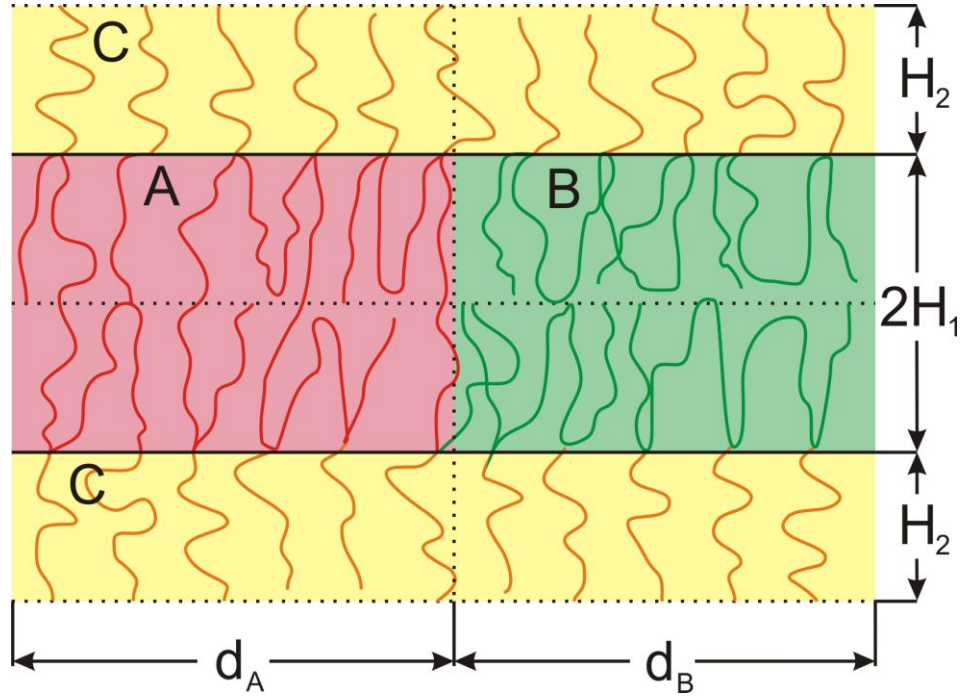
Figure 4.13. Schematic illustration of the perpendicular lamellar-*in*-lamellar structure.

After minimization of the free energy (4.35) with respect to the variables H_1, H_2, d_A, d_B, Σ_{AC}, Σ_{BC}, Σ_{AB} using eqs. (4.36-4.38) we find for the periods of the lamellar structure

$$2(H_1 + H_2) = 2\sqrt{\frac{2}{3}} R_0 \left[\frac{\varphi_B \sqrt{N\chi_{BC}} + (1-\varphi_B)\sqrt{N\chi_{AC}}}{m^2(4-3\phi_C)} \right]^{\frac{1}{3}};$$

$$2(d_A + d_B) = 2\sqrt{\frac{2}{3}} R_0 (1-\phi_C)^{2/3} (N\chi_{AB})^{1/6} \tag{4.39}$$

Using these, the free energy (4.35) becomes

$$F_\perp^{A/B/C} = 1.5 \left[(1-\phi_C)^{1/3} (N\chi_{AB})^{1/3} + m^{2/3}(4-3\phi_C)^{1/3} \left[(N\chi_{AC})^{1/2}(1-\varphi_B) + (N\chi_{BC})^{1/2}\varphi_B \right]^{2/3} \right]$$

$$\tag{4.40}$$

4.2.4.2 Parallel lamellar-*in*-lamellar structure

Another possibility is to have the AB interface parallel to the AC and BC interfaces as illustrated in Fig. 4.14. Now the stretching of the C blocks and the "short" A and B sections occurs only in the direction perpendicular to the interfaces between the components. The C blocks that are connected to the A blocks are stretched over a distance H_{C1} and the C blocks connected to the B blocks are stretched over a distance H_{C2}. The A blocks are stretched over a distance H_A and the B blocks over a distance H_B. Hence, the period of the lamellar structure is $H_{C1} + H_{C2} + H_A + H_B$.

The stretching free energies are given by

$$F_A = 4m_A \frac{3H_A^2}{2n_b a^2}; \quad F_B = 4m_B \frac{3H_B^2}{2n_b a^2}$$

$$F_C = m_A \frac{3H_{C1}^2}{2n_C a^2} + m_B \frac{3H_{C2}^2}{2n_C a^2}$$

(4.41)

And the interfacial free energies by

$$F_{AB} = \Sigma \gamma_{AB}; \quad F_{AC} = \Sigma \gamma_{AC}; \quad F_{BC} = \Sigma \gamma_{BC}$$

(4.42)

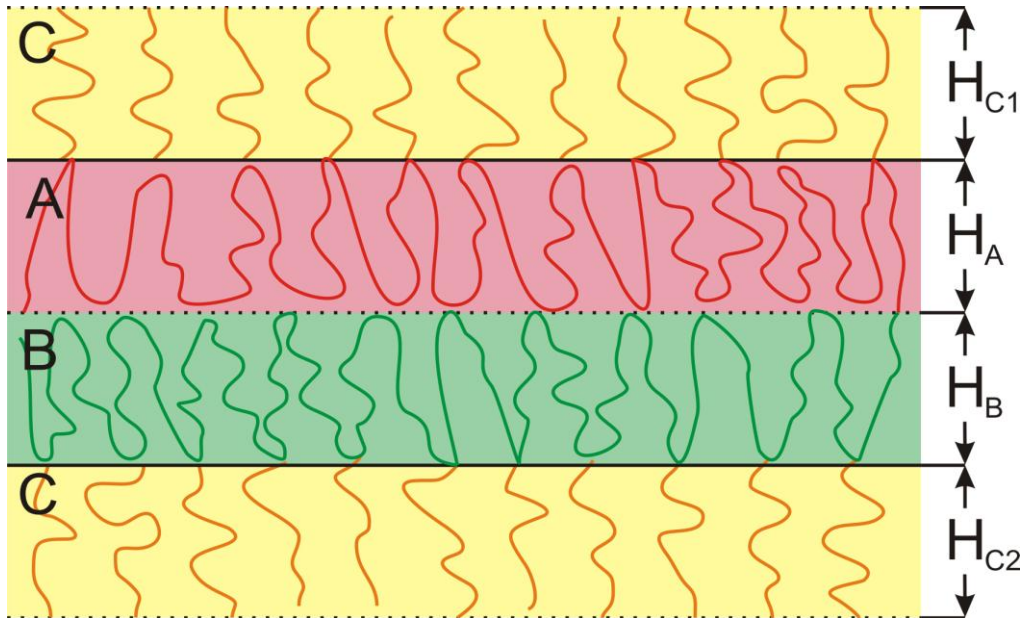**Figure 4.14.** Schematic illustration of parallel lamellar-*in*-lamellar structure**.**

Incompressibility implies

$$2N(1-\phi_C)\varphi_A \upsilon = \Sigma H_A; \quad 2N(1-\phi_C)\varphi_B \upsilon = \Sigma H_B;$$
$$2N\phi_C\varphi_A \upsilon = \Sigma H_{C1}; \quad 2N\phi_C\varphi_B \upsilon = \Sigma H_{C2} \tag{4.43}$$

Here Σ is the interfacial area per copolymer chain (section) of the different components. After substitution of eqs. (4.41 -4.42) in the free energy eq. (4.35) and minimization, the period is found to be

$$H_{C1} + H_{C2} + H_A + H_B = \sqrt{\frac{2}{3}}R_0 \left[\frac{(\sqrt{N\chi_{AC}} + \sqrt{N\chi_{BC}} + \sqrt{N\chi_{AB}})}{m^2\left((1-\varphi_B)^3 + \varphi_B^{\,3}\right)(4-3\phi_C)} \right]^{\frac{1}{3}} \tag{4.44}$$

With this the free energy becomes

$$F_{\parallel}^{A/B/C} = 1.5m^{2/3}\left(\varphi_B^3 + (1-\varphi_B)^3\right)^{1/3}\left(4-3\phi_C\right)^{1/3}\left[\sqrt{N\chi_{AC}} + \sqrt{N\chi_{BC}} + \sqrt{N\chi_{AB}}\right]^{2/3} \tag{4.45}$$

The free energy of the parallel lamellar-*in*-lamellar structure is a function of $\left(\varphi_B^3 + (1-\varphi_B)^3\right)^{1/3}$ with a minimum at $\varphi_B = 0.5$.

4.2.4.2 Hexagonally packed disks in lamellar structure

When the volume fraction of the B or A component is sufficiently small, microphase separation inside the AB layers may result in hexagonally packed disks with the core of the disks formed by the minority component (Fig. 4.15). Suppose the B blocks form the core and the A blocks the matrix. The C blocks form lamellar layers. The thickness of the C-layers is $2H_2$ and the thickness of the AB layers is $2H_1$.
As always, the free energy of the structure can be written as the sum of the elastic and the interfacial free energies (4.35).The stretching free energies of the different blocks are given by

$$F_A = F_{A,x} + F_{A,y} = \frac{3}{8}\frac{R_{in}^2}{N_A a^2}\ln\frac{1}{\varphi_A} + m_A\frac{3(2H_1)^2}{2n_b a^2}$$
$$F_B = F_{B,x} + F_{B,y} = \frac{\pi^2}{16}\frac{R_{in}^2}{N_A a^2} + m_B\frac{3(2H_1)^2}{2n_b a^2} \tag{4.46}$$
$$F_C = F_{C,y} = m_C\frac{3H_2^2}{2n_C a^2}$$

The interfacial energies F_{AB}, F_{AC}, F_{BC} are

$$F_{AB} = 4\pi R_{in} H_1 \gamma_{AB} Q^{-1}; \quad F_{BC} = 2\pi \left(R_{ex}^2 - R_{in}^2 \right) \gamma_{BC} Q^{-1}; \quad F_{AC} = 2\pi R_{in}^2 \gamma_{AC} Q^{-1} \tag{4.47}$$

where Q is the number of copolymer chains per disk.
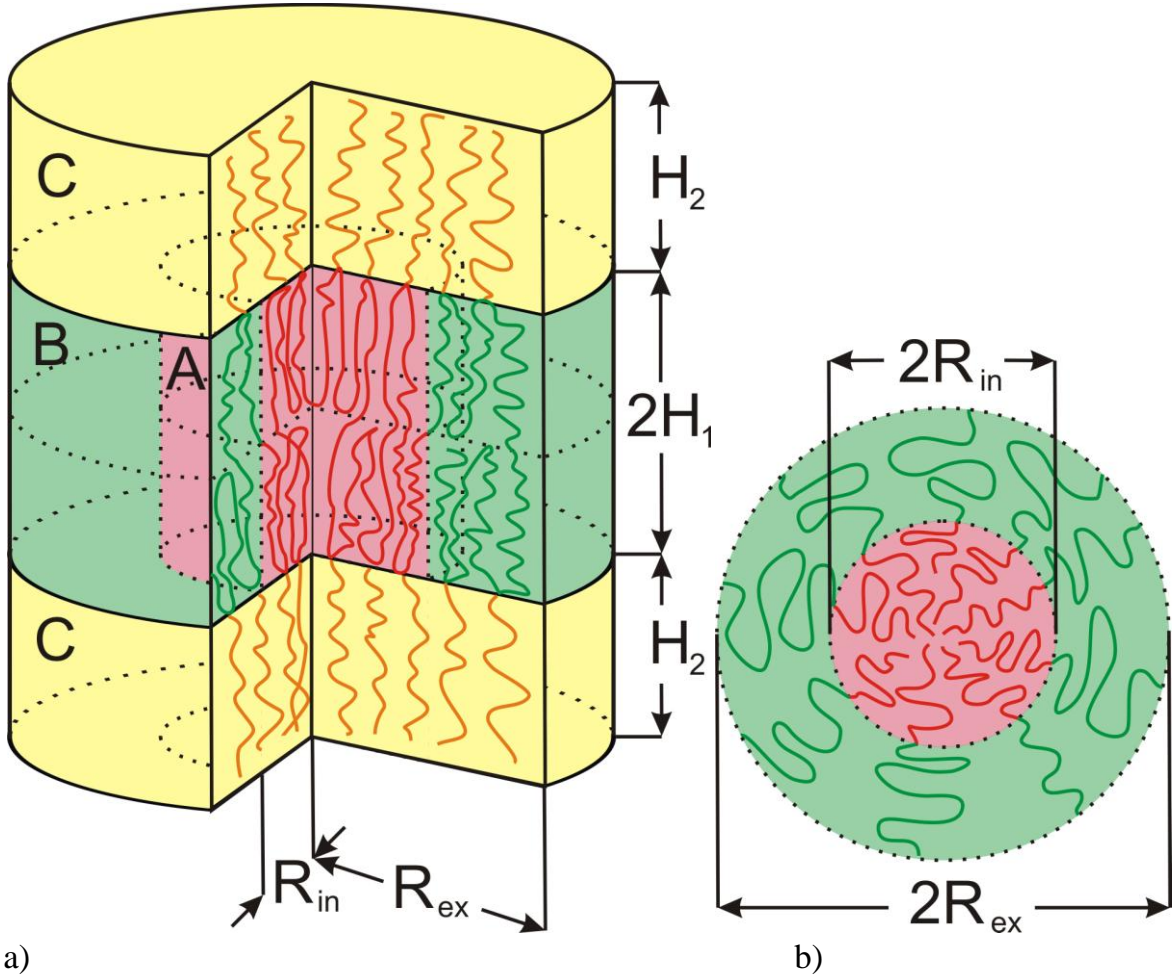
Figure 4.15. Schematic illustrations of hexagonally packed disks inside a lamellar structure a) three dimensional view, b) interface between AB and C bocks. .

Incompressibility implies

$$2\pi R_{ex}^2 H_1 = (N_A + N_B)\upsilon Q; \quad 2\pi R_{in}^2 H_1 = N_A \upsilon Q; \quad 2\pi R_{ex}^2 H_2 = N_C \upsilon Q \tag{4.48}$$

When $Q \gg 1$ (this condition will be verified afterwards) minimization of the total free energy (4.35) with respect to parameters of the hexagonal structure using eqs. (4.46-4.48) results in a period $2(H_1 + H_2)$ and a radius R_{in} given by

$$2\left(H_1+H_2\right)=2\sqrt{\frac{2}{3}}R_0\left[\frac{\varphi_A\sqrt{N\chi_{BC}}+\left(1-\varphi_A\right)\sqrt{N\chi_{AC}}}{m^2\left(4-3\phi_C\right)}\right]^{\frac{1}{3}}$$

$$R_{in}=R_0\left[\frac{4\varphi_A^2\left(1-\phi_C\right)^2}{\sqrt{6}\left(\frac{\pi^2}{16}-\frac{3}{8}\ln\varphi\right)}\right]^{\frac{1}{3}}\left(N\chi_{AB}\right)^{1/6} \tag{4.49}$$

This results in a free energy given by

$$F_{HEX_B^{A/B/C}}=1.5m^{2/3}\left(4-3\phi_C\right)^{1/3}\left[\left(1-\varphi_A\right)\sqrt{N\chi_{AC}}+\varphi_A\sqrt{N\chi_{BC}}\right]^{2/3}+$$
$$2.08\varphi_A^{2/3}\left(1-\phi_C\right)^{1/3}\left[\frac{\pi^2}{16}-\frac{3}{8}\ln\varphi_A\right]^{1/3}\left(N\chi_{AB}\right)^{1/2} \tag{4.50}$$

The number of chains per disk is found to satisfy

$$Q=7.2\pi N^{1/2}\frac{\varphi_A^{1/3}\left(\varphi_A\sqrt{N\chi_{BC}}+\left(1-\varphi_A\right)\sqrt{N\chi_{AC}}\right)^{1/3}\left(N\chi_{AB}\right)^{1/3}}{m^{2/3}\left(\pi^2-6\ln\varphi_A\right)^{2/3}}\frac{\left(1-\phi_C\right)^{4/3}}{\left(4-3\phi_C\right)^{1/3}} \tag{4.51}$$

In order to prove the assertion that $Q\gg1$, Q is plotted in Figs. 4.16 and 4.17 as a function of the composition resp. as a function of the interaction parameters. Figure 4.16 demonstrates that for $\varphi_A>0.1$ and $\phi_C<0.95$ the number of chains $Q>10$ for interaction parameter values satisfying $N\chi_{AB}=100$, $N\chi_{AC}=N\chi_{BC}=200$.

Figure 4.17 shows Q as a function of the interaction parameters $N\chi_{AB}$, $N\chi_{AC}$, $N\chi_{BC}$ at fixed volume densities when the hexagonal structure is formed. Starting from $N\chi=50$ the number of chains remain at Q>10.
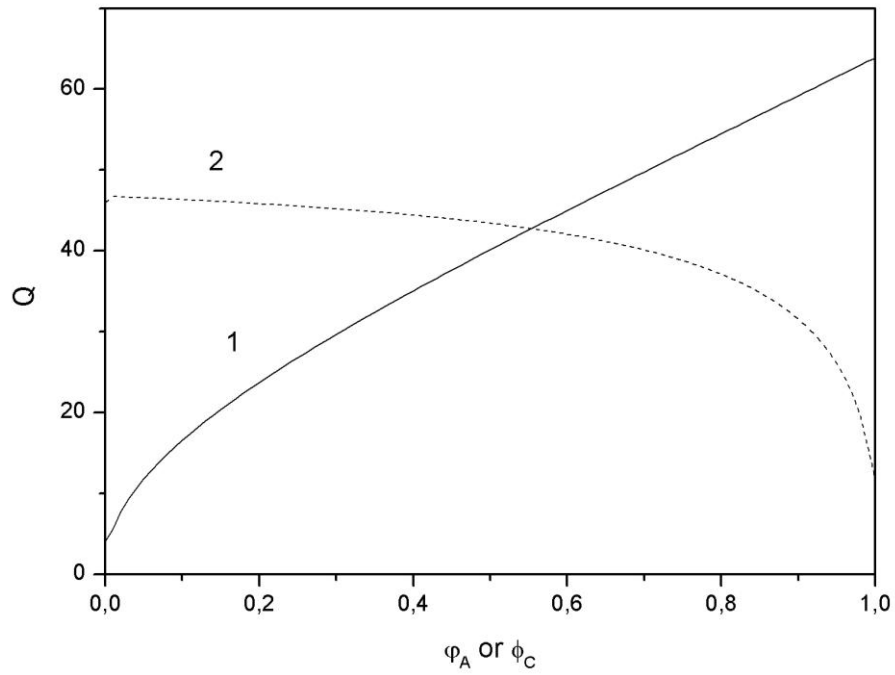
Figure 4.16. The number of chains Q per disk as a function of different volume factions: 1) φ_A at fixed $\phi_C = 0.7$, 2) ϕ_C at fixed $\varphi_A = 0.5$. All calculations were performed at fixed $N\chi_{AB} = 100$, $N\chi_{AC} = N\chi_{BC} = 200$.
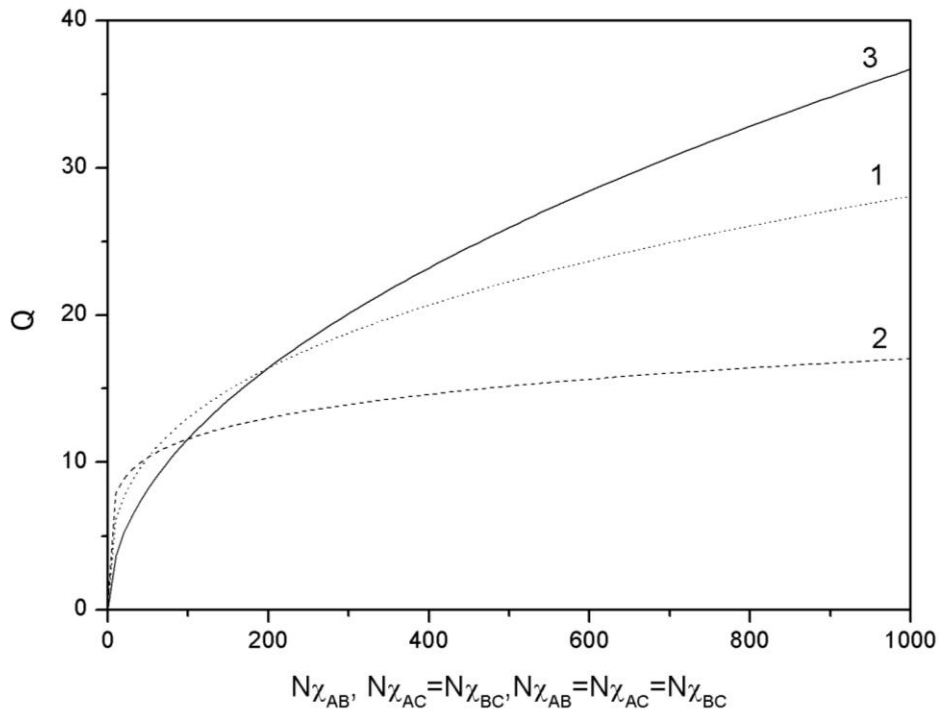
Figure 4.17. The number of chains Q per disk as a function of the Flory-Huggins interaction parameters 1) $N\chi_{AB}$, 2) $N\chi_{AC} = N\chi_{BC}$, 3) $N\chi_{AB} = N\chi_{AC} = N\chi_{BC}$ at fixed $\varphi_A = 0.1$, $\phi_C = 0.9$. Extreme values were chosen to prove that Q does not drop below 10.

4.2.4 Results and discussion

We will now discuss several scenarios. We start with fixed volume fractions $\phi_C = 0.7$, $\varphi_A = \varphi_B = 0.5$ and plot phase diagrams in the ($N\chi_{AB}, N\chi_{AC} = N\chi_{BC}$)-plane for different values of the number of side chains *m*. Because of the volume fractions selected only lamellar domains are possible (cf. Fig. 4.12). At sufficiently small values of the Flory-Huggins interaction parameters $\chi_{AB}, \chi_{AC}, \chi_{BC}$ the disordered state DIS is stable. By increasing the interaction between the A and B blocks, keeping the interaction between backbone and side chains fixed, the system self-assembles in the lamellar state LAM$^{AC/BC}$ with alternating layers formed by AC and BC mixtures. As discussed above, this regime corresponds to that of simple symmetric diblocks with effective Flory-Huggins parameter $(1-\phi_C)^2 \chi_{AB}$. On the other hand, if the interaction between the A and B blocks remains sufficiently small and the interaction between the backbone and the side chains increases, at some point a lamellar state $LAM^{AB/C}$ will be formed with alternating layers consisting of C side chains and AB mixtures. At sufficiently high values of all three interaction parameters all three components will microphase separate from each other. Then two types of lamellar phases are possible, one where the layers formed by the A or B blocks are aligned perpendicularly with respect to layers formed by the C blocks, $LAM_\perp^{A/B/C}$, and one where all layers are parallel, $LAM_\parallel^{A/B/C}$. Figure 4.18a presents the phase diagram for *m* = 2. The transition between the partially and fully micro phase separated states occurs at small values of $N\chi_{AB}$ (from $LAM^{AC/BC}$ to $LAM_\perp^{A/B/C}$) and small values of $N\chi_{AC} = N\chi_{BC}$ (from $LAM^{AB/C}$ to $LAM_\parallel^{A/B/C}$). The border between parallel lamellar-*in*-lamellar and perpendicular lamellar-*in*-lamellar is the straight line $N\chi_{AB} = 2N\chi_{AC} = 2N\chi_{BC}$. At *m* = 3 (Fig. 4.18b) the region of parallel lamellar-*in*-lamellar $LAM_\parallel^{A/B/C}$ becomes smaller and the straight transition line between $LAM_\parallel^{A/B/C}$ and $LAM_\perp^{A/B/C}$ changes into $N\chi_{AB} = 0.28N\chi_{AC} = 0.28N\chi_{BC}$. At higher values of *m* the parallel lamellar-*in*-lamellar phase disappears (Fig. 4.18c). Increasing the number of side chains *m* the chain sections between consecutive side chains and the side chains become shorter and higher values of the Flory-Huggins parameters are required to induce microphase separation. As a consequence, the stability regions of $LAM^{AB/C}$, $LAM^{AC/BC}$ and the disordered phase *DIS* all increase. The parallel lamellar-*in*-lamellar phase becomes unfavorable due to the high AB interfacial energy. In Fig. 4.19 the free energies of the parallel and perpendicular lamellar phases are shown as a function of the number of side chains *m*. For the fixed values of the other parameters selected, the free energies become approximately the same for *m* = 3.
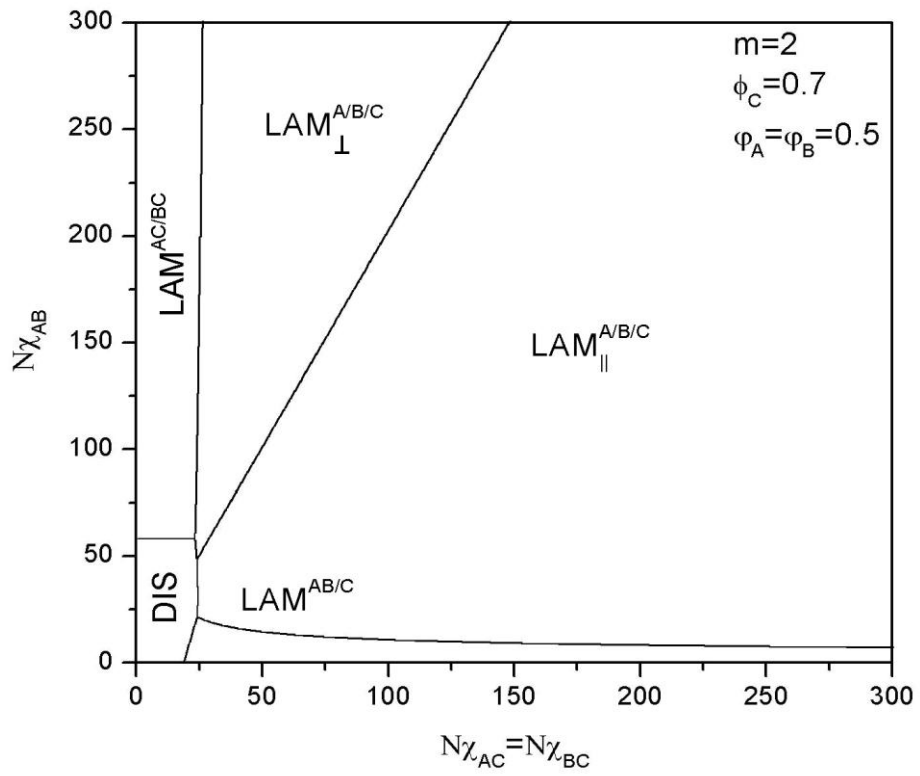
a)
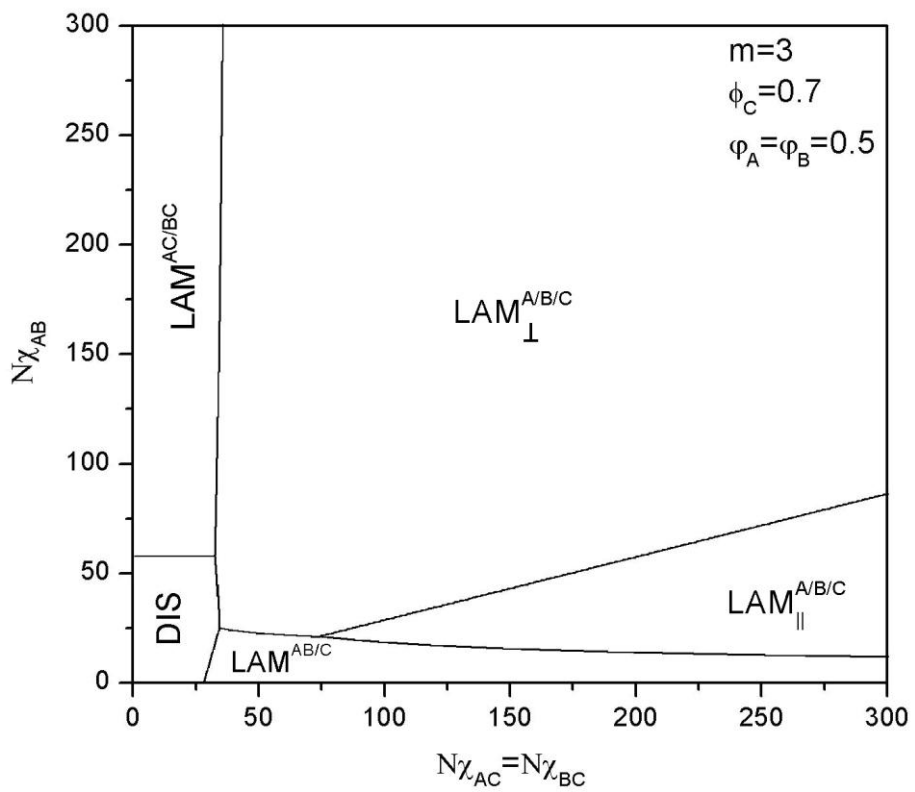
b)
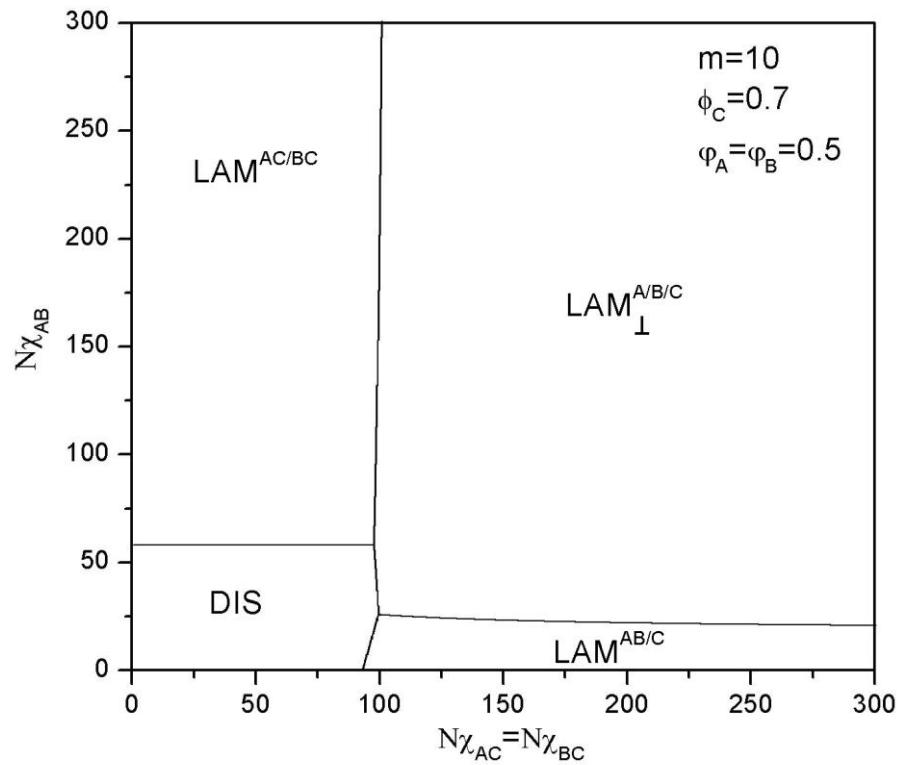
c)

Figure 4.18. Phase diagrams of the lamellar phases of (A-*comb*-C*)-b*-(B-*comb*-C) as a function of the Flory-Huggins interaction parameters $N\chi_{AB}$ and $N\chi_{AC} = N\chi_{BC}$ for fixed $\phi_C = 0.7$, $\varphi_A = \varphi_B = 0.5$ a) $m = 2$; b) $m = 3$; c) $m = 10$
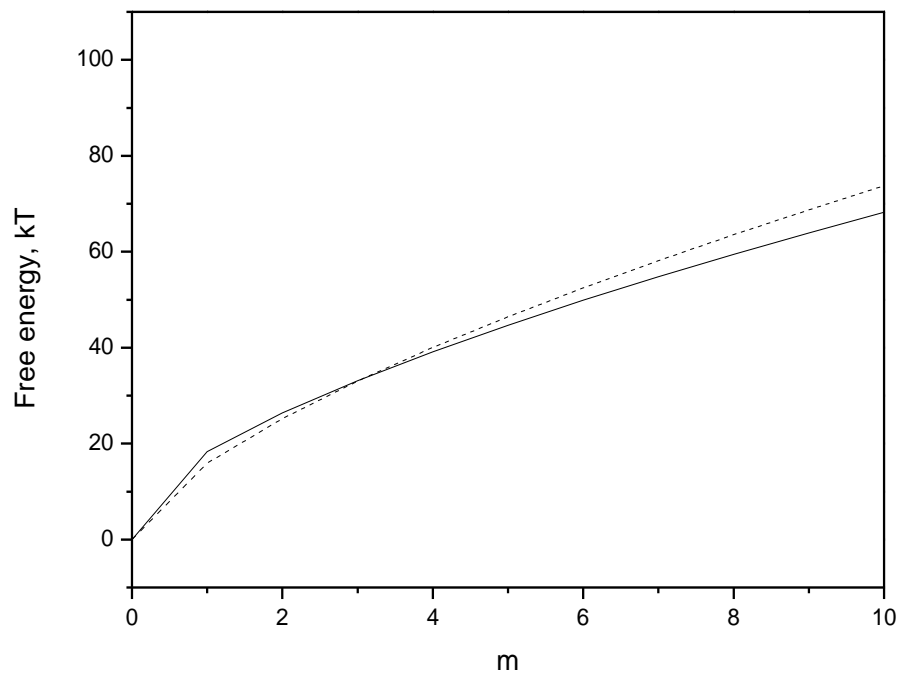
Figure 4.19. Free energy of the lamellar phases as a function of the number of side chains *m*. Solid line represents free energy of the perpendicular lamellar-*in*-lamellar phase and the dotted line the parallel lamellar-*in*-parallel lamellar phase.

Next we turn our attention to asymmetric diblock backbones. Figure 4.20 presents phase diagrams as a function of the Flory-Huggins interaction parameters $N\chi_{AC} = N\chi_{BC}$ and the volume fraction φ_B of B. The diagrams are calculated at a fixed volume fraction of C blocks $\phi_C = 0.7$, because in that case the fully separated system consists of alternating C and AB layers with different internal structures in the AB layers. Figure 4.20a corresponds to $m = 10$, $N\chi_{AB} = 200$. In this case, as long as $N\chi_{AC} = N\chi_{BC} < 100$, the phase behavior has already been presented in phase diagram Fig. 4.5. When $N\chi_{AC} = N\chi_{BC} > 100$, four different phases are stable. As a function of the volume fraction φ_B these are the lamellar $LAM^{AB/C}$ phase, the disk-*in*-lamellar phase $HEX_B^{A/B/C}$ (Fig. 4.15, core formed by B), the perpendicular lamellar-*in*-lamellar structure $LAM_\perp^{A/B/C}$, the disk-*in*-lamellar phase $HEX_A^{A/B/C}$ (core formed by A) and again the lamellar $LAM^{AB/C}$ phase. For sufficiently low or high volume fraction φ_B the A and B blocks form a disordered phase and the system essentially resembles a simple comb copolymer system. When $m = 2$ (Fig. 4.20b) the parallel lamellar-*in*-lamellar state $LAM_\parallel^{A/B/C}$ appears in the range $0.385 < \varphi_B < 0.615$. At $\varphi_B = 0.5$ the lowest transition point occurs at $N\chi_{AC} = N\chi_{BC} \approx 98$. The border line between the fully microphase separated system and AC/BC phases shifts to smaller values of Flory-Huggins interaction parameters $N\chi_{AC} = N\chi_{BC} \approx 25$.

Decreasing $N\chi_{AB}$ to 100 changes the phase diagram considerably (Fig. 4.20c). The BCC phases are not stable anymore and the width of disordered state area increases.

a)

b)

c)
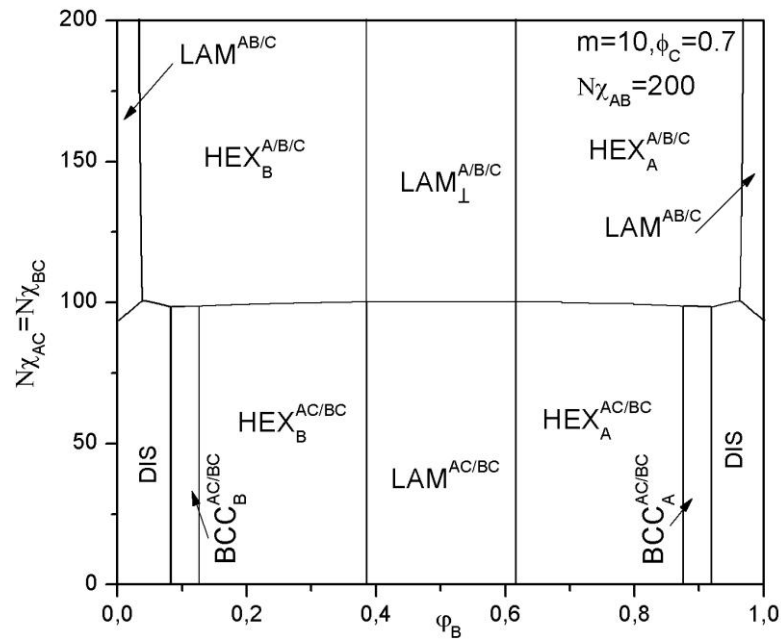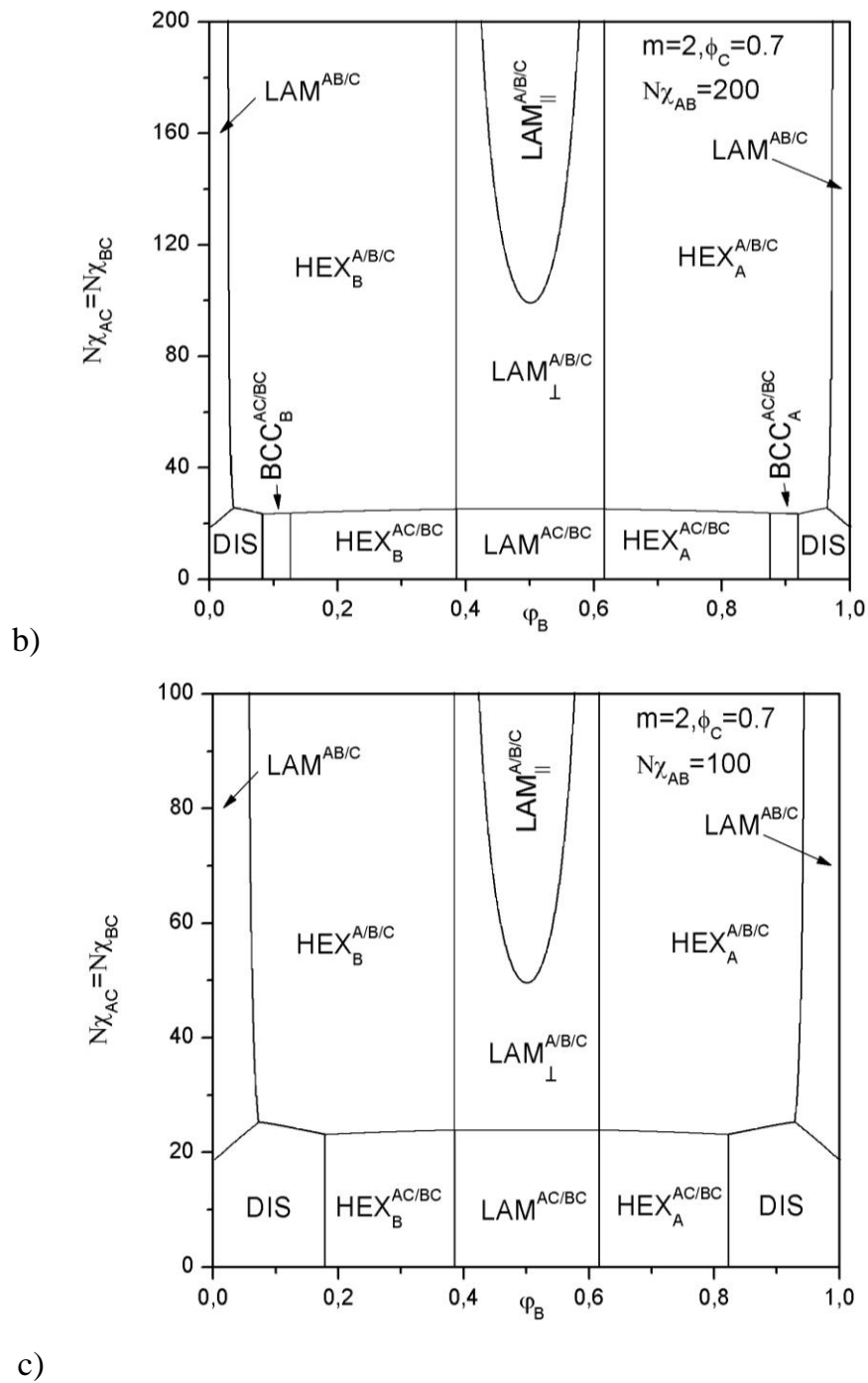
Figure 4.20. Phase diagrams of (A-*comb*-C*)-b*-(B-*comb*-C) in terms of Flory-Huggins parameters $N\chi_{AC} = N\chi_{BC}$ versus volume fraction φ_B:

a) $m = 10$, $N\chi_{AB} = 200$, $\phi_C = 0.7$ b) $m = 2$, $N\chi_{AB} = 200$, $\phi_C = 0.62$;

c) $m = 2$, $N\chi_{AB} = 100$, $\phi_C = 0.7$

Figure 4.21 presents another series of phase diagrams, now in terms of the Flory-Huggins interaction parameters $N\chi_{AB}$ and the volume fraction of B blocks φ_B. For fixed values $m = 20$, $N\chi_{AC} = N\chi_{BC} = 200$, $\phi_C = 0.7$ four different structures are possible.

At small values of $N\chi_{AB} < 24$ the lamellar phase with mixed AB blocks $LAM^{AB/C}$ is formed. The borders between the different structures are similar to the borders in the phase diagram for simple diblock copolymers with the noticeable exception that the BCC structure is absence. Of course, the disordered state of the latter is replaced by the $LAM^{AB/C}$, the *HEX* by $HEX^{A/B/C}$ and the simple lamellar by $LAM_{\perp}^{A/B/C}$. The reason becomes clear by comparing the free energy of the structures considered with the free energy of simple diblocks. The difference is the extra energy due to the C side chains, however, this extra energy is the same for all structures considered.

When $m = 3$, the diagram is no longer similar to that of simple diblocks due to the appearance of $LAM_{\parallel}^{A/B/C}$. Its stability region is restricted to $12 < N\chi_{AB} < 57$ for $N\chi_{AC} = N\chi_{BC} = 200$, $\phi_c = 0.7$ (Fig. 4.21 b). Increasing the AC and BC interaction to $N\chi_{AC} = N\chi_{BC} = 400$ (Fig. 4.21c) the stability region of $LAM_{\parallel}^{A/B/C}$ also increases to $10 < N\chi_{AB} < 113$.
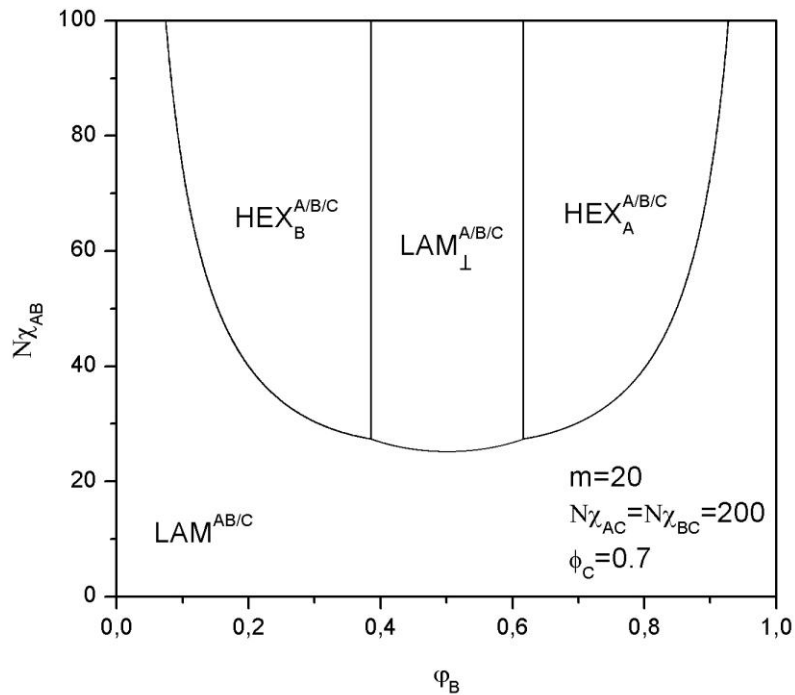
a)
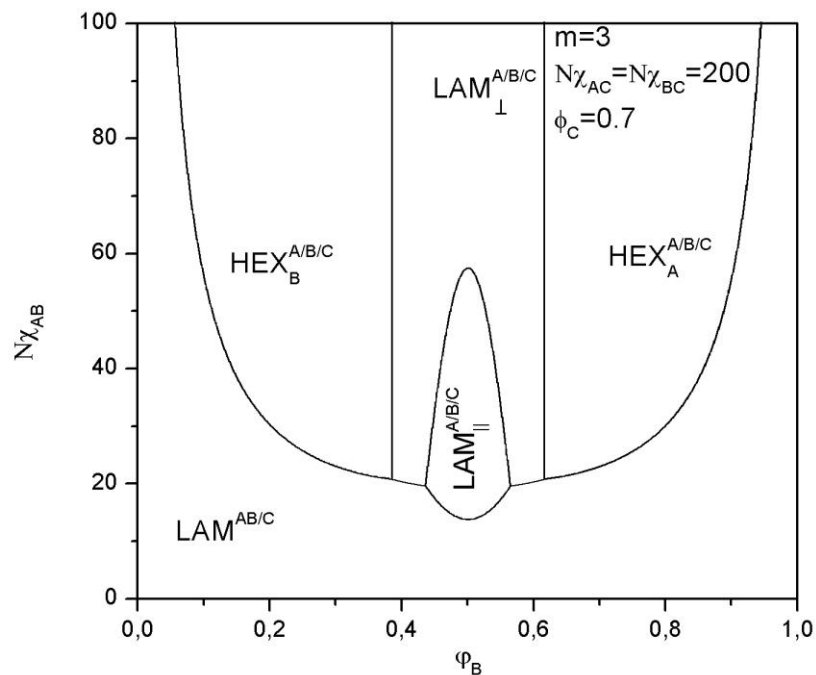
b)
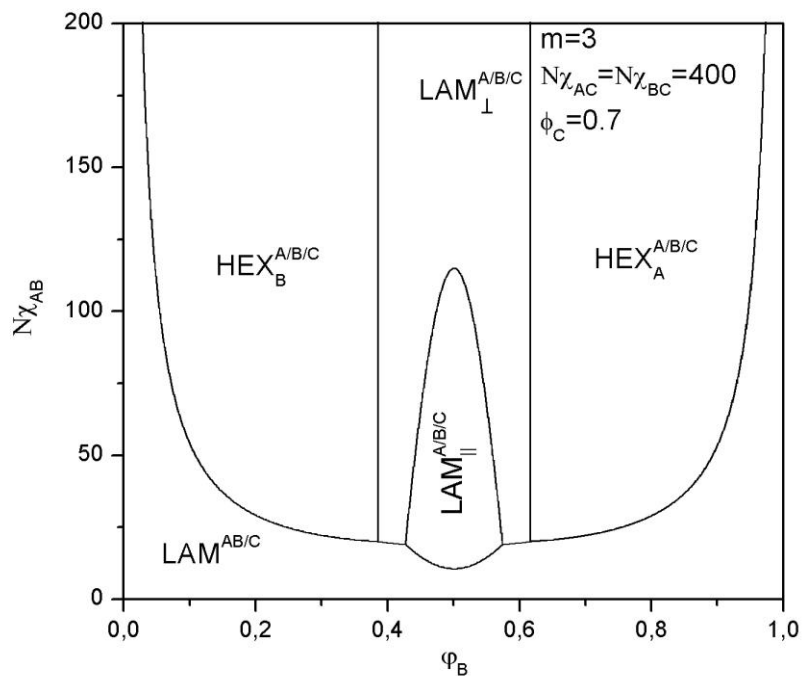
c)

Figure 4.21. Phase diagrams of (A-*comb*-C*)-b-*(B-*comb*-C) in terms of Flory-Huggins interaction parameter $N\chi_{AB}$ versus volume fraction φ_B:

a) $m = 10$, $N\chi_{AC,BC} = 200$, $\phi_C = 0.7$ b) $m = 2$, $N\chi_{AC,BC} = 200$, $\phi_C = 0.7$;

c) $m = 2$, $N\chi_{AC,BC} = 400$, $\phi_C = 0.7$.
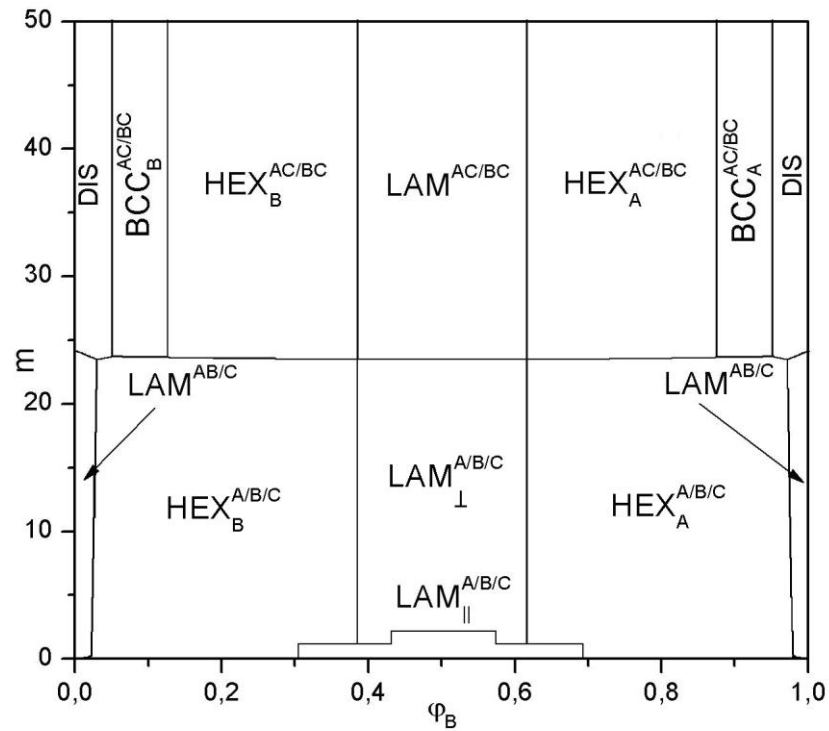
a)

]
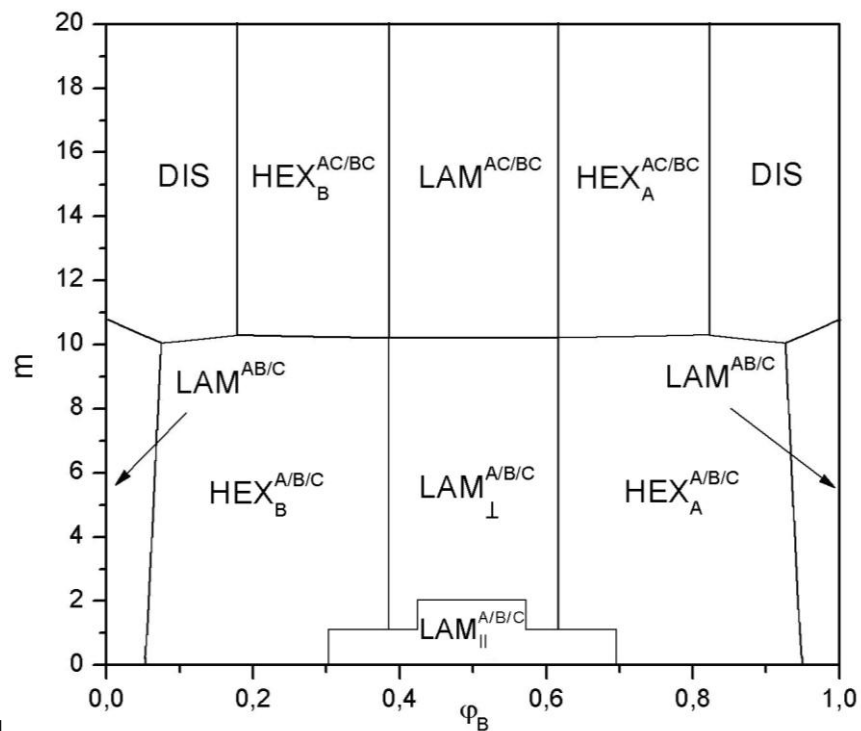
b)

Figure 4.22. Phase diagrams in terms of grafting density m versus volume fraction φ_B of B blocks.

a) $N\chi_{AB} = N\chi_{AC} = N\chi_{BC} = 200, \ \phi_C = 0.62$

b) $N\chi_{AB} = N\chi_{AC} = N\chi_{BC} = 100, \ \phi_C = 0.7$.

113

Finally, in Fig. 4.22 phase diagrams are presented in terms of the grafting density m versus the volume fraction φ_B of B blocks. For increasing m the number of segments of the repeat unit $n = 2N/m$ decreases and these diagrams are a kind of inverted versions of Fig.4.20 with two differences. Due to the integer values of m we have horizontal borderlines and secondly $n\chi_{AB}$ is not fixed any more The most striking observation concerns the stability region of $LAM_{\parallel}^{A/B/C}$, which strongly depends on m, the larger m, the smaller the region.

4.2.5 Concluding remarks

Using the strong segregation theory the self-assembly of diblock copolymer-based comb copolymers with chemically identical side chains (A-*comb*-C)-*b*-(B-*comb*-C) was investigated. Different regimes were considered. When the repulsion between the C side chains and the AB backbone is insufficient, the C blocks are mixed with the AB blocks with the A blocks microphase separated from the B blocks. In that case the behavior is equal to that of simple diblock copolymers with a renormalized Flory-Huggins parameter $(1-\phi_C)^2 \chi_{AB}$. The second case is characterized by mixed A and B blocks microphase separated from the C side chains. Due to the side chain architecture the phase stability region of the lamellar phase is shifted to $0.6 < \phi_C < 0.8$. For the specific case considered ($\varphi_A = \varphi_B = 0.5; m = 20$) the hexagonal structure with the core of the cylinders formed by loops from the A and B blocks is no longer stable. Furthermore, the stability region of the BCC structure where the core of the spheres is formed by the C side chains is significantly increased compared to the simple diblock case. All these observations are in excellent agreement with previously reported results by Milner on the effect of chain architecture on the asymmetry in copolymer phase behavior [35]. The final case considered concerned the most interesting situation where all three components microphase separate from each other and hierarchically ordered structures are formed. The volume fraction of C side chains was assumed to satisfy $0.6 < \phi_C < 0.8$ so that only lamellar structures, where one layer is formed by the C side chains and the other by the AB backbones, are stable. Perpendicular lamellar-*in*-lamellar and parallel lamellar-*in*-lamellar and disk-*in*-lamellar phases were found and characteristic phase diagrams presented. In the case of a lamellar-*in*-lamellar morphology, the perpendicular lamellar-*in*-lamellar is usually the preferred state. Only when the grafting density is relatively small, i.e. $m \leq 4$, does the parallel lamellar-*in*-lamellar state become possible.

4.3 Comb-like diblock copolymers: dissipative particles dynamics investigation

In order to verify some results obtained by SSL theory it was decided to use dissipative particle dynamics (DPD) [44-46]. This simulation technique was chosen because the collection of many monomers into a few bead-and-spring particles allows us to investigate the molecular behavior on a longer time- and length-scale. From the beginning DPD was proposed to simulate fluids, that is why it can be used to investigate dynamics of polymer melts.

4.3.1 Model and calculation details

The comb-like diblock copolymer DPD model is represented in Fig. 4.23. In our DPD simulations the lengths of the backbone and the side chains were taken to be 11 and 3 DPD, respectively. The spacing between the side chains was fixed at 1 DPD bead, i.e. a side chain is attached to every other backbone bead. Hence, the volume fractions of the backbone and the side chains equal $f_{bb} = 0,38$ and $f_C = 0.62$, respectively. These numbers were selected because this should give rise to large length scale lamellar structures, as demonstrated in Part 4.2 of this thesis. The size of simulation box was chosen to be almost twice as large as the backbone length $L_{box} = 20$ to avoid boundary effects. The coefficients for the DPD soft-core potential are presented in Table 1.

a_{ij}	A	B	C
A	25	120	120
B	120	25	120
C	120	120	25

Table 1. Potential coefficients for different types of beads.
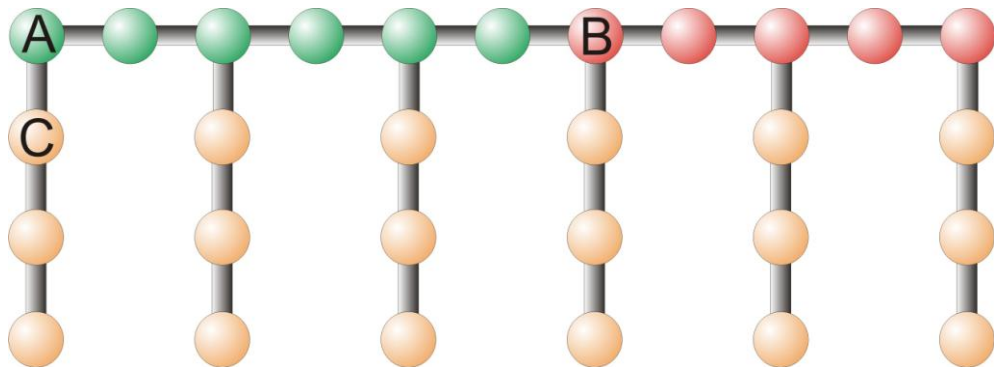
Figure 4.23. Comb-like diblock copolymer DPD model, with $N_A = 6$ $N_B = 5$ $N_C = 18$.

4.3.2 Results and discussion

We start with the most asymmetric backbone where $N_A = 1$, $N_B = 10$, $N_C = 18$. When all interactions are strongly unfavorable the chains align well into a lamellar structure, where one type of layers consists of C beads and the other of A and B beads. The thickness of the alternating layers is different due to the unequal volume fractions of backbone and side chains. Because the repulsion between the A and B beads was taken to be high, a second scale microphase separation exists inside the AB layers. Since only one side chain is connected to the A block, the A beads are located at the interface between the C and B blocks (fig. 4.24a,b). There is not enough material to form A layers, so the A beads form a kind of disks. The radius of these disks is not large enough to have a hexagonal ordering (fig. 4.24c). They are too far apart and do not affect each other. The structure formation within the successive AB layers is independent from each other because they are screened by C layers. Hence there is no alignment between the A domains in the different layers.

a)   b)

c)
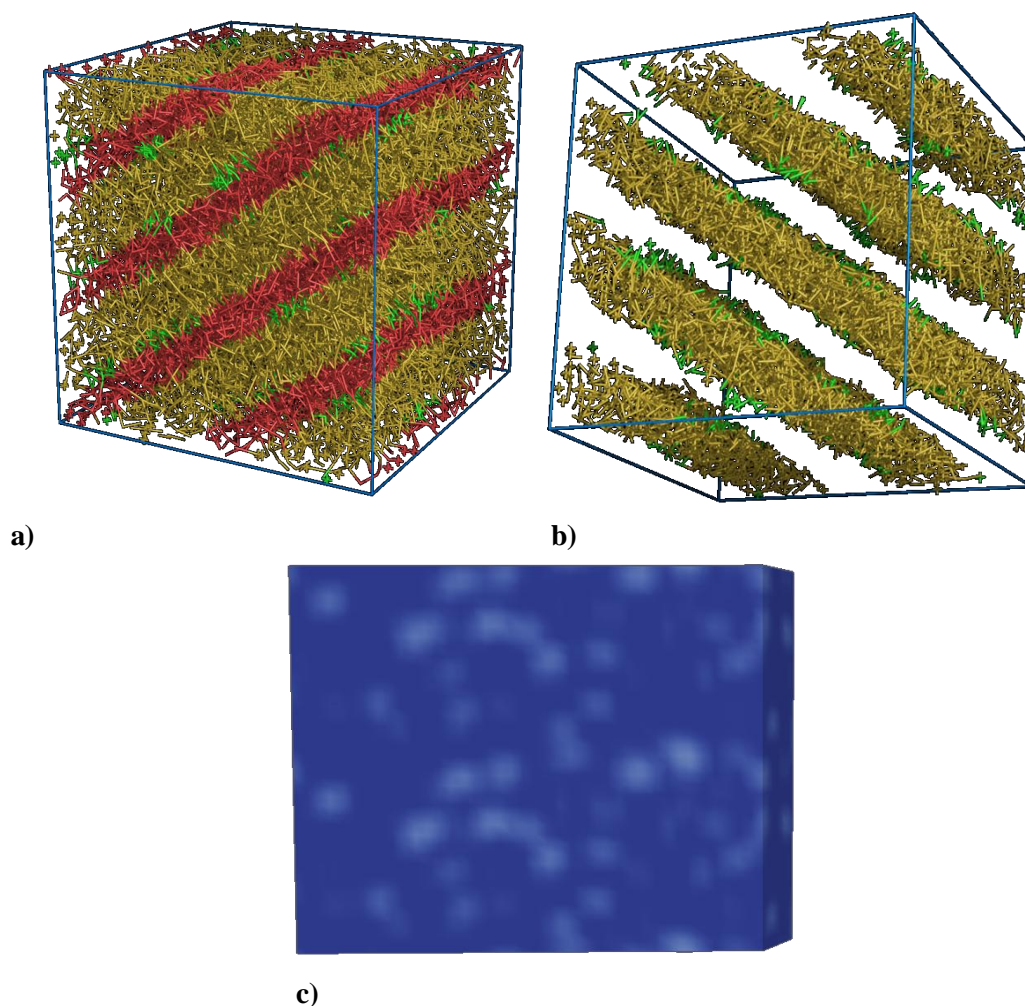
Figure 4.24. $N_A = 1$, $N_B = 10$, $N_C = 18$. a) Snapshot; b) Snapshot without B component; c) Density volume fraction profile of BC interface. White color represents B component.

In the present study the interactions between the backbone beads A, B on the one hand and the side chain C beads on the other were taken to be equal. This results in a flat interface between the C and AB compounds. Otherwise, if the interaction between A and C differs from that between B and C it is possible that the interface is no longer flat, because system will try to find a balance between interfacial and stretching energies. In that case the stretching of the C blocks becomes more complex and long range correlation between different AB layers can appear.

When the volume fraction of the A species increases (N_A = 2 or 3) the A type domains become bigger. The primary structure remains lamellar because of the volume fraction of C and A, B blocks. As shown by the SSL investigation, a cylindrical structure of the A domains appears at the same volume fraction ratio as for simple diblock copolymers. And, indeed, in our DPD simulations for N_A = 2 or 3 we observe this cylindrical structure. Fig. 4.25a shows a snapshot of a characteristic disks-*in*-lamellar structure. Fig. 4.25b and c show one AB layer where it is clearly showing the hexagonal ordering of the A domains. By increasing the volume fraction f_A, the radius of the cylinders increases. As in the previous case there is no correlation between the microphase separated structures in different layers.

a)   b)

c)
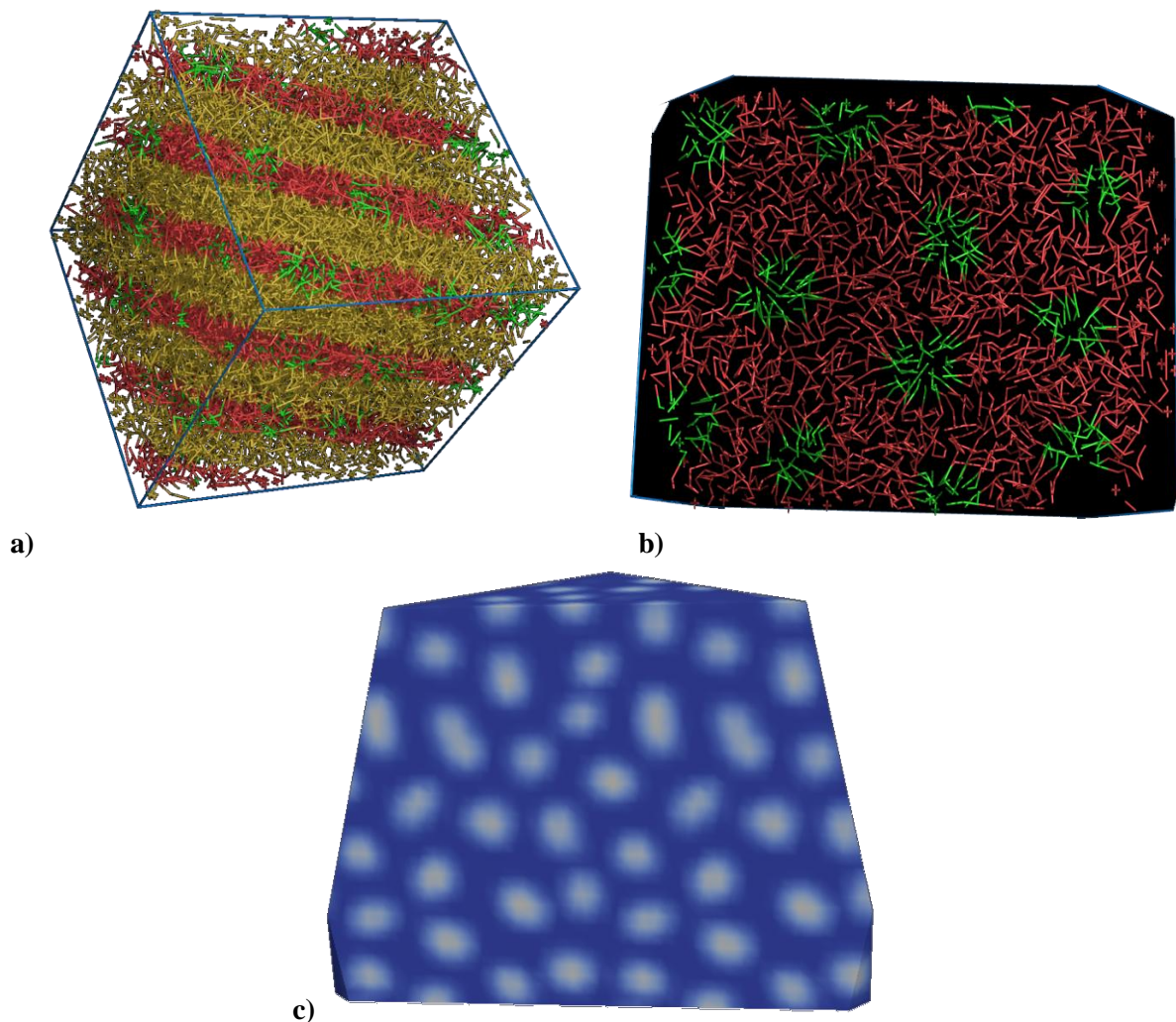
Figure 4.25. N_A = 2, N_B = 9, N_C =18. a) Snapshot; b) Single AB layer, C component is not shown; c) Volume fraction profile of AB layer. White color represents A component.

The most interesting case is the near symmetric backbone case when $N_A = 5$ or 6. For a simple AB diblock copolymer there should be a well-defined lamellar structure. Characteristic snapshots clearly show that a lamellar-like AB morphology is also established for our comb-like structures, Fig. 4.26. The A and B blocks self-assemble in stripes in each layer, but these stripes are not always well aligned. Fig 4.27 presents several volume fraction profiles for the A blocks. Well-aligned (Fig. 4.27b and c) and stripes that change direction (rotation on 90 degrees) are observed (Fig. 4.27a). This rotation can be explained by the kinetics of the strip formation. For example two centers with different directions of growth appear at the beginning of the microphase separation and after some time they will grow to maximum size and split with each other, because there are constrains by the side chains such a situation becomes quite stable and this defect has a very long relaxation time.

It is should be mentioned that there is only a small amount of chains that belong to more than one layer. Never more than 10 chains on a total number of chains per simulation box equal to approximately 827.
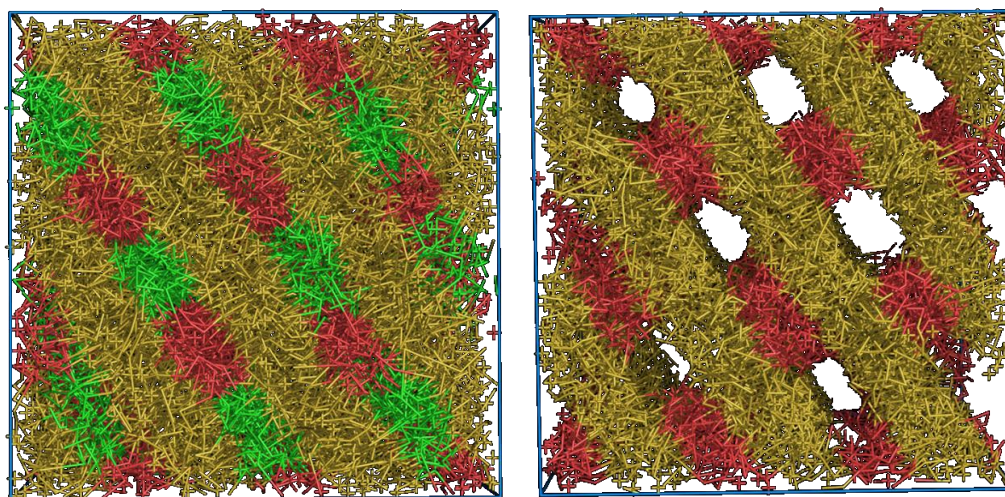
Figure 4.26. $N_A = 5$, $N_B = 6$, $N_C = 18$. a) Snapshot; b) Snapshot without A component.

a)   b)   c)
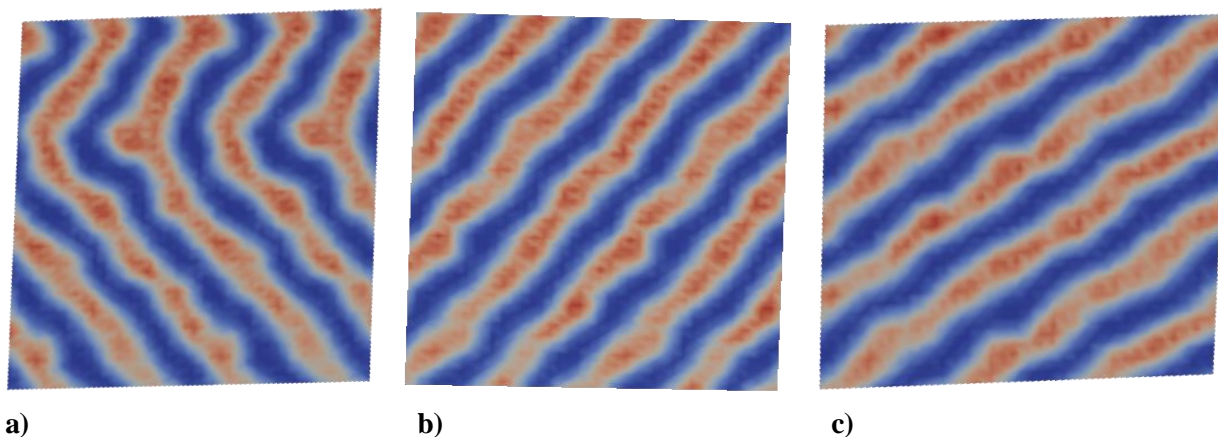
Figure 4.27. $N_A = 5$, $N_B = 6$, $N_C = 18$. Volume fraction profiles of A species in different layers, obtained by the annealing method. Red color represents maximum of volume fraction of B component.
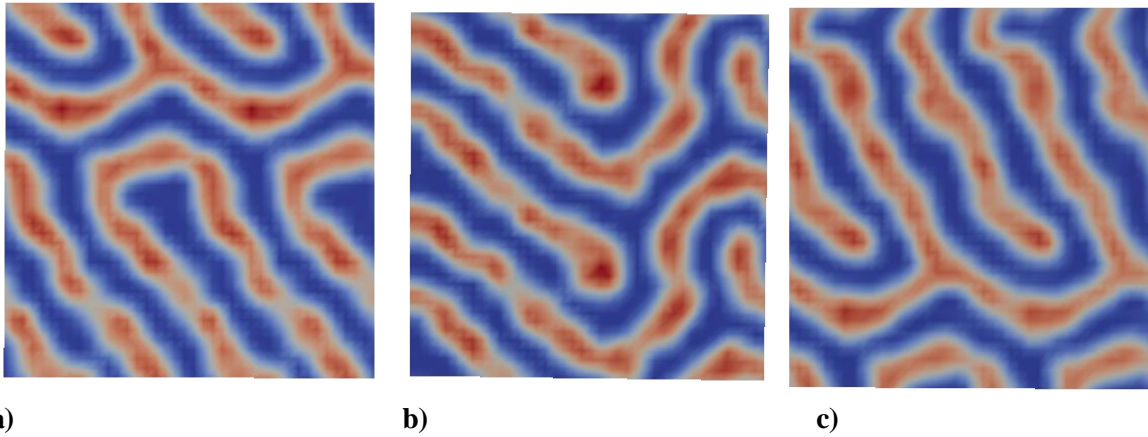
Figure 4.28. $N_A = 5$, $N_B = 6$, $N_C = 18$. Volume fraction profiles of A species in different layers obtained by fast cooling method. Red color represents maximum of volume fraction of B component.

The "quality" of the A- and B-stripes in the layers strongly depends on the method they were obtained. In principle there are two different methods. One is so-called fast cooling. In this case the interaction parameters change value in one step. If the parameters of the system change fast, the system can freeze in a metastable phase. The fast cooling method is good to find new phases, because such metastable states may be stable under certain conditions. The other method is annealing where the interaction parameter values change slowly. It our case the parameter values changed from their initial value to their end value during $2 \cdot 10^6$ DPD time steps. Usually, the structures formed using the annealing technique have less defects. Fig. 4.27 presents volume fraction profiles of different layers obtained with the annealing method and Fig. 4.28 those obtained with the fast cooling technique. The stripes in the first case are either straight or with one defect like changing direction with 90 degrees. In the second case the stripes are not straight and are connected to each other. Due to the comb-like architecture, the side chains strongly restrict the possibility for chains reconfiguration. As a consequence, such non-aligned stripes were stable during the calculation time of $5*10^6$ DPD time steps.

To study the dynamics of the A, B strip formation inside the layers, the order parameter S based on the Saupe tensor (Eq. 4.52) [47]) was calculated.

$$Q_{\alpha\beta} = \frac{3}{2}(r_\alpha r_\beta - \delta_{\alpha\beta}) \qquad 4.52$$

Here **r** is a unit vector directed either along the bond which connects the A and the B beads or the bonds that connect the A and B beads with the attached side chain. The characters α and β are Cartesian indices, δ is the Kronecker symbol. The order parameter S is equal to the largest eigenvalue of the volume average of $Q_{\alpha\beta}$. S is zero in the completely disordered state, and it should be equal to one if the system is perfectly aligned. Values of the other eigenvalues indicate the degree of ordering in secondary directions. If **r** is a unit vector directing along the bond which connects the DPD A,B

with C beads we address ordering of C layers. Fig. 4.29 shows the order parameter dependence on time in DPD time steps. In the case of fast cooling the order parameters increased to fixed values in the first $3*10^2$ time steps and remain the same during subsequent calculation time. The graph shows that the ordering between the backbone and the side chains goes faster than that between the A and B blocks. In the case of the annealing procedure the formation consist of two parts. First blobs are formed during 10^6 steps, than there is jump when the blobs connect to each other and form stripes. From time 10^6 to $1.7*10^6$ the system undergoes ordering and after that the order parameters do not change until the end of the experiment. The value of S for the ordering between the A and B blocks is far less than for the ordering between side chains and backbone. This is due to the fact that the orientation of A and B strips in different layers is not correlated. Comparing values of S for fast cooling and for annealing, they are as expected higher in the latter case.

a)   b)
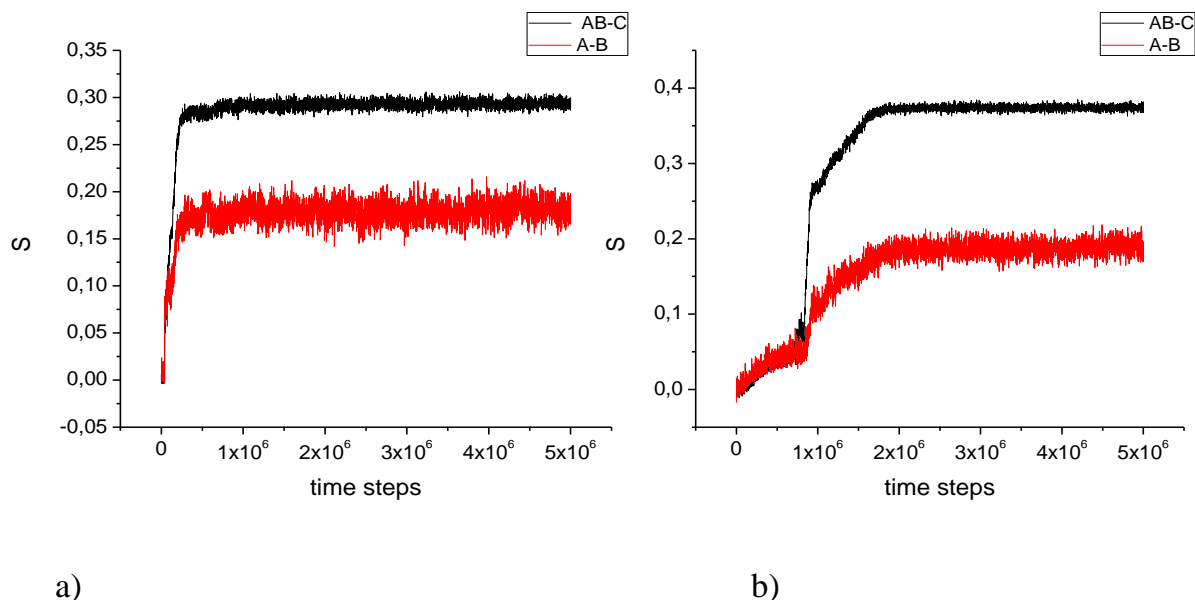
Figure 4.29. Order parameter dependence on time. Black line describes ordering between backbone and side chains, red line describes ordering between A and B blocks in the layers. a) Fast cooling, b) Annealing.

4.3.3 Concluding remarks

Using dissipative particle dynamics, a comb like diblock copolymer melt was investigated. Only one type of polymers was considered with a fixed grafting density and fixed volume fraction of side chains. It was found that three types of structures are possible for this system. For all backbone compositions the C side chains formed nearly perfectly ordered layers. The difference is only in the structures formed inside the AB layers. For the smallest A fraction, the A blocks form not ordered disks. These disks pack

hexagonally at higher A fractions. Finally near symmetric backbone compositions lead to lamellar ordering or more accurately stripes. There is no correlation between the AB ordering in the successive AB layers. To achieve highly ordered structures the so-called annealing procedure is preferred. The morphologies observed are in excellent agreement with the theoretical SSL predictions.

4.4 Summary

Self-Assembly of (A-*comb*-C)-*b*-(B-*comb*-C) block copolymers in a melt was investigated using two different approaches. A theoretical study was presented using the strong segregation theory. Three major cases were considered. In the first case both disordered comb blocks are microphase separated from each other, in case 2 the side chains C are microphase separated from the disordered A-*b*-B diblock backbones and, finally, in case 3 all species A, B and C are microphase separated from each other. In the first case the phase behavior is almost the same as for simple diblock copolymers. The only difference is a renormalized Flory-Huggins interaction parameter. In the second case the region of stability of the different phases is significantly changed compared to simple diblocks due to the comb architecture. The fully microphase separated case is characterized by hierarchical structure formation. We restricted the analysis to systems where self-assembly results in the formation of alternating C-layers and internally microphase separated AB layers. The latter consist of either alternating A- and B-stripes or disks of the minority component. In the former case, the A- and B-stripes are generally perpendicular to the C-layers. The parallel orientation is only possible for small grafting densities. As a second approach the DPD simulation technique was used to investigate only the fully microphase separated case with fixed volume fraction of side chains and fixed grafting density. The DPD simulations confirmed the structures found in the SSL theory. Aspects of the dynamics of the lamellar(stripes)-*in*-lamellar formation were discussed.

4.5 References

1. L. Leibler, *Macromolecules,* **1980**, *13*, 1602.
2. A.N. Semenov, *Sov. Phys. JETP*, **1985**, *61*, 733.
3. F.S. Bates and G. H. Fredrickson, *Annu. Rev. Phys. Chem.*, **1990**, *41*, 525.
4. M.W. Matsen and M. Schick, *Phys. Rev. Lett.*, **1994**, *72*, 2660.
5. M.W. Matsen and F.S. Bates, *Macromolecules*, **1996**, *29*, 1091.
6. I.W. Hamley, *The Physics of Block Copolymers*, Oxford University Press, Oxford, 1998.
7. C.A. Tyler and D.C. Morse, *Phys. Rev. Lett.,* **2005**, *94*, 208302.
8. M. Tanaka, T. Wakada, S. Akasaka, S. Nishitsuji, K. Saijo, H. Shimizu, M. I. Kim, H. Hasegawa, *Macromolecules*, **2007**, *40*, 4399.
9. F.S. Bates and G.H. Fredrickson*, Phys. Today*, **1999**, *52*, 32.
10. V. Abetz, P.F.W. Simon, *Adv. Polym. Sci.,* **2005***, 189*, 125.
11. C. Park, J. Yoon, and E.L. Thomas, Polymer, **2003**, *22*, 6725.
12. I.W. Hamley, *Angew. Chem. Int. Ed.,* **2003**, *42*, 1692.
13. M. Lodge, *Macromol. Chem. Phys.*, **2003**, *204*, 265.
14. M. Lazzari, G. Liu, S. Lecommandoux, Block Copolymers in Nanoscience, Wiley-VCH, Weinheim, **2006**.
15. T.H. Epps III, E.W. Cochran, C.M. Hardy, T.S. Bailay, R.S. Waletzko, F.S. Bates, *Macromolecules,* **2004** *,37*, 7085.
16. I.Y. Erukhimovich, *Eur. Phys. J. E,* **2005***, 18*, 383.
17. J. Masuda, A. Takano, Y. Nagata, A. Noro, Y. Matsushita, *Phys. Rev. Lett.,* **2006**, *97*, 098301.
18. Y. Smirnova, G. ten Brinke, I.Y. Erukhimovich, *J. Chem. Phys.,* **2006**, *124*, 054907.
19. Y. Matsushita, *Macromolecules,* **2007**, *40*, 771.
20. K. Hayashida, T. Dotera, A. Takano, Y. Matsushita, *Phys. Rev. Lett.,* **2007***, 98*, 195502.
21. Z. Guo, G. Zhang, F. Qiu, H. Zhang, Y. Yang, A-C. Shi, *Phys. Rev. Lett.,* **2008**, *101*, 028301.
22. M. Sun, P. Wang, F. Qiu, P. Tang, H. Zhang, Y. Yang, *Phys. Rev. E,* **2008**, *77*, 016701.
23. J. Qin, F.S. Bates, D.C. Morse, *Macromolecules,* **2010**, *43*, 5128.
24. G. Zhang, F. Qiu, H. Zhang, Y. Yang, A-C. Shi, *Macromolecules,* **2010**, *43*, 2981.
25. M. Olvera de la Cruz, I.C. Sanchez, *Macromolecules,* **1986**, *19*, 2501.
26. H. Benoit, G. Hadziioannou, *Macromolecules,* **1988**, *21*, 1449.
27. A.V. Dobrynin, I.Y. Erukhimovich, *Macromolecules,* **1993**, *26*, 276.
28. A. Shinozaki, D. Jasnow, A. C. Balazs, *Macromolecules,* **1994**, *27*, 2496.
29. D. P. Föster, D. Jasnow, A. C. Balazs, *Macromolecules,* **1995**, *28*, 3450.
30. L. Wang, L. Zhang, J. Lin, *J. Chem. Phys.,* **2008**, *129*, 114905.
31. C. Lee, S. P. Gido, Y. Poulos, N. Hadjichristidis, N. B. Tan, S. F. Trevino, J. W. Mays, *J. Chem. Phys.*, **1997**, *107*, 6460.
32. C. Lee, S. P. Gido, Y. Poulos, N. Hadjichristidis, N. B. Tan, S. F. Trevino, J. W. Mays, *Polymer,* **1988**, *39*, 4631.
33. M. Xenidou, F.L. Beyer, N. Hadjichristidis, S.P. Gido, N.B. Tan, *Macromolecules,* **1998**, *31*, 7659.
34. F.L. Beyer, S.P. Gido, C. Büschl, H. Iatrou, D. Uhrig, J.W. Mays, M.Y. Chang, B.A. Garetz, N.P. Balsara, N.B. Tan, N. Hadjichristidis, *Macromolecules,* **2000**, *33*, 2039.

35. S.T. Milner, *Macromolecules,* **1994**, *27*, 2333.

36. R.J. Nap, C. Kok, G. ten Brinke and S.I. Kuchanov, *European Phys. J. E,* **2001**, *4*, 515.

37. R.J. Nap, G. ten Brinke, *Macromolecules,* **2002**, *35*, 952.

38. J. Ruokolainen, R. Mäkinen, M. Torkkeli, T. Mäkelä, R. Serimaa, G. ten Brinke, O. Ikkala, *Science,* **1998**, *280*, 557.

39. J. Ruokolainen, G. ten Brinke, O. Ikkala, *Adv. Mater.*, **1999**, *11*, 777.

40. O. Ikkala, G. ten Brinke, *Science,* **2002**, *295*, 2407.

41. H.L. Chen, J.S. Liu, C.H. Yu, C.L Yeh, U.S. Jeng, W.C. Chen, *Macromolecules,* **2007**, *40*, 3271.

42. W.S. Chiang, C.H. Lin, B. Nandan, C.L. Yeh, M.H. Rahman, W.C. Chen, H.L. Chen *Macromolecules,* **2008**, *41*, 8138.

43. A. H. Hofman, M. Faber, G. ten Brinke, and K. Loos (unpublished).

44. R.D. Groot, T.J. Madden, *J. Chem. Phys.*, **1998,** *108*, 8713.

45. R.D. Groot, P.B. Warren, *J. Chem. Phys.*, **1997,** *107*, 4423.

46. P. Español, P.B.Warren, *Europhys. Lett.*, **1995,** *30*, 191.

47. A. Saupe, Angewandte Chemie, **1968**, *7*, 97.

Chapter 5

DNA-*b*-PFO block copolymers and SWNT complexes

5.1 Introduction

The characteristics properties of nanomaterials may depend strongly on the size. A good example is provided by single wall carbon nanotubes (SWNT), where changes in structure at the atomic scale can influence electronic and optical properties in a discontinuous manner. For most practical technologies it is therefore important to have control over the size of the nanostructures. The strong correlations between physical properties and size forced researches to find ways to prepare samples of SWNTs with well-defined geometrical properties, such as diameter, length and chirality. There are several approaches to sort SWNTs: selective chemistry, electrical breakdown, dielectrophoresis, chromatography, ultracentrifugation and improving monodispersity while growing SWNTs [1-7]. One of the latest surfactant-based separation methods of the purification process, the so-called density gradient ultracentrifugation, makes it possible to obtain narrow distributions of SWNTs in which over 97% of the SWNTs are within a 0.02-nm-diameter range [8]. Using more complex dispersing agents, such as poly(9,9-di-n-octylfluorenyl-2,7-diyl) (PFO) it is possible to selectively solubilize certain semiconducting nanotube chiralities [9].

One of the most interesting macromolecules is DNA. In recent years researches started to use DNA as highly flexible building blocks for devices [10–12]. Due to its amphiphilicity DNA can wrap around SWNTs and make them soluble in water [13]. It was shown that using specific oligonuceotide (ODN) sequences and chromatography it is possible to isolate individual SWNT species in solvent [13]. Other features of DNA can be used for non-destructive functionalization of SWNTs. Using hybridization of DNA highly ordered structures from SWNTs can be prepared [14,15]. Usually in studies of DNA and SWNT complexes, the macromolecules are bound by covalent bonds [16] or DNA is chemically modified [17,18]. DNA hybridization is hindered in such techniques due to the strong interaction between sidewalls and ODNs [19]. Another way is to combine two approaches by using a dispersant to isolate individual SWNTs and using DNA with a predefined structure to manipulate these SWNTs [20].

DNA – SWNT complexes were also studied by computer simulations [21-25]. Recent molecular dynamics simulations [24] of a SWNT interacting with DNA demonstrated that the DNA could be spontaneously encapsulated inside a SWNT in water. The van der Waals attraction between the nanotube and the DNA was found to be the main driving force for this phenomenon. However, the behavior of DNA depends on the diameter of the SWNT and on the initial position of both. If they are not specifically tuned, DNA wraps around SWNT [25].

In order to make water soluble CNT complexes with the ability to control the diameter of the carbon nanotube, nanotube/PFO-*b*-DNA block copolymer complexes were prepared. To proof that the PFO part of PFO-*b*-DNA is responsible for the selectivity properties, computer simulations were performed.

5.2 Model and Molecular Dynamics properties

The Molecular Dynamics computer simulations performed used the freeware package, Gromacs [28] v 3.3.1, with the following force fields: amber99p [29] for simulation ssDNA interactions and OPLS force field [30] for PFO and DNA interactions. The 5'-end of a 22mer ssDNA (5′-CCT CGC TCT GCT AAT CCT GTT A-3′) was connected via phosphodiester linkage to PFO consisting of 6 monomer (9,9-dioctylfluorene) units with phenyl group at the open end. The length of the SWNT used was approximately the same as the length of the PFO block to reduce simulation time and to completely cover the SWNT length by one PFO molecule. The molecular complexes were dissolved in a periodic $11 \times 13 \times 12$ nm box with TIP3P water [31] as the solvent. The number of Na^+ ions was equal to the number of negative charges on the oligonucleotides to make the system charge neutral. The carbon nanotube was generated using parameters listed in Table 5.1 [32]. The carbon atoms of nanotubes were treated as uncharged Lennard-Jones particles and the force field parameters are shown in Table 5.2.

Name	Parameter or formula
C–C bonding length a_{C-C}	0.142 nm
Unit vector R_1, R_2	(1, 0), (1/2, √3/2)
Chiral vector $B\_$	$\vec{B} = n\vec{R}_1 + m\vec{R}_2$
Circumference of nanotube L	$L = a_{c-c}\sqrt{3(n_2 + nm + m_2)}$
1-D translation vector $\vec{T}$	$\vec{T} = t_1\vec{R}_1 + t_2\vec{R}_2$
Length of $\vec{T}$	$\left|\vec{T}\right| = \sqrt{\dfrac{3L}{d}}$
Number of atoms per unit cell N	$N = \dfrac{4(n_2 + nm + m_2)}{d}$
Chiral angle θ	$\theta = \arctan(\dfrac{\sqrt{3}m}{2n + m})$

Table 5.1. Selected parameters for (*n, m)* CNTs.
d is the highest common divisor of (2n + m, 2m + n).

$K_{Cr} = 478.9$ kJ mol^{-1} Å^{-2}	$r_C = 1.418$ Å
$K_{C\theta} = 562.2$ kJ mol^{-1}	$\theta_C = 120.0$ º
$K_{C\varphi} = 25.12$ kJ mol^{-1}	$\gamma = 2.1867$ Å^{-1}
$\varepsilon_{C-C} = 0.4396$ kJ mol^{-1}	$\sigma_{C-C} = 3.851$ Å

Table 5.2. Force field parameters for CNT interaction potentials[8]. K_{Cr}, r_C, and γ are the parameters of the Morse potential, $K_{C\theta}$ and θ_C the angle parameters, and $K_{C\varphi}$, is the torsion parameter; E_{C-C} and σ_{C-C} are the Lennard-Jones parameters for the carbon-carbon interaction.

5.3 Results

In the initial state, the CNT and the DNA-*b*-PFO block copolymers were aligned along the nanotube. The total simulation time was equal to 8 ns. Two cases were investigated. First, at the initial state the DNA part of the diblock copolymer (PFO-*b*-DNA) was closer to the CNT than the PFO block (fig. 5.1). During the first 100 ps some monomer units of DNA adsorbed onto the CNT surface. The more monomers adsorbed the closer the PFO block becomes to the CNT. When the distance between CNT and PFO became sufficiently small, PFO rapidly adsorbed on the CNT surface. The number of adsorbed DNA monomer units is highly fluctuating due to the thermal motion of its free end.

In the second case, in the initial state the PFO part of the diblock copolymer (PFO-*b*-DNA) was closer to the CNT than the DNA block. In a time less than 50 ps the distance between the PFO block and the CNT surface rapidly decreased. While the CNT is covered by PFO blocks, DNA blocks were stable in water showing free waving during the whole simulation time. Some part of the DNA can be adsorbed by the CNT, but because of the entropy loss it again detaches rapidly from the CNT surface.

By putting five PFO-*b*-DNA block copolymers and one CNT in the simulation box it was shown that only four diblocks are enough to cover the surface of the CNT. The length of the alkyl tails determines how many PFO blocks are needed to cover the whole surface of the CNT. In our experiments this length was equal to 5 monomer units. The distance between CNT and the adsorbed PFO was measured to be 4.4 Å. Both CNT and PFO are hydrophobic molecules which is responsible for the strong interaction between them in water. Another point is that PFO is a stiff flat molecule which increases the surface contact between PFO and CNT. Hence PFO displaces DNA from the CNT surface, creating a dense hydrophobic core with a hydrophilic shell of DNA chains.

In conclusion, our simulations demonstrate that because only the PFO block from the PFO-*b*-DNA diblock binds to SWNT, it becomes possible to extract from solution SWNTs with precisely defined diameter. The length of the alkyl subchains of the PFO block determines how many diblocks can bind to SWNT. This implies that SWNTs with different diameters will bind different number of diblocks. This then allows to extract SWNTs with a precisely predetermined diameter from solution.

Figure 5.1. Snapshots of two DNA-*b*-PFO block copolymers and one SWNT at different time steps, where at the initial point the DNA block was closer to the SWNT.
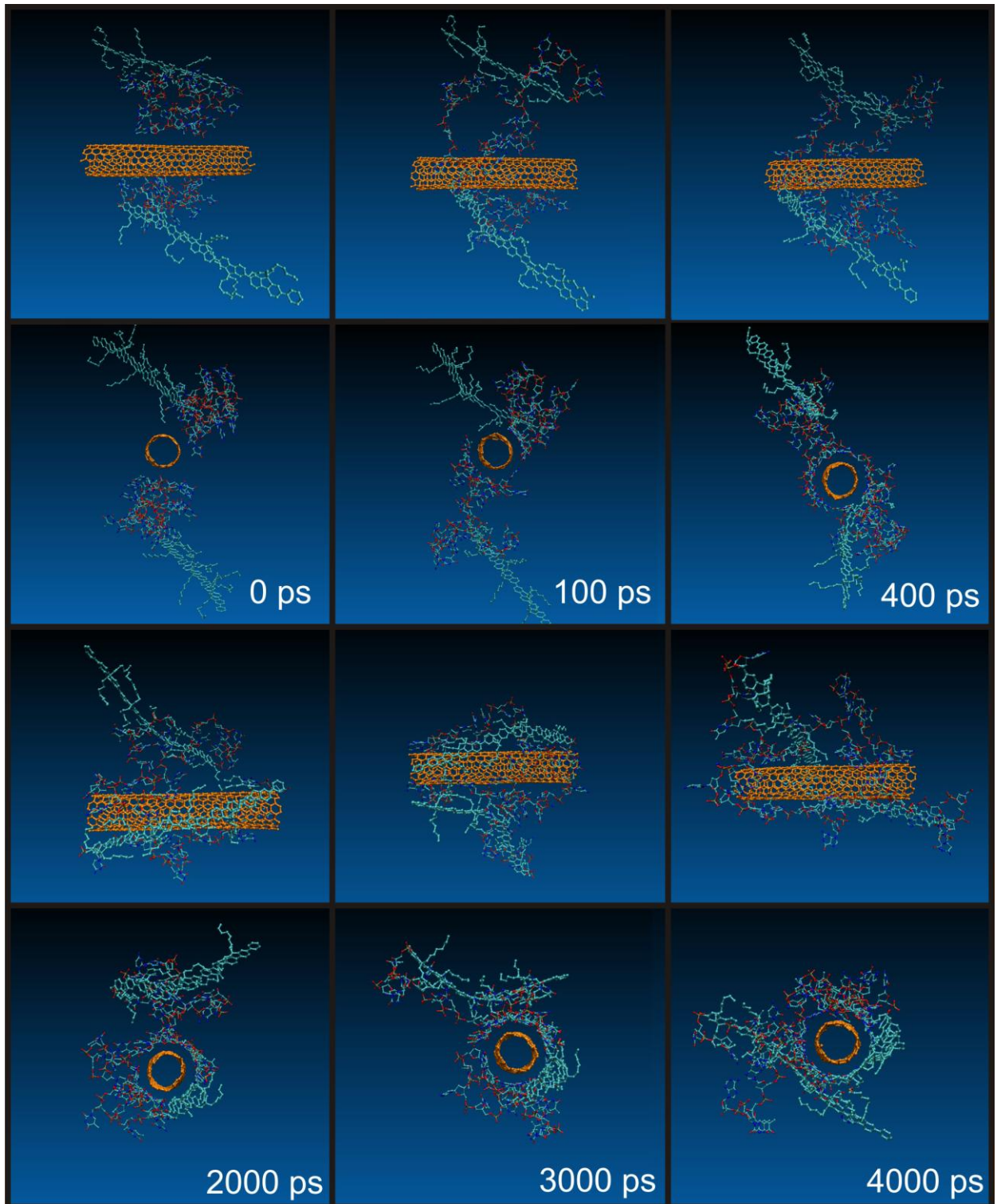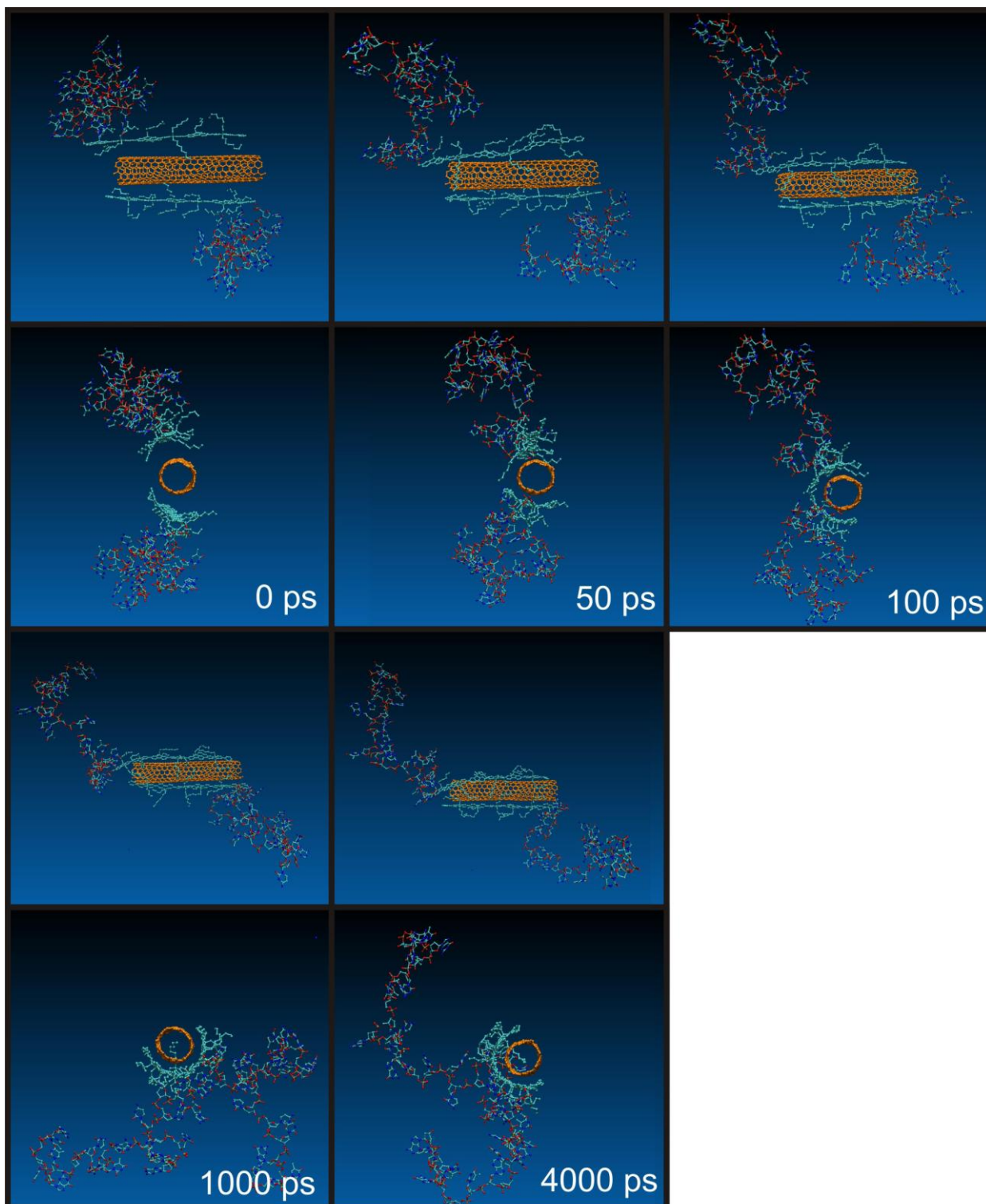
Figure 5.2. Snapshots of two DNA-*b*-PFO block copolymers and one SWNT at different time steps, where at the initial point the PFO block was closer to the SWNT.
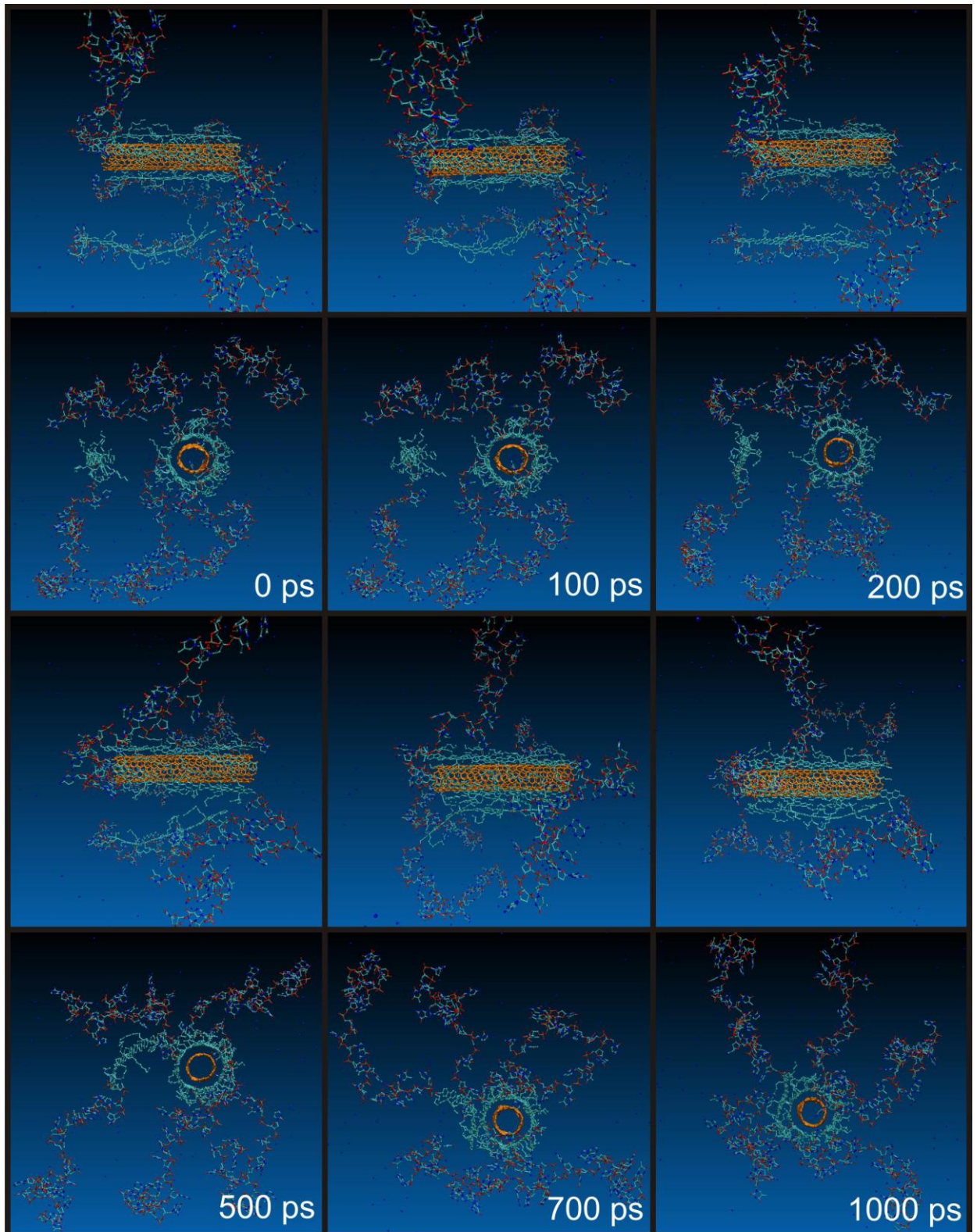
Figure 5.3. Snapshots of two DNA-PFO block copolymers and one SWNT at different timesteps, where at initial point block copolymer was closer to SWNT by PFO block

5.4 References

1. M. Hersam, *Nature Nanotechnol.*, **2008,** *3*, 387.
2. D. Tasis, N. Tagmatarchis, A. Bianco, M. Prato, *Chem. Rev.*, **2006**, *106*, 1105.
3. M. Tchoul, W. Ford, G. Lolli, D. Resasco, S. Arepalli, *Chem. Mater.,* **2007**, *19*, 5765.
4. M.J. O'Connell1, S.M. Bachilo, C.B. Huffman, V.C. Moore, M.S. Strano, E.H. Haroz, K.L. Rialon, P.J. Boul, W.H. Noon, C. Kittrell, J. Ma, R.H. Hauge, R.B. Weisman, R.E. Smalley, *Science,* **2002**, *297*, 593.
5. V.C. Moore, M.S. Strano, E.H. Haroz, R.H. Hauge, R.E. Smalley, *Nano Lett.*, **2003**, *3*, 1379.
6. J. Amiran, V. Nicolosi, S.D. Bergin, U. Khan, P.E. Lyons, J.N. Coleman, *J. Phys. Chem. C*, **2008**, *112*, 3519.
7. M.S. Arnold, A.A. Green, J.F. Hulvat, S.I. Stupp, M.C. Hersam, *Nature Nanotechnol.,* **2006**, *1*, 60.
8. A. Nish, J. Hwang, J. Doig, R. Nicholas, *Nature Nanotechnol.,* **2007**, *2*, 640.
9. M. Zheng, A. Jagota, E.D. Semke, B.A. Diner, R.S. Mclean, S.R. Lustig, R.E. Richardson, N.G. Tassi, *Nature Mater.*, **2003**, *2*, 338.
10. P.W.K. Rothemund, *Nature*, **2006**, *440*, 297.
11. N.C. Seeman, *Nature,* **2003**, *421*, 427.
12. J. Sharma, R. Chhabra, A. Cheng, J. Brownell, Y. Liu, H. Yan, *Science,* **2009**, *323*, 112
13. X. Tu, S. Manohar, A. Jagota, M. Zheng, *Nature*, **2009**, *460*, 250.
14. Y. Chen, H. Liu, T. Ye, J. Kim, C. Mao, *J. Am. Chem. Soc.*, **2007**, *129*, 8696.
15. W. Yanga**,** M.J. Moghaddama**,** S. Taylora**,** B. Bojarskia**,** L. Wieczorek**,** J. Herrmann**,** M.J. McCall**,** *Chem. Phys. Lett.*, **2007**, *443*, 169.
16. H.T. Maune, S. Han, R.D. Barish, M. Bockrath, W.A. Goddard, P.W.K. Rothemund, E. Winfree, *Nature Nanotechnol.*, **2010**, *5*, 61.
17. J.F. Campbell, I. Tessmer, H.H. Thorp, D.A. Erie, *J. Am. Chem. Soc.*, **2008**, *130*, 10648.
18. Z. Zhou, H. Kang, M.L. Clarke, S.H. De Paoli Lacerda, M. Zhao, J.A. Fagan, A. Shapiro, T. Nguyen, J. Hwang. *Small,* **2009**, *5*, 2149.
19. E. Jeng, A. Moll, A. Roy, J. Gastala, M. Strano, *Nano Lett.,* **2006**, *6*, 371.
20. K. Müller, S. Malik, C. Richert, *ACS Nano,* **2010**, *4*, 649.
21. H.T. Maune, S. Han, R.D. Barish, M. Bockrath, W.A. Goddard, P.W.K. Rothemund, E. Winfree, *Nature Nanotechnol.*, **2010**, *5*, 61.
22. G. Dovbeshko,O. Repnytska , E. Obraztsova, Y. Shtogun, *Chem. Phys.Lett.,* **2003***, 372*, 432.
23. M. O'Connell, P. Boul, L. Ericson, C. Huffman, Y. Wang, et al., *Chem. Phys. Lett.,* **2001***, 342*, 265.
24. H. Gao, Y. Kong, D. Cui,CS Ozkan, *Nano Lett.,* **2003***, 3*, 471.
25. H. Gao, Y. Kong, Annu. Rev. Mater. Res., **2004**, *34*, 123, 50.
26. van der Spoel, D. et al. Gromacs User Manual. Version 3.1.1 edn, (University of Groningen, 2002).
27. E.J. Sorin, V.S. Pande, *BioPhys. J.,* **2005**, *88*, 2472.
28. W.L. Jorgensen, D.S. Maxwell, J. Tirado-Rives, *J. Am. Chem. Soc.*, **1996**, *118*, 11225.
29. W.L. Jorgensen, J. Chandrasekhar, J.D. Madura, R.W. Impey, M.L. Klein, *J. Chem. Phys.,* **1983**, *79*, 926.
30. M.S. Dresselhaus, G. Dresselhaus, P.C. Eklund, Science of Fullerenes and Carbon Nanotubes: Their Properties and Applications, *Academic Press*, **1996**.
31. J.H. Walther, R. Jaffe, T. Halicioglu, P. Koumoutsakos, *J. Phys. Chem. B,* **2001**, *105*, 9980.

Chapter 6.

6.1 Summary

In the main body of this thesis a theoretical study of the self-assembly in a special class of block copolymers melts is presented. Block copolymers are macromolecules consisting of chemically different blocks. Due to unfavorable interactions between the connected blocks, described by the Flory-Huggins parameter χ, copolymer melts undergo microphase separation into well-ordered nano structures. In this work results obtained by three different theoretical approaches are presented. In the first one, the so called strong segregation limit theory (SSL) introduced by Semenov, it is assumed that $\chi N \gg 10$ (N being the chain length). In this case the interface thickness is small and the chains are considerably stretched. This allows us to describe the polymer conformations by the most probable ones. The second approach concerns computer simulations based on the dissipative particle dynamics (DPD) simulation technique. Here a number of monomers, usually of the order of a Kuhn segment, are represented by a single DPD bead. Beads are connected by a spring type potential and their mutual interaction is described by a soft repulsive potential. The final approach is the self-consistent field theory (SCFT). Here the main idea is that the interaction between a particle and all other particles can be described by an external field that has to be determined self-consistently.

The first chapter starts with an overview of self-assembly in simple diblock copolymer melts. Block copolymers with a more complex molecular architecture in some cases self-assemble in hierarchically ordered structures with two characteristic length scales. An experimental and theoretical overview of secondary characteristic length scale phenomena in block copolymer melts is given in the final part.

Lamellar-in-lamellar self-assembly in linear ternary multiblock copolymers is investigated in Chapter 2. Our main goal was to find correlation between the number of blocks m in the middle multiblock part of the copolymers under investigation and the number of "internal" layers k of the lamellar-*in*-lamellar self-assembled state of C-*b*-(B-*b*-A)$_m$-*b*-B-*b*-C multiblock copolymers. In our analysis it is assumed that the C end blocks are of the same length and that the volume fraction of C equals the volume fraction of the A, B multiblock part, where the latter consists of A and B blocks of equal length. Furthermore we take $\chi N \gg 10$ for all types of monomers. Due to these assumptions self-assembly results in a lamellar-*in*-lamellar state. In the first part of this chapter this is studied by the SSL approach using the Alexander-de Gennes approximation for the chain trajectories. The simplified description allows us to predict the number of internal layers as a function of the interaction parameters and the number of blocks in the multiblock middle part. The results are in good agreement with a more detailed theoretical study performed before and with experimental studies. Increasing the unfavorable interactions between the A and B components, the structure with a minimal number of internal layers becomes favorable. The opposite behavior is observed when the

interaction between the B and C components is increased. These tendencies follow simply from the fact that the system tries to minimize the most unfavorable contacts by stretching the chains involved. In the second part of this chapter we show that these theoretical predictions are in good agreement with DPD simulations.

If the assumption that $\chi N \gg 10$ is not valid for all types of monomers involved, different microphase separated states become possible. In the experimental work by Bates and co-workers it was shown that A-b-(B-b-A)$_2$-b-C type block copolymers can self-assemble in *perpendicular* lamellar-*in*-lamellar states rather than the *parallel* considered above. In the third chapter we study this *parallel* versus *perpendicular* lamellar-*in*-lamellar self-assembly for A-b-(B-b-A)$_2$-b-C linear ternary multiblock copolymer melts. The volume fractions are assumed to satisfy $f_A = f_B = 0.25$ and $f_C = 0.5$, in agreement with the above mentioned experimental study. In this case only lamellar states are possible. This issue is studied by the three different approaches, 1) SSL theory, 2) DPD simulation and 3) SCFT.

In the first part the SSL approach was used to investigate phase behavior of ternary block copolymer A-b-(B-b-A)$_n$-b–C melt. Four different states are considered: disordered, simple lamellar, parallel and perpendicular lamellar-*in*-lamellar. The influence of the copolymer chain length N, the value of the Flory-Huggins interaction parameters $\chi_{AB}, \chi_{AC}, \chi_{BC}$ and the number of blocks n in the AB multiblock chain on the phase behavior is discussed. We show that in the limiting case of $n \gg 1$ the perpendicular lamellar-*in*-lamellar state becomes stable when the interaction parameters satisfy the relation $0 < \chi_{BC} < 0.22\,\chi_{AC}$. Two different phase diagrams in terms of ($\chi_{AB}N$, $\chi_{BC}N$) for $n = 2$, $n = 10$ and $N\chi_{AB} = N\chi_{AC}$, $N\chi_{AB} = 1.6N\chi_{AC}$ are calculated.

The results of dissipative particle dynamics simulations of A-b-(B-b-A)$_2$-b–C and (B-b-A)$_2$ –b–C ternary multiblock copolymers are presented in the second part of this chapter. It is shown that at small unfavorable interactions a highly fluctuating disordered structure appears as an intermediate state in between the disordered and the lamellar state. When $\chi_{AC}N$ is large, but $\chi_{BC}N$ is small the inverted lamellar-*in*-lamellar structure is favorable. Here the order of the blocks in the ordered state is ABC, whereas in the copolymer chain itself it is BAC. Morphology diagrams in terms of ($\chi_{AB}N$, $\chi_{BC}N$) for $N\chi_{AB} = 2N\chi_{AC}$ are calculated for both multiblock copolymers. It is shown that there is a stronger tendency to form a perpendicular lamellar-*in*-lamellar state for A-b-(B-b-A)$_2$ -b–C than for (B-b-A)$_2$ –b–C.

The last part of Chapter 3 is devoted to a SCFT investigation of the A-b-(B-b-A)$_2$-b–C and (B-b-A)$_2$–b–C ternary multiblock copolymers. We show that for a range of $\chi_{AB}, \chi_{AC}, \chi_{BC}$ values the common solution procedure does not work. A new approach is introduced that allows us to calculate the phase behavior on, close and far away from the so-called Hildebrandt approximation. Stability regions for the shifted and not shifted perpendicular lamellar-*in*-lamellar states are found. In the shifted state the internal AB layers in successive AB layers are shifted over half a period with respect to each other. It was shown that the distribution of the C end block can reduce the free

energy of the shifted structure compared to the not shifted structure. Phase diagrams in terms of (χ_{AB}N, χ_{BC}N) at $N\chi_{AB} = 2N\chi_{AC}$ for both polymer structures are calculated and found to be in good agreement with the results from the DPD investigation. In the parallel lamellar-*in*-lamellar structure at sufficient small χ_{BC}N the B blocks were shown to penetrate into the AC interface to reduce the interfacial tension. Decreasing the BC interaction even further leads to SCFT restrictions, but this case was already covered by the DPD study.

In Chapter 4 the self-assembly of diblock copolymer-based comb copolymers with chemically identical side chains (A-*comb*-C)-*b*-(B-*comb*-C) was investigated. When the repulsion between the C side chains and the AB backbone is small whereas it is large for the A and B blocks, the C blocks are mixed with the AB blocks while the A blocks microphase separate from the B blocks. In that case the behavior is equal to that of simple diblock copolymers with a renormalized Flory-Huggins parameter. The second case is characterized by mixed A and B blocks that microphase separate from the C side chains. Due to the side chain (graft) architecture, the phase stability region of the lamellar phase is shifted to C volume fractions satisfying $0.6 < \phi_C < 0.8$. For the specific case considered ($\varphi_A = \varphi_B = 0.5; m = 20$) the hexagonal structure with the core of the cylinders formed by loops from the A and B blocks is no longer stable. Furthermore, the stability region of the BCC structure where the core of the spheres is formed by the C side chains is significantly increased compared to the simple diblock case. All these observations are in excellent agreement with previously reported results by Milner on the effect of chain architecture on the asymmetry in copolymer phase behavior. The final case considered concerned the most interesting situation where all three components microphase separate from each other and hierarchically ordered structures are formed. The volume fraction of C side chains was assumed to satisfy $0.6 < \phi_C < 0.8$ so that only lamellar structures, where one layer is formed by the C side chains and the other by the AB backbones, are stable. Perpendicular lamellar-*in*-lamellar and parallel lamellar-*in*-lamellar and disk-*in*-lamellar phases were found and characteristic phase diagrams presented. In the case of a lamellar-*in*-lamellar morphology, the perpendicular lamellar-*in*-lamellar is usually the preferred state. Only when the grafting density is relatively small, i.e. $m \leq 4$, the parallel lamellar-*in*-lamellar state become possible.

Chapter 5, finally, is devoted to the question how DNA-*b*-poly(9,9-di-n-octylfluorenyl-2,7-diyl) (PFO) diblock copolymers bind to single wall nanotubes (SWNT) in a water solution. It is shown that the PFO part preferentially binds to the SWNT. If both DNA and PFO block would bind to SWNT it would be impossible to get from solution SWNTs of selected diameters. When only the PFO block from the PFO-*b*-DNA diblock binds to SWNT, it becomes possible to extract from solution SWNTs with selected diameter. The length of the alkyl subchains of the PFO block determines how many diblocks can bind to SWNT. To SWNT with different diameters different number of diblocks can bind, which allows to extract SWNT with a precisely predetermined diameter from solution.

6.2 Samenvatting

Dit proefschrift beschrijft het resultaat van een theoretisch onderzoek naar de zelf-assemblage in een bijzondere klasse van blokcopolymeren. Blokcopolymeren zijn macromoleculen die bestaan uit chemisch verschillende polymeerblokken. Ten gevolge van de karakteristieke ongunstige interactie tussen chemisch verschillende stoffen, voor polymeersystemen uitgedrukt door de Flory-Huggins interactieparameter χ, treedt in blokcopolymeren microfasescheiding in geordende nanostructuren op. Hier beschouwen we dit met behulp van een drietal verschillende benaderingen. De eerste is de zogenaamde sterke segregatie limiet theorie (SSL), geïntroduceerd door Semenov, waarbij wordt aangenomen dat χN >> 10 (N is de ketenlengte). In deze limiet is er sprake van scherpe grensvlakken en aanzienlijk uitgerekte ketens. Dit maakt het mogelijk om in plaats van alle mogelijke polymeerconformaties alleen de meest waarschijnlijke mee te nemen. De tweede benadering betreft computersimulaties met behulp van de "dissipative particle dynamics" (DPD) simulatietechniek. Hierbij worden een aantal monomeren samengenomen in één DPD deeltje. Deze deeltjes, voor zover behorend tot dezelfde polymeerketen, zitten aan elkaar vast met behulp van een veerachtige potentiaal. Hun onderlinge interactie wordt beschreven door een zachte repulsieve potentiaal. De laatste theoretische benadering betreft de zelf-consistente veldtheorie (SCFT).De belangrijkste aanname binnen deze theorie is dat de interactie van een deeltje met alle andere deeltjes kan worden beschreven door een uitwendig veld, een veld dat vervolgens zelf-consistent moet worden bepaald.

In hoofdstuk 1 beginnen we met een overzicht van de zelf-assemblage in simpele diblokcopolymeren om vervolgens blokcopolymeren met een meer complexe moleculaire architectuur te behandelen. In het bijzonder wordt aandacht geschonken aan systemen die een hiërarchische ordening vertonen, een ordening op meerdere lengteschalen. Er wordt een kort overzicht gegeven van experimentele en theoretische resultaten in het eenvoudigste geval van twee verschillende lengteschalen.

Het resultaat van het onderzoek naar gelaagde laag-in-laag structuren voor ternaire multiblokcopolymeren wordt gepresenteerd in Hoofdstuk 2. De belangrijkste onderzoeksvraag betreft het verband tussen het aantal interne "dunne" lagen k als functie van het aantal blokken m in het multimiddenblok voor C-b-(B-b-A)$_m$-b-B-b-C multiblokcopolymeren. Onze analyse beperkt zich tot het symmetrische systeem met C eindblokken van gelijke lengte en A en B blokken van gelijke lengte, waarbij verder de volumefractie van C 50% bedraagt. Verder wordt aangenomen dat χN>>10 voor elk van de drie verschillende polymeerparen. Door deze aannames resulteert zelf-assemblage in een laag-in-laag structuur. In het eerste deel van dit hoofdstuk beschouwen we dit systeem in de sterke segregatie benadering waarbij we verder gebruik maken van de Alexander-De Gennes benadering voor de ketenconformaties. Deze vereenvoudiging stelt ons in staat om het aantal interne lagen te voorspellen als functie van het aantal blokken in het midden multiblok en als functie van de interactiesterkte. De resultaten zijn in goede

overeenstemming met de resultaten van een meer gedetailleerde theoretische beschouwing en met de weinige beschikbare experimentele gegevens. Wanneer de interactie tussen de A en B componenten ongunstiger wordt worden structuren met minder interne lagen gevormd. Het omgekeerde gedrag wordt gevonden als de interactie tussen de B en C componenten ongunstiger wordt. Dit gedrag volgt eenvoudig uit het feit dat het systeem het aantal ongunstige interacties tracht te minimaliseren door het uitrekken van de betreffende polymeerblokken. In het tweede deel van dit hoofdstuk laten we zien dat deze theoretische voorspellingen goed overeenkomen met de DPD simulaties.

Wanneer de aanname $\chi N \gg 10$ niet voor alle monomeerparen geldt is het mogelijk dat de parallelle laag-in-laag structuur plaats maakt voor een loodrechte laag-in-laag structuur. Bates and co-workers lieten experimenteel zien dat bepaalde A-*b*-(B-*b*-A)$_2$-*b*-C type blokcopolymeren deze structuur aannemen. In het derde hoofdstuk beschouwen we deze twee mogelijkheden nader voor A-*b*-(B-*b*-A)$_n$-*b*-C multiblokcopolymeren. Voor de volumefracties nemen we $f_A = f_B = 0.25$ en $f_C = 0.5$, in overeenstemming met de experimentele situatie. De parallel versus loodrecht optie wordt bestudeerd met de eerder genoemde drie verschillende benaderingen: 1) SSL theorie, 2) DPD simulaties en 3) SCFT.

De SSL benadering gebruiken we om vier verschillende structuren te vergelijken: niet-geordend (homogeen), simpel gelaagd, parallelle en loodrechte laag-in-laag. We onderzoeken de invloed van de totale polymeerlengte *N*, de waarde van de interactieparameters $\chi_{AB}, \chi_{AC}, \chi_{BC}$ en het aantal blokken *n*. In het limietgeval $n \gg 1$ blijkt de loodrechte laag-in-laag structuur stabiel te zijn voor $0 < \chi_{BC} < 0.22\chi_{AC}$. Twee verschillende fasediagrammen in het $(\chi_{AB}N, \chi_{BC}N)$-vlak worden berekend voor $n = 2$ en $n = 10$ en $N\chi_{AB} = N\chi_{AC}, N\chi_{AB} = 1.6N\chi_{AC}$.

Vervolgens worden DPD simulaties toegepast op A-*b*-(B-*b*-A)$_2$-*b*–C en (B-*b*-A)$_2$ –*b*–C. Voor relatief kleine waarden van de interactieparameters wordt een sterk fluctuerende ongeordende structuur gevonden als een tussentoestand tussen homogeen ongeordend en de gelaagde structuur. Voor $\chi_{AC}N$ groot en $\chi_{BC}N$ klein wordt een geïnverteerde laag-in-laag structuur gevonden. De volgorde van de lagen is ABC terwijl de volgorde in het blockcopolymeer BAC is. Fasediagrammen worden gepresenteerd in het $(\chi_{AB}N, \chi_{BC}N)$-vlak voor $N\chi_{AB} = 2N\chi_{AC}$. De tendens op vorming van de loodrechte laag-in-laag structuur is groter voor A-*b*-(B-*b*-A)$_2$ -*b*–C dan voor (B-*b*-A)$_2$ –*b*–C.

Het laatste deel van Hoofdstuk 3 is gewijd aan de SCFT studie van A-*b*-(B-*b*-A)$_2$-*b*–C en (B-*b*-A)$_2$–*b*–C. Voor een gebied van $\chi_{AB}, \chi_{AC}, \chi_{BC}$-waarden blijkt de gangbare oplosmethode niet te werken. Omdat het hier juist om het meest interessante gebied gaat wordt er een nieuwe benadering geïntroduceerd. Stabiliteitsgebieden voor twee verschillende loodrechte laag-in-laag structuren worden gevonden, nl. de verschoven en de niet-verschoven toestand. In het eerste geval zijn de interne A en B lagen in de opeenvolgende AB lagen over een afstand van een halve periode verschoven. Fasediagrammen in het $(\chi_{AB}N, \chi_{BC}N)$-vlak worden gepresenteerd voor $N\chi_{AB} = 2N\chi_{AC}$ en

deze blijken goed overeen te komen met de DPD simulaties. Voor kleine $\chi_{BC}N$ waarden blijken de B blokken voor de parallelle laag-in-laag structuur in het AC grensvlak te penetreren om zo de grensvlakspanning te reduceren. Voor nog lagere waarden van $\chi_{BC}N$ werkt ook de nieuwe oplossingsmethodiek niet meer. Om daar toch iets over te kunnen zeggen moeten we een beroep op de DPD simulaties doen.

In Hoofdstuk 4 beschouwen de zelf-assemblage van op diblokcopolymeren gebaseerde kamcopolymeren met chemisch identieke zijketens: (A-*comb*-C)-*b*-(B-*comb*-C). Eerst beschouwen we de situatie waarin de repulsieve interactie tussen de zijketens C en beide hoofdketens A en B relatief gering is en die tussen de beide hoofdketens A en B groot. De C ketens mengen met de A en B ketens die onderling microfasescheiden. Het fasegedrag is vergelijkbaar met dat van simpele diblokcopolymeren, maar met een gerenormaliseerde Flory-Huggins interactieparameter. In het omgekeerde geval zijn de gemengde A en B blokken fasegescheiden van de C zijketens. Ten gevolge van de vertakte moleculaire architectuur verschuift de lamellaire structuur, in vergelijking met het diblokcopolymeer fasediagram, naar volumefracties $0.6 < \phi_C < 0.8$. Voor een symmetrische hoofdketen met 20 zijketens blijkt de hexagonale structuur met cilinders gevormd door de A en B ketens zelfs niet langer stabiel te zijn. Daarnaast neemt het stabiliteitsgebied van de BCC structuur met bollen gevormd door de C zijketens aanzienlijk toe vergeleken met simpele diblokken. Deze vindingen komen goed overeen met de theoretische voorspellingen van Milner over het effect van de ketenarchitectuur op het copolymeer fasediagram. Tenslotte beschouwen we in detail de meest interessante situatie waarbij alle drie de componenten onderling fasescheiden waardoor er hiërarchische structuurvorming optreedt. We nemen voor het gemak aan dat de volumefractie C voldoet aan $0.6 < \phi_C < 0.8$, zodat alleen de gelaagde structuur, met de opeenvolgende lagen gevormd door de C ketens en de AB ketens, stabiel is. De hiërarchische structuurvorming treedt op door de verdere fasescheiding in de AB lagen. Loodrechte en parallelle laag-in-laag structuren en schijf-in-laag structuren worden gevonden. Voor de laag-in-laag structuur blijkt de loodrechte versie veelal de meest stabiele te zijn. Alleen als de vertakkingsgraad klein is, wordt de parallelle toestand ook mogelijk.

Hoofdstuk 5, behandelt een enigszins ander vraagstuk. Bekeken wordt hoe DNA-*b*-poly(9,9-di-n-octylfluorenyl-2,7-diyl) (PFO) diblokcopolymeren zich binden aan enkelwandige koolstofbuisjes (SWNT) in een water oplossing. Omdat alleen het PFO blok van het PFO-*b*-DNA diblokcopolymeer zich aan de SWNT blijkt te binden wordt het mogelijk om op deze wijze SWNT's met gewenste diameter uit een oplossing te selecteren. De lengte van de alkiel zijketens van het PFO blok bepaalt hoeveel diblokken zich aan één SWNT binden. SWNT's met een verschillende diameter binden zich met een verschillend aantal diblokken. Dit maakt het mogelijk om SWNT's met een gewenste diameter te extraheren.

Chapter 7.

Appendix

7.1 Dissipative Particle Dynamics

Dissipative particle dynamics (DPD) is a stochastic simulation technique for simulating the dynamic and rheological properties of simple and complex fluids. DPD was originally proposed by Hoogerbrugge and Koelman [1, 2] to avoid the lattice artifacts of the so-called lattice gas automata and to increase hydrodynamic time and space scales compare to those available with molecular dynamics (MD). Later it was reformulated and slightly modified by Español [3, 4] to ensure the proper thermal equilibrium state. Mapping onto the Flory-Huggins theory was done by Groot and Warren [4].

DPD is an off-lattice mesoscopic simulation technique which involves a set of particles moving in continuous space and discrete time. DPD particles represent whole molecules or part of macromolecule or fluid regions. Atomistic details are not considered. The particles internal degrees of freedom are integrated out and replaced by simplified pairwise dissipative and random forces, so as to conserve momentum locally and ensure correct hydrodynamic behavior. The main advantage of this method is that it gives access to longer time and length scales than are possible using traditional MD simulations. Simulations of polymeric fluids in volumes up to 100 nm in linear dimension for tens of microseconds are now feasible.

7.2 Implementation

The time evolution for a set of interacting particles is found by solving Newton's equations of motion.

$$\dot{\vec{r}}_i = \vec{v}_i, \ \dot{\vec{v}}_i = \frac{\vec{f}_i}{m_i}$$

(A0)

The force acting on the i-th particle $\vec{f}_i$ due to particle j is the sum of a conservative force $\vec{F}_{ij}^C$, a dissipative force $\vec{F}_{ij}^D$, and a random force $\vec{F}_{ij}^R$

$$\vec{f}_i = \sum_{j \neq i} \left(\vec{F}_{ij}^C + \vec{F}_{ij}^D + \vec{F}_{ij}^R \right) \qquad (A1)$$

where the sum is over all other particles within a certain cut-off radius r_c. Since r_c is the only length scale it is used as the unit of length and thus set equal to 1. The conservative force $\vec{F}_{ij}^C$ is a soft repulsive force given by

$$\vec{F}_{ij}^C = \begin{cases} a_{ij}(1 - \dfrac{r_{ij}}{r_c})\vec{e}_{ij}, r_{ij} < r_c \\ 0, r_{ij} \geq r_c \end{cases} \qquad (A2)$$

where a_{ij} is the repulsive interaction parameter between particles i and j, $\vec{r}_{ij} = \vec{r}_i - \vec{r}_j$, $\vec{e}_{ij} = \dfrac{\vec{r}_{ij}}{|\vec{r}_{ij}|}$, $r_{ij} = |\vec{r}_{ij}|$. The dissipative force $\vec{F}_{ij}^D$ is a hydrodynamic drag force and is defined by

$$\vec{F}_{ij}^D = \begin{cases} -\gamma \omega^D(r_{ij})(\vec{e}_{ij} \cdot \vec{v}_{ij})\vec{e}_{ij}, r_{ij} < r_c \\ 0, r_{ij} \geq r_c \end{cases} \qquad (A3)$$

where γ is a friction parameter, ω^D is a r-dependent weight function. The random force $\vec{F}_{ij}^D$ describes thermal noise

$$\vec{F}_{ij}^R = \begin{cases} \sigma \omega^R(r_{ij}) \dfrac{\theta_{ij}}{\sqrt{\Delta t}} \vec{e}_{ij}, r_{ij} < r_C \\ 0, r_{ij} \geq r_C \end{cases} \qquad (A4)$$

where σ is the noise amplitude, ω^R is a weight function, and θ_{ij} is a random variable with normal distribution, Δt is a time step. The dissipative force slows down the particles by removing the kinetic energy from them and this effect is balanced by the random force due to thermal fluctuations. Friction γ and noise σ are related by [3]:

$$\sigma^2 = 2\gamma \, k_B T \tag{A5}$$

The associated weight functions satisfy the fluctuation-dissipation theorem if the following relation is satisfied [5]

$$\omega^D = \left(\omega^R(r)\right)^2 \tag{A6}$$

The standard choice for ω^D is

$$\omega^D = \begin{cases} (r_C - r_{ij})^2, & r_{ij} < r_C \\ 0, & r_{ij} \geq r_C \end{cases} \tag{A7}$$

The spring force $\vec{F}_i^{\,S}$ that acts on bead i due to its connection with beads j satisfies

$$\vec{F}_i^{\,S} = \sum_j C\vec{r}_{ij} \tag{A8}$$

where C is a harmonic type spring constant, which is chosen to be equal to 4 (in terms of k_BT) [5].

A modified version of the velocity-Verlet algorithm is used to solve Newton's equations of motion [5]

$$
\begin{aligned}
r_i(t + \Delta t) &= r_i(t) + v_i(t)\Delta t + 0.5 f_i(t)\Delta t^2 \\
\tilde{v}_i(t + \Delta t) &= v_i(t) + \lambda f_i(t)\Delta t \\
f_i(t + \Delta t) &= f_i[r_i(t + \Delta t), \tilde{v}_i(t + \Delta t)] \\
v_i(t + \Delta t) &= v_i(t) + 0.5\Delta t[f_i(t) + f_i(t + \Delta t)]
\end{aligned}
\tag{A9}
$$

Groot and Warren [7] presented a detailed investigation of the effect of λ on the steady state temperature and showed that for a particle density $\rho=3$ and noise $\sigma=3$, the optimum value is given by $\lambda=0.65$ for which the temperature control can be maintained even at large time-steps of $\Delta t=0.06$. For our calculations we took accordingly $\lambda=0.65$, $\Delta t=0.06$, $\rho=3$ and $\sigma=3$.

Following the work of Groot and Warren [7], the repulsive parameters between the same types of particles is taken as $a_{ii}=25$. For different types of particles a_{ij} can be chosen from the relation between the energy parameter a_{ij} and the Flory–Huggins interaction parameter χ_{ij}

$$a_{ij} = a_{ii} + 3.497\, \chi_{ij} \tag{A10}$$

Model Parameters	
m	mass of DPD particles
r_c	range of DPD interactions (cutoff radius)
γ	friction coefficient
σ	noise amplitude
L	size of simulation box $V = L_d$
N	number of particles
Derived Parameters	
T_0	equilibrium temperature $T_0 = mv_0^2 = m\sigma^2/2\gamma$
n	number density $n = N/L_d$
n_c	number of particles in interaction sphere $n_c = n(\sigma_d r_c^d)$
t_c	traversal time of interaction sphere $t_c = r_c/v_0$
ω_0	collision frequency $\omega_0 = \dfrac{1}{d} n[w]\gamma \propto n_c\gamma$
t_0	collision time $t_0 = 1/\omega_0$
l_0	dynamic distance (mean free path) $l_0 = v_0 t_0$

t_γ	friction time $t_\gamma = 1/n[w]\gamma = t_0/d$
l_γ	dynamic friction distance $l_\gamma = v_0 t_\gamma = l_0/d$
Dimensionless Parameters (n[w] = 1)	
Ω_0	dynamic overlapping $\Omega_0 = r_c/l_0$
Ω_γ	dynamic friction overlapping $\Omega_\gamma = dr_c/l_\gamma = d/n_c \Omega_0$
Ω_L	dimensionless box length $\Omega_L = r_c/L$

Table. 1 The model parameters of dissipative particle dynamics [20, 21].

7.3 References

1.   P. J. Hoogerbrugge and J. M. V. A. Koelman, *Europhysics Letters*, **1992**, 19, 155.
2.   J. M. V. A. Koelman and P. J. Hoogerbrugge, Europhysics Letters, **1993**,21, 363
3.   P. Español, P. Warren, *Europhys. Lett.*, **1995**, 30, 191
4.   P. Español, *Europhys. Lett.*, **1997**, 40, 631.
5.   R.D. Groot, P.B. Warren, *J. Chem. Phys.*, **1997**,107, 4423.
6.   M. Ripoll, M.H. Ernst, and P. Español, *J. Chem. Phys.*, **2001**, 115, 7271.
7.   M. Ripoll, P. Español and M.H. Ernst., *Int. J. Mod. Phys. C*, **1998**, 9, 1329.

List of publications.

1. **Lamellar-in-lamellar self-assembled C-b-(B-b-A)(m)-b-B-b-C multiblock copolymers: Alexander-de Gennes approach and dissipative particle dynamics simulations,**
    T. Klymko, V. Markov, A. Subbotin and G. Ten Brinke,
    Soft Matter, **2009**, 5 (1), 98-103.

2. **Parallel versus perpendicular lamellar-within-lamellar self-assembly of A-b-(B-b-A)(n)-b-C ternary multiblock copolymer melts,**
    A. Subbotin, V. Markov and G. Ten Brinke,
    Journal of Physical Chemistry B, **2010**, 114 (16), 5250-5256.

3. **DNA Block Copolymer Doing It All: From Selection to Self-Assembly of Semiconducting Carbon Nanotubes,**
    M. Kwak, J. Gao, D. Prusty, A. Musser, V. Markov, N. Tombros, M. Stuart, W. Browne, E. Boekema, G. ten Brinke, H. Jonkman, B. van Wees, M. Loi and A. Herrmann,

    Angewandte Chemie International Edition, **2011**, 50, 3206-3210.

4. **Self-assembly of (*A*-comb-*C*)-*b*-(*B*-comb-*C*) diblock copolymer-based comb copolymers,**
    V. Markov, A. Subbotin, and G. ten Brinke,
    Physical Review E, **2011**, 84, 041807.

Acknowledgments

Here I would like to acknowledge all the people who supported me in different ways during my PhD research. This dissertation could not have been written without my promotor Prof. Dr. Gerrit ten Brinke. I am very thankful to him for giving me the opportunity to perform the research that led to this thesis, for the many interesting scientific discussions, for understanding, for the opportunity to work with different people and for stimulating me to take part in different conferences. Special thanks for fixing my English and teaching me how to write articles.

I am very grateful to my copromotor Dr. Andrei Subbotin for teaching me the correct way of thinking to make theoretical investigations successful. Our discussions were very helpful in improving my understanding of the Strong Segregation Theory approach.

I would never have been able to fully understand the Self-Consistent-Field Theory without the enormous help from Prof. I.Ya. Erukhimovich and Dr.Yu.A. Kriksin. Thank you for showing me the fundamental problems of the SCFT approach, for helping me with preparing articles and for the many discussions on unexpected results.

I would like to thank the members of the reading committee, Prof. dr. I.Ya. Erukhimovich, Prof. dr. J.J.M. Slot and Prof. dr. F.A.M. Leermakers for careful reading my thesis manuscript.

Thanks to all the members of the Polymer Chemistry Department for creating a nice working atmosphere. Special thanks to all my group mates: Tetyana Klymko, Yulya Smirnova, Evgeny Polushkin, Sergei Ivanov, Wendy van Zoelen, Joost de Wit, Gerrit Gobius du Sart, Martin Faber and Ivana Vukovich. Yulya, thank you for helping me in the beginning when I just arrived in the Netherlands. Tanya, thank you for our collaboration and for being such a friendly officemate. Sergey, thanks for the many discussions, for helping with the computer cluster maintenance, for programming advices and for allowing me to stay at your place when it needed.

Many thanks to the people from the Polymer Chemistry Department with whom I had a direct collaboration: Martin Faber and Minseok Kwak. Martin, thanks for bringing some of my ideas back to the real world. Minseok, thanks for giving me the opportunity to contribute to your research, resulting in a joint paper.

Very special thanks to my wife, Olya, for supporting me, for giving me strength and for being with me in happiness and grief.

Last but not least I thank my dear parents. Thank you for supporting me on this not so simple road.

28.11.2011   Vladimir.
Groningen